University of Technology, Sydney

School of Civil and Environmental Engineering

Faculty of Engineering and Information Technology

Dynamic Performance of Timber and Timber-Concrete Composite Flooring Systems

By

Rajendra Rijal

BEng. (Civil), MEStud (Structure)

Thesis submitted for fulfilment of

requirements for the degree of

Doctor of Philosophy

2013

CERTIFICATE OF ORIGINAL AUTHORSHIP

I certify that the work in this thesis has not previously been submitted for any degree nor has it been submitted as part of requirements for a degree except as fully acknowledged within the text.

I also certify that the thesis has been written by me. And help that I have received in my research work and the preparation of the thesis itself has been acknowledged. In addition, I certify that all information sources and literature used are indicated in the thesis.

Rajendra Rijal

February 2013

To My Wife & “Doshi” Raju Dai

ACKNOWLEDGEMENT

This PhD project would not have been possible without the assistance, understanding and guidance rendered by numerous kind people, to only some of whom it is possible to give particular mention here, throughout the project.

Above all, I offer my sincerest gratitude to my principal supervisor, Professor Bijan Samali for his patience, outstanding guidance, knowledge, motivation, wisdom and caring support provided throughout my thesis. It was an honour and a pleasure to be his student. His exceptional personality and positive attitude became a source of inspiration and a role model for my professional and personal development. Utmost gratitude is also forwarded to my co-supervisor, Professor Keith Crews for his guidance, fatherly advice, motivation and support throughout my study. It was possible to fulfil my dream of completing PhD due to their invaluable advice, kind response to my interest and support given from beginning of my study.

I also gratefully acknowledge the financial assistance provided by Structural Timber Innovation Company (STIC), University of Technology Sydney (UTS) provided as International Research Scholarship and Centre for Built Infrastructure Research (CBIR), UTS.

I am heartily thankful to Dr. Rijun Shrestha for his encouragement, guidance and unfailing assistance throughout this study. His brilliant and sharp mind combined with his extensive technical knowledge, experience and dedication contributed largely to the success of this project. I would also like to thank Dr. Christophe Gerber for his invaluable assistance during this study. I am really grateful to his technical guidance on experimental works since the beginning of this project.

This thesis would not have been completed without generous assistance and expertise of Dr. Jianchun Li and Dr. Ulrike Dackermann. They have been very helpful throughout this project especially with their expert guidance on the modal testing and experimental modal analysis.

I would also like to acknowledge Dr. Ali Saleh, Dr. Hamid Valipour, Dr. Shami Nejadi, and Dr. Fook Choon Choi for their helping hand on various aspects at different stages of this project. I wish to acknowledge my colleagues, especially those involved in this project such as Zhinus Zabihi, Farzad Moshiri, Nima Khorsandnia and Mulugheta Hailu for providing generous help during this study.

The assistance from the staff in Structures and Material Testing Laboratories at UTS has been very important in completing the tests included in the thesis. I would like to thank Mr. Rami Haddad, Peter Brown, David Dicker and David Hooper. Special thanks go to Peter Brown for his invaluable help in completing experimental modal analysis and testing, and to David Dicker for his expertise in specimen handling. I would like to thank Mr Laurence Stonard and Scott Graham from the Materials Testing Lab for their support in completing the tests. Working in the lab would never have been easy without the assistance provided by all these people.

I wish to thank my family for their love and support to complete my study. My special thanks also go to Manu DD, Subash Dai, Prem Dai and Sunita Vabi, and Dilli Dai for their support and motivation. I offer my regards and blessings to all of those who supported me in any respect during the completion of this study.

Lastly, I would like to dedicate this thesis to my beloved wife, namely, Manju and family, especially my elder brother "Doshi" Raju Dai for their continuous love, assistance and encouragement.

Rajendra Rijal
February 2013

LIST OF PUBLICATIONS

Journal Papers

Rijal, R., Samali, B., Shrestha, R. & Crews, K., "Dynamic performance of timber-concrete composite beams: Experimental and analytical investigations", *Journal of Construction and Building Materials,* under review.

Rijal, R., Samali, B., Shrestha, R. & Crews, K., "Dynamic performance of timber floor modules (Timber beams): Experimental and analytical investigations", *Journal of Construction and Building Materials,* under preparation.

Dackermann, U., Rijal, R., Li, J. & Samali, B., "A novel dynamic-based method for the estimation of the loss of composite action in timber composite systems", *Journal of Non-destructive Testing and Evaluation International, NDT & E International,* under preparation.

Conference Papers

Rijal, R., Samali, B., Crews, K. & Shrestha, R. (2010), "Dynamic behaviour of timber-concrete composite flooring systems", *Proceedings, Eleventh World Conference on Timber Engineering, WCTE 2010,* Trentino, Italy, 20-24 June.

Rijal, R., Samali, B. & Crews, K. (2010), "Dynamic performance of timber-concrete composite flooring systems", *Proceedings, 21st Australasian Conference on the Mechanics of Structures and Materials, ACMSM 21,* Melbourne, Australia, 7-10 December.

Rijal, R., Samali, B., Shrestha, R., Gerber, C. & Crews, K. (2012), "Dynamic performance of timber flooring systems", *Proceedings, 22nd Australasian Conference on the Mechanics of Structures and Materials, ACMSM 22,* Sydney, Australia, 11-14 December.

Dackermann, U., Li, J., Rijal, R. & Samali, B. (2013), "A vibration-based approach for the estimation of the loss of composite action in timber composite systems", *Proceedings, 2nd International Conference on Structural Health Assessment of Timber Structures, SHATIS'13,* Trento, Italy, 4-6 September, to be presented.

LIST OF NOTATIONS

α	damage severity estimator
γ	shear bond coefficient
δ	mid span deflection
δ_k	damping factor for mode *k*
λ_1	calibration factor for $LCAI_1$
λ_2	calibration factor for $LCAI_2$
λ_k	pole value for mode *k*
v	unit impulse velocity response
ξ, D	damping ratio
ρ	density
σ_x	standard deviation
υ	poisson's ratio
φn	normalised modal amplitude
Ψ	matrix of eigenvectors
Ψn	original modal amplitudes obtained before mass normalisation
ω_{dk}	damped natural frequency of mode *k*
ω_n	circular natural frequency
βij	damage indicator for the DI method
ϕ_i''	second derivative or curvature of i^{th} mode shape with respect to x
ω	frequency variable (Chapter 3)
*	complex conjugate (Chapter 3); denotes the damaged state (Chapter 6)
$\chi_m(f)$	magnification function
D_{max}	dynamic magnification factor
ρ_{max}	maximum harmonic response amplitude
$\bar{\omega}$	forcing frequency
$[m]$	mass matrix
$[\Lambda]$	diagonal matrix of poles
$\{\emptyset_n\}$	normalised modal vector
$\emptyset_i$	i^{th} mode shape

Δ	elastic deflection of the system
Δ_B	mid span deflection of the floor beam due to flexure and shear
Δ_G	deflection of the girder at the beam support due to flexure and shear
Δ_S	deflection of the supports such as column or wall due to axial strain
1-D	one-dimensional
2-D	two-dimensional
3-D	three-dimensional
a	flexibility coefficient; distance of load point from nearest support (Chapter 3)
A	area under $\chi_m^2(f)$
A_0	initial amplitude of the flooring system from heel drop test; mass modified stiffness matrix (Chapter 3)
A_1	mass modified damping matrix (Chapter 3)
a_o/g	acceleration limit
a_p/g	predicted acceleration ratio due to walking excitation
A_r	area associated with the resonance bandwidth ($f_n/\sqrt{2} < f < \sqrt{2}f_n$)
b	floor width
B	number of bits used to represent a sample in the ADC
B_c	width of concrete topping
B_0, B_1	force distribution matrices
c	damping coefficient
$LCAI_1$	first loss of composite action index
$LCAI_2$	second loss of composite action index
C_B	frequency coefficient
Cc	critical damping coefficient
CO_2	carbon dioxide
d	diameter of the shear connector
D_C	theoretical full composite deflection
D_I	measured partial composite deflection
D_N	theoretical fully non-composite deflection
D_w	depth of LVL web
$D_{xx}(\tau)$	auto RanDec function
$D_{xy}(\tau)$	cross RanDec function

E	modulus of elasticity; efficiency of composite systems (Chapter 2 - Section 2.11); dynamic-based degree of composite action (Chapter 6)
E_{cj}	mean MOE of concrete at the appropriate age
EI	flexural stiffness
$(EI)_b$	bending stiffness of the floor about an axis parallel to the beams
$(EI)_{ef}$	effective bending stiffness
$(EI)_l$	bending stiffness of the floor about an axis perpendicular to the beams
E_x	mean modulus of elasticity of LVL in x-direction
$f(\omega)$	input signal
F, P	point load
f'_b	characteristic bending strength
f'_c	characteristic compression strength parallel to grain
f'_p	characteristic compression strength perpendicular to grain
f'_s	characteristic shear strength
f'_{sj}	characteristic shear strength at joint details
f'_t	characteristic tensile strength
f_1	fundamental frequency
f_a & f_b	natural frequency corresponding to the first, *a*, and second point, *b*, of the *HBM*
f_b	mean bending strength
f_c	mean compression strength
f_{cm}	mean value of the compressive strength of concrete at the relevant age
f_{damped}	damped natural frequency
F_{ij}	fractional modal strain energy for undamaged beam
F_{max}	theoretical maximum Nyquist frequency limit
f_n	natural frequency
$f_{n(Exp)}$	experimental natural frequency
$f_{n(FE)}$	natural frequency from FE model
F_{Nyq}	nyquist frequency
F_{samp}	sampling frequency
f_t	mean tensile strength
$f_{undamped}$	undamped natural frequency
f_v	mean shear strength

g	acceleration due to gravity (9.81 m/s^2)
G	shear modulus
$g(\omega)$	output signal
$G_{ff(\omega)}$	input auto spectrum
$G_{fg(\omega)}$	cross input-output spectrum
$G_{gg(\omega)}$	output auto spectrum
$H(\omega)$	matrix of FRFs
$H_1(\omega)$	frequency response function
$H_{ij(j\omega)}$	FRF between the respond DOF *i* and reference DOF *j*
I	moment of inertia
i, n, M	mode number
k	stiffness
$k17$	factor for multiple nailed joints
K_{serv}	serviceability limit state stiffness
K_u	ultimate limit state stiffness
L, l	span
L_b	shear-free span between load points
m	mass of the floor ; mass per unit length (Chapter 7); mass per unit area (Section 7.1.4)
M_i	initial mass of moisture content test piece
M_o	dry weight of moisture content test piece
N	number of averaged time segments (Chapter 2); number of modes of vibration (Chapter 3); number of accelerometers (Chapter 6)
n_{40}	number of first-order modes with natural frequencies up to 40 Hz
$NFerror$	natural frequency difference between FE and experimental models
P_o	excitation force
Q_k	strength of shear connectors
R_d	deformation response factor
r_{ijk}	residue value for mode *k*
s_e	spacing of the shear connectors at the ends of the beam
S_{eff}	effective constant spacing of the shear connectors
s_m	spacing of the shear connectors in the middle of the beam
T_c	thickness of concrete topping

T_f	thickness of LVL flange
T_w	thickness of LVL web
$Tx(t_i)$	triggering condition applied to time history x(t)
W	effective weight of the floor
w	maximum short-term deflection; uniformly distributed load per unit length (Chapter 7)
$x(k)$	discrete series
x(t)	response time history
y(t)	response time history
y_0	maximum deflection
y_1 & y_2	amplitudes of the response peaks of the 1st and 2nd cycle
y_n	amplitude of n^{th} cycle response
y_{n+m}	amplitude of the $(n + m)^{th}$ cycle response
y_w	weighted average value of the static deflection
Z_{ij}	normalised damage indicator

LIST OF ACRONYMS

ADC	analogue-to-digital converter
BM	bird-mouth
CA	composite action
CMSE	cross-modal strain energy
COMAC	coordinate of modal assurance criterion
CoV	coefficient of variation
DD	damage detection
DI	damage index
DOF	degree of freedom
MOE	modulus of elasticity
EBM	equivalent beam method
EMA	experimental modal analysis
FDPI	frequency domain direct parameter identification
FE	finite element
FEA	finite element analysis
FEM	finite element model
FFT	fast Fourier transform
FRF	frequency response function
FRST	foundation for research science and technology
FWPA	forest and wood products Australia
Glulam	glue laminated timber
HBM	half-power bandwidth method
IRF	impulse response function
LCA	loss of composite action
LCAI	loss of composite action index
LDA	logarithmic decrement analysis
LVDT	linear variable differential transformer
LVL	laminated veneer lumber
MAC	modal assurance criterion
MC	moisture content

MDI	modified damage index
MDOF	multi degree of freedom
MT	modal testing
NDI	non-destructive inspection
NS	normal screw
NZ	New Zealand
Pty Ltd	proprietary limited
R & D	research and development
RanDec	random decrement
RMS	root mean square
SCC	steel-concrete composite
SDOF	single degree of freedom
SLS	serviceability limit state
STIC	structural timber innovation company
TCC	timber-concrete composite
ULS	ultimate limit state
UTS	University of Technology Sydney

TABLE OF CONTENTS

LIST OF FIGURES

LIST OF TABLES

ABSTRACT

In recent years, there has been an increasing trend in Australia and New Zealand towards the use of long-span timber and timber-concrete composite (TCC) flooring systems for the construction of multi-storey timber buildings. The popularity of these flooring systems is because of their low cost, easy construction and the use of environmentally sustainable materials. Due to their light-weight, such long-span floors are however highly susceptible to vibrations induced by service loads. Although long-span timber and TCC flooring systems can easily be designed to resist the static loads using currently available design guidelines, it is crucial to also investigate the dynamic behaviour of these floors as the occupant discomfort due to excessive vibration may govern the design. Moreover, many structural failures are caused by dynamic interactions due to resonances, which highlight the importance of investigating the dynamic behaviour of flooring systems. To date, there are very limited design guidelines to address the vibration in long-span floors, especially composite floors, due to a lack of sufficient investigation.

In 2009, a research consortium named Structural Timber Innovation Company (STIC) was founded, with the aim to address various issues encountered with structural timber buildings including timber and TCC flooring systems. STIC is conducting Research and Development (R & D) work in a number of key areas to provide a new competitive edge for commercial and industrial structural timber buildings. The R & D work is undertaken with three parallel objectives at three universities, namely, the University of Technology Sydney (UTS), the University of Canterbury (UC) and the University of Auckland (UA). The focus of UTS is the assessment of various performance issues of long-span timber only and TCC flooring systems for multi-storey timber buildings. The work presented in this thesis deals with the investigation of the dynamic performance of timber only and TCC flooring systems, which is one of the sub-objectives of the research focus at UTS.

In particular, the presented research assesses the dynamic performance of long-span timber and TCC flooring systems using different experimental und numerical test structures. For the experimental investigations, experimental modal testing and analysis

is executed to determine the modal parameters (natural frequencies, damping ratios and mode shapes) of various flooring systems. For the numerical investigations, finite element models are calibrated against experimental results, and are utilised for parametric studies for flooring systems of different sizes. Span tables are generated for both timber and TCC flooring systems that can be used in the design of long-span flooring systems to satisfy the serviceability fundamental frequency requirement of 8 Hz or above. For floors where vibration is deemed to be critical, the dynamic assessment using the 8 Hz frequency requirement alone may not be sufficient and additional dynamic criteria such as response factor, peak acceleration and unit load deflection need to be satisfied. To predict the fundamental frequency of various TCC beams and timber floor modules (beams), five different analytical models are utilised and investigated.

To predict the cross-sectional characteristics of TCC systems and to identify the effective flexural stiffness of partially composite beams, the "Gamma method" is utilised. Essential input parameters for the "Gamma method" are the shear connection properties (strength, serviceability stiffness and ultimate stiffness) that must be identified. Therefore, a number of experimental tests are carried out using small scale specimens to identify strength and serviceability characteristics of four different types of shear connection systems and three of them were adopted in the TCC beams. The connections included two types of mechanical fasteners (normal wood screw and SFS screw) and two types of notched connectors (bird-mouth and trapezoidal shape) with coach screw.

Traditionally, the composite action of a system is determined from static load testing using deflection measurements. However, static load testing is expensive, time consuming and difficult to perform on existing flooring systems. Therefore, two novel methods are developed in this thesis that determines the degree of composite action of timber composite flooring systems using only measurements from non-destructive dynamic testing. The core of both methods is the use of an existing mode-shape-based damage detection technique, namely, the Damage Index (DI) method to derive the loss of composite action indices (*LCAIs*) named as $LCAI_1$ and $LCAI_2$. The DI method utilises modal strain energies derived from mode shape measurements of a flooring system before and after failure of shear connectors. The proposed methods are tested and

validated on a numerical and experimental timber composite beam structure consisting of two LVL components (flange and web). To create different degrees of composite action, the beam is tested with different numbers of shear connectors to simulate the failure of connection screws. The results acquired from the proposed dynamic-based method are calibrated to make them comparable to traditional static-based composite action results. It is shown that the two proposed methods can successfully be used for timber composite structures to determine the composite action using only mode shapes measurements from dynamic testing.

University of Technology, Sydney

CHAPTER 1

INTRODUCTION

1 Introduction

1.1 Background

Timber is the oldest and the only renewable natural building material. It was the primary structural material until the beginning of the 20th century (Lam 2009). Therefore, it has a very old history in the construction of the buildings and footbridges in Australia, Europe and the rest of the world. Further, timber is a widely available and flexible building material. It is more suitable than the other building materials such as concrete and steel for many reasons such as cost, ease of workmanship, customer preference for natural materials, environment friendly and thermal insulation properties of wood.

Timber has been dominated by concrete and steel since the 20th century, but emission of greenhouse gases is the main concern during the production of concrete and steel. In addition, the price and shortage of concrete and steel is increasing due to rapid growth in infrastructure construction. Thus, there is increasing interest in alternative, low embodied energy building materials such as timber. Research has proven that timber construction produces much less greenhouse gases such as carbon dioxide (CO_2) compared to concrete and steel. Hence, in recent times 'light frame timber construction' has become more popular. The demand for structural timber and wood products keeps increasing as a building material for single and multi-family housing and low-rise commercial buildings. For example, more than 90% of residential buildings in North America and Japan are built with timber frame or post and beam systems where over two million building units are built annually (Lam 2009).

However, light-weight floor constructions are susceptible to vibrations and have low impact sound insulation due to inherent low density, low stiffness and poor damping of the timber. In recent times, the floor vibration problem is increasing in the flooring systems of the offices and hospitals where they need very low-vibration environment and residential buildings due to recent trends towards long-span and light-weight construction. Occupants of the buildings can cause vibration of the light-weight floors and resonance at low frequencies causing discomfort to them, therefore, specific construction techniques is essential to minimize the transmission of vibrations and sound to the adjoining units**.**

Timber-concrete composite (TCC) floor construction is a new construction technique to resolve vibration susceptibility and low impact insulation issues concerned with light-weight timber floors. In the construction, a thin layer of concrete is cast on the top of timber elements and connectors in between are essential to transfer shear force from concrete topping to the timber joist as shown in Figure 1.1. Concrete performs well in compression while timber is stronger in tension, therefore, the tensile resistance of the timber joist can be used in a similar fashion as conventional reinforcement in conventional concrete construction. The cross-section needs to be designed in such a way that the concrete topping is in compression and the area in tension is replaced with timber to utilize the strength and stiffness of both materials for greatest advantage. Hence, the concrete topping can be used to resolve many issues encountered in timber only flooring systems, especially vibration.

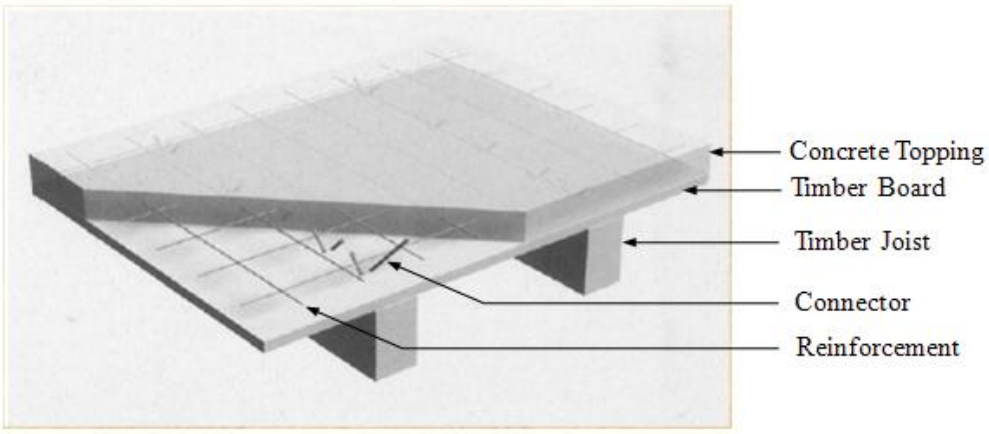

Figure 1.1 Typical TCC flooring system (Kolb 2008).

Normally, composite flooring systems are designed against the static actions, but the dynamic actions are also of great importance nowadays as they have also been the cause of many structural failures. Hence, there is a growing need for measurement of modal parameters such as natural frequencies, damping ratios, mode shapes and modal masses of the flooring systems as design parameters. Initially, the vibration issues of different types of composite flooring systems was identified through experimental investigations under the action of human activities by Chien & Richie (1984) and was followed by Bachmann & Ammann (1987); Allen & Murray (1993); Williams & Waldron (1994), and Nor Hayati, Deam & Fragiacomo (2009). Moreover, da Silva et al. (2003), Hicks (2004) and Ebrahimpour & Sack (2005) investigated the response of the flooring

systems against vibration caused by human activities with the use of finite element method.

A number of design guidelines such as Wyatt (1989); Murray (1990); Murray, Allen & Ungar (2003), and Eurocode 5 (2008) are available to design composite flooring systems. Empirical methods are presented in the guidelines to estimate first natural frequency of the flooring systems, but very limited solutions can be found to estimate higher natural frequencies. In this thesis the reliability of the empirical methods are checked. This research is part of Structural Timber Innovation Company's (STIC) research and development programme. Some details about STIC are presented in Section 1.2.

1.1.1 History of TCC Flooring Systems

The TCC system is a relatively young technology. The first attempts to combine wood and concrete were done in the 1920's and 1930's. Bathon (2000) reported that Otto Schaub was the first inventor in Germany to apply for a patent that consisted of a TCC element in 1939. Hotel "Zum guten Hirten" is the first project where concrete was cast on top of the existing timber floor to upgrade its performance in 1960. The first design models were introduced based on experimental tests in 1984 and it was concluded that the composite action increases the overall capacity of TCC floors against timber floors by a factor of 2.5. A new type of fastener, known as the double-headed screw for the new type of TCC system, was invented in 1985. In 1987, Küng used the advantages of the light-weight concrete-composite systems to renovate a timber-beamed-floor. A glued connection system was introduced in 1993 to provide a rigid connection between timber and concrete (Bathon 2000). The technology has become more acceptable with more successful applications since the 1980's (Steinberg, Selle & Faust 2003).

1.1.2 Advantages of TCC Flooring Systems

Structural performance of the full timber flooring system can be improved by using TCC construction. A number of advantages of this system against timber, steel, and reinforced concrete floors are listed below:

- *Higher stiffness and strength* compared to timber-only floors. If the timber and concrete are well connected in the systems, the strength and flexural rigidity of

the systems can be up to three and six times of timber only flooring systems, respectively. The improved strength and flexural stiffness could allow composite floors to span up to 12 m (ABD. Ghafar 2008).They can resist design imposed actions higher than the standard 1.50 kPa and the span can be increased by about 1.5 times when 50 mm thick concrete layer is cast by using typical shear connectors to a timber floor (Steinberg, Selle & Faust 2003).

- *Less susceptible to vibrations* than timber only floors as they have damping ratio of about 2% while timber only floors have damping of about 1%. Higher damping reduces the annoying springiness effect on the floors caused by human activities (Hu, Chui & Onysko 2001).
- *Lighter in weight*. They are relatively lighter than reinforced concrete and steel-concrete composite flooring systems as timber has much lower density than concrete and steel. As a consequence, the reduced permanent action allows larger spans to be achieved and reduces the size of the foundation, which ultimately saves money. The density of normal weight concrete is about 2,400 kg/m^3 while for timber it ranges from 310 to 700 kg/m^3 (Lam 2009). Moreover, the permanent action of a TCC floor can be reduced by 15% if light-weight concrete with a density of 1,600 kg/m^3 instead of a normal weight concrete of 2,300 kg/m^3 is used (Steinberg, Selle & Faust 2003).
- *Greater thermal mass*. The high thermal mass of the concrete topping stabilises the internal temperature of the building, reducing heating and cooling costs.
- *More effective acoustic separation*. Both air-borne and impact noise insulation is improved relative to full timber flooring systems, owing to the increased mass and greater damping, respectively.
- *More economical* than reinforced concrete slab, particularly when prefabrication construction is adopted and the total installed cost is considered, owing to number of factors such as quick construction, little or no formwork, less propping, less wastage, and reduced foundations.
- *They are efficient as shear-walls* as the concrete topping gives racking strength and the timber joists' stiffness against out-of-plane buckling (Ceccotti 2002).
- *They have such large in-plane rigidity* that they keep their shape, and in turn the shape of the whole building, during an earthquake, permitting the use of simplified seismic analysis procedures. The timber joists and the concrete

topping should be well connected to masonry walls to take this advantage (Ronca, Gelfi & Giuriani 1991).

- *Local resource consumption*. They can optimize consumption of local timber resource**.**
- *Less environmental impact*. TCC systems are superior to reinforced concrete floors as lower energy is required to produce timber instead of steel or concrete and timber is sustainable with net CO_2 emission being zero during its full life-cycle (Steinberg, Selle & Faust 2003).
- *Use of lightness.* The system can be used to increase height (or storeys) of the existing structures due to its lightness compared to the concrete and steel.
- *Preservation of historical timber floors.* The system can be used to upgrade strength and stiffness of the existing timber floors.

1.1.3 Importance of Composite Action in the TCC Flooring Systems

The two major components of TCC flooring systems such as timber joists and concrete topping need to be connected by mechanical fasteners to transfer shear forces from concrete topping to the timber joists. There is a crucial role for connection system in order to achieve composite action so that the dynamic and static performance of the systems can be improved. The two components act independently if the system is fully non-composite and the system performs poorly under the static and dynamic actions while the system performs well when the system is fully composite. The higher composite action results in better performance. Therefore, the transfer of the shear force across the concrete-timber interface is critical in design of the system.

1.2 Structural Timber Innovation Company

"Structural Timber Innovation Company (STIC) is a research consortium developing and commercialising new technologies that will enable structural timber to compete more effectively in the building and construction market" (STIC Ltd 2009).

It was registered in New Zealand and its seven shareholders are Carter Holt Harvey Ltd, Nelson Pine Industries Ltd, Wesbeam Pty Ltd, Building Research Association New Zealand Inc, NZ Pine Manufacturers Association, Auckland Uniservices Ltd (University of Auckland) and University of Canterbury. In addition, it has two major

financial stakeholders such as Forest and Wood Products Australia (FWPA), and Foundation for Research Science and Technology (FRST).

It is developing new technologies to construct multi-storey commercial and long-span industrial portal framed buildings with easy design and rapid construction techniques using pre-fabricated engineered timber products such as laminated veneer lumber (LVL) and glue laminated timber (Glulam) so that timber can compete effectively with the two current construction dominant materials, namely, concrete and steel. In addition, it has the following missions (STIC Ltd 2009):

- Contract and manage the required research and development to enable the vision to be achieved.
- To manage the intellectual property developed and to ensure its availability to relevant segments of the building and construction industry value chain.
- To facilitate and promote the implementation and transfer of the newly developed intellectual property into the Trans-Tasman building and construction industries.
- Provide new timber building solutions to the industry and add value to building owners/developers, constructors, architects, engineers and fabricators.

It is conducting research and development (R & D) in a number of key areas to provide a new competitive edge for commercial and industrial structural timber buildings. Further, it is developing design guidelines, analysis packages, and recommendations and supporting data sets that will provide Architects, Engineers, Quantity Surveyors, Fabricators and Constructors with the information they need to design and construct these next generation of timber buildings with confidence and minimal inconvenience. The current R & D programme is being carried out in three parallel objectives at three universities as shown in Figure 1.2.

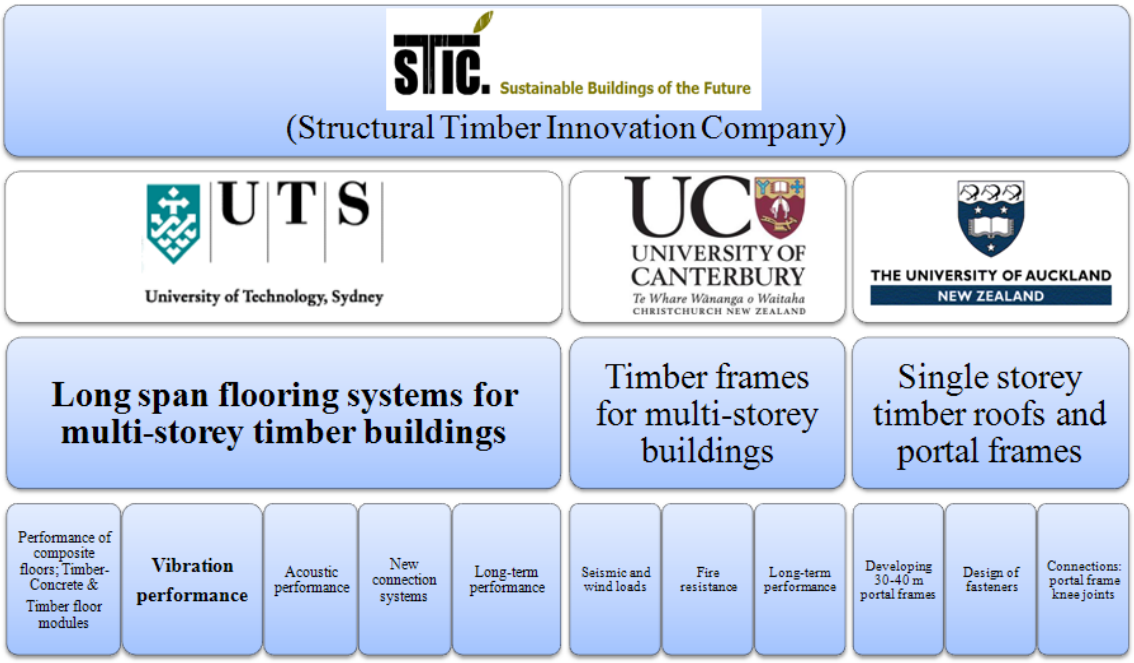

Figure 1.2 A summary of STIC's objectives.

UTS research project is a part of STIC's R & D programme and its focus is mainly to assess a number of performance issues of the long-span TCC and timber only flooring systems for multi-storey timber buildings. This thesis is focused on assessing "Vibration Performance" of the flooring systems, which is one of the sub-objectives of the UTS project, by evaluating their modal parameters. An overview of the experimental work is depicted in Figure 1.3. The tests surrounded by broken line in the figure are covered in this thesis and the rest of the tests are part of the future work of the UTS ongoing project.

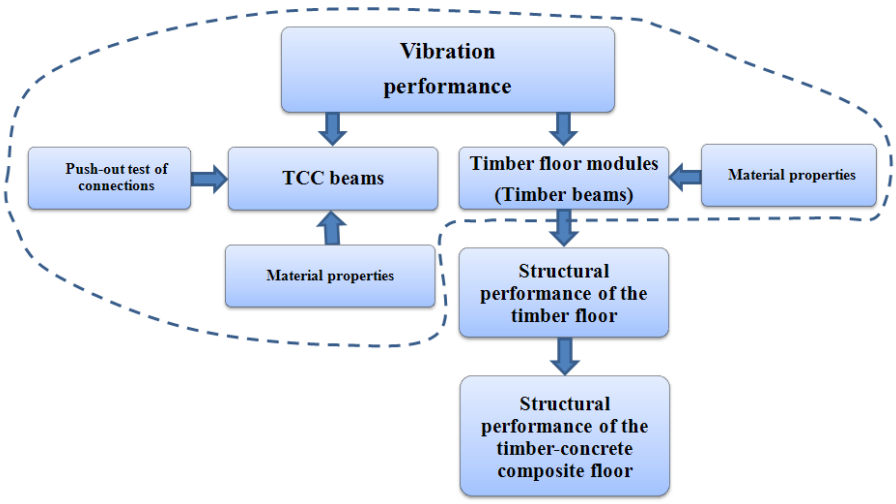

Figure 1.3 An overview of experimental work.

1.3 Basic Vibration Terminologies

(a) Dynamic loadings

Mathematically, dynamic loadings can be classified as harmonic, periodic, transient, and impulsive as shown in Figure 1.4. Harmonic loads are usually caused by rotating machinery and periodic loads are caused by rhythmic human activities such as dancing and aerobics, and machinery. Transient loads occur from the movement of people, including walking and running. Impulsive loads are consequence of single jumps and heel drop impacts and the like.

(b) Vibration period and natural frequency

Vibration period is the time interval between successive peaks of repeating events such as harmonic and periodic dynamic loads as shown in Figure 1.4. Frequency is the inverse of period and is usually expressed in Hertz.

(c) Steady state and transient motion

Steady state motion on the flooring system is caused by a continuous harmonic load and the motion has a constant frequency and amplitude. If the system is subjected to the impulsive loads such as hammer and heel drop impacts, the resulting motion will be subsided by damping in the system as shown in Figure 1.5, which is a transient motion.

(d) Natural frequency

Natural frequency is the frequency of a structure in free vibration, expressed in cycles per second (Hz) or rad/sec (ω).

(e) Damping, critical damping and damping ratio

Damping is the property of the system which dissipates vibration energy. Damping ratio is expressed as the ratio of actual damping to critical damping. Critical damping is the smallest amount of viscous damping which inhibits oscillation.

(f) Step frequency

Step frequency is the frequency of human activities imparted to the flooring systems.

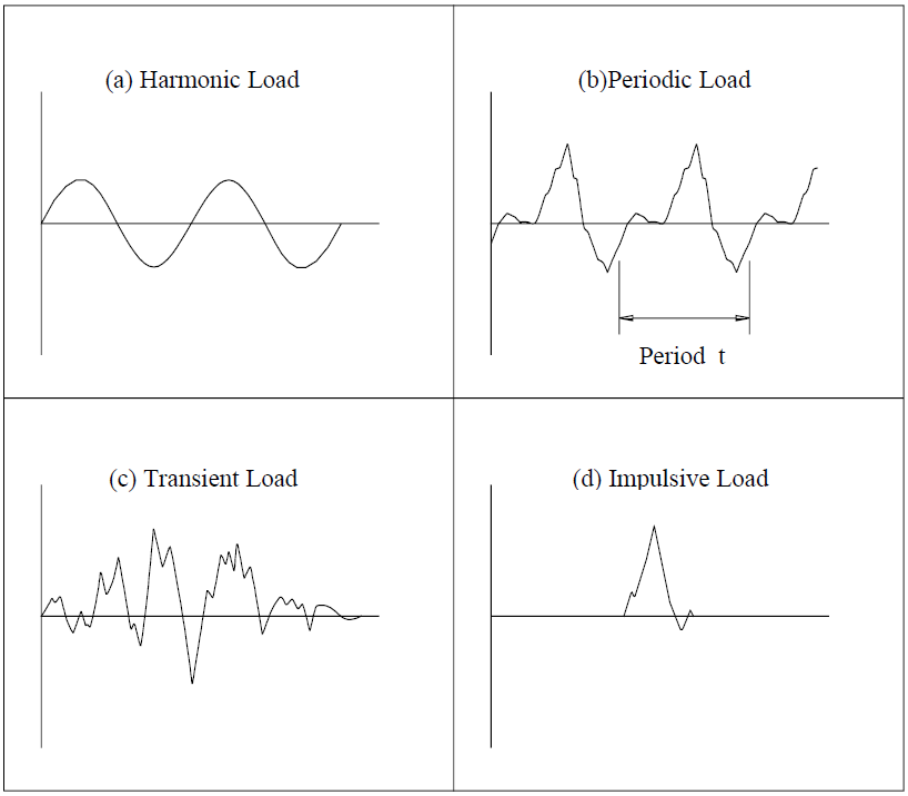

Figure 1.4 Types of dynamic loading (Murray, Allen & Ungar 2003).

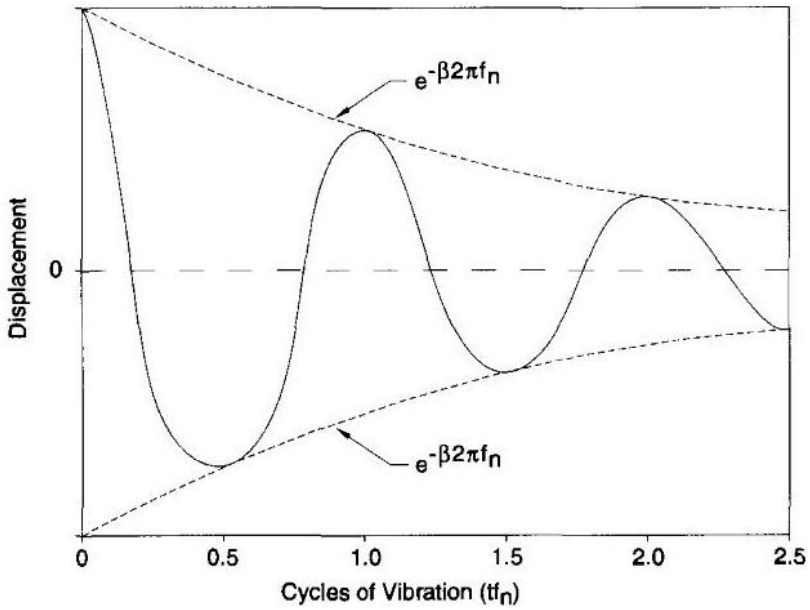

Figure 1.5 Transient vibration with viscous damping (Murray, Allen & Ungar 2003).

(g) Harmonic

Harmonic is the multiple frequency of the step frequency caused by repetitive forces such as human activities and machinery (Murray, Allen & Ungar 2003).

(h) Resonance

Resonance will occur in the flooring systems when exciting frequency coincides with the natural frequency of the system resulting in very large amplitude of motion.

(i) Vibration modes

Vibration modes or resonances are inherent properties of the systems as they depend upon the material properties such as mass, stiffness, and damping properties, and boundary conditions of the systems. Each mode is defined by a modal natural frequency, modal damping, and mode shape. The overall vibration shape of the systems at or close to the natural frequency of a mode will be dominated by the mode shape at resonance (Schwarz & Richardson 1999).

(j) Vibration mode shape

Vibration mode shape of the systems is their vibration shape when they are allowed to vibrate freely in a particular mode. Each natural frequency has a mode shape associated with it. Figure 1.6 depicts typical mode shapes for a simple beam and flooring system (Murray, Allen & Ungar 2003).

(a) 2nd flexural mode of a typical beam

(b) 4th flexural mode of a typical beam

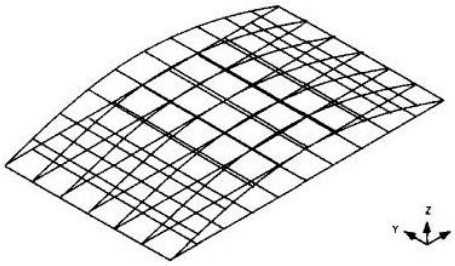

(c) 1st or fundamental flexural mode of a typical floor

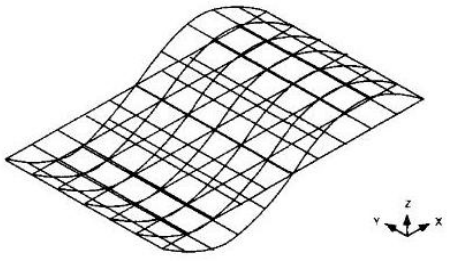

(d) 2nd flexural mode of a typical floor

Figure 1.6 Typical beam and floor system mode shapes (Murray, Allen & Ungar 2003).

(k) Modal analysis

Modal analysis is a computational analytical or experimental method to determine the modal parameters such as natural frequencies, damping ratios and mode shapes of a structure to a given excitation. The response of individual modes can be superimposed to obtain an overall response of the structure (Murray, Allen & Ungar 2003).

(l) Spectrum

A spectrum depicts the variation of relative amplitude with frequency of the vibration components that contribute to the load or motion as shown in Figure 1.7.

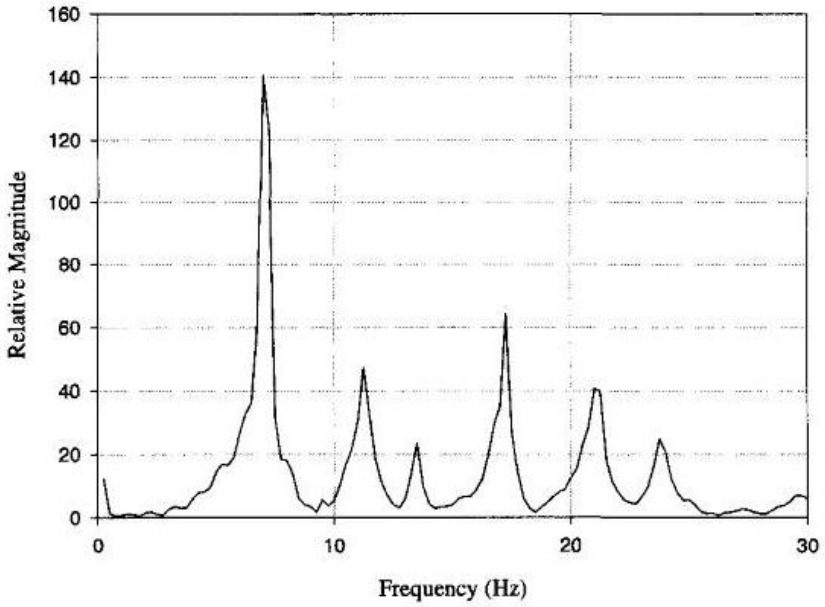

Figure 1.7 Frequency spectrum (Murray, Allen & Ungar 2003).

(m) Fourier transformation

Fourier transformation is the mathematical procedure to convert a time history response of a system into a frequency spectrum without loss of information.

(n) Acceleration ratio

Acceleration ratio is the ratio of acceleration of the system to the acceleration of gravity. Usually the peak acceleration of the system is used (Murray, Allen & Ungar 2003).

(o) Frequency response function

The frequency response function (FRF) is a fundamental measurement to be made for experimental modal analysis that isolates the inherent dynamic properties of a structure. FRFs are usually used to describe the input (or excitation force) and output (or response) relationships of the system. FRF measurements are also used to obtain experimental modal parameters such as natural frequencies, damping ratios and mode shapes. The FRF formulations are presented in Table 1.1 (Schwarz & Richardson 1999; Dackermann 2010).

Table 1.1 Frequency response function formulations

Receptance	Acceleration/Force
Effective mass	Force/Acceleration
Mobility	Velocity/Force
Impedance	Force/Velocity
Dynamic compliance	Displacement/Force
Dynamic stiffness	Force/Displacement

1.4 Research Objectives

The main aim of this research is to investigate the dynamic behaviour of TCC beams with different connection systems for evaluation of their serviceability. Further, dynamic-based composite action methods are developed for the determination of the degree of composite action of a composite flooring system. The specific objectives of this research work are as follows:

- To assess the dynamic performance of TCC beams and timber floor modules (timber beams) based on the structures' dynamic parameters, i.e. natural frequencies, damping ratios and mode shapes. The aim of this study is to maximize the span length of TCC sections (with different connection systems) under consideration of limited vibration responses.
- To study the long-term dynamic behaviour of TCC systems and to determine if creep effects alter the dynamic characteristics.

- To develop a method based on dynamic test measurements for the determination of the degree of composite action of a composite system.
- To identify natural frequencies, in particular the fundamental frequencies, of TCC and timber beams using available analytical prediction models and validate their reliability by correlating predicted values acquired from these models with test results of the corresponding beams.
- To establish the serviceable span range for TCC beams and timber floors that satisfy serviceability limit state, especially vibration characteristics, by performing parametric analyses on corresponding FE models.

1.5 Research Scope

This research is concerned with the study of the dynamic behaviour of TCC flooring systems. The scope of this work is limited to the following areas:

- The dynamic assessment of four identical long-span TCC beams (5.8 m clear span) with different connection systems based on their dynamic parameters, especially natural frequencies.
- The study of the long-term dynamic behaviour of TCC beams to determine if creep effects alter the dynamic characteristics.
- The investigation of the performance of different type of shear connectors used in TCC beams.
- The dynamic assessment of six long-span timber beams, three with 6 m clear span and three with 8 m clear span, based on their dynamic parameters, especially natural frequencies.
- The evaluation of existing analytical natural frequency prediction models applied to composite flooring systems.
- The development of novel dynamic-based loss of composite action (LCA) identification schemes suitable for composite flooring systems.
- The numerical verification of the proposed LCA identification schemes using finite element models.
- The experimental validation of the developed LCA identification procedures using laboratory test structures.

1.6 Research Significance and Contribution to Knowledge

The serviceability of light-weight and long-span flooring constructions is greatly restricted by their vibrational behaviour. Hence, the dynamic assessment of these structures has become an integral part in the design process and guidelines. The current research is concerned with the vital study of the dynamic behaviour of newly developed TCC flooring systems with different connection systems using dynamic parameters such as natural frequencies, damping ratios and mode shapes. Further, a dynamic-based testing method is developed to assess the loss of composite action of a composite flooring system due to the failure of shear connectors. The original contributions of this study include:

- The assessment of the dynamic behaviour of TCC beams with different connection systems of 5.8 m span length and timber floor modules with spans of 6 and 8 m. The dynamic parameters (natural frequencies, damping ratios and mode shapes) of experimental and corresponding numerical structures are determined using experimental modal testing and analysis procedures. Based on this study, the maximum span length of various TCC sections is determined under consideration of limited dynamic responses. In addition, natural frequencies of these beams are predicted using existing analytical prediction models and the results are correlated with experimental results to identify the reliability of these models as natural frequency measures are one of the important dynamic serviceability design criteria.
- The long-term performance of TCC beams in relation to their dynamic behaviour is investigated. Three dynamic tests are undertaken over a period of 15 months for different TCC beams to determine the effects of long-term static action, variation in temperature, relative humidity and moisture content to the dynamic behaviour, i.e. the modal parameters (especially fundamental frequencies). It is found that variations in the moisture content of LVL timber have a significant effect on the dynamic characteristics. In particular, the natural frequencies increase with the decrease in moisture content and vice versa. Furthermore, creep effects in different components such as timber, concrete and connection systems of beams also influence the dynamic performance as percentage of increment or decrement of natural frequencies of corresponding

beams was found to be different for the same decrement or increment of moisture content in the LVL timber.

- Push-out tests are conducted on four different types of shear connectors to characterise their properties and identify the most effective shear connector. The bird-mouth notched connection is found to be the most efficient connection type.
- Two novel dynamic-based methods are developed for the identification of the composite action for composite flooring systems using the dynamic mode shape measurements as input parameters. Both developed techniques are based on the Damage Index (DI) method to derive the indices $LCAI_1$ and $LCAI_2$, respectively, which evaluate the degree of composite action. Higher amplitudes of the indices represent higher loss of composite action. The proposed algorithms are capable of determining the composite action of a composite structure using only mode shape measurement obtained from dynamic testing.
- The two developed loss of composite action (LCA) methods are validated on numerical and experimental timber composite beam structures consisting of two LVL components. In numerical modelling, 2-D FE models are generated and real testing limitations, such as limited number of accelerometers, are incorporated in the models to simulate real life conditions as closely as possible. In an experimental investigation, a simply supported timber composite beam is dynamically tested and analysed. To create different degrees of composite action, the composite beam structure is tested with different numbers of shear connectors to simulate the failure of connection screws. The results from the proposed methods are correlated against outcomes from traditional static-based method.

1.7 Layout of the Thesis

This thesis is organised into nine chapters and their content is as follows:

Chapter 1: An introduction and background to the research topic, objectives of the study, significance of the work and contribution to knowledge, and vibration terminologies have been described in this chapter.

Chapter 2: This chapter provides a review of literature on the dynamic performance of flooring systems under dynamic actions induced by human activities and describes the

current vibration design methods. Further, it describes the modal parameters prediction methods and vibration problems remedial measures on the existing flooring systems. It also presents previous experimental testing methods and numerical investigations on the flooring systems. Finally, it covers a general review of damage detection methods and importance of various components of the TCC flooring systems and identified the gaps in current knowledge.

Chapter 3: This chapter presents the details of the experimental work which includes the details of the push-out tests conducted on TCC connections to characterize their properties, dynamic tests conducted on 6 m long TCC beams and the corresponding long-term dynamic tests as well. Results of these tests and concluding remarks are also presented in this chapter.

Chapter 4: This chapter presents the details of the experimental work such as dynamic test conducted on timber floor modules (timber beams) having 6 and 8 m spans. A summary of modal parameters to assess their dynamic performance is also presented.

Chapter 5: This chapter provides an overview of FE models development for the TCC and timber beams, which were studied experimentally in Chapters 3 and 4, respectively. The results from experiment and FE models are correlated. These FE models of the beams are calibrated and validated with dynamic and static test results.

Chapter 6: This chapter covers a summary of dynamic tests performed on a 3.5 m span timber beam to investigate degree of composite action of the composite systems using recent damage detection methods. Results from this test are also discussed. It also provides an overview of FE models development for the beam. The results from experiments are used in the calibration and validation of the FE models.

Chapter 7: Available analytical models to predict natural frequencies of the beams and flooring systems are summarized in this chapter. Further, natural frequencies of the tested TCC and timber beams presented in Chapters 3 and 4 are predicted using these analytical models and correlated with experimental results.

Chapter 8: This chapter presents parametric analyses performed on FE models of the TCC beams and timber beams described in Chapters 3 and 4, respectively. The FE

models were extended to longer spans and at the same time cross-sectional dimension of the beam models were changed.

Chapter 9: The main contributions of this research and recommendations for future research are highlighted in this chapter.

References to literature referred in this study and appendices are presented at the end of this dissertation.

University of Technology, Sydney

CHAPTER 2

LITERATURE REVIEW

2 Literature Review

2.1 Introduction

This chapter provides an overview of dynamic loads and their effect on structures, particularly on flooring structures, followed by vibration serviceability criteria, and vibration design criteria of the flooring systems. Then a review of predicting the modal parameters such as natural frequency and damping ratio is also summarised. The available vibration remedial measures of the existing flooring systems are subsequently reviewed. A number of available non-destructive dynamic test methods that have been used to excite the floors for determining their dynamic characteristics are then presented and is followed by finite element simulation of the flooring systems. Further, a summary of different components of the TCC flooring systems and their influence on the dynamic performance of the systems is presented. Evaluation of the efficiency of the composite flooring system and some recent damage detection techniques are included in the last part of the literature review. This chapter is ended with identifying the gaps in the present state of knowledge and contributions to the current research.

2.2 Type of Dynamic Loads on Structures

Structures are subjected to a number of dynamic loads throughout their life span. Dynamic loads may cause catastrophic structural failure when the effect of dynamic loads is not taken into design consideration. Failure of Tacoma Narrows Bridge in 1940 and just in four months after its completion is a well-known disaster due to a windstorm in 1940. In addition, collapses of the World Trade Centre in 2001, wobbling of the Millennium Footbridge in London and Tsunami wave attack in Japan in 2011 are a few examples of recent and well-known incidents involving dynamic loads (Dallard et al. 2001a; Dallard et al. 2001b). The main sources and origins of the dynamic loads can be categorized as earthquake, wind, traffic, explosion, machinery and human.

Earthquake and wind are the naturally occurring dynamic loads on structures. An earthquake is the result of sudden release of energy in the outermost layer of the earth that generates seismic waves and the waves are propagated through the surface material of the earth causing the structure to vibrate. Tsunamis are the consequence of tectonic

earthquakes that are associated with the earth's crustal deformation; when occurring beneath the sea. Wind is the most common natural source of dynamic load and needs to be considered in the design of bridges and tall structures.

Moving traffic generates oscillations on structures such as bridges and parking floors. The generated waves propagate to the surrounding buildings through the earth surface causing them to vibrate (Hunadidi 2000). An explosion or bomb releases an extremely sudden and violent energy causing catastrophic damage and vibrates the structures through both ground and atmosphere transmitted mechanical stresses. Installed machinery and human activities are considered to be the two most important sources of excitation in timber-framed residential floors and cause a number of serviceability issues on the long-span and light-weight floors (Eurocode 5 2008). Footbridges, shopping malls, concert halls, dance halls, gymnasiums and sport halls are vulnerable to the vibration induced by human activity. It is desirable to consider dynamic vibration criteria in conjunction with static deflection criteria in the design of floors.

Mathematically, the dynamic actions can be classified as harmonic, periodic, transient, and impulsive. Harmonic loads are represented by sine functions and are consequence of human walking and dancing, and rotating machinery. Periodic load is a load in which a portion of load defined over time repeats itself at regular intervals. The cause of periodic loads is rhythmic activities such as dancing and aerobics, periodically impacting parts and unbalanced masses. Transient loads do not show any periodical repetition in time and are caused by the movement of people such as walking and running, earthquakes and wind. Impulsive loads are forces that act for a very short duration. Impulsive loads are of great importance in the design of flooring systems as the systems everyday encounter the source of impact loads such as human activities and machinery operation. Damping has minimal influence in controlling the maximum response of a structure to impulsive load compared to harmonic and periodic loads as the maximum response reaches in a very short time. Single jumps, heel drop impacts and blast waves are examples of impulsive loads.

2.3 Serviceability Limit State

To satisfy the serviceability limit state criteria, a structure must remain functional for its intended use subject to everyday loading, and as such the structure must not cause

occupant discomfort under routine conditions. There are a number of serviceability criteria such as deflection, vibration, acoustic, fire, crack width etc. A structure is said to have satisfied the deflection limit state when the structural elements deflect less than certain limits specified in the design standards. The floors should satisfy vibration criteria and other possible requirements such as deflection, fire and acoustic as required by the applicable building codes. With the increasing trend on the use of long-span and light-weight floors, design of such floors may be governed by the serviceability limit states, especially vibration and deflection rather than ultimate strength limit state. Vibration criteria are briefly summarized in this section. The details of vibration design criteria are described in Section 2.4.

2.3.1 Vibration

Vibration of flooring systems is to and fro motion in the vertical direction caused by a number of dynamic forces such as human activities, operation of machines on the floor, and transmission of the vibration from adjoining floors and the ground through buildings columns (Allen & Pernica 1998).

The daily human activities such as walking, jumping, dancing or running on the floor may load to an uncomfortable feeling to the users when magnitudes of the vibration are uncontrolled. The main factors contributing to annoying levels of floor vibrations are reduced natural frequencies of the floors as a result of long-span and light-weight construction, an increase in the number of rhythmic human activities such as aerobics and decrease in damping due to usage of fewer non-structural components on the floors.

The primary cause of vibration issues and failure of the structures is resonance. If the frequency of the applied dynamic loads on the flooring systems is identical or close to the natural frequency of the systems, the resonance occurs and consequences are most severe. Vibration amplitude of the systems attains its peak when resonance occurs. Figure 2.1 shows the floor acceleration due to a cyclic force with a range of natural frequencies. The floor attains maximum acceleration when the ratio of natural and forcing frequency is one. The amplitude of the peak is dependent on the amount of damping in the structural system and the amplitude will be higher if the system has lower damping. For vibration to be acceptable, the natural frequency of the designed flooring systems must be higher than the forcing frequency (Allen & Pernica 1998).

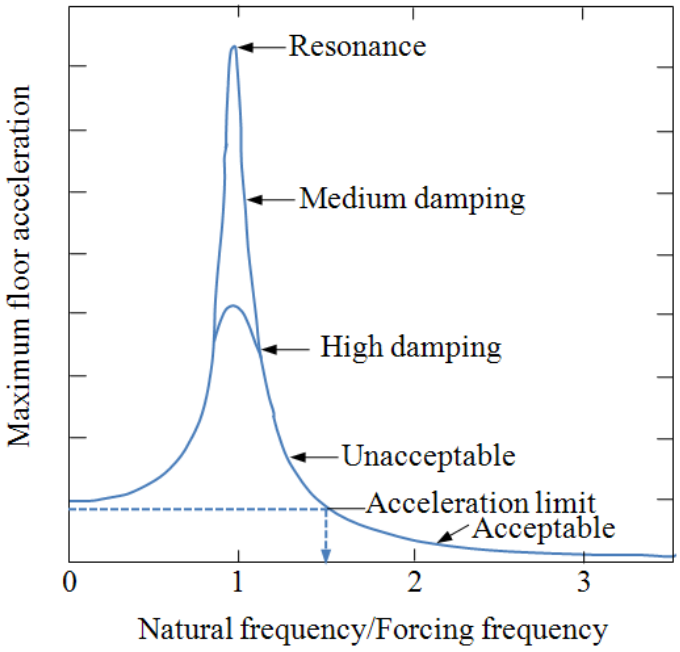

Figure 2.1 Floor acceleration due to a cyclic force (Allen & Pernica 1998).

2.4 Floor Vibration Design Criteria

The response of the people to floor vibrations depends upon the perception of the vibration, which varies from person to person and depends upon the activities they are involved in. Three design criteria pertaining to floor vibrations, namely, acceleration, natural frequency and unit point load deflection limit can be found in the design standards and literature to design the flooring systems so that the systems perform well under dynamic actions.

2.4.1 Acceleration Limit

Human perception plots were developed from the acceleration responses as main design tools against floor vibrations. Reiher & Meister (1931); Murray (1990); Allen & Murray (1993); Murray, Allen & Ungar (2003); and Allen & Pernica (1998) introduced acceleration limits for flooring systems and design charts for buildings.

Reiher & Meister (1931) developed a well-known criterion for acceleration limits based on the group of standing people's perception to steady state vibrations due to walking with variation of frequency from 1 to 100 Hz and displacement amplitude from 0.00254 to 2.54 mm as shown in Figure 2.2. The floor vibration is divided into six categories

based on the subjective perception and response of the people as (a) not perceptible (b) slightly perceptible (c) distinctly perceptible (d) strongly perceptible (e) disturbing and (f) very disturbing. From Figure 2.2 it can be concluded that larger displacements are acceptable if the frequency is lower. For example, 0.0508 mm displacement is not perceptible if the frequency is 1 Hz while the same displacement is distinctly perceptible if the frequency is 10 Hz.

However, Lenzen modified the Reiher-Meister scale based on his investigations on timber-concrete floor systems in 1960's (Figure 2.3). The modified Reiher-Meister scale was obtained from original scale by multiplying a factor of 10. The modified scale was applicable to lightly damped flooring systems with damping ratios below 5% (Naeim 1991). The floor vibration is categorised as (a) vibration, though present, is not perceived by the occupants (b) vibration is perceived but does not annoy (c) vibration annoys and disturbs and (d) vibration is so severe that it makes occupants ill**.** A flooring system, to be acceptable, must fall into the first two categories and the structural design needs a criterion to determine the suitability of a proposed flooring system (Murray 1990).

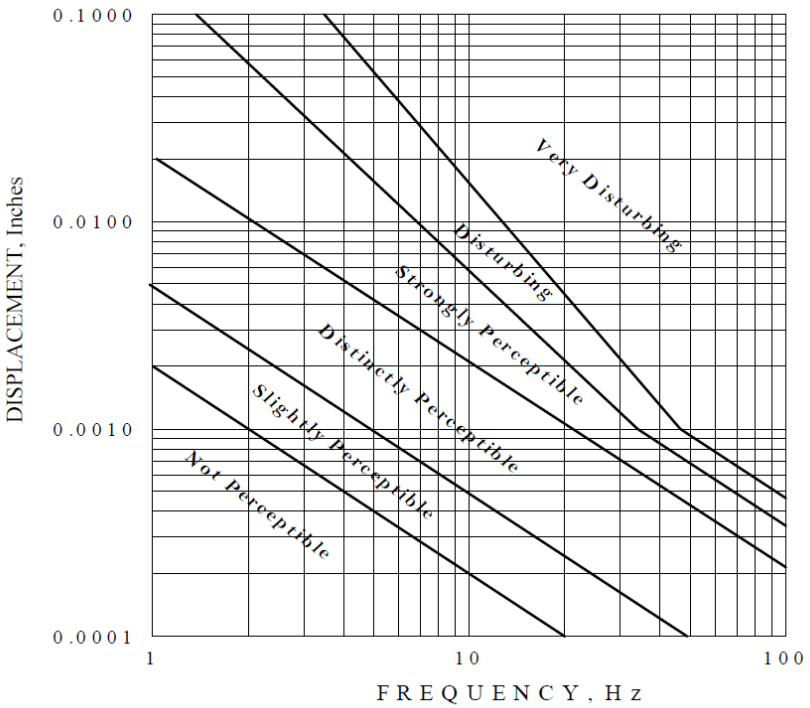

Figure 2.2 Reiher-Meister scale.

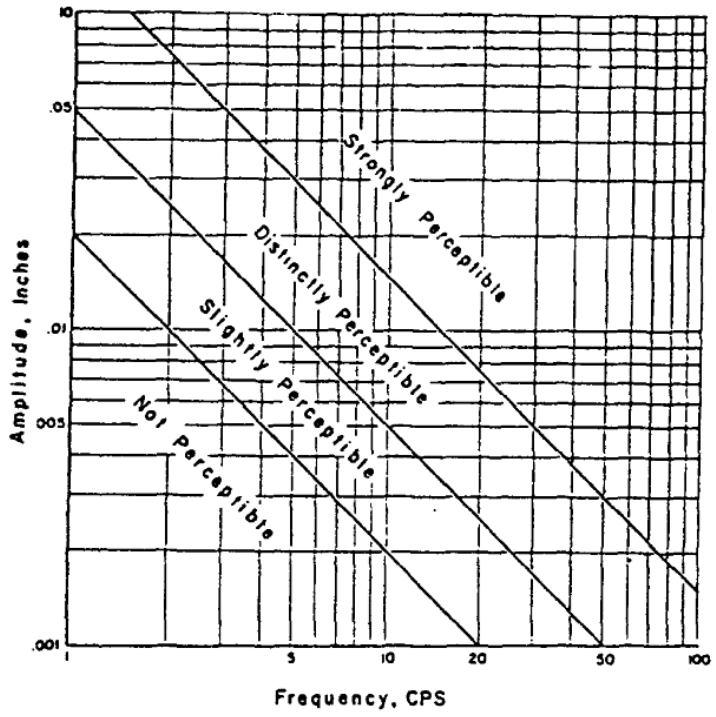

Figure 2.3 Modified Reiher-Meister scale (Naeim 1991).

The modified scale does not consider damping explicitly and, therefore, this scale is frequently used with another additional method to pass judgement on perceptibility as a design criterion. Murray (1981) presented an inequality based on the results of 90 in-situ tests of office and residential flooring systems under normal human activities to address the limitation of the modified scale as expressed in Equation (2.1). The inequality criterion presented is to be used along with the modified scale to address the presence of damping. The motion of the flooring system due to human activities will not be objectionable to the occupants if the condition given in Equation (2.1) is satisfied.

$$D > 35\, A_0 f_1 + 2.5 \tag{2.1}$$

where D is the percentage of damping, A_0 is the initial amplitude of the flooring system from heel drop test (inch) and f_1 is the fundamental frequency of the flooring system (Hz).

The required damping ratios, ξ, are presented in Section 2.6. The assessment also needs amplitude, A_0, which can be obtained from experimental heel drop test on the floor. The fundamental frequency, f_1, can be estimated using the simplified analytical models, which are adequate, as described in Section 2.5 or finite element model (FEM) for desired level of accuracy.

Allen & Murray (1993) proposed a criterion based on the dynamic response of the steel joist supported flooring systems such as for offices, residences, shopping malls and footbridges to walking excitation. The criterion was developed from the acceleration limits in terms of RMS acceleration recommended by ISO 2631-2 (1989) using multipliers for intended occupancy (see Figure 2.4). The multiplier to ISO 2631-2 (1989) acceleration limits for offices and residences was 10, for indoor footbridges and shopping malls was 30 and 100 was for outdoor footbridges (Murray, Allen & Ungar 1997).

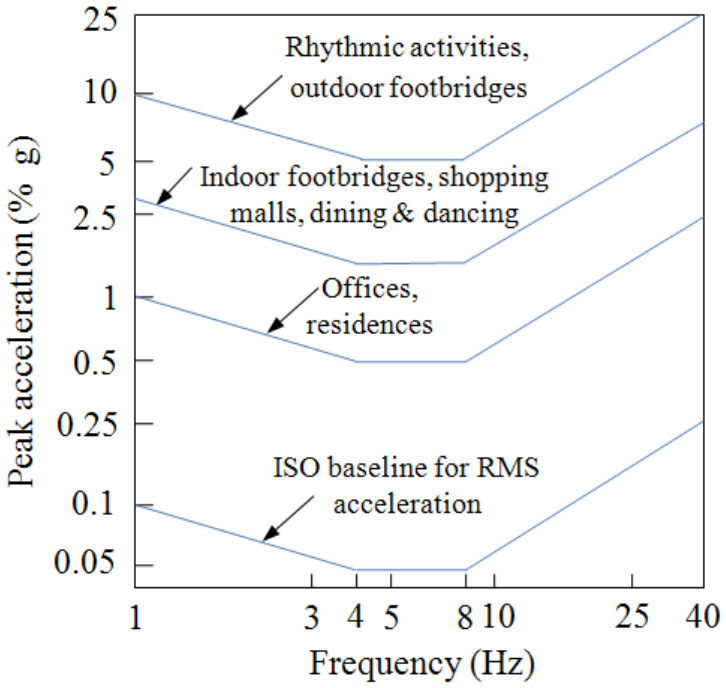

Figure 2.4 Acceleration limit for human comfort for vibrations caused by human activities (Allen & Murray 1993; ISO 2631-2 1989).

Murray, Allen & Ungar (2003) presented a new procedure in American Institute of Steel Construction (AISC) to evaluate floor vibrations due to human activity such as walking excitation. The criterion is satisfied if

$$\frac{a_p}{g} = \frac{P_o e^{-0.35 f_1}}{\xi W} < \frac{a_o}{g} \tag{2.2}$$

where a_p/g is the predicted accelaration ratio due to walking excitation, P_o is a constant excitation force, f_1 is the fundamental natural frequency, ξ is the damping ratio, W is the effective weight of the floor and a_o/g is the acceleration limit.

Recommended values of P_o, ξ and a_o/g are given in Table 2.1. The damping ratio for office, residence and church floors with few non-structural components is 0.02 (which can occur in open work areas and churches), with only small demountable partitions is 0.03 and with full height partitions up to the ceiling is 0.05.

Table 2.1 Recommended values of parameters (P_o, ξ and a_o/g)

	P_o (kN)	ξ	a_o/g x 100 (%)
Offices, Residences, Churches	0.29	0.02 - 0.05	0.5
Shopping Malls	0.29	0.02	1.5
Indoor Footbridges	0.41	0.01	1.5
Outdoor Footbridges	0.41	0.01	5.0

Rhythmic activities are also a cause of increasing vibration issues in the building as cyclic floor accelerations of about 0.5g result in fatigue problems in the structure. NBC (1990) stated that vibration issues of the floors with fundamental frequency below 5 Hz are caused by resonance due to human activities. The flooring systems having fundamental frequency up to 10 Hz can also have vibration problems due to resonance caused by repetitive human activities such as dancing. The following acceleration limits were introduced in NBC (1990) to resolve fatigue problems in the structures due to rhythmic activities (Murray, Allen & Ungar 2003).

Table 2.2 Acceleration limits

Occupancies affected by the vibration	Acceleration limit (% g)
Office or residential	0.4 - 0.7
Dining or weightlifting	1.5 - 2.5
Rhythmic activity only	4.0 - 7.0

2.4.2 Natural Frequency Limit

The serviceability design of flooring systems requires an assessment of the first natural frequency in order to check the vibration behaviour of the floor and occupant comfort. Hanes (1970) reported that the designer must be aware of very low first natural frequency (below 3 Hz) of the systems to avoid walking resonance. Further, he

mentioned that the natural frequency of human internal organs is in the 5-8 Hz and this range was established based on automobile and aircraft passenger comfort studies. Murray (1991) investigated more than 100 problematic floors and the frequency of most of these floors was between 5-8 Hz. Hence, the following frequency ranges must be avoided:

- Frequency below about 3 Hz to prevent walking resonance.
- Frequency range of 5-8 Hz to prevent human discomfort.

For residential/office floors, a natural frequency greater than 10 Hz shall be targeted (Hanes 1970). A special investigation is needed if the predicted fundamental frequency of the floors is less than 8 Hz (Eurocode 5 2008). A stringent fundamental frequency limit for both occupied and unoccupied wood-light-weight floors are given by Dolan et al. (1999). The minimum frequency limit for unoccupied floors is 15 Hz while for occupied floors is 14 Hz. Smith & Chui (1988) have recommended that the fundamental frequency of the floors should exceed 8 Hz to avoid human discomfort. From all of these, it can be concluded that frequency of the flooring systems above 10 Hz is sufficient.

Repeated forces applied on the floor by people during any human activities are known as step frequency and the resonance occurs when the step frequency coincides with the natural frequency of the structure. Furthermore, resonance can occur not only at the step frequency, but also at its multiples if the repeated force has an impact component. For example, an aerobics class jumping to a step frequency of 2.5 Hz will produce harmonic vibrations at multiples of step frequency, i.e. at 2.5 Hz (1^{st} harmonic), at 5 Hz (2^{nd} harmonic), at 7.5 Hz (3^{rd} harmonic) etc. The resonance problems are more likely to occur as a consequence of second and third harmonics since the natural frequency of the floors are usually more than 3 Hz and fall in the range of 4 to 8 Hz. However, lower the harmonic, the larger are the vibration produced. Minimum acceptable natural frequencies for different combinations of human activities and flooring systems are given in Table 2.3 (Allen & Pernica 1998). The resonance problem can also happen on the floors having fundamental frequencies greater than 8 Hz if the damping is low. Hence, it can be concluded that vibration causes discomfort to the occupants to a wide range of natural frequencies of the flooring systems. It is necessary to investigate the

vibration behaviour of the floors as vibration issues are increasing in recent times due to an increasing trend towards light-weight and longer span construction.

Table 2.3 Minimum floor natural frequencies (Hz)

Rhythmic activity	Steel/concrete floor	Light-frame floor
Dancing and dining	5	10
Aerobics	9	13

In the Eurocode 5 (2008), installed machinery and human activities are considered as the two most important sources of excitation in timber-framed residential floors. If the residential floors have a fundamental frequency below 8 Hz, a special investigation should be made. If the predicted fundamental frequency of the residential floors is above 8 Hz, the following Equations (2.3) and (2.4) should be satisfied:

$$w/F = a \ \ (\mathrm{mm/kN}) \tag{2.3}$$

where w is the maximum short-term deflection (mm) due to a static point load F (kN) applied at any point on the floor and a is the flexibility coefficient of the floor.

$$v \leq b^{(f_1\xi-1)} \ \ \mathrm{m/(Ns^2)} \tag{2.4}$$

where v ($\mathrm{m/Ns^2}$) is the unit impulse velocity response (m/s) due to an ideal unit impulse (1 Ns) applied at the point of the floor where it gives maximum response and its maximum limiting value is resulting from natural frequency up to 40 Hz and ξ is the damping ratio. The approximate value of v can be predicted by using Equation (2.5).

$$v = \frac{4(0.4 + 0.6\, n_{40})}{mbl + 200} \tag{2.5}$$

where n_{40} is the number of first-order modes with natural frequencies up to 40 Hz and its value can be calculated using Equation (2.6), m is the mass of the floor per unit area ($\mathrm{kg/m^2}$), b is the floor width (m) and l is the floor span (m).

$$n_{40} = \left\{\left(\left(\frac{40}{f_1}\right)^2 - 1\right)\left(\frac{b}{l}\right)^4 \frac{(EI)_l}{(EI)_b}\right\}^{0.25} \tag{2.6}$$

where $(EI)_b$ is the equivalent plate bending stiffness (Nm^2/m) of the floor about an axis parallel to the beams, where $(EI)_b < (EI)_l$.

The range of limiting values of *a* and *b* and their relationship is shown in Figure 2.5. If the value of flexibility coefficient, *a* (mm/kN) is below 2, the floor shows better performance, otherwise, it belongs to poorer performance category.

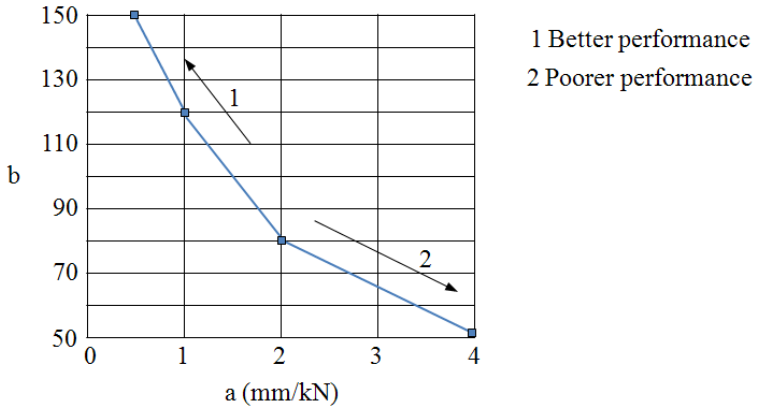

Figure 2.5 Relationship between *a* and *b* (Eurocode 5 2008).

2.4.3 Unit Load Deflection Limit

Allen & Pernica (1998) reported that the unit point load deflection criterion should be applied to the light-frame floors design when the vibration due to walking is an issue. The unit point load deflection criterion is shown in Figure 2.6. For floors with spans below 3 m, the limit for unit load deflection is ≤ 2 mm and the deflection limit for span ≥ 3 m decreases exponentially as shown Figure 2.6. The deflection of about 0.6 mm under the application of 1 kN point load is acceptable to all floor spans.

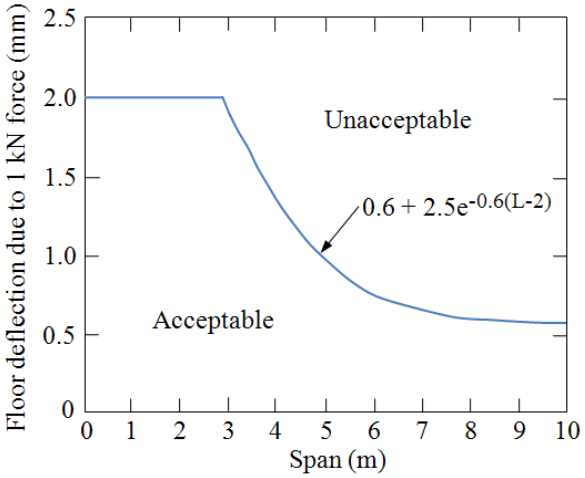

Figure 2.6 Design criterion for light-frame floors (Allen & Pernica 1998).

2.5 Natural Frequency

A structure vibrates at a certain frequency when it is applied some initial conditions such as displacement and velocity, and allows to vibrate freely. The number of oscillation cycles per second is called natural frequency. All structures have a number of natural frequencies and the lowest frequency, which is called the fundamental frequency, is the main concern of the designer. The natural frequency, especially fundamental frequency, is the most important parameter to assess dynamic performance of the flooring systems. It primarily depends on mass and stiffness of the systems. For a single degree of freedom (SDOF) system, the natural frequency can be estimated using Equation (2.7).

$$\omega_n = \sqrt{k/m} \tag{2.7}$$

where ω_n is the circular natural frequency (rad/sec), k is the stiffness of the system (N/m) and m is the mass (kg).

2.5.1 Simplest Natural Frequency Prediction Analytical Models

A number of methods are available to predict natural frequency of the flooring systems. The methods summarised in this thesis are Wyatt (1989); Allen (1990); Murray, Allen & Ungar (2003) and Eurocode 5 (2008). All prediction methods are essentially based on the fundamental frequency prediction relationship for a simple spring-mass system as given in Equation (2.8) and further expressed in terms of elastic deflection of the system due to its self-weight and imposed action Equation (2.9). The details of natural frequency prediction methods are presented in Chapter 7. The fundamental frequency of the tested TCC and timber beams are predicted using these methods. Further, the predicted values are correlated with test results to evaluate their reliability.

$$f_1 = 1/2\pi \sqrt{k/m} \tag{2.8}$$

where k is the stiffness of the system and m is the mass of the system.

$$f_1 = 1/2\pi \sqrt{g/\Delta} \tag{2.9}$$

where g is the acceleration due to gravity (9.81 m/s^2) and Δ is the elastic deflection of the system.

The natural frequency of the structure does not depend on the source of excitation, but damping in the system influences it slightly compared to that of an undamped system. The damped natural frequency, f_{damped}, of the systems for free vibration can be predicted using Equation (2.10). If the vibration is forced vibration, the effect of damping is dependent on the type of forcing function. For a harmonic excitation the damped natural frequency occurs below the undamped fundamental frequency and is calculated by using Equation (2.11). However, in the case of rotating mass type excitation the damped fundamental frequency occurs above the undamped fundamental frequency, f_{undamped} and its value can be calculated using Equation (2.12) (Soltis et al. 2002).

$$f_{damped} = f_{undamped}\sqrt{1-\xi^2} \tag{2.10}$$

$$f_{damped} = f_{undamped}\sqrt{1-2\xi^2} \tag{2.11}$$

$$f_{damped} = f_{undamped}\frac{1}{\sqrt{1-2\xi^2}} \tag{2.12}$$

2.6 Evaluation of Damping

2.6.1 Damping Coefficients

Vibration of the structure produces mechanical energy and to dissipate this energy damping is essential. Mechanical energy is dissipated in the form of thermal and sound energy. Damping is the governing parameter to control the transient response of the structural systems. When idealised as proportional damping, it depends on the mass and stiffness of the structural system. It is not only associated with the structural components of the systems but also mostly associated with non-structural components such as partitions, false floors, suspended ceilings, ducts, furniture, and standing objects such as occupancy on the floor (Saidi et al. 2006). The non-structural components provide higher damping on a light-weight floor compared to heavy floors (Kullaa & Talja 1999). Viscous damping also depends on the nature of the boundary conditions of the systems. The damping can be categorised into two groups as internal and external. The damping due to the material or contact areas inside the structures such as joints and

bearings is grouped as internal while damping due to external non-structural components is grouped as external damping (Mahrenholtz & Bachmann 1995).

The energy dissipated in a cycle of free and forced harmonic vibration is measured by damping coefficient, *c*. The damping ratio, denoted by ξ or *D*, is defined as the ratio of damping coefficient of the system to the critical damping, which inhibits oscillation completely. The damping ratio is a dimensionless measure of damping and the governing mathematical expression is given in Equation (2.13) (Chopra 2005).

$$\xi = {}^{c}/_{C_c} = {}^{c}/_{2m\omega} \tag{2.13}$$

where *Cc* (= 2*mω*) is the critical damping coefficient, *m* is the mass of the system and *ω* is the circular natural frequency (rad/sec).

In commercial environments such as shopping malls, the sources of excitation are human activities such as walking and running, which are almost continuous. In such situations the floor vibration is almost steady-state and damping is not as critical as for office/residential environments. In such cases, control of the stiffness of the structural system is the best solution rather than damping (Murray 1990).

Elnimeiri & Iyengar (1989) recommended a damping ratio of 3.0% and 4.5 - 6.0% for open floors and finished floors with partitions, respectively, based on his research. Maurenbrecher (1997) considered the effect of occupancy of the structures on the damping and suggested a damping ratio of 1% for footbridges, 2% for shopping malls and 2 - 5% for offices and residences. The presence of occupants on a flooring system could increase damping up to 10% (Brownjohn 2001). Moreover, dynamic tests conducted on a full-scale function hall showed that the harmonic resonance vibration was fully damped out by seated people. De Silva (2007b) has reported damping criteria for light-weight floors with a number of non-structural components in his literature review. The damping ratio of 2.0 - 2.5% was reported for an electronic office with few number of cabinets and with no full-height partitions while damping ratio for an open office with cubicles and without full-height partitions was 2.5 - 3.0%. The damping ratio for an office library with full-height bookcases was 2 - 4%.

2.6.2 Methods to Determine Damping Coefficients

The mass, stiffness and natural frequency of the floor can be estimated with higher accuracy than damping. For example, the measured damping of a floor was significantly lower than the generally assumed values, which verify the difficulty of damping estimation in Osborne & Ellis (1990). The determination of damping coefficient using generalized damping expression is not feasible as the basic energy-loss mechanism in real structures is not fully understood. Therefore, direct experimental methods are suggested to evaluate damping of structures (Clough & Penzien 1993). There are a number of factors that affect the accuracy of results obtained from prediction methods. One of the major factors is noisiness of the data (Haritos 1993). Nevertheless, there are a number of methods to estimate the damping ratio of the structural system using either time or frequency domain analysis as described in the following sub-sections.

2.6.2.1 Logarithmic Decrement Analysis

The damping ratio of flooring systems can be determined from free vibration time history response of the systems using Logarithmic Decrement Analysis (LDA). Figure 2.7 depicts a typical free vibration response of a system. LDA uses the amplitude of the peaks of the response such as y_1 and y_2, which are the amplitude of the peaks of the 1st and 2nd cycle, respectively, as shown in Figure 2.7. The damping ratio of the lightly damped systems can be estimated from amplitude of two peaks "m" cycles apart using Equation (2.14) (Saidi et al. 2006). LDA method is the simplest method and suited for better approximation of damping of SDOF systems. It can also be used for multi degree of freedom (MDOF) systems to determine damping of each mode, but the initial excitation should be in such a way that the decay of vibration takes place primarily in a single mode (De Silva 2007a). A special software package also can be used to filter the unwanted modes from the response of the systems.

$$\xi = \frac{1}{2m\pi} log_e \frac{y_n}{y_{n+m}} \tag{2.14}$$

where y_n is the amplitude of n^{th} cycle and y_{n+m} is the amplitude of the $(n + m)^{th}$ cycle of vibration. For any two successive positive peaks consideration, $m = 1$.

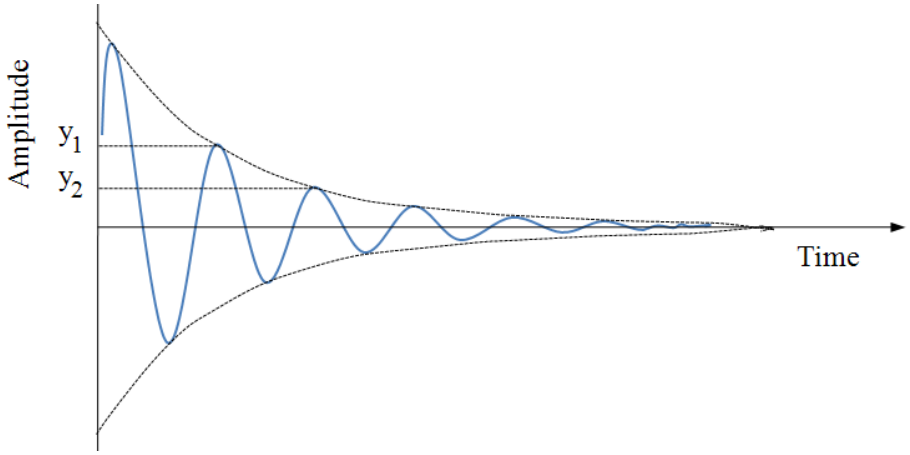

Figure 2.7 A typical free vibration response (Saidi et al. 2006).

2.6.2.2 Half-power Bandwidth Method

Half-power Bandwidth Method (HBM) is a commonly used method to estimate damping level of the systems without knowing the applied force. HBM uses a measured frequency response curve obtained from forced vibration tests and deformation response factor, R_d, is an important property of the curve. The half-power bandwidth of the curve is defined in Figure 2.8. The maximum amplitude divided by square root of two is called "half power point". The points "*a*" and "*b*", as depicted in Figure 2.8, are the first and second half power points of the bandwidth, respectively. The width of the plot between points "*a*" and "*b*" is 2ξ and the damping ratio can be estimated using Equation (2.15) (Chopra 2005).

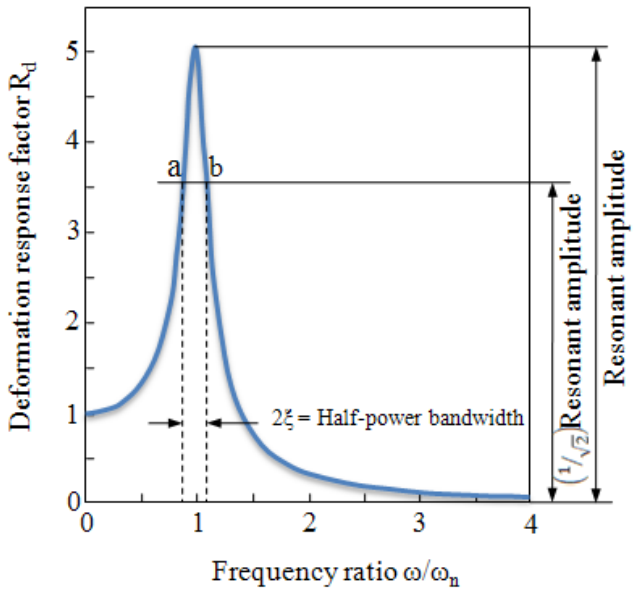

Figure 2.8 Half-power bandwidth (Chopra 2005).

$$\xi_n = \frac{f_b - f_a}{2f_n} \tag{2.15}$$

where f_n is the n^{th} natural frequency, f_a and f_b are the natural frequencies corresponding to the first, *a*, and second point, *b*, of the half-power bandwidth, respectively.

HBM can be used for both SDOF and MDOF systems having low damping, but gives better results for SDOF systems (Olmos & Roesset 2010). For MDOF systems HBM assumes that each peak in the frequency response function is dominated by the mode under consideration, but it is challenging for the closely spaced modes having close natural frequencies, as that might lead to mode coupling. The degree of mode coupling in the systems depends on its damping distribution, geometric characteristics and type of excitation (Papagiannopoulos & Hatzigeorgiou 2011).

2.6.2.3 Equivalent Area Method

Equivalent area method is an optimised method investigated by Haritos (1993) to obtain the damping level of the systems using Equation (2.16). Basically this method uses the area under the measured frequency response function trace. The principal advantage of this method is that the influence of noisiness is minimised as the integration is a form of smoothing operation. This method gives fairly accurate results for systems having damping levels below 8%.

$$A = \int_0^\infty \chi_m^2(f)df = \frac{\pi f_n}{4\xi}\frac{1-2\xi}{\sqrt{1-\xi^2}} \approx \frac{\pi f_n(1-2\xi)}{4\xi} \approx \frac{\pi f_n}{4\xi} \tag{2.16}$$

where A is the area under $\chi_m^2(f)$, $\chi_m(f)$ is the structure magnification function, f_n is the natural frequency. For light damped SDOF systems the area, A, is dominated by the area, A_r, associated with the resonance bandwidth ($f_n/\sqrt{2} < f < \sqrt{2}f_n$) and approximate damping value can be evaluated using Equation (2.17). The area, A_r, can be determined using standard numerical integration such as Simpson's rule, but Haritos (1993) used a Monte Carlo style simulation to identify the statistical characteristics of predicted damping levels of a SDOF.

$$A_r = \int_{f_n/\sqrt{2}}^{\sqrt{2}f_n} \chi_m^2(f)df \approx \frac{\pi f_n}{4\xi}\frac{1-2\xi}{\sqrt{1-\xi^2}} \tag{2.17}$$

2.6.2.4 Resonant Amplification Method

The damping ratio of the systems can be determined from a frequency-response curve using resonant amplification method. Figure 2.9 depicts a typical frequency-response curve for a medium damped system. The curve can be obtained by plotting the steady-state amplitudes of relative-displacement response caused by different harmonic loadings having amplitude of P_0 at discrete values of forcing frequency, $\bar{\omega}$, over a wide range of natural frequency (Clough & Penzien 1993).

The actual dynamic magnification factor $D_{max} = {\rho_{max}}/{\rho_0}$ occurs at the forcing frequency, $\bar{\omega} = \omega\sqrt{1-2\xi^2}$ and is given by $D_{max} = 1/2\xi\sqrt{1-\xi^2}$; however, the approximate value of damping can be determined using Equation (2.18). The damping ratio can be determined from the experimental data using Equation (2.19).

$$D_{max} = D(\beta = 1) = 1/2\xi \tag{2.18}$$

$$\xi = \rho_0/2\rho_{max} \tag{2.19}$$

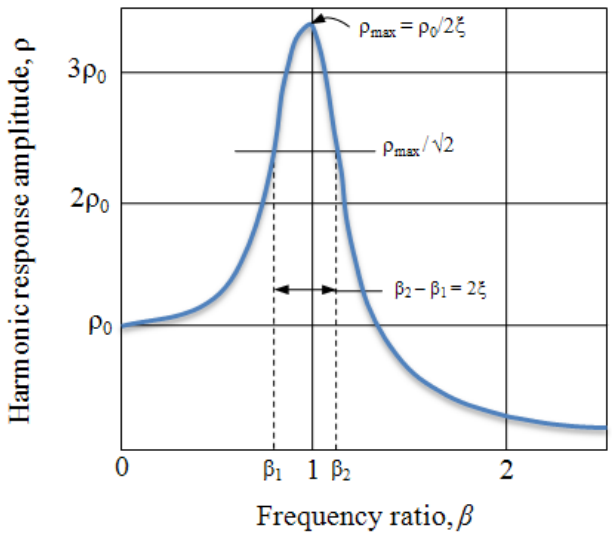

Figure 2.9 A typical frequency-response curve (Clough & Penzien 1993).

2.6.2.5 Random Decrement Technique

The random decrement (RanDec) technique was developed by Henry Cole to measure damping and identify the structural deterioration of aeroplane wings due to wind flutter excitation in the late 1960s. The RanDec technique is a fast-converging method to

extract information from random data. The basic concept of this technique is that segments of the random vibration response of the structure subjected to random excitation are ensemble averaged to form a signature. The signature represents the free vibration decay curve of the structure. The random response of the structure comprises three components such as the response of the structure to an initial displacement and velocity, and a random input load. Averaging enough segments of the same response with the same initial conditions will eliminate the forced vibration component. The number of segments to be averaged depends on shape of the signal; normally 400 to 500 averages are enough to produce a repeatable signature. The damping ratio and natural frequency of the structure can be extracted from the free vibration decay trace. The basic concept of RanDec technique is shown in Figure 2.10 (Al-Sanad, Aggour & Yang 1983; Brincker, Krenk & Jensen 1991; Rodrigues & Brincker 2005).

Considering two response time histories x(t) and y(t), simultaneously measured, the auto $D_{xx}(\tau)$ and cross $D_{xy}(\tau)$ RanDec functions can be mathematically defined by Equations (2.20) and (2.21) (Rodrigues & Brincker 2005).

$$D_{xx}(\tau) = \frac{1}{N}\sum_{i=1}^{N} x(t_i + \tau)\Big|Tx(t_i) \tag{2.20}$$

$$D_{xy}(\tau) = \frac{1}{N}\sum_{i=1}^{N} y(t_i + \tau)\Big|Tx(t_i) \tag{2.21}$$

where N is the number of averaged time segment and $Tx(t_i)$ is the triggering condition applied to time history x(t).

To evaluate RanDec functions, it is possible to consider different triggering conditions $Tx(t_i)$. The most common triggering conditions considered in the RanDec technique are:

(a) Level crossing (illustrated in Figure 2.10);

$$Tx(t_i) = \{x(t_i) = a\} \tag{2.22}$$

(b) Positive points;

$$Tx(t_i) = \{a \leq x(t_i) < b\} \tag{2.23}$$

(c) Zero crossing with positive slope;

$$Tx(t_i) = \{ x(t_i) = 0, \dot{x}(t_i) > 0\} \tag{2.24}$$

(d) Local extremum.

$$Tx(t_i) = \{a \leq x(t_i) < b, \dot{x}(t_i) = 0\} \tag{2.25}$$

where $\dot{x}(t_i)$ is the velocity.

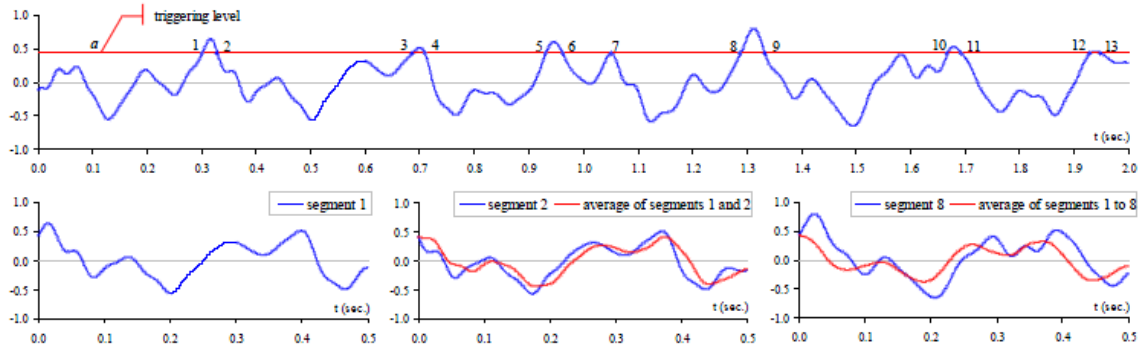

Figure 2.10 Basic concept of the RanDec technique (Rodrigues & Brincker 2005).

To obtain the free vibration curve, a triggering level and segment length need to be defined as shown in the above figure. One important aspect of the application of RanDec technique is the definition of the triggering level ($Tx(t_i)$) in Equations (2.20) and (2.21) and the length of time segments that are extracted from a time history. In general, it is advantageous to use a large number of triggering points. However, in order to eliminate the effect of noise, a large value of triggering levels a and b in Equations (2.22) and (2.23) should be specified as the lower values of triggering points in the time history might be more contaminated by the noise compared with larger values. Hence, a balance must be achieved between the large number of triggering points and having a high value of triggering level. A good option is to consider the positive points triggering condition with the levels a = σ_x and b = **∞,** where σ_x is the standard deviation of the response time history to be analysed. For level crossing triggering condition, the optimum triggering level is a = $\sqrt{2}\sigma_x$ (Rodrigues & Brincker 2005).

Length of the time segments, which are extracted from the response time histories, is another important aspect of the RanDec technique. For the time domain modal identification methods, the RanDec functions must have enough points to allow an over-determination of the equations from the system matrices to be estimated. For the frequency domain modal identification methods, the RanDec functions are evaluated with enough time length to have a complete decay within that length. In general, this

corresponds to a larger time length compared to the one required for the time domain methods (Rodrigues & Brincker 2005).

2.7 Remedial Measures to Floor Vibration Problems

There are a number of design guidelines that provide design criteria against vibration of flooring systems; nevertheless, existing floors can exhibit excessive vibrations causing human discomfort. Hence, it is essential to have a better understanding of the vibration response of the systems at design stage rather than spending huge amounts of money to retrofit the systems after construction. Murray, Allen & Ungar (2003) reported the following procedures and methodologies to minimize vibration problems of the existing floors.

2.7.1 Reduction of Effects

In some cases, use of very simple measures that reduce the annoyance associated with vibration can be sufficient to resolve vibration issues. These measures include removing or changing non-structural components configuration on the floor. The source of annoying vibration such as noise due to rattling can also be eliminated to minimize the vibration problems.

2.7.2 Relocation of Activities

The sources of vibration such as aerobics, machinery and sensitive occupants or equipment may be relocated to remedy the vibration problems. For example, aerobics exercise facility can be relocated from upper floor of a building to the ground or floors below. The sensitive people or equipment can be relocated to areas where vibration is less likely to occur. For example, vibration close to a column is less severe than towards the middle of the span.

2.7.3 Increasing Stiffness

Vibration caused by rhythmic activities and walking can be improved by increasing the stiffness of the structural system. Stiffening the flooring systems is enough to resolve vibration problems due to small dynamic loadings such as walking while whole building should be considered for severe dynamic loadings, like, rhythmic activities and heavy equipment. Adding new columns between existing columns supporting the

affected floor to the foundations are quite effective to increase the stiffness of the flexible floors. The stiffness of the members such as beams or joists of the light-frame flooring systems can be increased by welding or clamping additional members to the bottom flange of the members as shown in the following figure. For this technique sufficient ceiling space is required.

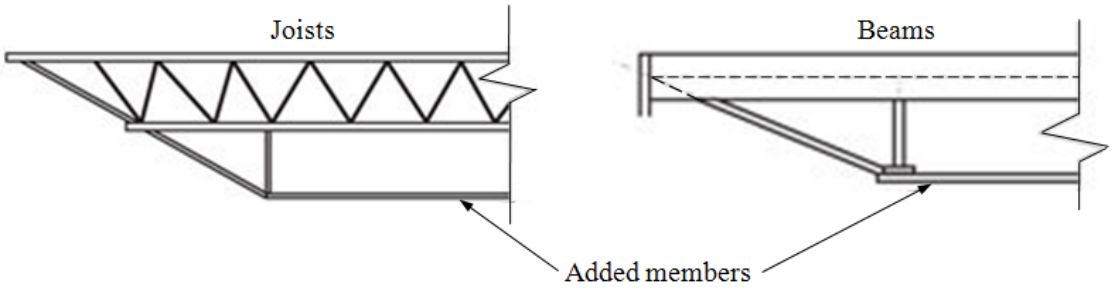

Figure 2.11 A stiffening technique for steel joists and beams (Allen & Pernica 1998).

2.7.4 Increasing Damping

Increasing the damping of the flooring system can be an option to improve the floor vibrations. The increment of damping will be more effective if the damping of the existing system is smaller. Damping of the systems can be increased by adding non-structural components such as dry wall partitions in the ceiling space that interact with the system. This method is effective for walking vibration of the system having low damping. The floor vibration can also be reduced effectively using damping devices such as tuned mass dampers.

2.7.5 Isolation

Isolation is an effective remedial measure to floor vibration due to machinery. The machinery can be placed on soft springs to isolate them from the floor and this technique reduces the transmission of vibration from the machinery to the floor.

2.8 Dynamic Tests on Floors

A number of dynamic tests can be conducted on flooring systems to assess their dynamic performance. In all tests, the floor is excited by some means and its response is measured. The modal parameters such as natural frequencies, damping ratios and mode shapes of the systems can be extracted from the dynamic response of the floors. The

performance of the floors can be accessed by evaluating their modal parameters. Several different testing procedures such as heel drop test, impact hammer test, forced vibration test or electro-dynamic shaker test, sand bag drop test, ambient test, walking test, burst random noise test and rotating mass type excitation, etc can be found in the literature. Only the first three most common non-destructive testing methods are discussed in the following sub-sections.

2.8.1 Heel Drop Test

Heel drop test is a well-known and well-calibrated test on floors as it is a very simple test that has been used for the last 30 years and is a part of several proposed design procedures (Blakeborough & Williams 2003). In this test, a person stands in the middle of the floor and rises on his toes and makes a sudden drop so that his heels strike the floor. Boice (2003) has defined the "standard heel drop" as the impact force exerted by the heels of a person with 77.3 kg weight on the floor after a drop of about 6.4 cm from a raised position as shown in Figure 2.12 (a). A heel drop of the humans creates a strong impulse on the light-weight floors and its idealised time history is depicted in Figure 2.12 (b). The maximum impact force induced by heel drop is 2,670 N and it dies out in 0.05 sec time duration. A typical heel drop time history is shown in Figure 2.12 (c) (Blakeborough & Williams 2003). The modal parameters can be calculated from the response of the floor caused by heel impact.

This test is easy to perform and does not require any expensive equipment compared to forced vibration test. The test also can be performed at a much quicker rate and the quality of frequency resolution is better than impact hammer test. It gives good resolution of natural frequencies of the floor in the range of 2-15 Hz and the range falls in the range of interest for floor vibration problems. The main limitation of the test is that it is an output-only test as only the response of the floor can be measured, but impact force is unknown and varies significantly from person to person and test to test. Output-only tests are not as good as modal tests such as impact hammer and forced vibration tests, in which both the exciting force and the floor response can be measured. Other tests such as instrumented impact hammers and forced vibration test or electro-dynamic shakers are often preferred due to this drawback of the test. Nevertheless, serviceability design evaluations of floor systems are based on this test.

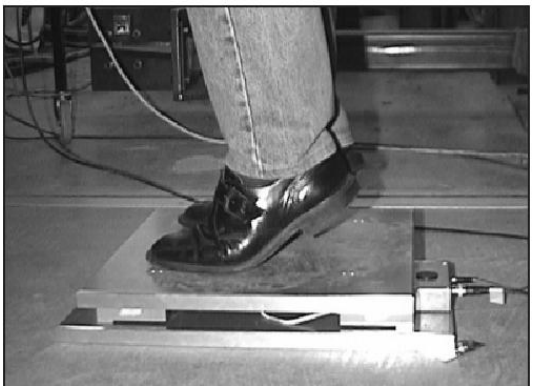

(a) Performing a heel drop test on the load cell

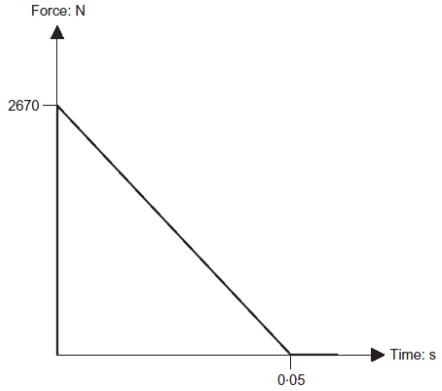

(b) Idealised heel drop time history

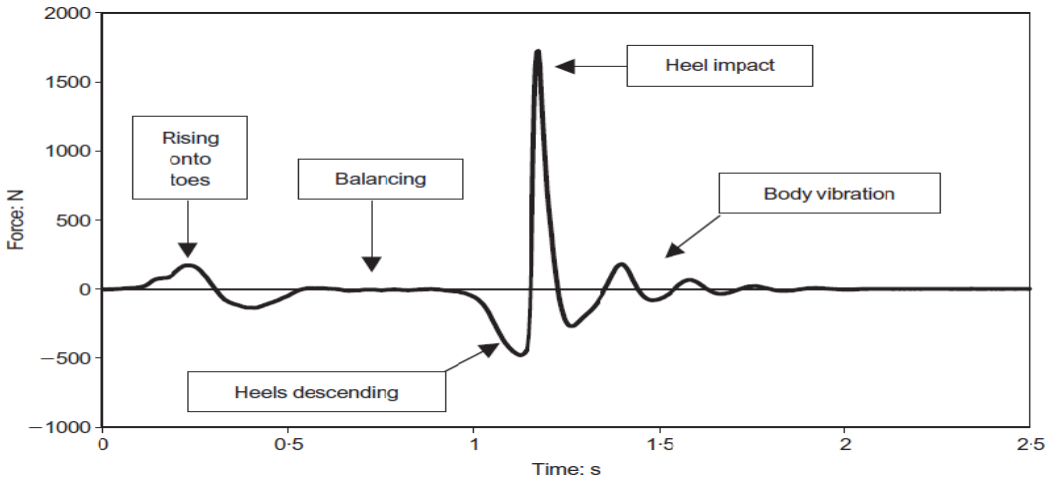

(c) Typical heel drop time history

Figure 2.12 Performance of heel drop test and heel drop time history (Blakeborough & Williams 2003).

2.8.2 Impact Hammer Test

Impact hammers are used in structural and modal analysis to assess dynamic performance of the flooring systems to impact force of varying amplitude and duration. This is the proposed test for the research project in this thesis. It has a force transducer in its head to measure exciting force, paired with an accelerometer on the system being tested to compare impact force and response of the system. A typical modal impact hammer is shown in Figure 2.13. The hammers are categorised in two groups as manually and remotely controlled hammers. The manually controlled hammer resembles an actual hand-held hammer and is used by manually striking the systems at appropriate locations while remote control hammers are either an automated piece of

machinery that the operator tells how much impact force to apply or else a hand-held power tool that is operated by actuating a switch.

The most critical parameters for impact hammers are the impact force and pulse duration as both parameters are rated with minimum and maximum values. The pulse duration is a measurement of the time of impact force applied on the systems, which is a very short span of time generally measured in milliseconds. The maximum frequency for which the response will be tested is also an important parameter. The frequency can be changed using different hammer tips with various materials and hardness allowing for different forces and response times (Figure 2.14). The figure depicts types of tip of a typical hammer with different colours. They are in the order of increasing hardness as black tip is the hardest tip. In general, harder tips have shorter pulse duration as they deform less than softer tips during impact and they are used to measure response at the higher frequencies. In addition, additional masses can be attached to the back of the hammer head to increase impact force beyond the force of the plain hammer. Different parameters such as hammer mass/tip, location and direction of hits, multiple hits "bounce", overload, and elastic range need to be considered in hammer tests (Ratcliffe 1998).

This test has number of advantages compared to other tests as it is cheaper and the test can be conducted during a shorter period of time. It also provides higher quality measurements of both the exciting force and the floor response. Furthermore, the excitation force can be applied at higher amplitudes to the floor than the forced-vibration test as the shaker in the forced-vibration test is limited by the force generated by the reaction mass moving at an acceleration of 1g (Howard 2005).

Figure 2.13 A typical impact hammer.

Figure 2.14 Types of hammer tip of a typical hammer.

2.8.3 Forced Vibration Test

Forced vibration test is the most comprehensive test used to measure the stiffness and mode shapes of the systems as it replicates the actual situations more accurately. Therefore, this test is used in vibration-proof tests for a wide range of applications in civil engineering and the automotive industry**.** The shaking system of the test requires a controller to provide both stability and a good replication of the given reference waveform. This system is based upon the principle that an electro-dynamic force is generated in proportion to an electric current applied to the coil existing in the magnetic field (Uchiyama, Mukai & Fujita 2009).

This test provides more consistent results than heel drop and hammer tests and the test can be used for a wide range of frequencies. However, the limitation on the operation of the shaker is that the acceleration has to be kept to less than 1g; otherwise the shaker will lift off the floor. The stroke of the moving mass has to be kept below 150 mm peak-to-peak, otherwise, it will strike the end stops. (Howard 2005).

2.9 Finite Element Modelling for Composite Flooring Systems

The finite element method (FEM) is a numerical modelling technique to determine the behaviour of real structures to external and internal loads by dividing it into several elements. It describes the response of each element and the behaviour of the whole system or structure can be obtained by reconnecting elements at nodes as if the nodes were the glue that holds elements together. It is one of the main computing tools for engineers due to its cheaper cost and time efficiency compared to the physical experiments. Some commercially available FE softwares are ANSYS, ABAQUS, SAP, LS-DYNA, ATENA, MICTROSTRAN, DIANA, ALGOR, and MFEAP.

Outputs from FE modelling are not necessarily 100% accurate, but can be obtained to a desired level of accuracy. The accuracy of the results from FE analyses depend upon the quality of the input data such as material properties: density, and elastic modulus just to mention a few. The FE model is considered accurate when it is updated based on experimental results. The updated model can be used for the parametric study and to demonstrate the performance of the test sample under the application of different types of action. Hence, a FE model needs to be calibrated against limited experiments to confirm whether results from it are acceptable.

FE modelling software ANSYS was adopted for the research project in this thesis to obtain relevant modal parameters to assess dynamic performance of the TCC and timber only flooring systems. In the literature, a number of FE models on timber only, TCC, steel-concrete composite (SCC) flooring systems and connections can be found, but there are very limited models on timber only and TCC flooring systems to acquire modal parameters to assess the systems.

Linden (1999) utilised FE model to study behaviour of TCC beams with different type of connectors and its configurations. Three elements, namely, shell, spring and beam elements were used to describe the concrete topping, mechanical connectors and timber joist of the beams as shown in Figure 2.15. Reinforcement was discarded in the model as it was used to prevent cracks due to shrinkage of the concrete and its contribution to the strength of the beam was assumed minimal.

Fragiacomo et al. (2004) developed a FE model to study collapse and long-term analysis of SCC beams as shown in Figure 2.16 and the model was calibrated against experimental results. They adopted the non-linear law proposed by Ollgard, Slutter & Fischer (1971) with unloading curve as shown in Figure 2.17 to model the head studs connector and an elastic-plastic with hardening law was assumed for the studs.

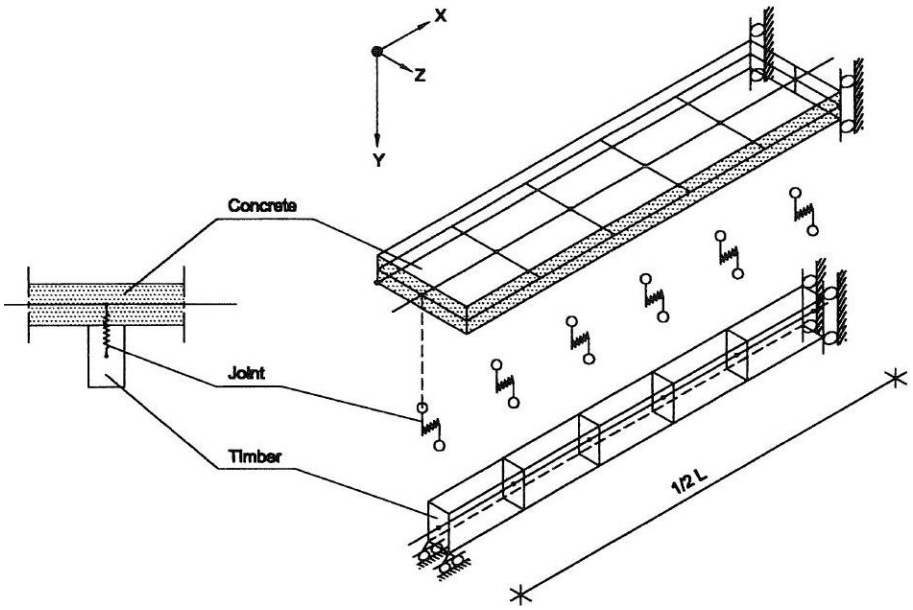

Figure 2.15 FEM model of a TCC beam (Linden 1999).

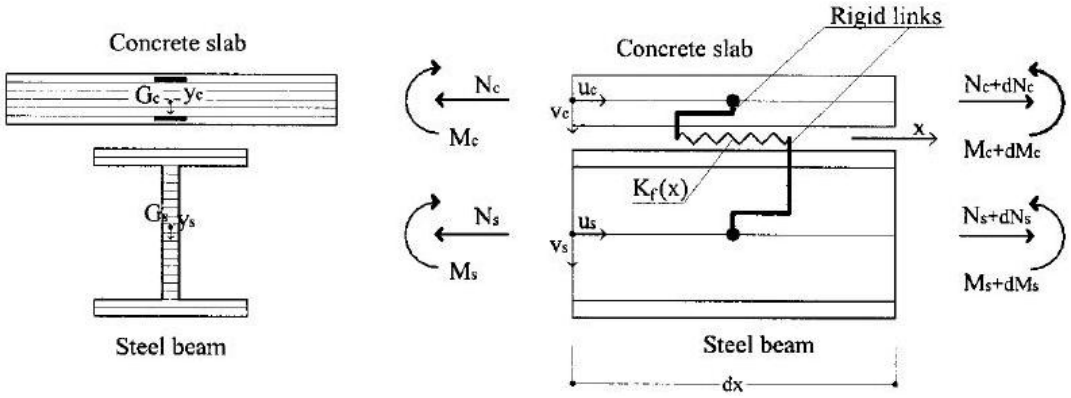

Figure 2.16 The finite element of the SCC beams (Fragiacomo et al. 2004).

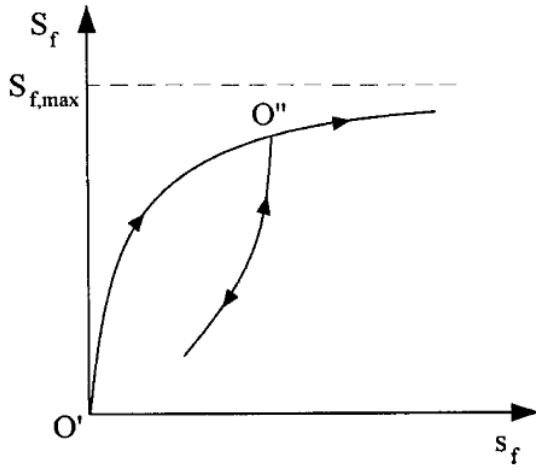

Figure 2.17 Shear force per unit length-slip law (Ollgard, Slutter & Fischer 1971).

Gerber, Crews & Sigrist (2005) created a FE model of a timber flooring system. Interface between timber deck and joists was modelled utilising an arbitrarily element and the connection system was assumed to be fully composite. The model was validated with the static tests and it was concluded that timber flooring system can be modelled quite precisely using FE modelling. Planinc et al. (2008) used a FE model by developing a new strain based FE to study non-linear analysis of composite timber beams with interlayer slips and the model was validated with experimental results. Four simply supported beams with different shear connector arrangements were tested under the application of static point load at mid span. The load-slip characteristic of the connector was used at timber interface to model the beam.

2.10 Components and Span of the TCC Flooring Systems

Concrete topping, timber joist and connection systems are three integral components of the TCC flooring systems. The connection systems are used to transfer shear forces from concrete topping to the timber joist. The thickness of the concrete topping, size and spacing of the timber joists, quality, spacing and the penetration depth of the connectors into timber joist, span of the flooring systems, all affect their performance. Hence, a number of parametric studies have already been done to optimize the system and a summary of each parameter is presented in the following sub-sections.

2.10.1 Concrete Topping Thickness

Thickness of concrete topping highly influences both the static and dynamic performance of the systems. Therefore, some researchers worked on overall depth of a TCC flooring system to optimise its performance in the past. The concrete is weak in tension while timber performs well in tension compared to concrete. Hence, to have the greatest advantages of both materials the section should be designed in such a way that the neutral axis lies at or near the interface between timber and concrete.

Gutkowski et al. (2007) remarked that the combined depth of wood and solid concrete of 150 mm is a reasonable depth for short span floors in office buildings. In their research 89 mm deep timber joist was combined with a 64 mm thick layer of concrete topping to produce about the same total floor depth. Steinberg, Selle & Faust (2003) constructed a TCC floor with a 50 mm thick concrete topping for testing. Brunner,

Romer & Schnuriger (2006) adopted three different thicknesses of concrete topping such as 80, 160 and 240 mm to manufacture the test specimens in order to determine the governing parameter influencing the displacement of the wet adhesive during the pouring of the wet concrete.

2.10.2 Joist Size and Spacing

A range of 300-600 mm joist spacing can be found in the literature to optimize the timber only and TCC flooring systems. Ahmadi & Saka (1993) fabricated five TCC floors using two different sizes of timber joists. First two identical floors were constructed using two timber joists having 75 x 100 mm cross-sectional dimension at spacing of 600 mm to investigate the influence of connectors in the composite action between timber and concrete while another three identical floors had 50 x 200 mm timber joists spaced at 300 mm apart to study efficiency of different types of connectors. They have stated that centre to centre spacing of joist of 300 mm is the current practice. Furthermore, they have concluded that the spacing between the timber joists can be increased using shear connectors between concrete topping and timber joists, and about 50% in the total number of joists in the flooring systems can be saved by utilising fully composite flooring systems using connectors. Therefore, the degree of composite action of the flooring systems is one of the parameters that influence the spacing of the joists. Soltis et al. (2002) tested three identical 6 m long flooring systems with different materials and degree of degradation to assess their dynamic performance. Each system had five pine joists (51 x 406 mm) spaced at 305 mm and the joists were laterally braced by cross bridging at 1.45 m distance along their span. In the Bernard (2004), a flooring system with fibre reinforced concrete on timber joists were constructed on solid LVL bearers. The system (2.4 x 4.8 m) was fabricated using five joists at spacing of 450 mm.

2.10.3 Shear Connector and its Types

A TCC flooring system where timber joists are connected with a concrete slab in order to achieve composite action is stronger and stiffer than a traditional timber floor. Shear connectors are required to transfer shear forces from the concrete slab to the timber joists and to provide composite action in the cross-section. In recent years, the optimisation of TCC systems is the main focus of the researchers all over the world.

Advantages of TCC systems cannot be achieved unless strong connection systems can be developed as the efficiency of the systems depends on the stiffness of the connection. Moreover, connectors ensure a ductile behaviour of the system under ultimate loading conditions. Hence, researchers are focusing on developing a range of shear connectors that allows a rigid connection between timber and concrete. A summary of the type of connectors that have been tested to improve performance of the systems is collated in the following sub-sections.

The load capacity and stiffness are the key parameters for the economic evaluation of the connectors. Connectors having higher stiffness reduce deflections due to increase in bending stiffness of TCC systems. In the literature, it is mentioned that spacing of the connectors should be set closer if the load capacity is not large enough to resist shear forces. The outcomes of push-out tests with connector E (see Figure 2.19) showed that vertical screws achieve only a low slip modulus, even with large diameters. Moreover, if the connectors are subjected to tension, they will perform more effectively (Steinberg, Selle & Faust 2003).

2.10.3.1 Mechanical Connector and its Spacing, and Penetration Depth

Mechanical linkage between hardened concrete and timber is provided through various sorts of mechanical connectors such as dowels, screws, nails and steel mesh inserted in the timber joist and concrete as appropriate. Stiffness, strength and cost of the connectors are the crucial parameters for their selection in the market. Screws installed at an angle of about 45° are very efficient, since the screws are loaded primarily in tension instead of shear. Early investigations in the field of TCCs revealed that slanted screws resulted in about twice the stiffness and load capacity compared to screws installed vertically (Küng 1987).

Ahmadi & Saka (1993) selected seven types, namely, types 3, 5, 6, 7, 8, 9 and 10 of shear connectors from the proposed ten different types as shown in Figure 2.18 to identify their shear strength and the selection was done based on their shear capacity, installation cost and corrosion resistivity investigated by the construction industry. Type 10 had maximum ultimate shear capacity among the nails. Three composite slabs were fabricated with different type of nails such as types 5, 9 and 10 to investigate the effect of nails on the performance of the slabs.

Steinberg, Selle & Faust (2003) tested various types of connectors as shown in Figure 2.19 for TCC flooring systems. From the push-out tests it was concluded that connector type A, B and D are more efficient.

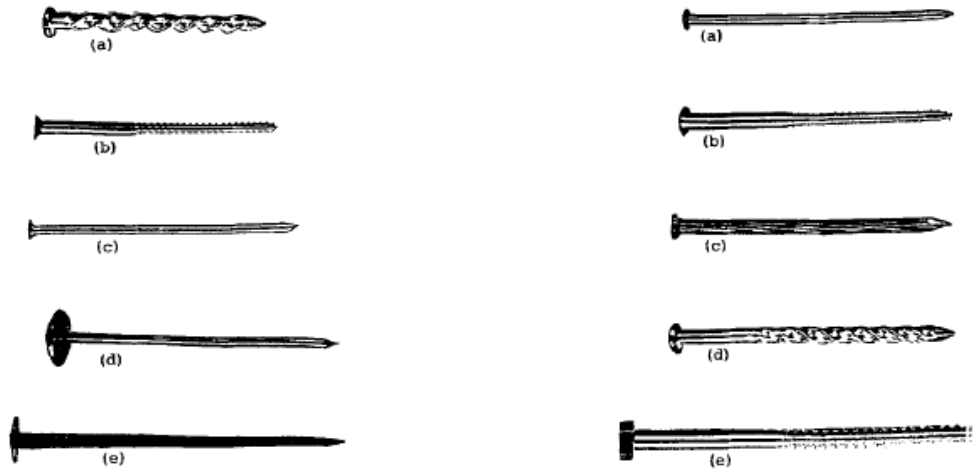

(a) Type 1, 75 mm asbestos nails;
(b) Type 2, 100 mm nickel screws;
(c) Type 3, 100 mm adler nails;
(d) Type 4, 100 mm umbrella nails;
(e) Type 5, 125 mm boat nails

(a) Type 6, 100 mm aluminium nails;
(b) Type 7, 100 mm brass screws;
(c) Type 8, 100 mm nissen nails;
(d) Type 9, 100 mm asbestos nails;
(e) Type 10, 150 mm bolts

Figure 2.18 Proposed 10 types of shear connectors in two groups (Ahmadi & Saka 1993).

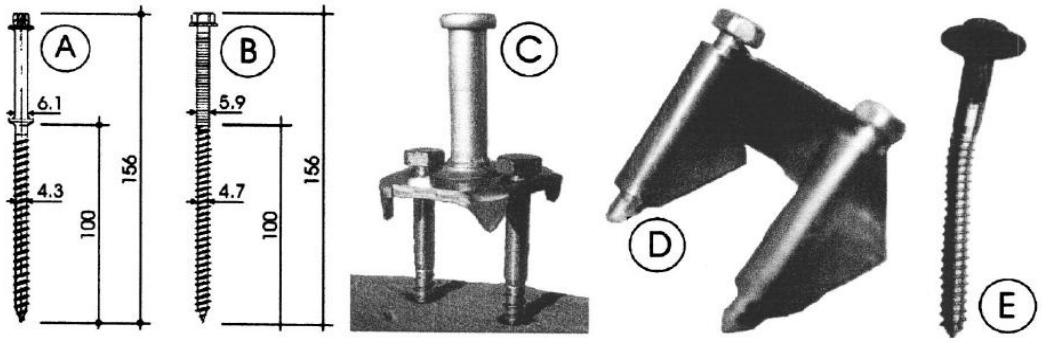

Figure 2.19 Different types of connector (mm).

Lukaszewska, Johnsson & Fragiacomo (2008) tested three different types of shear connectors to optimise the prefabricated TCC systems as shown in Figure 2.20. The connectors were embedded into prefabricated off-site concrete slab as shown in Figure 2.21 and connected to the timber joists on site. Push-out test was conducted on four small timber-concrete blocks and mechanical properties of the connectors such as stiffness (slip modulus), shear strength and ductility was identified. The outcomes of this study showed that fully prefabricated TCC is feasible.

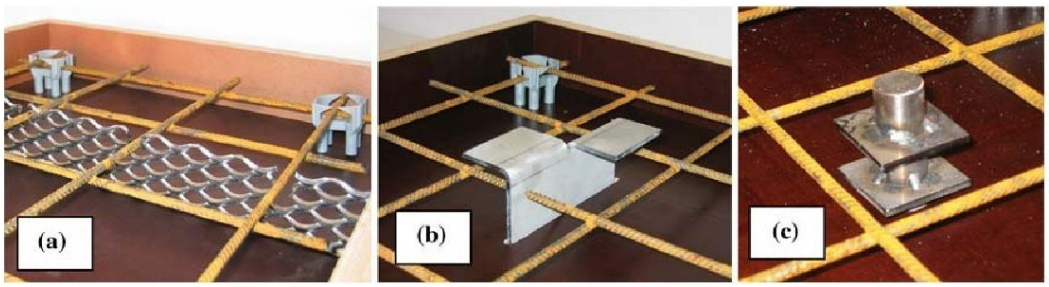

Figure 2.20 (a) Continuous steel mesh, (b) Folded steel plate, (c) Steel dowel with flanges (Lukaszewska, Johnsson & Fragiacomo 2008).

Figure 2.21 Prefabricated concrete slabs with inserted connectors: (a) Continuous steel mesh, (b) Folded steel plate, (c) Steel dowel with flanges (Lukaszewska, Johnsson & Fragiacomo 2008).

In this thesis three different type of connectors as shown in Figure 2.22 were used to fabricate TCC beams to investigate the effect of different type of connectors in both dynamic and static (short-term & long-term) performance of the beams. SFS screws and normal screws were inserted in the beams without any glue and notches while coach screws were combined with notch connection (Rijal, Samali & Crews 2010). Further details of these connectors can be found in Chapter 3.

Screw Type:	SFS screw	Coach Screw	Normal Screw
Diameter:	6 mm	16 mm	5 mm
Length:	22 cm	21 cm	10 cm

Figure 2.22 Different types of mechanical connectors.

A wide range of spacing of mechanical connectors have been used for testing in the past research to optimise the composite systems and implemented in real practice. The shear force at the interface determines the spacing of connectors and it might not be uniform throughout the span of the systems. For a beam subjected to uniformly distributed load, maximum internal shear force is developed near the supports and is reduced gradually toward mid span and become zero at the centre of the beam. Therefore, connectors are spaced closer near the supports than towards the centre. Commercially available connectors in Europe are set usually 100-500 mm apart from each other**.** Steinberg, Selle & Faust (2003) spaced shear connectors at spacing of 300 mm in their research and Bernard (2004) used nails at spacing of 150 mm. Ceccotti (2002) assumed an effective constant spacing, S_{eff}, to determine efficiency factor, γ of connection system and it was calculated using Equation (2.26).

$$s_{eff} = 0.75\, s_e + 0.25\, s_m \tag{2.26}$$

with $s_e < s_m < 4s_e$ where s_e is the spacing at the ends of the beam and s_m is the spacing in the middle.

Ahmadi & Saka (1993) adopted three different penetration depths of shear connectors such as 8d, 11d, and 15d, where *d* is the diameter of the connector, into the timber joist to find optimum depth of shear connectors so that sufficient strength could be achieved.

Test results showed no significant difference between the strength of the nails driven in the timber joists up to 11d and 15d. Hence, these experimental studies concluded that 11d is the required penetration depth to obtain sufficient strength.

2.10.3.2 Notch Connection

Notch connection is a common type of connection system in the TCC flooring systems. The indentations are carved on the timber joist and concrete is cast on its top. From literature, common shapes of indentations are rectangular, trapezoidal, and triangular or bird-mouth notch as shown in Figure 2.23. Normally, notch connection type is used in combination with mechanical connectors in the systems.

(a) Rectangular notch (b) Trapezoidal notch (c) Triangular notch

Figure 2.23 Common types of notch connection.

2.10.3.3 Glue Connection

A glued connection is also possible. The Swiss adhesive producer SIKA has developed a special adhesive connector such as masterseal compound, which is capable of bonding the concrete both wet and hardened (Brunner, Romer & Schnuriger 2006). Indeed, the use of an adhesive could distribute the shear forces uniformly over the entire surface and thus avoid the local force concentrations which are inevitable when mechanical connections are used. The adhesive connection is also quite slip-free, which helps to reduce the deflections. Figure 2.24 depicts glue connection between flange and web.

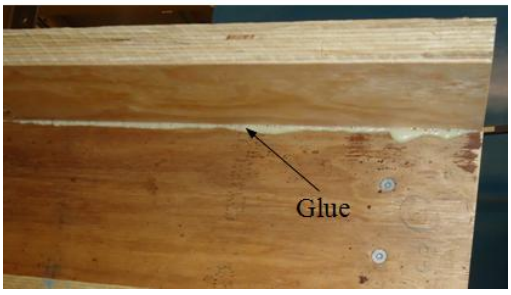

Figure 2.24 Glue connection.

2.10.3.4 Combined Connection

A notched connection with mechanical connectors such as coach screws has proven more effective. However, it is more time consuming and labour intensive compared to mechanical fasteners only connection systems and as a consequence it can be more expensive compared to them. A typical combination of different types of notch connection and mechanical connector such as coach screw is shown in Figure 2.25. Glue connection is also usually used with mechanical connectors, especially for timber-timber flooring systems. However, the load-slip behaviour of a glued and mechanical joint is different. Failure mode of glued connection can be brittle and may need to combine with mechanical connector to resolve fall-back issues and enhance plastic failure at joints. Connectors also help to set different components of the flooring systems in place after application of glue.

(a) Rectangular notch with coach screw (ABD. Ghafar 2008)

(b) Trapezoidal notch with coach screw

(c) Triangular or bird-mouth notch with coach screw

Figure 2.25 A typical combination of notch and mechanical connection.

2.10.4 Span

In recent years, trend demands are on long-span floors, but serviceability issues such as excessive deflection and vibration, has limited the span length. The floor vibrations depend on static stiffness, mass, natural frequency and damping of the systems (Hveem

1990). From the experimental results it was concluded that dynamic parameters such as natural frequencies and damping ratios reduce with increase in span length (ABD. Ghafar 2008). The economically competitive span limit to timber flooring construction using engineered wood products such as LVL and Glulam is likely to be around 8 or 9 m. Generally spans of around 6 m are the maximum used in practice with engineered wood products and other systems available at present (John et al. 2008). The improved stiffness and strength due to use of LVL instead of Glulam timber joist could allow TCC floors to span up to 12 m (ABD. Ghafar et al. 2008). Bathon & Cloustan (2004) performed bending tests on full scale semi-prestressed members with a maximum span of about 10 m. Their research proved that the system is well suited for long-span applications found in residential and commercial buildings. In recent times, new light-weight I-joists have been developed and are in common use. Floor construction with these joists may achieve a maximum span of 8 m if based on the *"maximum deflection of 0.9 mm at a point load of 1 kN placed over the middle of one joist"* criterion.

2.11 Efficiency of the Composite Flooring Systems

The transfer of the shear force across the concrete-timber interface is critical to the design of the system. Effective bending stiffness is highly dependent on the shear bond coefficient, γ of the interface. A shear bond coefficient of $\gamma = 0$ means the layers are acting totally independently and there is no force couple resisted by the composite section. A shear bond coefficient of $\gamma = 1$ represents a homogenous composite action with no slip in the interface. The shear bond coefficient for a given geometry and material properties is dependent on the stiffness of the connectors, the so-called slip modulus, and their spacing (Kuhlmann & Schänzlin 2007).The performance of the composite systems depends on the efficiency of connection systems. The efficiency of the composite systems can be determined using Equation (2.27) (Gutkowski et al. 2007).

$$\text{Efficiency, } E = (D_N - D_I)/ (D_N - D_C) \text{ x } 100 \qquad (2.27)$$

where D_C is the theoretical full composite deflection calculated using transformed section method, D_N is the theoretical fully non-composite deflection (no shear transfer between layers) and D_I is the measured deflection for partial composite action of the system.

2.12 Damage Detection

The damage detection (DD) can be defined as methods that capture the changes in structural characteristics caused by damage or degradation. DD methods can be categorised into two groups as global and local techniques. Many DD methods assess the structures (globally and locally) without causing any damage to their integrity and those methods are categorised as non-destructive inspection (NDI). Modal based DD methods are non-destructive methods and they are utilised in this study to detect presence of damage, geometric location of the damage, and the severity of the damage on the connection system of the TCC flooring systems. These methods identify the damage using changes in modal parameters such as natural frequency, modal damping, and mode shape as a consequence of changes in the physical parameters, namely, mass, damping and stiffness of the systems. Damage generally decreases mass and stiffness, but increases damping ratio. Dynamic approaches have been used to detect damage in structures extensively (Choi 2007). Modal strain-based damage detection methods are summarised in Chapter 6.

2.13 Summary and Contribution to the Current Research

The findings from previous work on vibration of flooring systems were quite useful to understand the fundamentals of dynamic assessment of the flooring systems and many innovative ideas were stimulated for the current research from the review, particularly in long-span timber only and TCC flooring systems. In the literature, limited works have been done on the long spanning flooring systems to assess their dynamic performance based on the dynamic parameters (natural frequency, damping ratio and mode shape). A number of analytical natural frequency prediction methods have been found in the literature and standards, nevertheless, very limited literature have determined the reliability of those methods in simply supported timber and TCC flooring systems. Further, there is no dynamic-based method to evaluate efficiency (degree of composite action) of the composite flooring systems. Dynamic approaches have not been applied to the TCC flooring system to detect damage of the connection system. Hence, it is necessary to extend the current knowledge on vibration of flooring systems.

University of Technology, Sydney

CHAPTER 3

DYNAMIC PERFORMANCE OF TCC FLOORING SYSTEMS

3 Dynamic Performance of TCC Flooring Systems

3.1 Push-out Test of TCC Connections - Test Setup and Testing

The design of TCC flooring systems requires an identification of shear connection properties such as strength, serviceability stiffness and ultimate stiffness. These properties are essential input to the "Gamma coefficients" method, which is presented in Eurocode 5 (2008), in order to predict the cross-sectional characteristics of the TCC systems. The method is adopted in Australia and New Zealand to design the flooring systems. A number of experimental tests were carried out to identify strength and serviceability characteristics of different types of connection systems for TCC systems.

This section presents an overview of tests conducted on four types of connections systems and three of them were adopted in TCC beams (Refer to Section 3.3), and their characteristics properties (5^{th} percentile for strength and average for stiffness). The results of these tests are presented in Section 3.2.

3.1.1 Test Specimens

Four types of shear connectors for TCC floors using small scale specimens were tested. Tested connections included two types of mechanical fasteners (normal and SFS screw) and two types of notched connectors (bird-mouth and trapezoidal shape) with coach screw. Refer to Section 3.4 for mechanical fasteners details. Summary of the test series is presented in Table 3.1. For normal screw type connection, four different series of asymmetrical specimens such as NS, 4NS50, 4NS100 and 4NS150 were tested and a series of specimens such as SFS were tested for SFS screw type connection. Typical geometry and components of the four normal screw series specimens are shown in Figures 3.1 to 3.4. The details of SFS series specimens are shown in Figure 3.5 and "Screw 1" in these specimens will be in tension while "Screw 2" will be in compression during loading in push-out test. For bird-mouth (BM) notched connection, five series of specimens, namely, B1, B2, B3, B4 and B5 were tested. The trapezoidal notched connection also had five series of specimens, namely, T1, T2, T3, T4 and T5. Figure 3.6

depicts typical geometric details of BM notched connection series specimens. The details of BM and trapezoidal notch are shown in Figures 3.7 and 3.8, respectively.

The tested specimens had LVL joist and a concrete layer, which was cast in-situ on top of the joist using a plywood formwork. The plywood formwork was removed from SFS and normal screw series specimens before testing them, but the notched connection series specimens were tested without removing the plywood formwork. The thickness of concrete was 65 mm for all connections. Diameters of the coach screw used in notched connection series specimens were 12 and 16 mm, and had a length of 200 mm. A gap of 15 mm was maintained between the concrete top and the coach screw head in notched connection series specimens. The widths of LVL joist used were 48, 63, 96 and 126 mm for the BM and Trapezoidal notch series specimens.

Table 3.1 A summary of NS and SFS series connections*

Type	Series	LVL joist width (mm)	Screw diameter (mm)	No. of specimens
Normal screw (NS)	NS	48	5	10
	4NS50	48	5	3
	4NS100	48	5	3
	4NS150	48	5	3
SFS screw	SFS	48	6	10
Bird-mouth (BM) notch with coach screw	B1	48	16	10
	B2	48	12	10
	B3	63	16	10
	B4	96	12	10
	B5	126	16	10
Trapezoidal notch with coach screw	T1	48	16	10
	T2	48	12	10
	T3	63	16	10
	T4	96	12	10
	T5	126	16	10

** Jointly conducted as part of a parallel PhD program undertaken by Ms Zhinus Zabihi, Mr. Nima Khorsandnia and Farzad Moshiri*

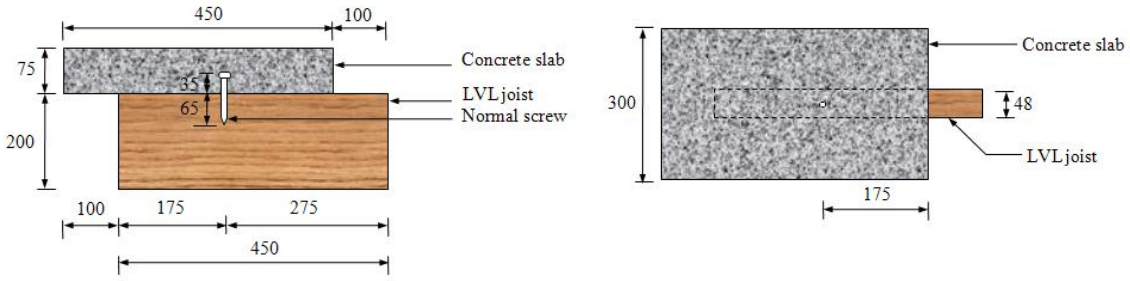

(a) Cross-section (b) Plan

Figure 3.1 A typical geometry and components of NS connection (mm).

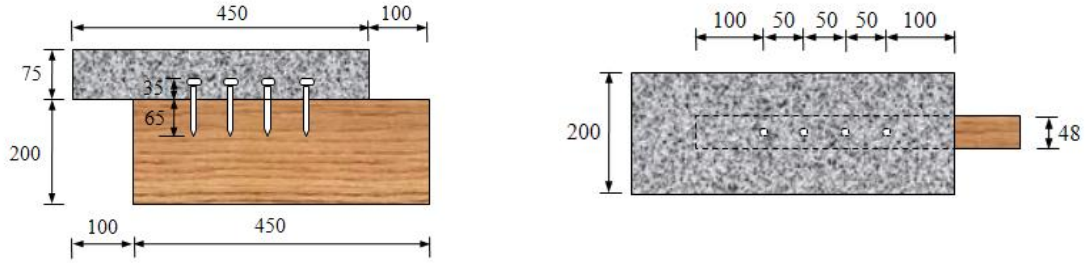

(a) Cross-section (b) Plan

Figure 3.2 A typical geometry and components of 4-NS50 connection (mm).

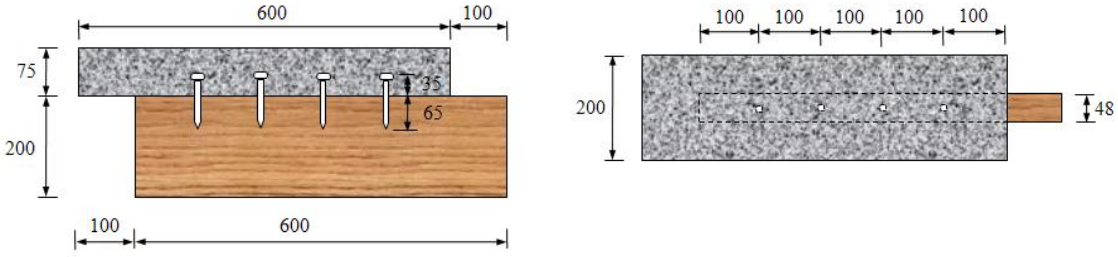

(a) Cross-section (b) Plan

Figure 3.3 A typical geometry and components of 4-NS100 connection (mm).

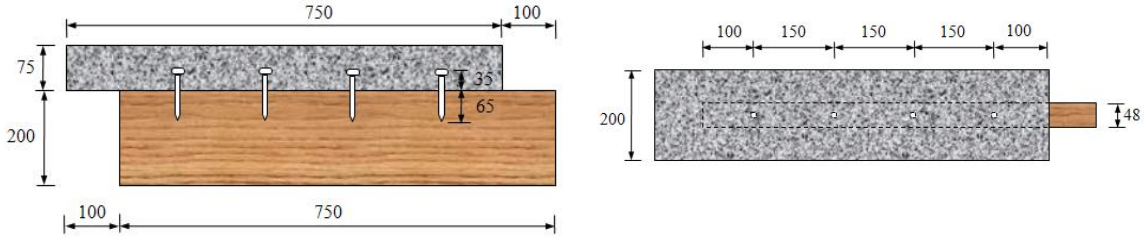

(a) Cross-section (b) Plan

Figure 3.4 A typical geometry and components of 4-NS150 connection (mm).

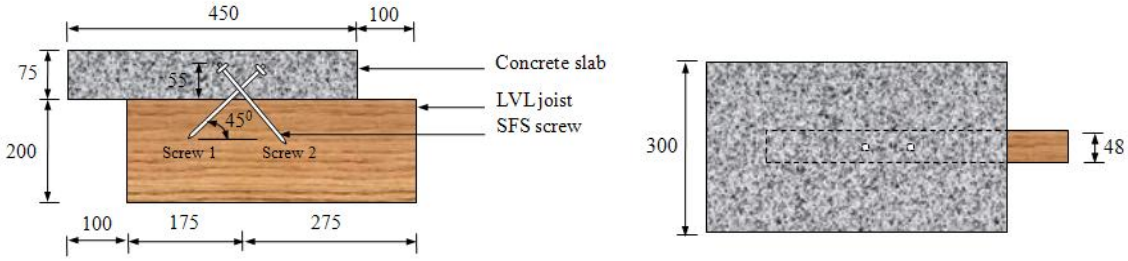

(a) Cross-section (b) Plan

Figure 3.5 A typical geometry and components of SFS series connection (mm).

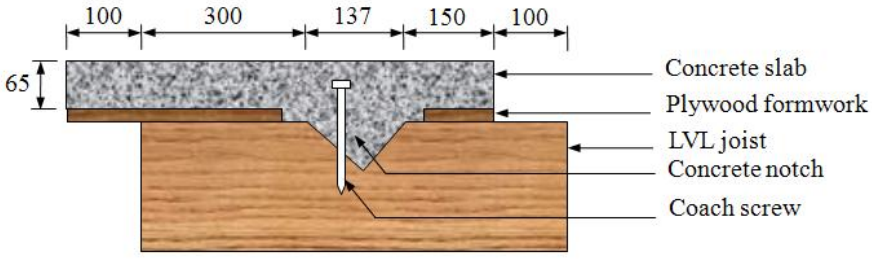

Figure 3.6 A typical geometry and components of BM series connection (mm).

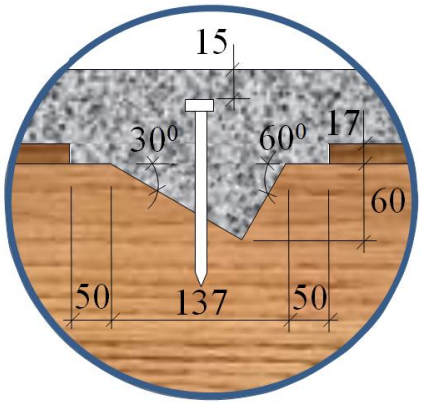

Figure 3.7 Geometric details of BM notched connections (mm).

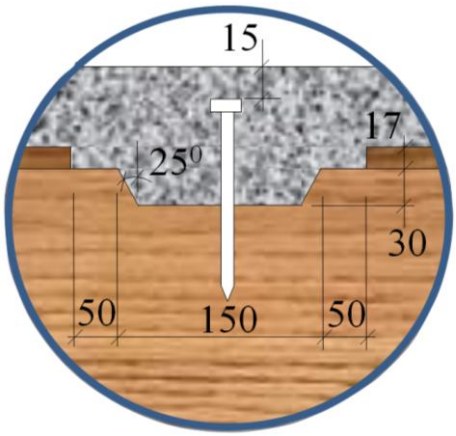

Figure 3.8 Geometric details of trapezoidal notched connections (mm).

3.1.2 Material Properties

The compressive strength and modulus of elasticity (MOE) of concrete was found in accordance with AS1012.9 (1999) and AS1012.17 (1997), respectively. The MOE was determined from three cylinders with 100 mm diameter. The mean 28 day compressive strength and MOE of concrete were 36.6 MPa and 24.5 GPa, respectively for NS and SFS series specimens. Experimental data from the material tests conducted on concrete used on NS and SFS series specimens are presented in Tables A.1 and A.2 (Appendix A). The mean 28 day compressive strengths of concrete used on BM and trapezoidal notched connection series specimens are summarised in Table 3.2.

Table 3.2 Mean compressive strength of concrete for notched connection series

Type	Series	Compressive strength (MPa)
Bird-mouth (BM)	B1	36.0
	B2	34.3
	B3	38.7
	B4	38.7
	B5	38.7
Trapezoidal	T1	38.7
	T2	34.3
	T3	38.7
	T4	38.7
	T5	38.7

3.1.3 Experimental Setup

An asymmetrical push-out test was conducted on all specimens. The experimental setup for the specimens is shown in Figure 3.9. The specimen placed on the test rig was loaded through the cross-head of the universal testing machine (Shidamzu REH 50) having maximum loading capacity of 500 kN. An overview of the universal testing machine is shown in Figure 3.10. Three linear variable differential transformers (LVDTs) were used to measure the relative displacements between the concrete slab and the LVL joist, two on either side of the joist and one at the centre while a fourth LVDT was used to measure the cross-head movement of the testing machine.

Notes on Figures 3.9 and 3.10:

1. Adjustable cross-head of universal testing machine
2. Spherical seating for loading
3. Rectangular metal plate

   It was placed on the top edge of LVL (as shown in the figure) to avoid stress concentration on LVL. The top edge of the LVL and the metal plate had to be aligned with the centre lines of the head to minimize load eccentricity.
4. LVDT left (25 mm travelling range)

   It was screwed on left hand side of the LVL.

5. LVDT right (25 mm travelling range)

   It was screwed on right hand side of the LVL.

6. Steel test rig

   It was designed to hold the specimen in place and no significant lateral load was expected during loading. Such a lateral load was not measured but the performance of the test rig was adequate to provide restraint against lateral movement.

7. Steel bracket

   There were two 'L' shaped stopping steel brackets, one on each side of the LVL, attached to the concrete using both sided tape. They were positioned about 200 mm from the bottom edge of the LVL.

8. LVDT centre (5 mm travelling range)
9. Steel blocks

   The blocks were used in the gap between concrete and test rig as shown in the figure to hold the specimen in position during loading.

10. LVDT cross-head
11. Load reader
12. Computer
13. Load control panel
14. Data logger

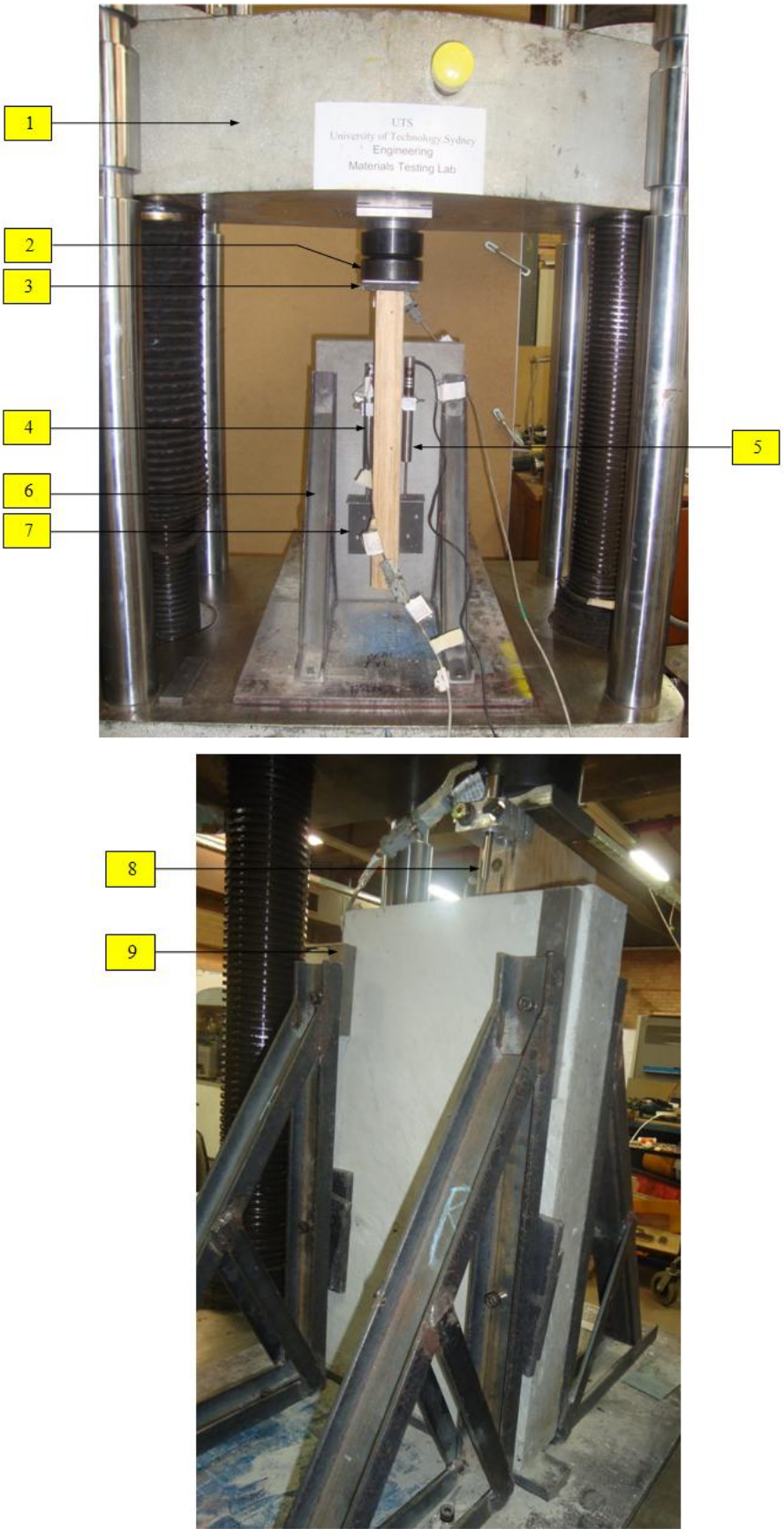

Figure 3.9 Push-out test setup of a test specimen.

Figure 3.10 Test environment showing the universal testing machine.

3.1.4 Loading Procedure

The loading procedure presented in European Standard EN26891 described by Dias (2005) as shown in Figure 3.11 was adopted for all tests. The load was applied in following steps.

1. The load is applied until about 40% of the estimated failure load. This stage is normally completed in about two minutes.
2. The load is maintained at about 40% of the estimated failure load for about 30 seconds.
3. The load is released until about 10% of the estimated failure load. This stage aims to last about one and a half minute.
4. The load is maintained at about 10% of the estimated failure load for some 30 seconds.
5. The load is (re-)applied until failure of the specimen. The loading rate should be close to the initial loading rate.

The reason to follow those loading steps is that it eliminates any internal friction in the connections. This is essential to ensure that when the specimen is tested to failure, it

does not fail due to initial slip or slack in the connection. A typical test would take about 10-15 minutes (600-900 seconds) to complete.

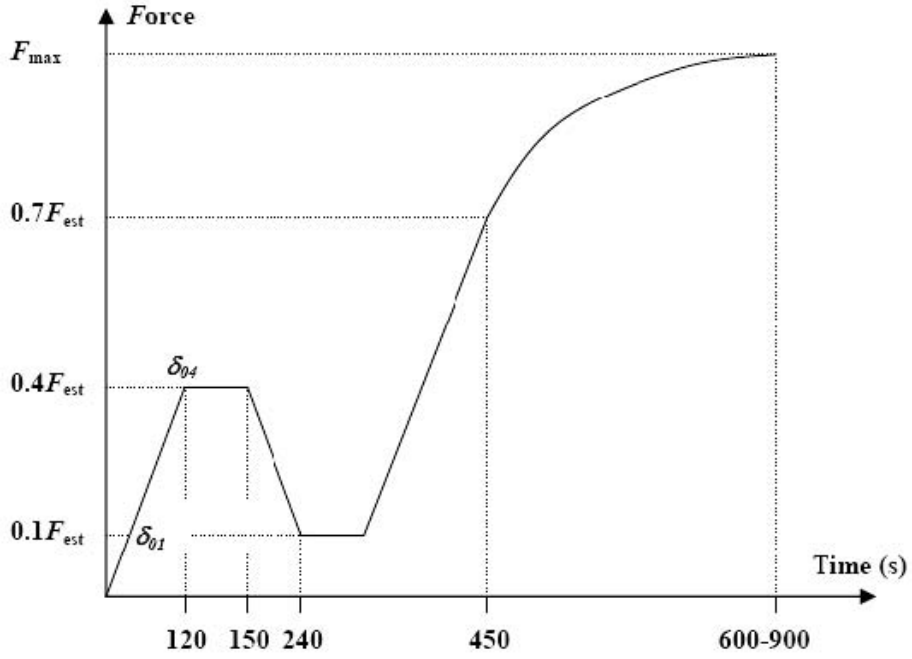

Figure 3.11 Loading regime as per EN 26891 (BSI 1991).

3.1.5 Test Criteria

The behaviour and effectiveness of the tested shear connections were assessed based on their strength, stiffness and failure mode.

The strength of the tested specimens is defined as the maximum load resisted by them in the push-out tests before their failure. The load carrying behaviour of the specimens, especially after failure, depends upon the failure mode such as brittle or ductile failure. Therefore, the failure modes have been well documented for the specimens. The efficiency of a shear connection is defined by one of the key parameters such as the connection stiffness (or slip modulus) as it represents the resistance to the relative displacement between the LVL joist and the concrete slab. Stiffness for the serviceability limit state (SLS) and ultimate limit state (ULS) are essential to characterise a shear connection. The stiffness for SLS (K_{serv}) corresponds to the slope of the load-slip curve between 10% and 40% of the failure load while the stiffness for ULS (K_u) corresponds to the slope of the load-slip curve between 10% and 60% of the failure load. In general, K_u is assumed as 2/3 of K_{serv}. The serviceability and ultimate stiffness are particularly important for serviceability and strength calculation.

3.2 Push-out Test of TCC Connections - Results

3.2.1 Introduction

This section presents the results for push-out tests conducted on four types of connections, mentioned in Section 3.1. This section should be read in conjunction with Section 3.1. Three types of these connections such as NS, SFS and Bird-mouth notched connections were adopted in the tested TCC beams (Refer to Section 3.4). The characteristic properties such as strength, stiffness and failure mode of each type of connection system is presented hereafter.

3.2.2 NS Series with Single Screw

Figure 3.12 depicts the load-slip response for NS series specimens with single screw. The load-slip behaviour basically consists of two linear parts with different stiffness which can be considered as elastic and plastic stiffness of the connection. Specimens NS1, NS2, NS3, NS5, NS7 and NS10 have similar response with gradual increase in load rate up to failure. Specimen NS8 had an unusual peak load compared to other specimens, and, therefore, the result for this specimen was excluded in the statistical analysis. The specimens NS4, NS6, NS8 and NS9 also showed unusually high stiffness which is attributed to possible rotation as the LVDTs may provide incorrect relative slip measurements if the rotation is present, and, therefore, were ignored in the statistical analysis to evaluate the stiffness of the connections. Friction at timber-concrete interface can also be one of the possible reasons of such unusual high ultimate load and stiffness.

The observation of all specimens of this series showed that the screw had snapped at the interface between LVL joist and concrete slab. Also, the LVL joist had crushed (Refer to Section 3.2.7) and, therefore, the ductility in the connection was provided by LVL crushing and not due to yielding of the screws. Crushing of LVL in connections NS1 and NS8 was relatively least visible while it was more prominent in connection NS4.

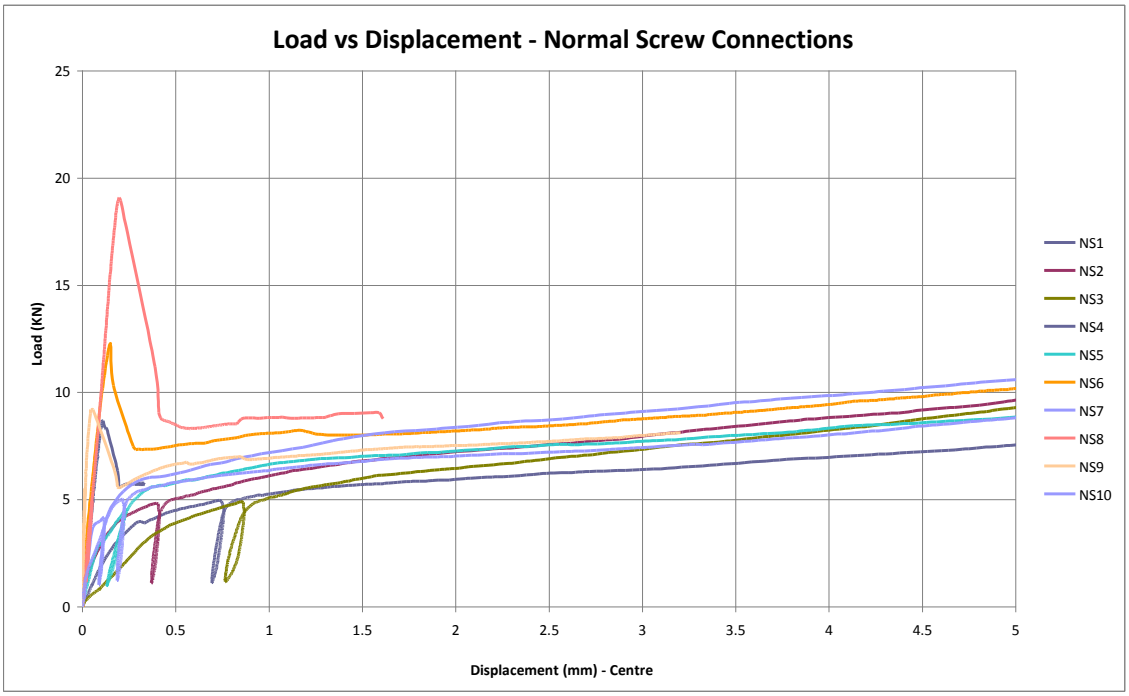

Figure 3.12 Load-slip plot for NS series with single screw.

3.2.3 NS Series with Four Screws (4NS50, 4NS100 and 4NS150 Connections)

The load-slip behaviour for NS series connection with four screws is shown in Figure 3.13. From Figure 3.13, it is apparent that there was no significant effect attributable to the spacing between the screws on the behaviour of the specimens as they had similar and consistent behaviour to push-out test results. This is also consistent with *k17* factor for multiple nailed joints, where its value is one if the number of rows is up to four (AS 1720.1 2010). The load-slip response of the connections was linear elastic up to the peak load and there was significant drop in stiffness after peak load. However, the peak load for connection 4NS100-2 was unusually high.

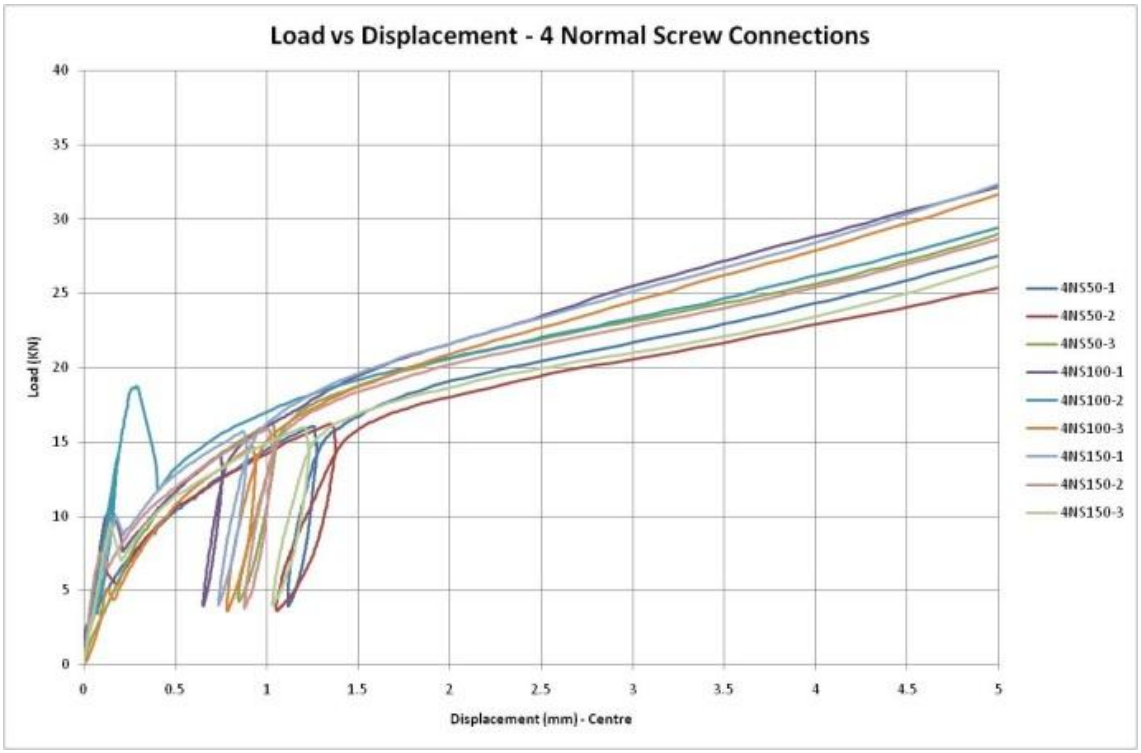

Figure 3.13 Load-slip plot for NS series with four screws.

3.2.4 SFS Series

Load-slip behaviour for SFS series connections are shown in Figure 3.14. The load-slip behaviour for the SFS screws are more consistent compared to the NS series connections except for connections SFS6 and SFS10 which had relatively high stiffness. The load-slip response of the SFS series connections showed relatively more ductile behaviour compared to the NS series connections.

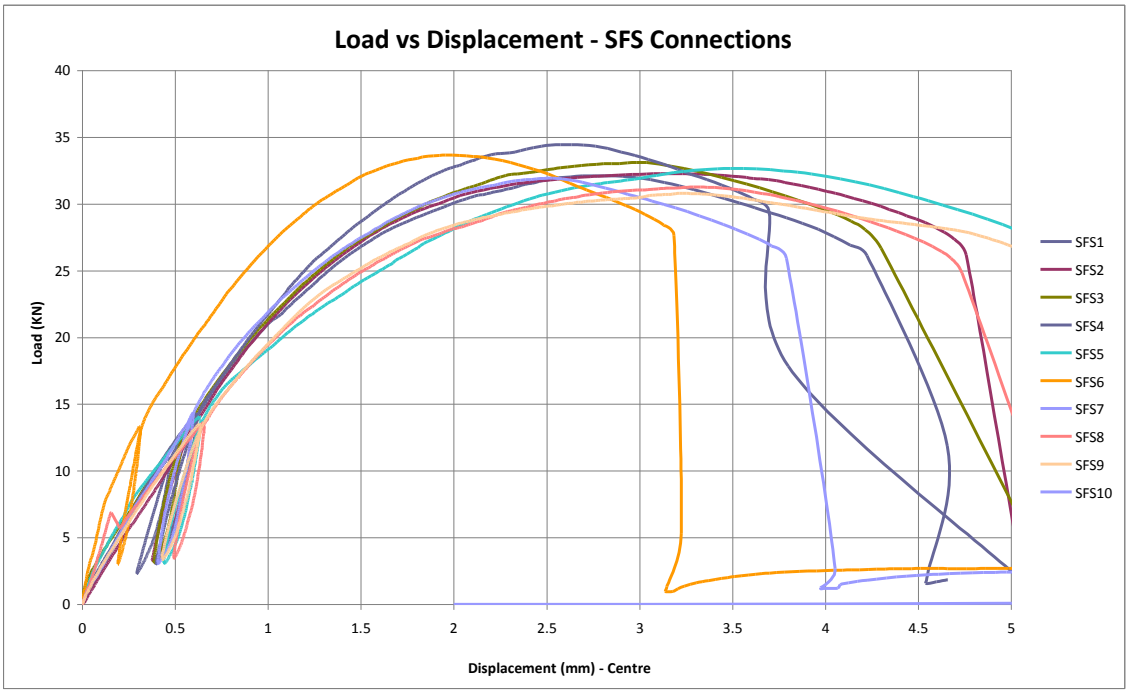

Figure 3.14 Load-slip plot for SFS series.

3.2.5 Bird-mouth Notched Connection Series

Typical load-slip behaviour for all bird-mouth notched connection series (5 series) are shown in Figure 3.15. The detailed load-slip behaviour of each specimen of these series can be found in Figures A.1 to A.4 (Appendix A). The load-slip response of the series connections showed ductile behaviour. The stiffness of the connections increased with increase in size of LVL joists. The B1 and B2 had 48 mm thick LVL joists and, therefore, had lower stiffness compared to other series specimens with 63 or 96 mm thick LVL joists. The load-slip behaviour of B1 and B2 series connections showed significant effect of the screw size in their performance, whereas, their effect was minimal in T1 and T2 series connections. The load-slip response revealed that the proportion of increase in strength and stiffness of the series B3 and B4, and B4 and B5 are significantly different. The results showed that the strength and stiffness of the series decreases if the screw diameter to the LVL joist thickness ratio is higher, as larger diameter of the screw results in splitting of LVL joist.

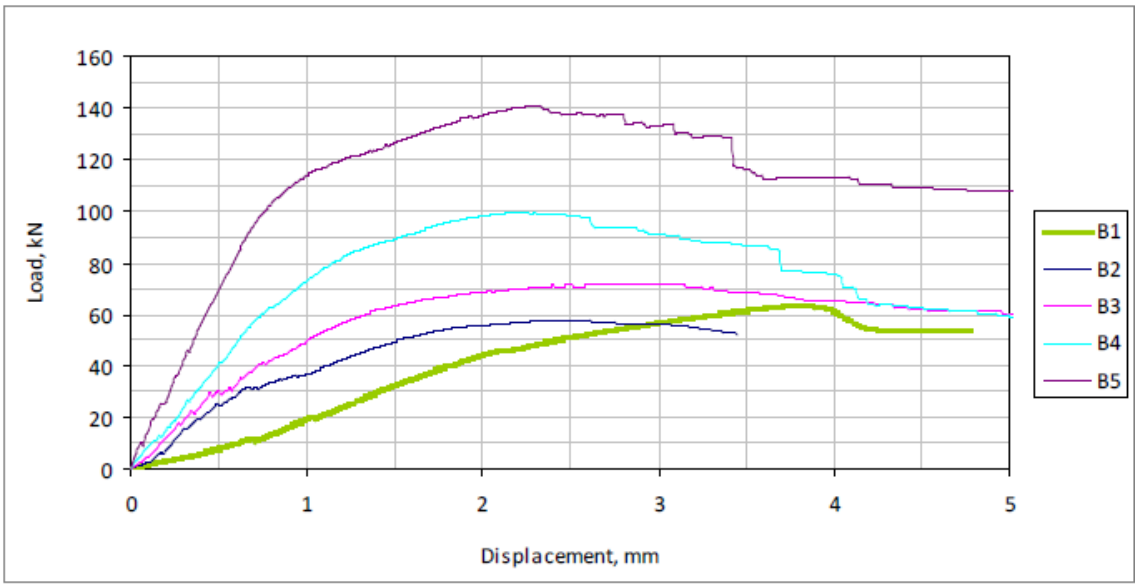

Figure 3.15 Typical load-slip behaviour for bird-mouth connection series.

3.2.6 Trapezoidal Notched Connection Series

Load-slip behaviour for all trapezoidal notched connection series (5 series) are shown in Figure 3.16. The detailed load-slip behaviour of each specimen of these series can be found in Figures A.5 to A.9 (Appendix A.3). The load-slip response of the connections showed ductile behaviour. The stiffness of the connections increased with increase in size of LVL joists. Stiffness and strength of T1 and T2 series connections is similar. They had the same thickness as LVL joist but the diameter of the coach screw was different. T1 and T2 series connections had coach screws with 16 and 12 mm diameter, respectively. The load-slip behaviour of T1 and T2 series showed minimal effect of screw size in their performance. Furthermore, the load-slip response revealed the proportion of increase in strength and stiffness of the series T3 and T4, and T4 and T5 is significantly different; concluding the increase in diameter of coach screw is more efficient with increase in thickness of LVL joist. The use of larger diameter screw in thinner LVL joist resulted in splitting of the joist. As a consequence, the characteristic values of the connections were relatively lower for T1 and T2 series.

In the comparison of load-slip behaviour of bird-mouth (BM) and trapezoidal notched connections, the behaviour of the corresponding series is similar. The stiffness of the B2, B4 and B5 series connections was greater than T2, T4 and T5 series connections, respectively. The load-slip behaviour revealed BM notched connections are more

efficient than trapezoidal notched connections. Further, BM notched connections are easier to fabricate as BM notch has only two faces, which simply can be cut using circular saw, while trapezoidal notch has three faces to be cut.

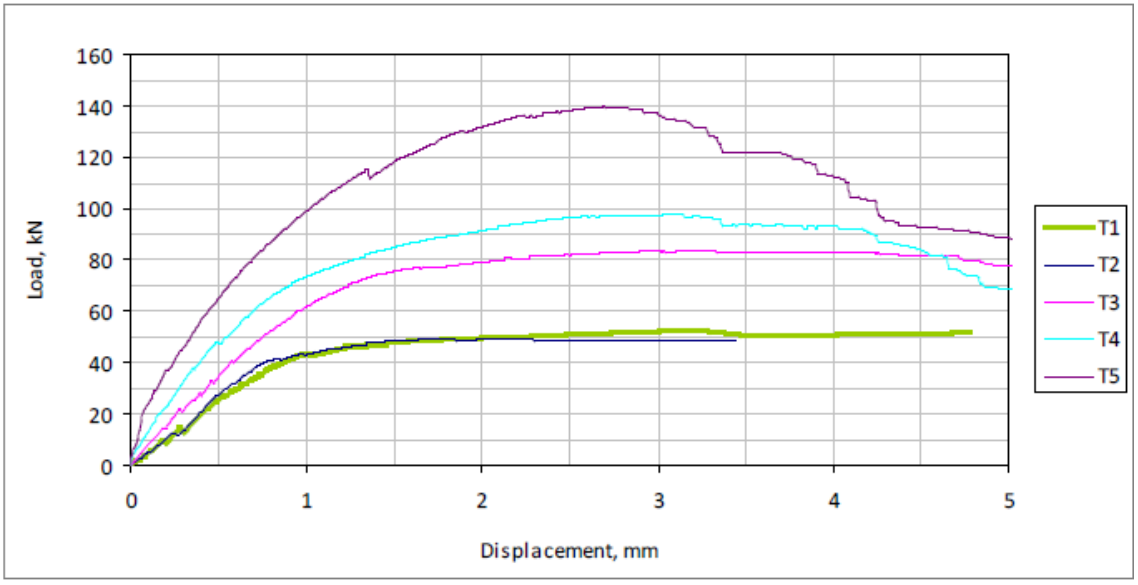

Figure 3.16 Typical load-slip behaviour for trapezoidal notched connection series.

3.2.7 Failure Mode

3.2.7.1 NS Series (with One and Four Screws) and SFS Series

The observed failure modes of NS series specimens are shown in Figures 3.17 to 3.20. The observation of the failed 4NS50 series specimens revealed splitting of LVL joist while no splitting of LVL joist was observed in other connections with four screws such as 4NS100 and 4NS150 series specimens. Nevertheless, the failure mode of the screws in all connections was identical where the screws snapped at the interface between the slab and the joist (see Figures 3.18 to 3.20), but the connection 4NS150-2 was an exception as the screws were actually pulled out from the LVL joist.

The observed failure modes of SFS series specimens are shown in Figures 3.21 and 3.22. Observation of the failed SFS series specimens showed that both screws were snapped in all connections except for connection SFS9 and SFS10. Also, during the test, it was observed that the screw installed in the direction of the load (Screw 1 in Figure 3.21 a, which is in tension) first failed which was then followed by failure of the second screw with large slip due to LVL crushing next to the second screw (which was under

compression). LVL was crushed at both screw locations in SFS9 and SFS10 specimens, but for both specimens the screw installed in the direction of the load was not broken.

(a) NS1 (b) NS2 (c) NS3

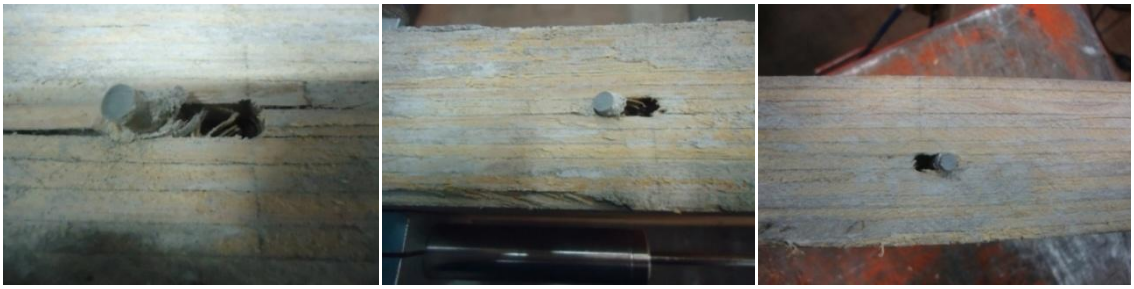

(d) NS4 (e) NS5 (f) NS6

(g) NS7 (h) NS8 (i) NS9

(j) NS10

Figure 3.17 Failed NS series with single screw (NS) specimens.

(a) 4NS50-1 (b) 4NS50-2 (c) 4NS50-3

Figure 3.18 Failed NS series with four screws (4NS50) specimens.

(a) 4NS100-1 (b) 4NS100-2 (c) 4NS100-3

Figure 3.19 Failed NS series with four screws (4NS100) specimens.

(a) 4NS150-1 (b) 4NS150-2 (c) 4NS150-3

Figure 3.20 Failed NS series with four screws (4NS150) specimens.

(a) SFS1

(b) SFS1

(c) SFS2

(d) SFS2

(e) SFS3

(f) SFS3

(g) SFS4

(h) SFS4

(i) SFS5

(j) SFS5

Figure 3.21 Failed SFS1-5 series specimens.

(a) SFS6

(b) SFS6

(c) SFS7

(d) SFS7

(e) SFS8

(f) SFS8

(g) SFS9

(h) SFS9

(i) SFS10

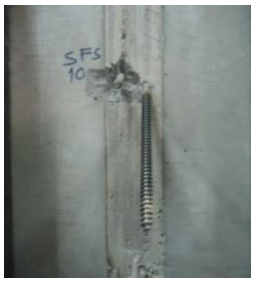

(j) SFS10

Figure 3.22 Failed SFS6-10 series specimens.

3.2.7.2 T (Trapezoidal Notched) and B (Bird-mouth Notched) Series

The observed failure modes of trapezoidal notched connection series specimens (T2 series) are shown in Figure 3.23. The observation of the failed specimens of the series revealed crushing of LVL joist and bending of the coach screw except for three specimens such as T2-7, T2-9 and T2-10. The observation also revealed splitting of crushed LVL joist in four specimens, namely, T2-1, T2-2, T2-6 and T2-8. The splitting of LVL joist in the specimen T2-2 was most severe.

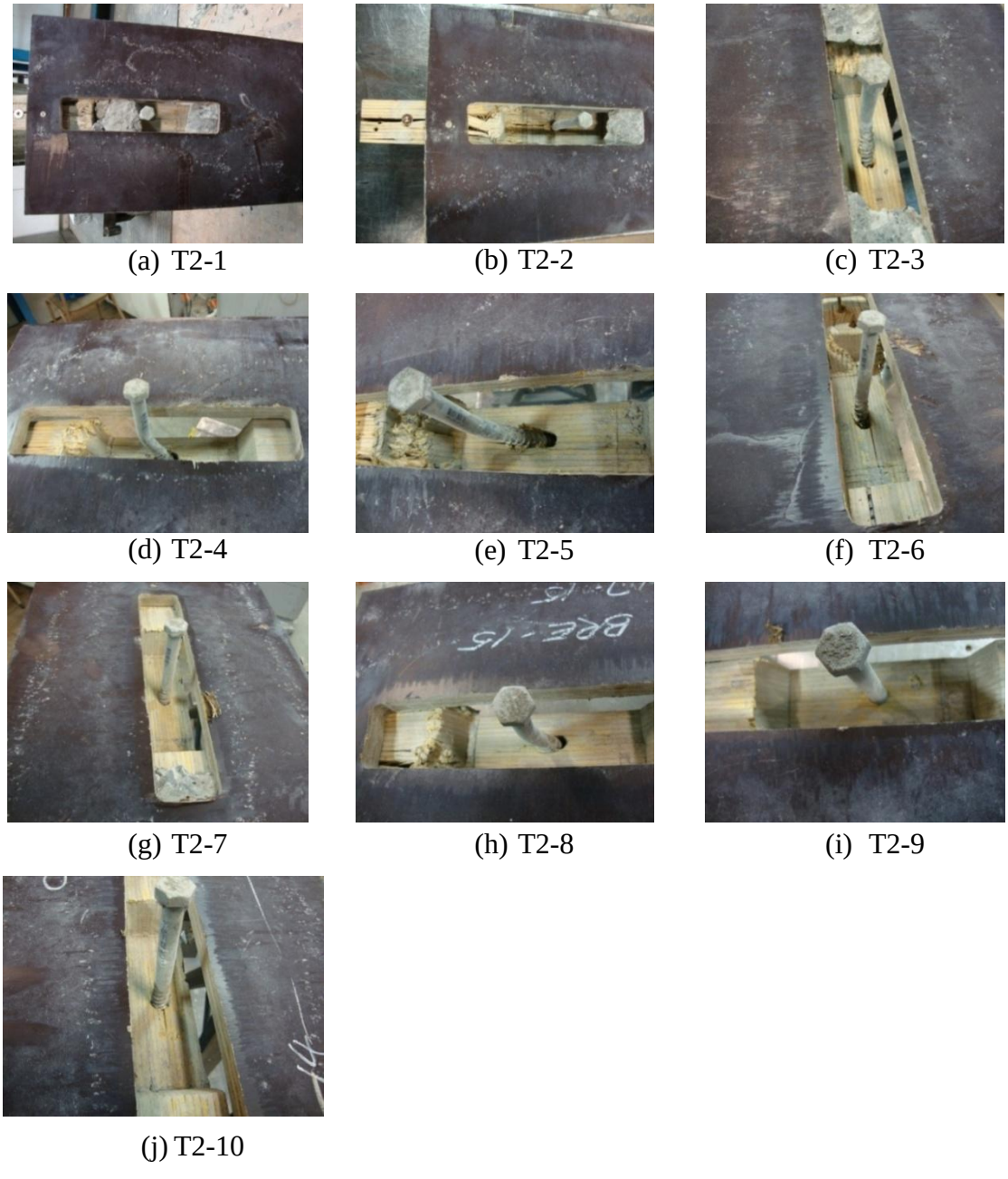

(a) T2-1 (b) T2-2 (c) T2-3

(d) T2-4 (e) T2-5 (f) T2-6

(g) T2-7 (h) T2-8 (i) T2-9

(j) T2-10

Figure 3.23 Failed T2 series specimens.

The observed failure modes of BM notched connection series (B2 series) specimens are shown in Figure 3.24. The failure mode of the specimens was totally different from T2 series specimens as no crushing and splitting of LVL joist of the B2 series specimens was observed. Furthermore, the observation revealed no bending of coach screw of the specimens, where two specimens B2-6 and B2-10 were an exception.

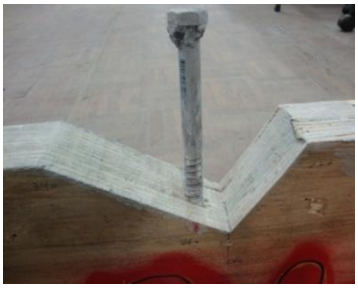

(a) B2-1

(b) B2-2

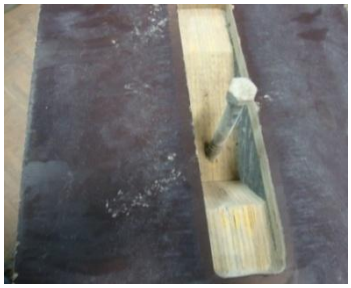

(c) B2-3

(d) B2-4

(e) B2-5

(f) B2-6

(g) B2-7

(h) B2-8

(i) B2-9

(j) B2-10

Figure 3.24 Failed B2 series specimens.

3.2.8 Characteristic Values for Four Connection Types

Summary of 5^{th} percentile values for strength evaluated based on log normal distribution and 50^{th} percentile or mean values for stiffness for each connection type along with coefficient of variation (CoV) are presented in Tables 3.3 to 3.5. The strength for NS series with single normal screw was determined based on 9 specimens (NS8 was ignored) and stiffness was evaluated based on 5 specimens only (NS4, NS6, NS8, NS9 and NS10 were ignored). Strength and stiffness results for each specimen of NS and SFS series are presented in Table A.3 (Appendix A). Similarly, these results for BM and trapezoidal notched connection series are presented in Tables A.4 and A.5 (Appendix A), respectively.

SFS connections were found to be more efficient compared to NS connections with single normal screw as they had relatively higher strength and stiffness. The strength for SFS screw connections, which is 30 kN, is three times higher than strength of single normal screw connections with CoV below 8%. The serviceability stiffness (K_{serv}) of these connections is higher than their ultimate stiffness (K_u). However, stiffness of single normal screw connections have significantly higher CoV (up to 41%) compared to SFS screw connections. The test results of NS series connections having four screws with different spacing exhibited similar characteristic values, where serviceability stiffness of the 4NS100 series connections was relatively much higher than 4NS50 and 4NS150 series connections. From the test results, it can also be concluded that performance of the notched connections (BM and trapezoidal) is better than the connections with mechanical fasteners only (NS and SFS connections) as notched connections had higher strength and stiffness. Nevertheless, the notched connections are more difficult to fabricate compared to non-notched connections as cutting notch in the timber joist needs additional instruments and consumes time. Among the notched connection types, the strength of B1, B2 and B4 series connections was greater than T1, T2 and T4, respectively, while stiffness of the B1 series connections was smaller than T1 series connections. The strength of B3 and B5 series connections was smaller than T3 and T5 series connections, respectively, but the stiffness of B5 series connections was greater than T5 series connections.

Table 3.3 Characteristic results for NS and SFS series connections

Connection description	Strength (kN)	Stiffness (kN/mm)	
	Q_k	K_{serv}	K_u
NS series with single screw	10 – 7.9%	49 – 33.0%	7 – 41.0%
SFS series	30 – 3.5%	58 – 21.2%	34 – 14.0%

Table 3.4 Characteristic results for NS series connections with four screws

Connection description	Strength (kN)	Stiffness (kN/mm)	
	Q_k	K_{serv}	K_u
4NS50	37 – 18.1%	34 – 12.7%	11 – 45.6%
4NS100	38 – 14.2%	62 – 48.5%	12 – 58.2%
4NS150	41 – 4.7%	32 – 24.4%	8 – 18.0%

Table 3.5 Characteristic results for BM and Trapezoidal notched connection series

Connection description	Strength (kN)	Stiffness (kN/mm)	
	Q_k	K_{serv}	K_u
B1 – 48mm LVL, 16mm screw	55 – 8.1%	37 – 12.4%	36 – 15.2%
B2 – 48mm LVL, 12mm screw	51 – 8.4%	115 – 48.4%	46 – 54.0%
B3 – 63mm LVL, 16mm screw	66 – 7.7%	98 – 12.9%	74 – 27.7%
B4 – 96mm LVL, 12mm screw	91 – 5.5%	156 – 19.8%	119 – 20.8%
B5 – 126mm LVL, 16mm screw	120 – 11.6%	213 – 34.2%	150 – 22.7%
T1 – 48mm LVL, 16mm screw	46 – 8.7%	87 – 20.5%	60 – 13.0%
T2 – 48mm LVL, 12mm screw	46 – 6.6%	106 – 15.0%	87 – 17.9%
T3 – 63mm LVL, 16mm screw	78 – 6.4%	109 – 19.3%	81 – 24.7%
T4 – 96mm LVL, 12mm screw	89 – 10.0%	110 – 34.8%	93 – 39.3%
T5 – 126mm LVL, 16mm screw	134 – 4.8%	124 – 41.3%	103 – 30.2%

Notes on Tables 3.3 to 3.5:

i) Integer = capacity; % = CoV

ii) Strength – 5th percentile based on a log normal distribution

iii) Stiffness – 50th percentile or mean

3.2.9 Concluding Remarks

These series of tests were important to characterise the shear connectors used in TCC beams (Refer to Section 3.3). The characteristic values are important for use in prediction models such as natural frequency prediction models for the tested TCC beams and design methods.

Test results showed that strength and stiffness variation in connectors using SFS screws are much less when compared to single normal screws and hence strength and stiffness of TCC beams and floor elements utilising such connectors can be predicted with confidence. With single normal wood screws, variation in the strength is 7.9%; however, the variation in stiffness is much higher. Connections using multiple normal screws with varying spacing between the screws were tested in order to investigate the use of push-out test to study the effect of connector spacing. However, the tests revealed that the push-out tests can not capture the effect of connector spacing on the overall effectiveness of the connectors and, therefore more comprehensive bending tests are suggested for future study on the effect of connector spacing.

A number of notched connections series were tested to investigate the effect of size of mechanical connectors (coach screw), thickness of LVL joist and shape of notches (bird-mouth and trapezoidal). The coach screw had longer length than normal wood screw and hence use of them had the advantage of deeper penetration depth inside the concrete slab. Hence, a single coach screw provided higher shear capacity compared to combination of four wood screws.

The bird-mouth type connections exhibited higher strength and stiffness than the trapezoidal notch connections. The bird-mouth notched connections were also superior to the trapezoidal notch connections. However, the fabrication of the trapezoidal notch connections is difficult as they have complex angle sequence. The bird-mouth type connections are on the other hand much easier to fabricate with simple cutting sequence and does not need special tools for fabrication. It should however be noted that the coach screws in bird-mouth notch provided only limited post peak plastic behaviour when compared to trapezoidal notch connections.

The failure mode of the bird-mouth notched connections was totally different from trapezoidal notched connections as typically T2 series specimens had crushing, and

splitting failure in the LVL along the glue line was observed in a number of test connections limiting the effectiveness of the shear connections, while there was no damage in the BM notched in B2 series connections. The effect of the ratio of coach screw diameter to LVL thickness is one of the parameters that need further investigation. Although poor gluing quality or variation in the LVL properties may have a role in such failure, effect of the ratio of coach screw diameter to LVL thickness needs to be verified.

From the test results it can also be concluded that performance of the notched connections (bird-mouth and trapezoidal) was better than the non-notched NS and SFS connections as the notched connections exhibited higher strength and stiffness.

3.3 Modal Testing and Experimental Modal Analysis Procedure

3.3.1 Introduction

Modal testing (MT) and experimental modal analysis (EMA) is a process of characterizing the dynamic properties of a test structure by exciting the structure artificially and identifying its modes of vibration (Ramsey 1982). EMA is the process of determining the modal characteristics such as natural frequencies, damping ratios and mode shapes from the experimental data while MT describes the performance of the testing and the acquisition of the modal data from the test structure. Signal processing, FRF and modal parameter estimation are three major steps to assess dynamic performance of the test structure.

3.3.2 Signal Processing

Basically, signal processing deals with the analysis of electrical signals obtained from dynamic test for assessment of the system. The discrete Fourier transform algorithm is needed to transform data from the time domain to the frequency domain once analogue electrical signals are converted into a corresponding sequence of digital values. The process of acquiring and converting physical quantities from analogue to digital electrical signals is shown in Figure 3.25. The estimated frequency response function includes errors such as digital signal processing errors (leakage and aliasing), noise

(power supply noise, cabling problems, rattles, and cable motion) and calibration error (system calibration and transducer calibration) (Allemang 1999).

Transducer captures the physical motion of the structure being tested and it converts vibration into analogue electrical signals. Piezoelectric accelerometer is the common transducer for vibration measurement. A signal conditioner converts the analogue signals from the transducer into voltage proportional to the measured physical quantities while amplifier increases the resolution of signal from conditioner and its signal-to-noise ratio (Dackermann 2010).

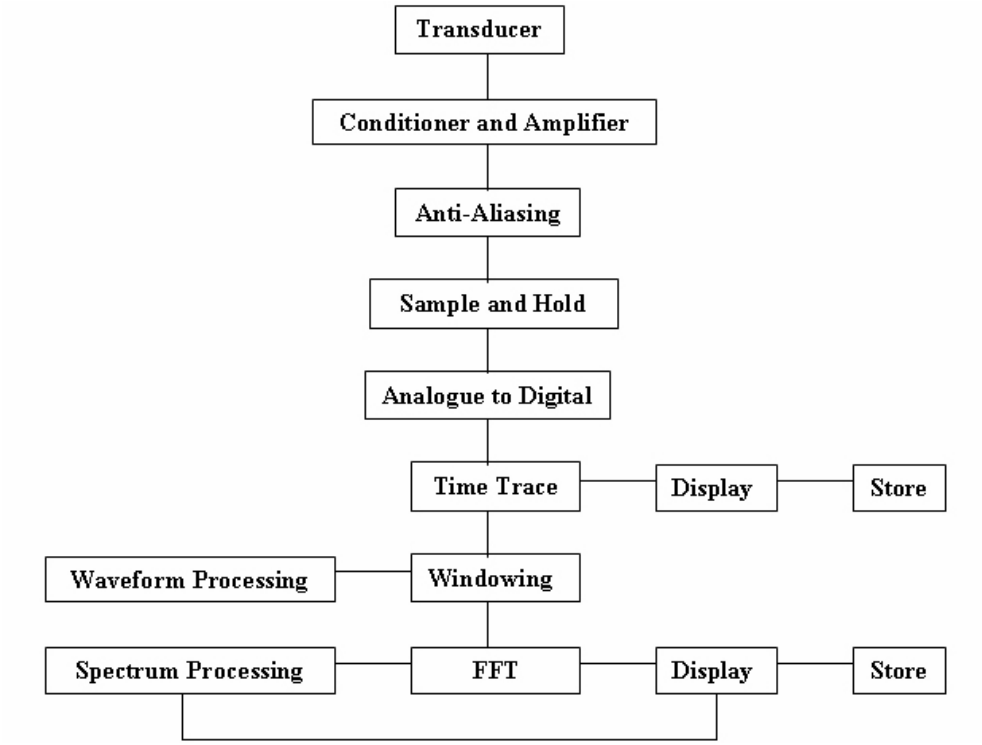

Figure 3.25 Digital signal processing (Abdul Rahman 1999).

In signal processing, there are some pitfalls such as aliasing and spectral leakage that might result in a loss of accuracy of the signal during the process. Aliasing is a phenomenon that occurs when the sampling rate is less than twice the highest frequency in the data. Aliasing produces a distorted representation of data and it also occurs when converting analogue data to digital data resulting in erroneous frequency interpretation in vibration analysis. Aliasing phenomenon is illustrated in Figure 3.26.

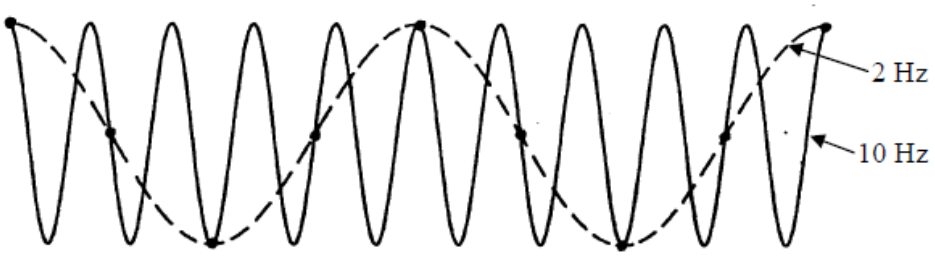

Figure 3.26 Aliasing phenomenon (Allemang 1999).

Aliasing can be minimised by using Nyquist-Shannon sampling theorem as expressed in Equations (3.1) and (3.2). This theorem states that a sampling rate of at least twice the highest frequency present in the data needs to be used to reduce aliasing. Alternatively, anti-aliasing filter, which is a low-pass filter, can be used to minimise aliasing as this filter automatically cuts-off frequencies set at or above half of the sampling frequency, F_{samp} (Allemang 1999).

$$F_{Samp} = \frac{1}{\Delta t} = F_{Nyq}\ x\ 2 \tag{3.1}$$

$$F_{Nyq} \geq F_{Max} \tag{3.2}$$

where F_{Nyq} is the Nyquist frequency and is the theoretical limit for the maximum frequency, F_{max}.

An analogue-to-digital converter (ADC) converts the analogue (continuous) input signal into a digital (discrete) form. The acquired continuous signal is first sampled and then converted into a discrete time series digital signal. The time interval between two samples is equal to the inverse of the sampling frequency. For example, time interval will be 0.001 sec if sampling frequency is 1000 Hz. The resolution of each digital signal sample is equal to 2^B, where B is the number of bits used to represent a sample in the ADC. For example, a 16-bit ADC will discretise the amplitude range of the signal to a resolution of 65536 grids.

After the digitising process, the continuous time signals are discretised into a sequence of values commonly known as discrete time series. A discrete time series has values that are defined only at discrete values of time. Discrete time signals are also known as time domain signals consisting many frequency components that are superimposed. Fast

Fourier Transform (FFT) can be used to convert a time domain signal into its various frequency components. The FFT algorithm is expressed as in Equation (3.3). During the process of FFT, some problems such as leakage may occur.

$$x\,(k) = \sum_{j=0}^{N-1} X\,(j)\, W_N^{-jk} \tag{3.3}$$

which represents the discrete series *x(k)* at the time instant *k* of a sampled data *N*, with *k* = 0, 1, 2, …, *N*-1 and *j* = 0, 1, 2, …, *N*-1 where $W_N = e^{-i2\pi/N}$. The concept of the discrete Fourier transform is shown in Figure 3.27.

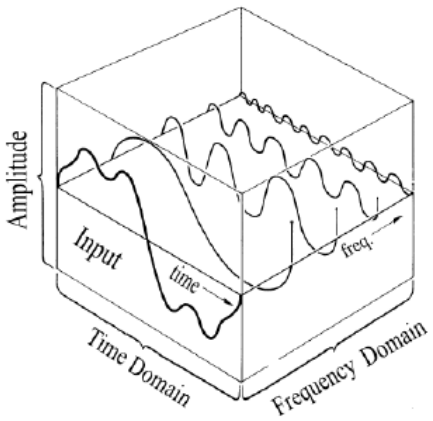

Figure 3.27 Discrete Fourier transform concept (Allemang 1999).

Leakage is the unwanted distortion caused by artificial truncation of sampled data (Maia et al. 1997). Windowing is a common tool that can be used to overcome the leakage problem. This function consists of a process of 'weighting' the original time history data to reduce the noise distortion and the effect of leakage. The common developed window functions to overcome the leakage problem are hanning, flattop, force and exponential windows. Last two window functions were used in this research and are briefly described below.

A force window is usually applied to the impact excitation such as hammer hit to remove noise from the impulse signal. Ideally, the impulse signal is non-zero for very short time interval of the excitation and zero for the remaining time. Therefore, any non-zero data following the impulse signal is assumed to be noise and thus is considered to be zero, as shown in Figure 3.28 (a). Exponential windows are commonly used for response signals, to ensure that the transient signal decays sufficiently at the end of the

sampling period, as illustrated in Figure 3.28 (b). This decay is employed by introducing artificial damping into the measurement data (Schwarz & Richardson 1999).

(a) Force window (b) Exponential window

Figure 3.28 Windowing functions.

3.3.3 Frequency Response Function

Frequency Response Functions (FRFs), also known as transfer function method are widely used for dynamic system identification in the industries, including the automotive, machine tool and structural engineering industries. The general procedure utilising the FRFs method for system identification is shown in Figure 3.29.

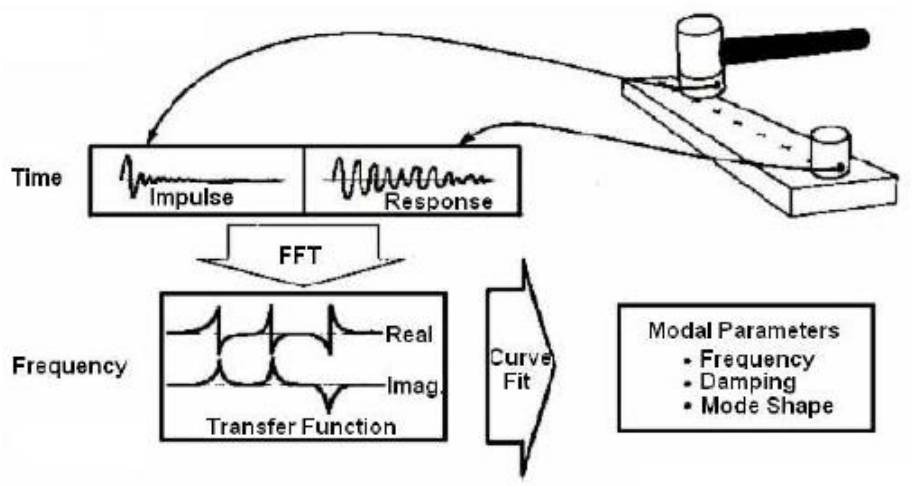

Figure 3.29 Transfer function method (Agilent Technologies 2000).

FRFs are used to describe the input-output (force-response) relationship of a system. To obtain FRF, one needs transducers such as accelerometers to record an output electric signal from the test structure, while the input signal is obtained from the source of excitation. For example, the input signal $f(\omega)$ with respect to frequency, ω, is the force applied to the structure using a modal hammer and the output signal $g(\omega)$ is the response motion signal obtained from the accelerometers attached to the system. The

FRF ($H_1(\omega)$) for each point on a system is the ratio of the output to the input after Fourier transformation as expressed in Equation (3.4).

$$H_1(\omega) = output/input = g(\omega)/f(\omega) \tag{3.4}$$

FRF can also be obtained from measured data using two methods. The first method normalises the cross input-output spectrum $G_{fg}(\omega)$ by the input auto spectrum $G_{ff}(\omega)$ as written in Equation (3.5).

$$H_2(\omega) = {G_{fg}(\omega)}\Big/{G_{ff}(\omega)} \tag{3.5}$$

where $G_{fg}(\omega) = f(\omega) \times g(\omega)$ is the cross spectrum, while $G_{ff}(\omega) = f(\omega) \times f(\omega)$ is the input auto-spectrum. The second method normalises the auto spectrum of the output $G_{gg}(\omega)$ by the cross input-output spectrum $G_{fg}(\omega)$, defined as:

$$H_3(\omega) = {G_{gg}(\omega)}\Big/{G_{fg}(\omega)} \tag{3.6}$$

where $G_{gg}(\omega) = g(\omega) \times g(\omega)$ is the output auto-spectrum.

FRF can be presented in rectangular coordinates such as real part vs. frequency, and imaginary part vs. frequency or in polar coordinates such as amplitude vs. frequency, and phase vs. frequency as shown in Figure 3.30 for a single degree of freedom system. At resonance, in the rectangular presentation, the imaginary part is a maximum and the real part is zero while in the polar system, the magnitude reaches a maximum and the phase lag approaches 90°. Hence, the modal parameters of a structure can be extracted from the FRF using these characteristics and the relationship between FRF and the modal parameters is given in Equation (3.7).

$$H_{ij}(j\omega) = \sum_{k=1}^{N} \left(\frac{r_{ijk}}{(j\omega - \lambda_k)} + \frac{r_{ijk}^*}{(j\omega - \lambda_k^*)}\right. \tag{3.7}$$

where $H_{ij(j\omega)}$ is the FRF between the response degree of freedom (DOF) i and reference DOF j, ω is the frequency (rad/sec), N is the number of modes of vibration that contribute to the structure's dynamic response within the frequency range under consideration, r_{ijk} is the residue value for mode k, λ_k is the pole value for mode k and * designates the complex conjugate. The pole value λ_k can be expressed as:

$$\lambda_k = \delta_k + j\omega_{dk} \tag{3.8}$$

where ω_{dk} is the damped natural frequency of mode k and δ_k is the damping factor of mode k.

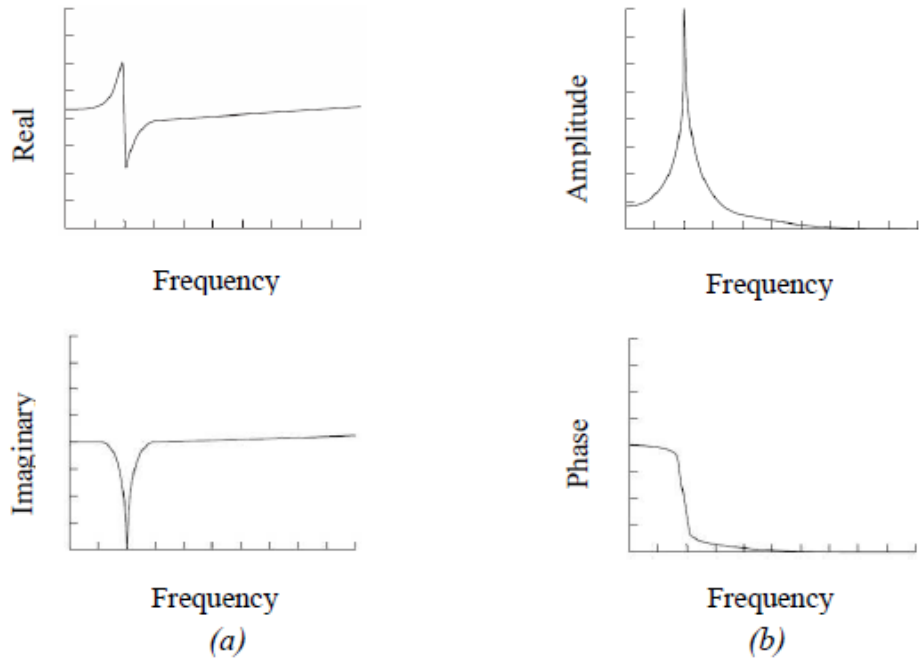

Figure 3.30 FRF graphs in (a) rectangular and (b) polar coordinates for a SDOF system.

3.3.4 Modal Parameter Estimation

Modal parameter estimation deals with the practical problem of estimating the modal parameters from the test data using a choice of mathematical model as justified by the EMA method (Structural Dynamic Research Laboratory 1999). Modal parameters such as natural frequencies, damping and mode shapes of the systems can be estimated utilising three different approaches. In analytical systems, the modal parameters are determined from the system matrices by formulating the Eigen solution of the system. In EMA, the modal parameters are extracted either from the measured FRFs in the frequency domain, or the Impulse Response Function (IRF) in the time domain. These three different methods of modal parameter estimation are shown in Figure 3.31.

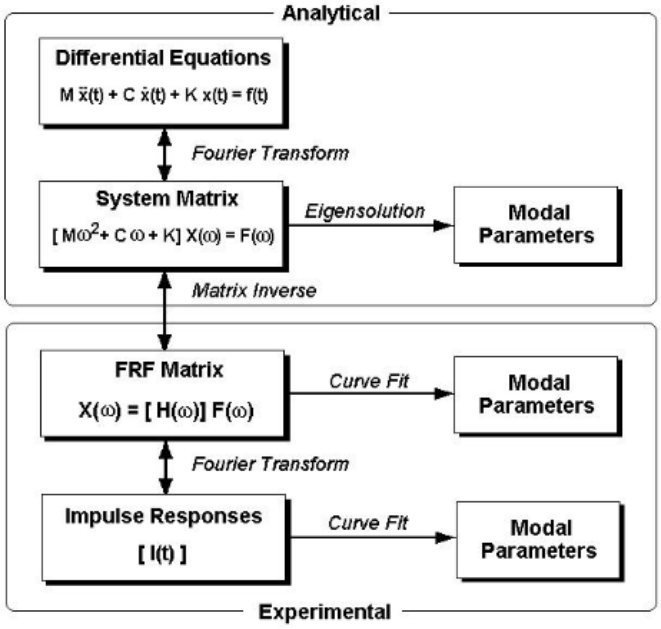

Figure 3.31 Modal parameter estimation methods (Schwarz & Richardson 1999).

In EMA, FRFs and curve fitting techniques are used to estimate the modal parameters mainly in the frequency domain. Curve fitting is defined as a process of matching a mathematical model to a set of measured data points. This is done by minimising the squared error or difference between the analytical function and the measured input-output data. Curve fitting methods are divided into four categories listed in order of increasing complexity which are local SDOF method, local MDOF method, global method and multi-reference (poly reference) method. SDOF methods estimate modal parameters, single mode at a time while MDOF, global and multi-reference methods can estimate modal parameters for two or more modes simultaneously (Schwarz & Richardson 1999).

In early applications of EMA, simple local SDOF curve fitting techniques were used to estimate frequency domain modal parameters. These methods were able to extract all three modal parameters, namely, frequency, damping and mode shape, directly from a set of measured FRFs. In recent times, most EMA methods are based on MDOF methods, which also use curve fitting methods to extract the modal parameters. Most of these methods use numerical techniques that separate the contributions of individual modes of vibration in measured FRFs by estimating the individual SDOF contributions to the MDOF measurement. This concept is shown in Figure 3.32.

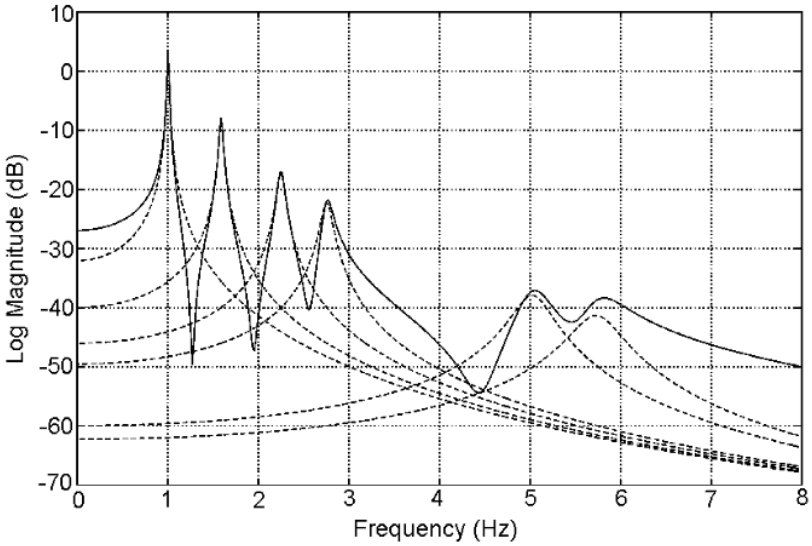

Figure 3.32 MDOF-SDOF superposition (Allemang 1999).

A number of MDOF-based methods such as the complex exponential, rational fraction polynomial, polyreference frequency domain and matrix decomposition methods were developed in the last few decades. In this study, Frequency Domain Direct Parameter Identification (FDPI) method is used to estimate the modal parameters. This method is based on MDOF method that is also capable of polyreference analysis. The principle of the FDPI method is briefly summarised as follows. Motion of a linear and time-invariant structure is expressed as below.

$$M\ddot{y}(t) + C\dot{y}(t) + Ky(t) = f(t) \tag{3.9}$$

When transformed into the frequency domain, this equation can be reformulated in terms of measured FRFs:

$$[-\omega^2 I + j\omega A_1 + A_0][H(\omega)] = j\omega B_1 + B_0 \tag{3.10}$$

where ω = frequency variable, $A_0 = M^{-1}K$ (the mass modified stiffness matrix), $A_1 = M^{-1}C$ (the mass modified damping matrix), $H(\omega)$ = matrix of FRFs, and B_0, B_1 are the force distribution matrices. When Equation (3.10) is assembled for all available FRFs the unknown matrix coefficients A_0, A_1, B_0 and B_1 can be determined from $H(\omega)$. Hence, measurement data $H(\omega)$ can be described by a second order linear model with constant matrix coefficients as written in Equation (3.11). For the identified matrices, the

system's poles (natural frequencies) and mode shapes can be estimated via an eigenvalue and eigenvector decomposition of the system matrix.

$$\begin{bmatrix} -A_1 & -A_0 \\ I & 0 \end{bmatrix} \tag{3.11}$$

This will yield the diagonal matrix [Λ] of poles and a matrix Ψ of eigenvectors. In the final step, the modal participation factors are estimated from another least squares problem, using the obtained [Λ] and Ψ matrices (CADA-X 1996).

3.4 Dynamic Test of TCC Beams - Test Setup and Testing

Four identical TCC beams with different shear connector arrangements were tested to evaluate their dynamic performance under the application of impact action. This section provides the details of the experimental investigation undertaken to assess the dynamic performance of the beams by evaluating modal parameters (natural frequencies, damping ratios and mode shapes). The tests were aimed at assessing the modal parameters of the beams and to investigate the efficiency of the different types of shear connector configurations. The results of these experimental works are presented in Section 3.5.

3.4.1 Test Program

The tested beams had an overall length of 6 m and a clear span of 5.8 m between supports. All beams were investigated under the pin-roller boundary conditions and free vibration was initiated with the use of instrumented modal hammer. A summary of the tested TCC beams and types of shear connector used in the beams is presented in Table 3.6.

Table 3.6 A summary of the tested TCC beams

Beam	Type of connector
Beam-1	SFS screw (Figure 3.34 a)
Beam-2	Normal screw (Figure 3.35 a)
Beam-3	Six bird-mouth notches with coach screw each (Figure 3.36 d)
Beam-4	Four bird-mouth notches with coach screw each (Figure 3.36 e)

3.4.2 Geometry of the TCC Beams

The tested beams were T-shaped and had identical geometry with an overall length of 6 m (see Figure 3.33). The laminated veneer lumber (LVL) joists were used as timber elements and concrete was cast on the top of joist. Either concrete notch or mechanical connectors were used to transfer shear from concrete topping to the joist. Concrete is stronger in compression while timber is stronger in tension and hence full advantage of both materials can be taken to the greatest advantage from the fabricated section as shown in Figure 3.33 (a).

The LVL joists were 250 mm deep and had a thickness of 48 mm, while the concrete slab, which was cast on the top of LVL joist, had a depth of 75 mm and a width of 600 mm. Concrete was poured directly on the LVL joist during fabrication and temporary formwork was used before pouring concrete.

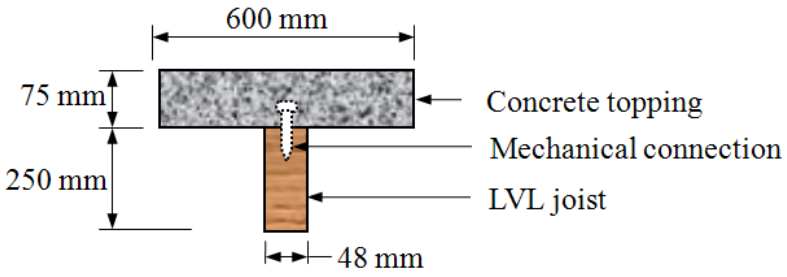

(a) Cross-sectional view of the beams

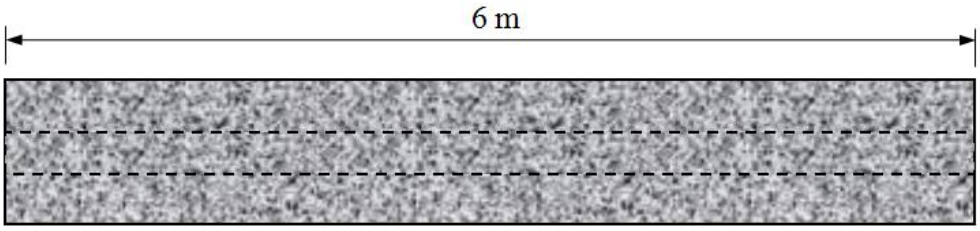

(b) Top view of the beams

Figure 3.33 Geometry of the TCC beams.

3.4.3 Types of Shear Connector and their Configuration in the Beams

Three different types of shear connectors were used in the four beams, namely, SFS screw, normal screw and bird-mouth notch combined with coach screw. A summary of the connection system for each beam is presented in Table 3.6. The details of the screw and connection arrangement on each beam before pouring concrete are depicted in Figures 3.34 to 3.36.

In Beam-1, the SFS screw (Type VB-4.8-7.5x165), which was specially designed for TCC system in Europe, was used as shear connector. Two screws were inserted at each location on LVL joist inclined at 45^o as shown in Figure 3.34 (b). The spacing of the screws was 300 mm for one-third span of the beam from the supports while spacing for one-third span at mid was 600 mm. As such, smaller spacing is used close to the support because of the higher shear force.

In Beam-2, the normal screw (Type 17 with gauge 14) was used as shear connector. The screws were inserted vertically on the LVL joist as shown in Figure 3.35 (b) at equal spacing of 500 mm (see Figure 3.35 c).

In Beams- 3 and 4, identical bird-mouth (or triangular) notch connector with coach screw as part of the connection system was used as shown in Figure 3.36 (b); with the only difference being the arrangement of the notch connections. Beam-3 had six notches spaced at 500 mm and Beam-4 had four notches spaced at 600 mm apart as shown in Figure 3.36 (d) and (e), respectively.

The SFS screw had a measured total length of 220 mm and a measured thread length of 135 mm (see Figure 3.34 a). The measured shank diameter was 6 mm. The 140 mm length was driven into the LVL joist at an angle of 45^o, leaving 80 mm length of the screw into the concrete as shown in Figure 3.34 (b). The normal screw had a measured total length of 100 mm and a measured thread length of 50 mm (see Figure 3.35 a). The measured shank diameter was 5 mm. The 65 mm length was driven into the LVL joist vertically; leaving 35 mm length of the screw into the concrete as shown in Figure 3.35 (b). The coach screw had a measured length of 210 mm and a measured thread length of 125 mm (Figure 3.36 a). The measured shank diameter was 16 mm. The 155 mm length

was driven into the LVL joist vertically, leaving 55 mm length of the screw into the concrete as shown in Figure 3.36 (b).

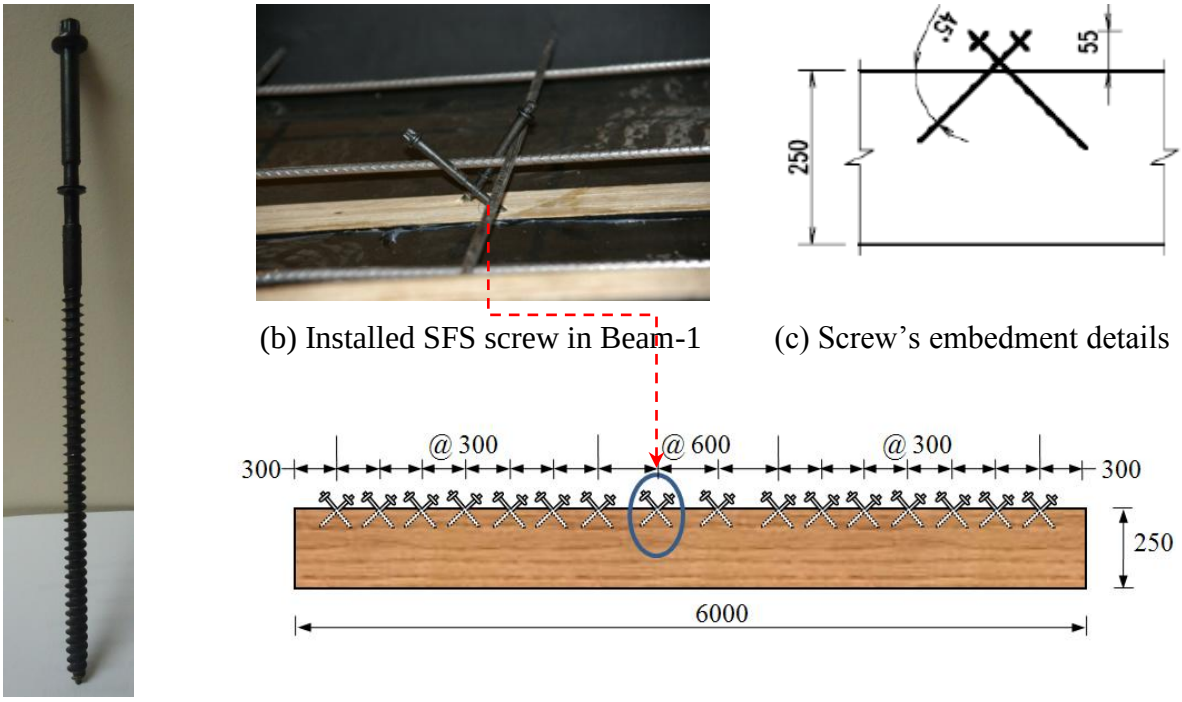

(a) SFS screw

(b) Installed SFS screw in Beam-1

(c) Screw's embedment details

(d) Connectors configuration in Beam-1 (mm)

Figure 3.34 SFS screws used as shear connector in Beam-1.

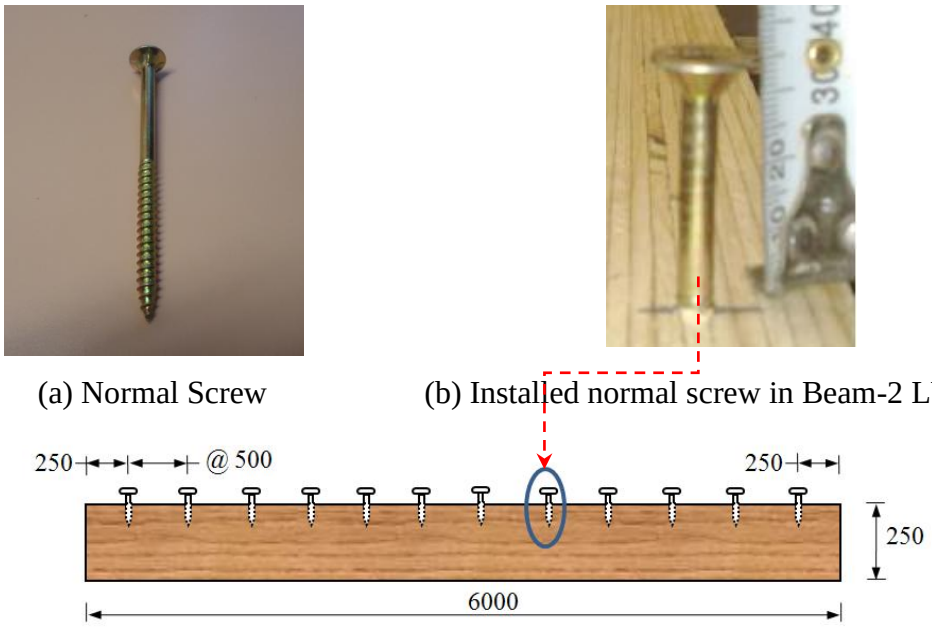

(a) Normal Screw

(b) Installed normal screw in Beam-2 LVL joist

(c) Connectors configuration in Beam-2 (mm)

Figure 3.35 Normal screws used as shear connector in Beam-2.

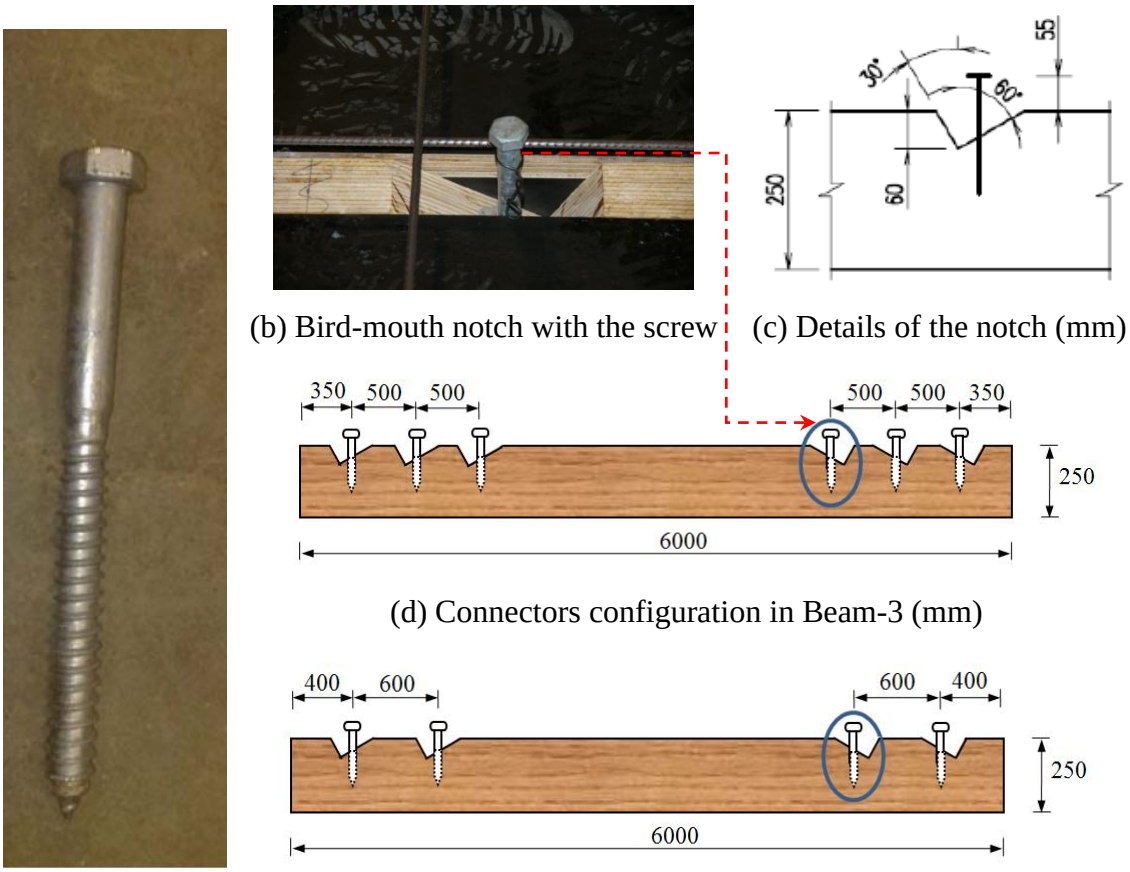

(a) Coach screw

(b) Bird-mouth notch with the screw

(c) Details of the notch (mm)

(d) Connectors configuration in Beam-3 (mm)

(e) Connectors configuration in Beam-4 (mm)

Figure 3.36 Bird-mouth notch with coach screw used in Beams- 3 and 4.

3.4.4 Fabrication of Specimens

These beams were fabricated in UTS laboratory. Formworks of four beams were put side by side before concrete pour as shown in Figure 3.37 (a). Each specimen had three components such as LVL joist, concrete topping and shear connectors. Ready mix concrete with 32 MPa was used for topping, which was compacted using a vibrator. A standard SL72 reinforcement mesh, 7 mm diameter bars at 200 mm spacing in both directions, was provided in the concrete slab to prevent shrinkage cracks. Beams after pouring concrete are depicted in Figure 3.37 (b).

(a) TCC beams before concrete pour

(b) TCC beams after concrete pour

Figure 3.37 Fabrication of TCC beams.

3.4.5 Material Properties

Material properties and general description of three components, namely LVL joist, concrete and shear connectors of the beams are presented in this section. Four point bending tests were conducted on LVL joist of each beam before and after pouring concrete. A summary of test results for each component is presented in the following sub-sections.

3.4.5.1 LVL Joist and TCC Beam

The joists used in TCC beams were made of 250 x 48 mm LVL. The properties of LVL vary from manufacturer to manufacturer as the properties depend upon the veneers used by manufacturer of the LVL. The characteristic values for these LVL joists are given in Table 3.7. Properties presented in this table were supplied by the manufacturer, namely Carter Holt Harvey while the structural properties were determined by testing in accordance to AS/NZS 4357.2 (2006).

Four point bending test was carried out on individual LVL joists of the tested TCC beams with and without notches (as relevant) before and after pouring concrete in accordance to AS/NZS 4357.2 (2006). Figure 3.38 shows the four point bending test set up for LVL joists. A summary of material properties for LVL joists and TCC beams is presented in Table 3.8. Detailed experimental procedure and test results of timber joist and TCC beams can be found in Vu Lam (2010). The density of LVL joist was 620 kg/m^3. MOE of LVL joist was determined using Equation (3.12).

$$E_{LVL} = (23\ P \times L^3)/(648\ \delta \times I) \quad (3.12)$$

where P is the static load (N), L is the span (mm), δ is the mid span deflection (mm), I is the moment of inertia of the section (mm^4).

The results from four point bending tests showed that TCC Beams- 1 and 2 had maximum and minimum stiffness, respectively. The LVL joists of the corresponding beams had slight MOE variation. LVL joist (without notch) used in Beam-2 had maximum MOE value of 16.2 GPa.

Table 3.7 LVL material properties

Properties	Characteristic value
Bending, f'_b	48 MPa
Tension, f'_t	33 MPa
Compression parallel to grain, f'_c	45 MPa
Compression perpendicular to grain, f'_p	12 MPa
Shear in beams, f'_s	5.3 MPa
Shear at joint details, f'_{sj}	5.3 MPa
Modulus of elasticity, E	13.2 GPa
Shear modulus, G	660 MPa
Density at 12% moisture content, ρ	620 Kg/m^3

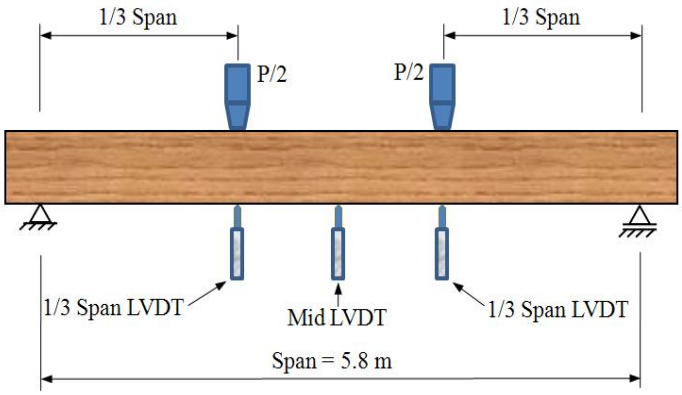

Figure 3.38 Four point bending test setup for LVL beam.

Table 3.8 Material properties of LVL joists and TCC beams (Vu Lam 2010)

Beam	Item	Load	Deflection	Stiffness	MOE (GPa)	
		P (kN)	δ (mm)	P/δ (kN/m)	LVL joist	Concrete
Beam-1	LVL joist without Notch	3.3	15.03	222	14.8	
	TCC Beam	13.5	10.06	1344		27.2
Beam-2	LVL joist without Notch	3.4	15.01	223	14.9	
	TCC Beam	8.2	10.04	811		27.2
Beam-3	LVL joist without Notch	3.7	15.04	243	16.2	
	LVL joist with Notch	3.3	15.08	217	14.4	
	TCC Beam	12.8	10.04	1276		27.1
Beam-4	LVL joist without Notch	3.6	15.08	237	15.8	
	LVL joist with Notch	3.4	15.14	225	15.0	
	TCC Beam	12.1	10.03	1210		27.2

3.4.5.2 Concrete

Normal weight concrete with a characteristic compressive strength of 32 MPa was used for the slab. Compressive strength test was conducted on twelve concrete cylinders on 7, 28, 56 and 91 days from the date of concrete pouring on the LVL joists. The average compressive strength was determined from three 100 mm diameter cylinders out of twelve cylinders each time as per AS 1012.9 (1999) at different stages and corresponding average MOE at the appropriate age was found as per AS 3600 (2001) using Equation (3.13). A summary of these test results for concrete specimens are presented in Table 3.9. Cylinders' compression test data are presented in Table A.6 (Appendix A). The average density of normal-weight concrete was 2,400 kg/m^3.

$$E_{cj} = (\rho)^{1.5}\, x\, \left(0.043\sqrt{f_{cmi}}\right) \tag{3.13}$$

where E_{cj} is the mean value of MOE of concrete at the appropriate age, ρ is the density of concrete (kg/m^3) and f_{cmi} is the mean value of the compressive strength of concrete at the relevant age.

Table 3.9 Summary of concrete properties for tested TCC beams

Test	Compressive strength	MOE
	(MPa)	(GPa)
7 days	23.7	24.6
28 days	39.6	31.7
56 days	44.3	33.6
91 days	50.3	35.8

3.4.5.3 Mechanical Connectors

Four different types of shear connector configurations were used in the four beams (Refer to Section 3.4.3 for details). Types of mechanical connectors used in these shear connector configurations are shown in Figure 3.39. In Beam-1, the SFS screw type VB-4.8-7.5x165 was used as shear connector. In Beam-2, the normal screw type 17 with gauge 14 was used as shear connector. Beams- 3 and 4 had six and four bird-mouth notches, respectively, and each notch had coach screw with 16 mm diameter and 210 mm overall length.

Screw Type:	SFS screw	Coach Screw	Normal Screw
Diameter:	6 mm	16 mm	5 mm
Length:	22 cm	21 cm	10 cm

Figure 3.39 Detail of the mechanical connectors.

3.4.6 Test Setup

All beams were tested under the identical boundary conditions using pin-roller supports at the two ends as shown in Figure 3.40. The pin and roller arrangements were supported on top of concrete blocks. The pin arrangement had a metal shaft between to metal plates having groove on both plates, which constrained horizontal movement, while there was no groove on plates for roller arrangement as it allows horizontal movement to replicate the pin and roller supports (see Figure 3.40). There was no mechanism to prevent vertical movement of the beams; nevertheless, no significant vertical movement was expected due to self-weight of the beam and hammer impact load was also applied gently during the test to minimize bouncing at the supports.

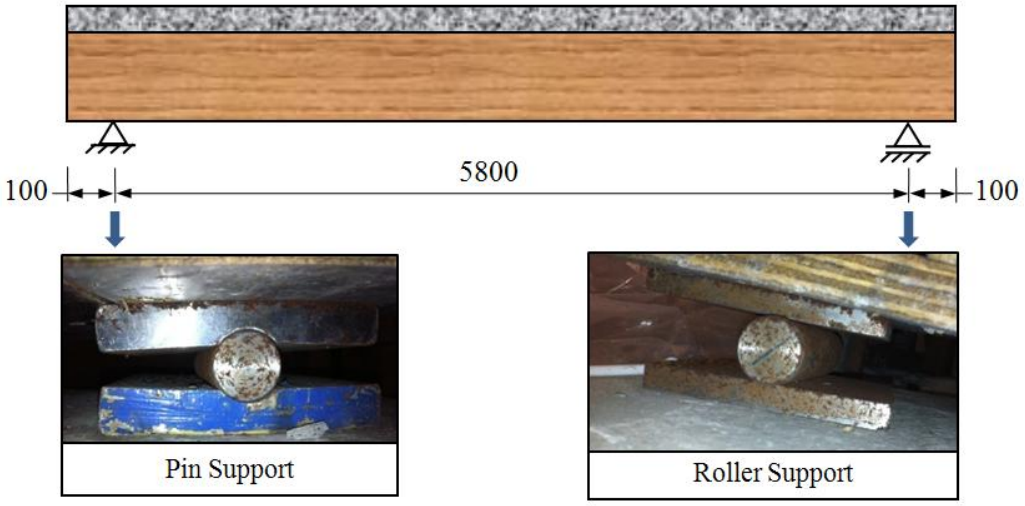

Figure 3.40 Experimental setup for the TCC beams (mm).

3.4.7 Instrumentation and Testing Procedure

Metal plates were attached on the concrete topping using epoxy glue while additional plates were screwed on the LVL joist as shown in Figure 3.41 (a) and (b), respectively, and accelerometers were attached to the plates with double sided tape. In total twenty uniaxial accelerometers, seventeen on the top surface of concrete slab and three at the bottom of LVL joist, were used on each beam to capture acceleration from different locations of the beam as shown in Figure 3.42. The instruments used in the tests are shown in Figure 3.43. The accelerometers (model ADXL320) as shown in Figure 3.43 (a) having a sensitivity of 3.45g per volt were used to capture the response of the beams. The accelerometers measure acceleration with a full-scale range of ±5g. Figure 3.42 depicts the configuration of the accelerometers on the beam as the accelerometers on the top of concrete were placed at equal spacing of 970 mm while spacing at bottom of LVL joist was 1,940 mm.

The locations and the number of accelerometers on the concrete topping were chosen based on the number of modes to be captured and accelerometers at the bottom of LVL joist were chosen to study the degree of composite action of the connection system of the beams. The purpose of using seven accelerometers on the concrete topping along its centreline was to accurately capture the first three flexural modes as shown in Figure 3.44, where numbers 1 to 5 are the nodal points of the three modes and one accelerometer was placed at each node. The natural frequency and damping ratio of

each mode was found. Two accelerometers at the supports were used to see whether uplifting motion is significant. Five accelerometers on the concrete topping along each of its longitudinal edges were used to capture the first two torsional modes and other three accelerometers on the bottom of LVL joist were used to investigate the degree of composite action between concrete topping and LVL joist. However, torsional natural frequencies are not presented in the thesis as flexural modes have more significance in the serviceability design of flooring systems rather than torsional modes and therefore, main focus of this project was on flexural natural frequencies of the beams. Results for the degree of composite action investigation are also not presented in the thesis due to inconclusive results.

All beams were subjected to free vibration initiated by impact from an instrumented modal hammer (PCB model 086D20) (see Figure 3.43 b). Impact force was applied on the top of concrete along its centreline at mid span (node 3) and 1/3 span (node 2) from pin support to excite the first three flexural mode shapes. The multi-channel signal conditioner (PCB model 483B03) as shown in Figure 3.43 (c) was used to amplify and condition the time history signals from the input channel for impact hammer force while output channels for the accelerometers were directly connected to the acquisition system as accelerometers had signal conditioned voltage outputs. The acquisition system had NI SCXI1000 chassis with NI SCXI-1102B cards with 16 bit resolution and sampling rate of 250 KS/sec. The time history signals were captured using LabVIEW (2009) software package.

For all tests, the sampling rate was set to 1000 Hz with 16,384 time domain data points recorded while this corresponds to a frequency bandwidth ranging from 0 to 500 Hz with 8,192 FRF data points giving a frequency resolution of 0.061 Hz in the frequency domain.

(a) Metal plate on concrete topping (b) Metal plate on LVL timber joist

Figure 3.41 An instalment of metal plates.

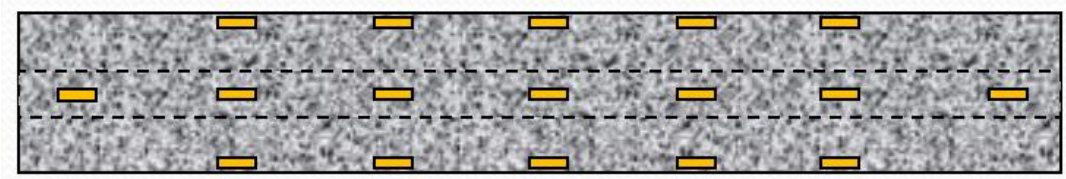

(a) Top view

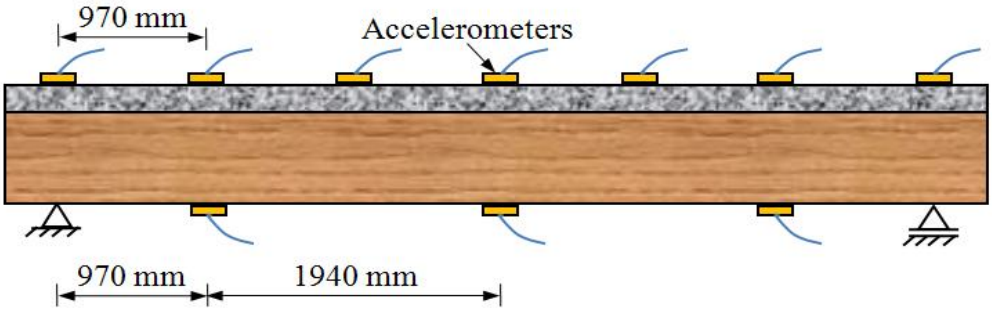

(b) Longitudinal/side view

Figure 3.42 Configuration of the accelerometers on the beam.

(a) Accelerometer

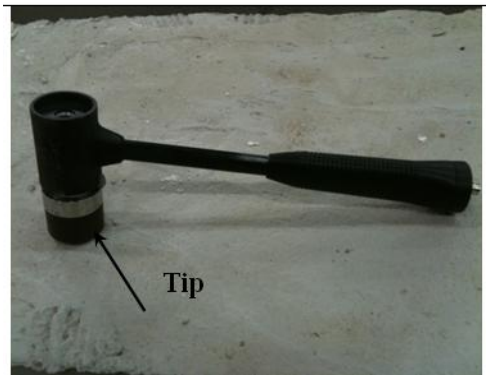

(b) Modal hammer

(c) Multi-channel signal conditioner

Figure 3.43 Test instruments.

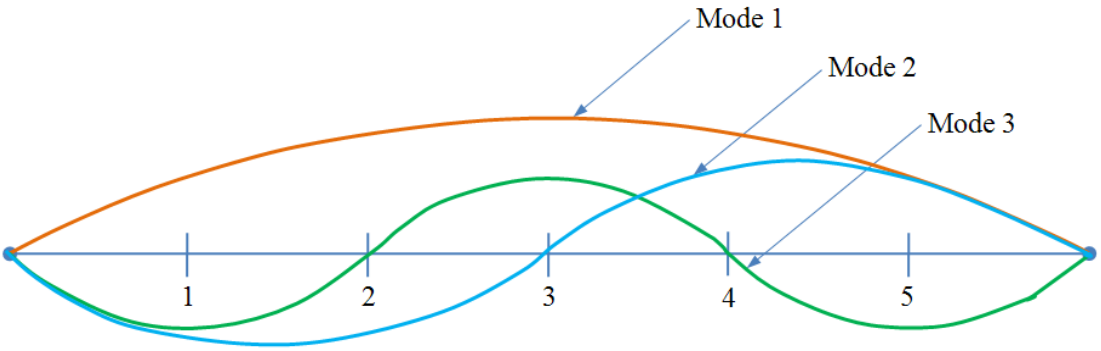

Figure 3.44 The first three flexural mode shapes and their node points.

3.4.8 Data Processing and Analysis

MT and EMA were performed to identify the modal parameters (natural frequencies, damping ratios and mode shapes) of the TCC beams. The MT and EMA configuration is shown in Figure 3.45. The Fourier transformation was used to convert time history signals obtained from impact hammer and accelerometers into frequency spectra. The FRFs were obtained from the ratio of the Fourier transformed output and input signals. For each beam, six test measurements were recorded for six different hammer hits at two different locations of the beams. The modal parameters of the beams were extracted from the FRFs with the use of post-processing module in CADA-X (1996) software package. The dynamic behaviour of the beams was assessed by evaluating their modal parameters and the results are presented in Section 3.5.

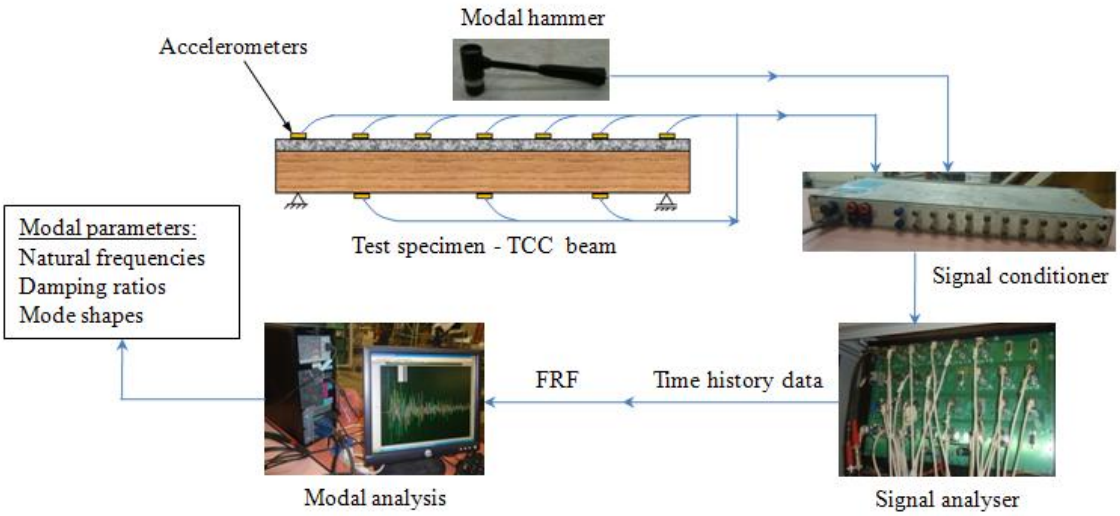

Figure 3.45 MT and EMA configuration.

3.5 Dynamic Test of TCC Beams - Results

3.5.1 Introduction

This section summarises dynamic test results of the four TCC beams with identical geometry, but different connection system and should be read in conjunction with the experimental programme described in Section 3.4. The tests were aimed at comparing the dynamic performance of the beams by evaluating their natural frequencies, damping ratios and mode shapes.

3.5.2 Modal Parameters

The time history signals obtained from accelerometers attached at mid and 1/3rd span of TCC Beam-1 as a sample are shown in Figures A.10 and A.11 (Appendix A), respectively. A typical FRF summation function obtained by adding up the FRFs of seven accelerometers used on the top of concrete topping along its centreline from Beam-1 is shown in Figure 3.46. In the figure distinct peaks are visible, which describe the first three flexural modes. In the displayed frequency bandwidth, ranging from 0 to 100 Hz, additional peaks are also observed. These peaks indicate other modes (torsional or transversal modes).

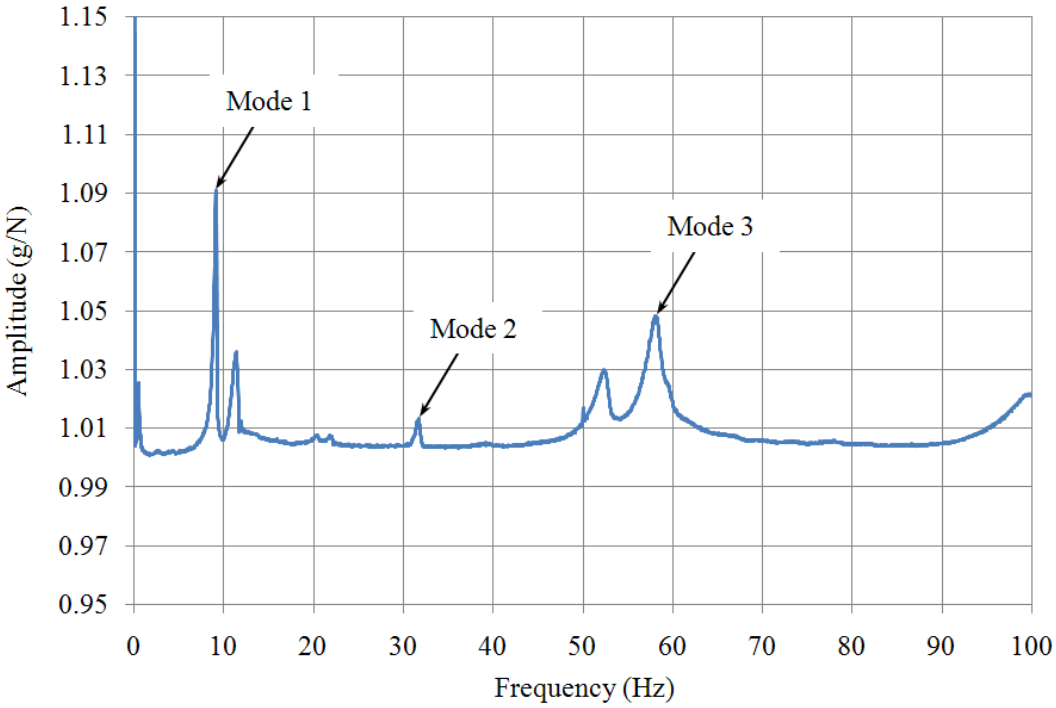

Figure 3.46 FRF summation function of the TCC Beam-1.

A summary of the natural frequencies of the first three flexural modes and the corresponding damping ratios of the beams are presented in Table 3.10. In the same table CoV of the results within each mode of the beams is also presented and it was evaluated based on three sets of data. The detailed results are given in Table A.7 (Appendix A). The results showed that natural frequencies are more consistent compared to damping ratios as the CoV for natural frequencies of the beams is below 1%, which is negligible, while for damping ratio it is below 10% except second mode of Beam-1. The possible cause of CoV can be impact locations, impact force and bouncing

at supports. No general trend is observed between the natural frequencies and damping ratios. In the comparison of natural frequencies of the same mode among the beams no significant difference is observed and the static test results were not consistent among the beams. This comparison shows that the dynamic test could not pick up the effect of different types of connection systems as clearly as the static test.

Fundamental frequency of the beams varies from 8.93 to 10.08 Hz. Beam-3 had the maximum fundamental frequency of about 10 Hz and Beam-2 had the lowest value of about 9 Hz. Results presented in Table 3.10 showed that the connection system in Beam-3 was superior as it had maximum frequency and damping ratio for the fundamental mode among the beams. The fundamental frequency of the Beams- 3 and 4, which had bird-mouth notch with coach screw, is greater than the Beams- 1 and 2 without any notches by about 1 Hz as expected. Hence, the fundamental frequency of the system can be increased by providing notches in the connection system. It is obvious that the dynamic performance is dependent on the screw provided in the notch. For Beams- 1 and 2 with only SFS and normal screws, respectively, no significant difference of the fundamental frequencies was observed (which is about 9 Hz). Between Beams- 3 and 4 there is an increment of frequency of only about 3%. Therefore, increase in the number of notches has minimal effect on the fundamental frequency of the beams. The damping ratio of Beams- 3 and 4 are 1.86 and 1%, respectively. Hence, it can be concluded that an increase in the number of notches has a significant effect on the damping ratio rather than on the fundamental frequency, but one can not rely on the damping ratio with full confidence as it is not as consistent as natural frequencies.

The captured first three flexural modes of Beam-1 are depicted in Figure 3.47. For all modes an uplifting motion was observed for all tested beams as there was no mechanism to constrain vertical motion at pin-roller supports. The bouncing at supports was observed to be higher for higher modes and thus result from higher modes may be affected due to the bouncing.

Table 3.10 First three natural frequencies and corresponding damping ratios of the TCC beams

Beam	Natural frequencies (Hz)			Damping ratios (%)		
	Mode 1	Mode 2	Mode 3	Mode 1	Mode 2	Mode 3
Beam-1	9.00	31.63	57.88	1.00	0.48	1.63
CoV (%)	0.27	0.17	0.06	8.15	13.85	4.59
Beam-2	8.93	30.23	52.90	1.01	0.78	2.37
CoV (%)	0.18	0.46	0.30	2.34	6.37	4.63
Beam-3	10.08	28.02	52.70	1.86	3.32	3.16
CoV (%)	0.16	0.63	0.41	1.78	6.20	5.98
Beam-4	9.76	29.71	52.34	0.97	2.11	1.95
CoV (%)	0.05	0.18	0.30	4.37	4.85	9.86

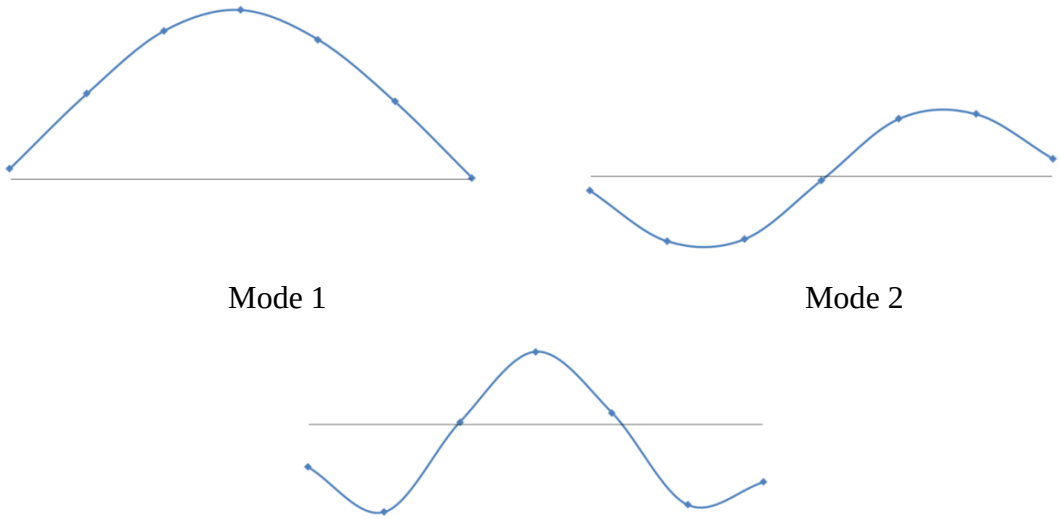

Figure 3.47 First three flexural mode shapes of Beam-1.

3.5.3 Concluding Remarks

Dynamic tests were conducted on four TCC beams with 5.8 m clear span to assess their dynamic performance by evaluating their modal parameters. The following conclusions can be drawn based on the experimental results.

- The results showed that natural frequencies are more consistent compared to damping ratios. The CoV for natural frequencies of the beams was below 1% while for damping ratio it was below 10 %, with the second mode of Beam-1 being an exception and no general trend was observed between the natural frequencies and damping ratios. The damping ratios of the beams were not as consistent as natural frequencies; therefore, it has less reliability.
- The most important modal parameter, namely, the fundamental natural frequency of all beams was above 8 Hz, which falls in the acceptable range. Beam-3 had a maximum fundamental frequency of 10 Hz and Beam-2 had a minimum fundamental frequency of 8.93 Hz. The damping ratio of the Beam-3 was about 1.9% while other three beams displayed a damping ratio of 1% for the fundamental mode.
- The test results showed that the connection system in Beam-3 was superior as it provided maximum frequency and damping ratio for the fundamental mode.
- The fundamental frequency of the beams with notch connection was higher than the beams without any notches by about 1 Hz as expected. Beams- 3 and 4 with notch connection had similar fundamental frequencies of about 10 Hz while Beams- 1 and 2 without notches also had similar frequencies of about 9 Hz. Hence, it can be concluded that bird-mouth connection system can be adopted as shear connectors on the beams to increase their stiffness.
- Further, increase in the number of notches from four to six (Beam-4 had four notches while Beam-3 had six notches) had minimal effect on the fundamental frequency of the beams, but had significant effect on the damping ratio. The fundamental frequency of Beam-3 was only 3% higher than Beam-4 frequency.
- In the comparison of natural frequencies of the same mode among the beams no significant difference was observed while the static test results were not consistent among the beams. This comparison shows that the dynamic test could not pick up the effect of different types of connection systems as significantly as the static test.

3.6 Long-term Dynamic Test of TCC Beams

The aforementioned four identical TCC beams were relocated to the fog room for long-term tests in controlled environmental conditions after conducting short-term static and dynamic tests. The room was sheltered and the beams were protected from direct sun radiation. The beams were loaded in the fog room as shown in Figure 3.48. In accordance with Eurocode 5 (2008), the loading condition may be defined as a long-term load as the load was applied for more than 6 months and less than 10 years.

The beams were loaded using lead bars and they were equally spaced such that a uniformly distributed load of 1.05 kN/m was applied. The load applied was about 41% of the service load. No plasticity in any material was expected to occur immediately after the application of this level of load. For timber-concrete composite floors, a maximum of 20% of the failure load including the self-weight of the floors could be expected for their normal use. The quasi-permanent loads applied on each beam are summarised in Table 3.11. Details of quasi-permanent load and long-term static investigation can be found in Hailu et al. (2012).

Table 3.11 Quasi-permanent load on test beams

Specimen	Shear connector	Uniform load (kN/m^2)
Beam-1	SFS screw	1.74
Beam-2	Normal screw	1.67
Beam-3	Six bird-mouth notches	1.74
Beam-4	Four bird-mouth notches	1.70

Three dynamic tests were conducted on the beams at different time intervals in the fog room as a part of long-term dynamic testing of the beams under identical pin-roller boundary conditions. The main objective of these tests was to evaluate the effects of long-term static loading, and variation in relative humidity and moisture content of the timber joist on the natural frequencies of the beams, especially fundamental frequency. The three tests conducted are summarized in the following sub-sections.

Figure 3.48 Beams under quasi-permanent loads (Hailu et al. 2012).

3.6.1 Dynamic Test 1

The first dynamic test was conducted on all TCC beams as a part of long-term dynamic testing of the beams under the identical pin-roller boundary condition as shown in Figure 3.49. The response signal was measured using a low impedance piezoelectric accelerometer (model PCB 356A08) with a sensitivity ranging from 94 to 100 mV/g as shown in Figure 3.50. The accelerometer was attached on the top of concrete topping close to mid span of the beams. The accelerometer could not be attached at the mid span of the beam as a strain gauge and LVDT were already installed at the mid span for long-term static investigations (see Figure 3.50). To minimize disturbance in the long-term static instrumentation and results, a minimum number of accelerometers and hit locations to excite the beams were chosen. An instrumented modal hammer with brown tip was used to excite the beams (see Figure 3.52 b).

Impact load was applied close to the mid span where accelerometer was attached and 3 sets of data for 3 different hits at the same location were taken for each beam. For all tests, the sampling rate was set to 1000 Hz with 16,384 time domain data points recorded while this corresponds to a frequency bandwidth ranging from 0 to 500 Hz with 8,192 FRF data points giving a frequency resolution of 0.061 Hz in the frequency domain.

There was imposed load and instrumentation on the beams for long-term static investigation when the dynamic test was performed. The dynamic tests had no influence on the static deflection of the beams before and after the tests except in Beam-1, where it was increased by 0.015 mm (which is negligible). Temperature and humidity in the fog room were recorded at 19.6°C and 50%, respectively on the day of testing. Moisture content of the LVL timber was 9.7% on the test day. The variation in moisture content in LVL joist of the beams were monitored using small moisture content sample blocks (100 x 100 x 45 mm). They were cut from the same batch of LVL and were kept in the fog room. Oven dry method was used to measure the changes in the moisture content level. Details about measurement of temperature, humidity and moisture content are presented in Hailu et al. (2012).

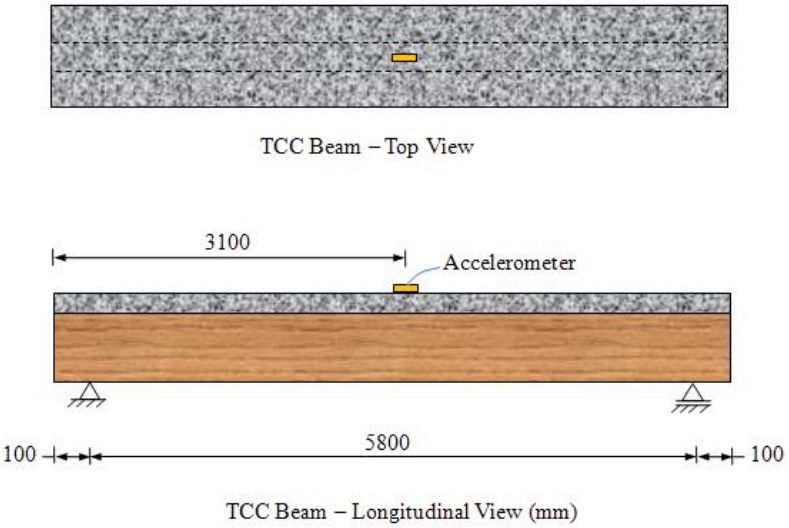

Figure 3.49 Dynamic test 1 setup and instrumentation.

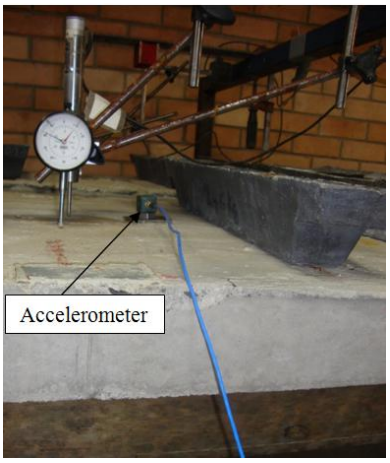

Figure 3.50 Accelerometer model PCB 356A08.

3.6.2 Dynamic Test 2

Dynamic test 2 was performed after about four months from the test 1 being conducted on all beams. The boundary conditions were identical with test 1 and test setup for this test is shown in Figure 3.51. Instruments used in the test are shown in Figure 3.52. Three uniaxial magnetic accelerometers (model PCB 337A26) as shown in Figure 3.52 (a) were used at the top of concrete topping to capture response of the beams from their three different sections as shown in Figure 3.51. An instrumented modal hammer with brown tip (a PCB model 086D20) as shown in Figure 3.52 (b) was used to excite the beams. The multi-channel signal conditioner (PCB model 483B03) as shown in Figure 3.52 (c) was used to amplify and condition the time history signals from the impact hammer and the accelerometers. The input and output channels from signal conditioners were connected to the data acquisition system through terminal block (model SCB - 68) as shown in Figure 3.52 (d), which merely conveyed the time history signals acquired from signal conditioners to the acquisition system without any modification. The acquisition system had two internally synchronised acquisition cards (model NI PCI - 6133 as shown in Figure 3.52 c) with resolution of 14 bit and sampling rate of 2.5 MS/sec, simultaneously.

Impact load was applied at the mid span on the top of concrete and 3 sets of data i.e. for 3 different hits at the same location were taken for each beam. Sampling rate was identical with the test 1. Temperature and humidity in the fog room were recorded at 20.6°C and 70%, respectively, on the day of testing. Moisture content of the LVL timber was 15.5% on the test day.

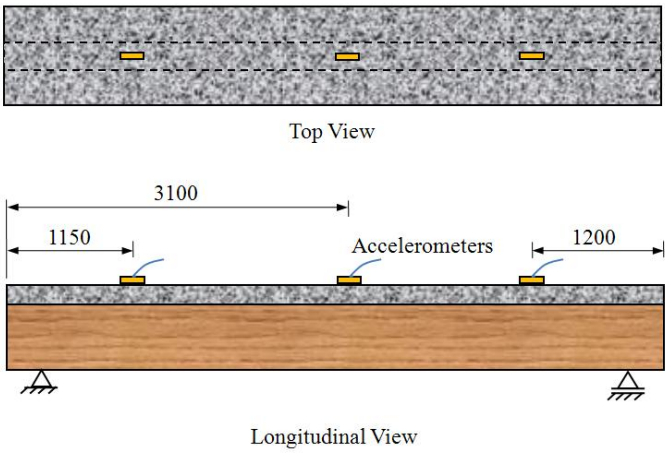

Figure 3.51 Dynamic test 2 setup and instrumentation.

(a) Accelerometer model PCB 337A26

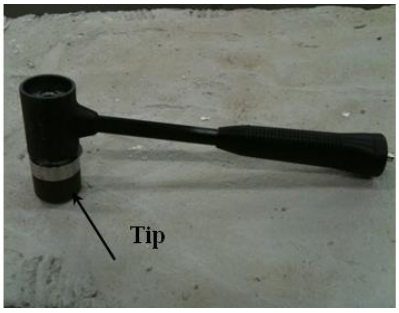

(b) Modal hammer

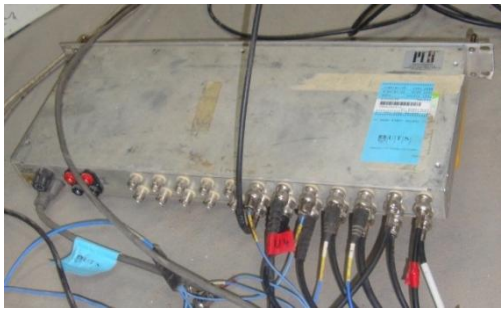

(c) Multi-channel signal conditioner

(d) Terminal block

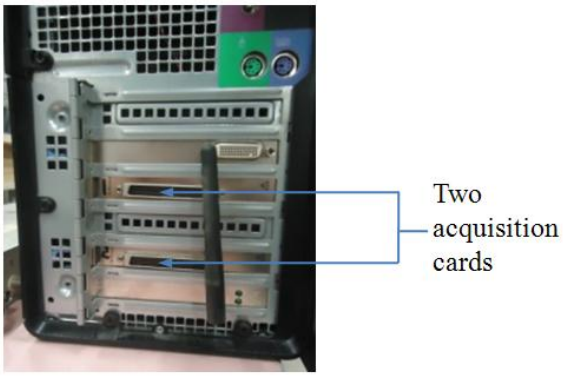

(e) Data acquisition system

Figure 3.52 Test instruments.

3.6.3 Dynamic Test 3

Dynamic test 3 was conducted on the beams after 11 months from test 2 being performed. This test had identical boundary conditions and instrumentation to test 2. Sampling rate was also identical with the tests 1 and 2. Temperature and humidity of the fog room were recorded at 22°C and 67.5%, respectively on the day of testing. Moisture content of the LVL timber was 9.7% on the test day.

3.6.4 Test Results

This section provides the results obtained from three different dynamic tests performed on four identical TCC beams with 5.8 m span as a part of long-term dynamic test. The tests were aimed at comparing the fundamental frequency of the beams at different stages of long-term investigation.

Environmental conditions such as temperature and relative humidity in the room, and moisture content of the LVL timber on the day of three different dynamic tests are summarised in Table 3.12. In test 2, moisture content was significantly higher than test 1, but test 3 had identical moisture content to test 1. Temperature was similar for all tests. Relative humidity of tests 2 and 3 was similar and significantly higher than test 1. The TCC beams were monitored under wetting and drying cycle for long-term investigations, especially static. The temperature and relative humidity presented in the table were measured on the test day and, therefore, moisture content of LVL joist measured on the test day may not be compared directly with the relative humidity as moisture content in the LVL does not change instantly.

A summary of the captured fundamental frequency of the beams acquired from three different tests is summarised in Table 3.13. For all beams, frequencies obtained from test 2 were higher than test 1, which was unexpected, as test 2 had higher moisture content, which increases mass and stiffness resulting in lower natural frequencies. The percentage of frequency increment was similar for Beams- 1 and 4, and the increment was around 5.50%. There was maximum increment of 8.74% for Beam-2 and minimum increment of 1.04% for Beam-3. For most of the beams, the results showed significant change in fundamental frequency with variation in moisture content of LVL timber.

In test 3, frequency of all the beams was lower than test 2. In this test, drop in frequency compared to test 2 was unexpected as moisture content of the LVL was lower than test 2. There was similar decrement of about 5.70% for Beams- 1 and 4. There was maximum decrement of about 30% for Beam-2 and minimum of 5.15% for Beam-3. For all beams, test 3 results also showed significant effect in fundamental frequency with variation in moisture content of LVL timber.

In overall comparison, percentage of increment of frequency of each beam in test 2 compared to the corresponding beam in test 1 and percentage of frequency decrement in test 3 compared to test 2 was significantly different for Beams- 2 and 3 while there was minimal discrepancies for Beams- 1 and 4. The moisture content of LVL timber in tests 1 and 3 was identical, and thus percentage of increment and decrement was expected to be similar. This showed that natural frequency of the flooring systems, especially TCC and timber floors are influenced by a number of factors such as environmental changes (temperature and relative humidity) resulting variation in moisture content of the timber components used in the systems.

Table 3.12 A summary of climate data and moisture content on the day of different tests

Dynamic tests	Temperature (°C)	Relative humidity (%)	Moisture content (%)
Test 1	19.6	50.0	9.7
Test 2	20.6	70.0	15.5
Test 3	22.0	67.5	9.7

Table 3.13 A summary of fundamental frequency of TCC beams

Beam	Shear connector	Fundamental frequency, Hz		
		Test 1	Test 2	Test 3
Beam-1	SFS screws	6.40	6.75	6.37
Beam-2	Normal screws	5.95	6.47	4.56
Beam-3	Six bird-mouth notches	6.73	6.80	6.45
Beam-4	Four bird-mouth notches	6.45	6.82	6.42

3.6.5 Concluding Remarks

The dynamic tests were conducted at different time intervals of a long-term static investigation on four TCC beams with 5.8 m clear span. The main objective of this study was to assess the effects of long-term static action, variation in temperature, relative humidity and moisture content of timber elements in dynamic performance of TCC beams by evaluating their modal parameters, especially fundamental frequency of

each beam. The following conclusions have been drawn based on comparison of three tests:

- Variation in moisture content of the LVL timber has a significant effect on dynamic performance as natural frequency varies with variation in moisture content of LVL timber. The results showed that natural frequency increases with increase in moisture content and vice versa, which is unexpected.
- Creep effects in the beams also influence the dynamic performance as percentage of increment or decrement of natural frequency of corresponding beams was not similar for the same decrement and increment of moisture content in the LVL timber.
- Variation in natural frequency was different for all beams and thus dynamic performance is dependent on shear connectors used in the beams.

University of Technology, Sydney

CHAPTER 4

DYNAMIC PERFORMANCE OF TIMBER FLOOR MODULES

4 Dynamic Performance of Timber Floor Modules

4.1 Introduction

This section provides a summary of dynamic tests performed on two sets of timber floor modules (timber beams). Floor modules in each set had identical geometry while the overall length of the floor modules in the two sets was 6.3 and 8.4 m. The tests were aimed at assessing the dynamic performance of the long-span timber beams by evaluating the modal parameters such as natural frequencies, damping ratios and mode shapes of the beams and to investigate the structural performance of a long-span timber flooring system for both commercial and multi-storey residential applications under the application of dynamic action using modal parameters.

4.2 Test Program

The tests were conducted in the Structural laboratory of UTS. The clear span for 6.3 and 8.4 m timber beams was 6 and 8 m, respectively. All beams were tested with the same pin-roller boundary condition and free vibration was initiated with the use of instrumented hammer. The nomenclature of the specimens is given in Table 4.1.

Table 4.1 A summary of nomenclature of timber beams

Beam	Description
L6-01	1st 6 m span beam
L6-02	2nd 6 m span beam
L6-03	3rd 6 m span beam
U8-01	1st 8 m span beam
U8-02	2nd 8 m span beam
U8-03	3rd 8 m span beam

4.3 Geometry of the Timber Beams

The design of both 6 and 8 m span beams were governed by serviceability limit state criteria (Zabihi et al. 2012), which is not uncommon for long-span timber beams. The shape of the sections was chosen based on the following number of advantages of using the sections to the floor construction.

- It has sufficient space between the webs for the installation of services.
- The space also allows for installation of acoustic insulation.
- It has versatile application in the floor construction as it can be used as upside-down in the modular construction and an additional layer such as concrete topping can be applied on the top of it to increase the stiffness of the flooring systems that reduces vibration and static issues.
- It is more stable compared to the "T" and "I" sections.

The cross sectional dimensions for the 6 m span beams are shown in Figure 4.1. Two types of LVL such as hySPAN Cross-banded and hySPAN PROJECT were used in the fabrication of the beams. The hySPAN Cross-banded LVL was used for top flange while webs and bottom flanges were made from hySPAN PROJECT LVL. The top flange was 600 mm wide and had a depth of 35 mm while the bottom flanges had a width of 120 mm and a depth of 35 mm. The webs were 180 mm deep and 45 mm thick.

The dimensions of the 8 m span timber beams are depicted in Figure 4.2. The top flange was identical with 6 m span beams but the bottom flanges had a width of 140 mm. The webs were 270 mm deep and had a thickness of 45 mm. The top and bottom flanges of all beams were glued and screwed to the web. Further details of the specimens can be found in Zabihi et al. 2012.

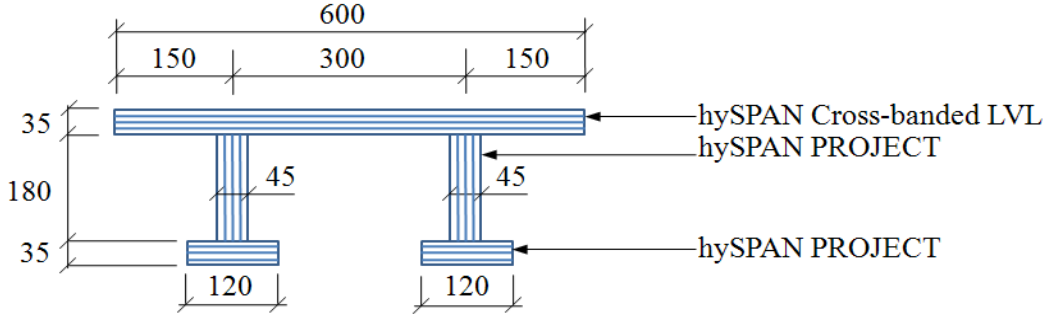

Figure 4.1 Dimensions of the 6 m span timber beams (mm).

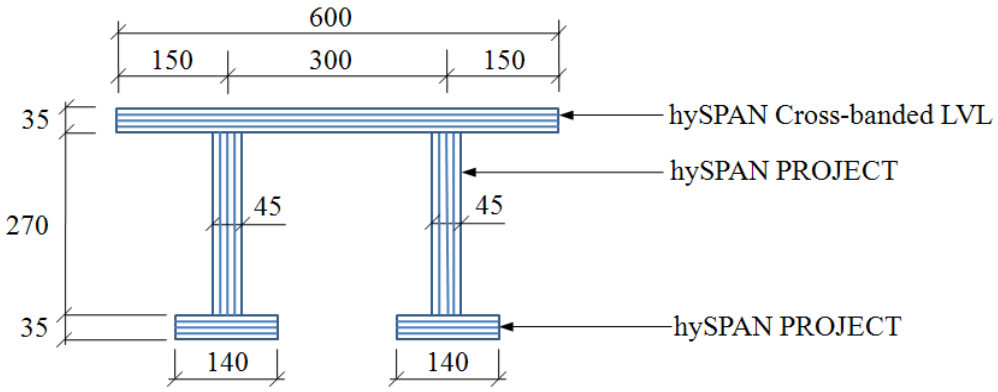

Figure 4.2 Dimensions of the 8 m span timber beams (mm).

4.4 Material Properties

4.4.1 LVL Timber

A number of bending, shear, compression, and tension tests were conducted on all components (top flange, webs and bottom flanges) of the timber beams at UTS to characterise the basic properties of the LVL. Flat-wise properties for the top and bottom flanges and edge-wise properties for the web were tested which replicate the orientation of the flanges and web in the tested beams.

A summary of the results (mean values) for individual components of the beams is presented in Table 4.2. The dynamic performance of the systems is highly sensitive to the MOE and density of the timber beams. A minimum of eleven samples were tested for each component to find MOE of the LVL and the flanges have higher variability in the MOE values within individual components compared to the webs. Bottom flanges have maximum CoV of 12.3%. The density of the components shows that there is no signification variation within individual components and among the components. The rest of the properties of each component also have significant variation within and among the components (Zabihi et al. 2012).

Moisture content (MC) of the four timber beams was measured on the day of testing in accordance to AS 1080.1 (1997) using oven dry method and the results are presented in Table 4.3. For each beam three small LVL timber blocks (test pieces) were used to measure the MC of the tested beams and the size of the pieces was 100 x 100 x 50 mm. The test pieces were put on top of tested beams one week before testing. On the day of

testing weight of the test pieces was measured by weighing with a balance and put in the drying oven for 24 hours at a temperature range of 102°C to 105°C. The dry weight of the test pieces was measured after 24 hours and was again put in the oven for a further 24 hours to ensure that moisture was removed completely. The MC values were calculated using mass of the test pieces before (initial weight) and after (dry weight) putting in the oven and the percentage of MC of a test piece was determined using Equation (4.1). The MC results show that there is no significant difference in the MC values of the timber beams and it varies from 8.2 to 10.0% among the timber beams which was tested over a period of 20 weeks. As such, the MC will not have any significant effect on the dynamic parameters of the tested beams.

$$MC = (M_i - M_o)/M_o \times 100 \quad (4.1)$$

where M_i is the initial mass of test piece, M_o is the oven-dry mass of test piece.

Table 4.2 Material properties of LVL timber (*Courtesy of Zhinus Zabihi as part of a concurrent PhD study*)

Component Name	MOE	Density	Bending	Shear	Compression	Tension	MoR
	E_x (GPa)	ρ (kg/m^3)	f_b (MPa)	f_v (MPa)	f_c (MPa)	f_t (MPa)	G (MPa)
Top flange	9.6	606.5	49.5	5.1	42.1	34.1	189.8
CoV (%)	10.7	1.0	19.4	7.2	7.8	6.5	16.6
Webs	13.3	603.7	66.1	6.7	51.1	37.4	554.3
CoV (%)	4.0	1.3	9.8	4.2	7.6	13.5	16.0
Bottom flanges	13.1	601.1	65.5	5.8	51.4	36.4	239.5
CoV (%)	12.3	1.8	17.1	15.0	8.2	4.7	25.5

Table 4.3 Moisture content of the beams

Beam	L6-01	L6-02	L6-03	U8-01	U8-02	U8-03
Moisture Content (%)	*	*	8.3	8.2	8.8	10

*Note: * The MC value was not measured.*

4.4.2 Mechanical Connectors

All beam components were connected with the combined use of glue and normal wood screw (Type 17) as shown in Figure 4.3 as shear connector to connect top and bottom flanges to the webs without any indentation on its LVL components. The screw had a measured total length of 90 mm and thread length was measured at 45 mm. The measured shank diameter was 5 mm. The screws were installed at a spacing of 375 and 385 mm for 6 and 8 m span beams, respectively. The interface between flanges and web was assumed to be fully composite as no slip was observed during the four point bending test under service load. Bond between flange and web were not expected to be broken when tested under hammer impact load.

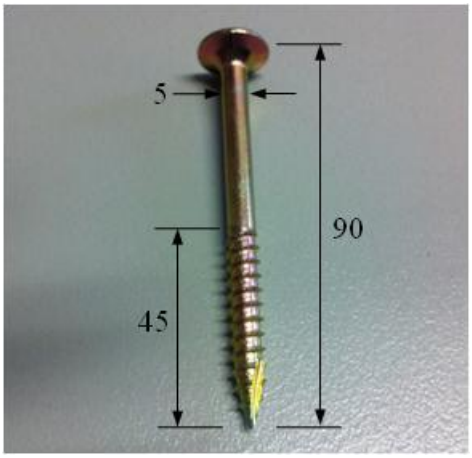

Figure 4.3. The dimensions of the screw used in the timber beams (mm).

4.5 Test Setup

All specimens were tested under the same boundary conditions using pin-roller supports. The pin and roller arrangements were supported on top of concrete block. The pin arrangement had a metal shaft between two metal plates having grooves on both plates, which constrain horizontal movement; while there was no grooves on top plate for roller arrangement as it allows horizontal movement to replicate the pin and roller supports (see Figure 4.4). There was no mechanism to prevent vertical movement due to large complex cross sectional geometry of the beams; nevertheless, no significant vertical movement was expected due to self-weight of the beam and hammer impact load was also applied gently during the test to minimize bouncing at the supports. The

schematic diagram of boundary conditions for 6 and 8 m span beams are depicted in Figures 4.4 and 4.5, respectively.

Figure 4.4 A schematic diagram of setup for 6 m span timber beam (mm).

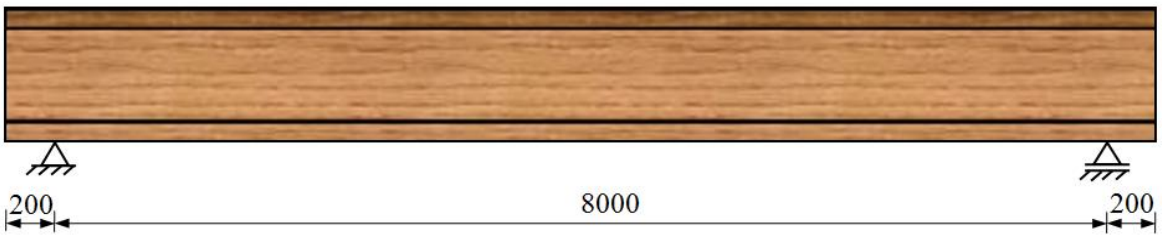

Figure 4.5 A schematic diagram of setup for 8 m span timber beam (mm).

4.6 Instrumentation and Testing Procedure

Fifteen magnetic uniaxial accelerometers were mounted at different locations of the beams to measure their responses as depicted in Figure 4.6 and their position at each section is shown in Figure 4.7. At mid span five accelerometers, two on the top flange, 1 at the bottom flange and two on the web were used as shown in Figure 4.7 (c). The instruments used in the test are shown in Figure 4.8. The accelerometers were ICP type with PCB model 352C34 and 337A26 as shown in Figure 4.8 (a) and (b), respectively, having a sensitivity of 100 mV/g. The full instrumentation for 6 m span beams is shown in Figure 4.9. The instrumentation for 8 m span beams was identical to 6 m span beams.

The purpose of using seven accelerometers on the top flange along its centreline was to capture the first three flexural modes accurately as shown in Figure 4.10, where numbers 1 to 5 are the nodal points of the three modes and one accelerometer was placed at each node. Two accelerometers at the supports were used to see whether bouncing is significant. Five accelerometers on the top flange on the side were used to capture the first two torsional modes and other five accelerometers on the web and bottom flanges were used to study the degree of composite action between flange and web.

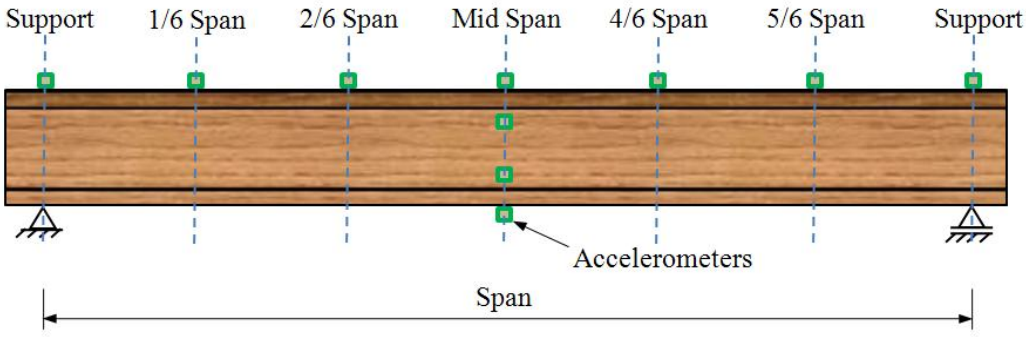

Figure 4.6 The arrangement of the accelerometers along the span.

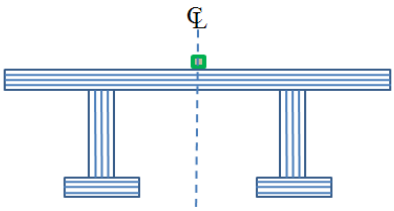

(a) Cross-section showing location of one accelerometer at supports

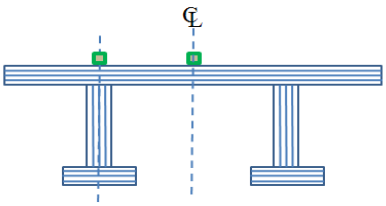

(b) Cross-section showing location of two accelerometers at 1/6, 2/6, 4/6 and 5/6 span

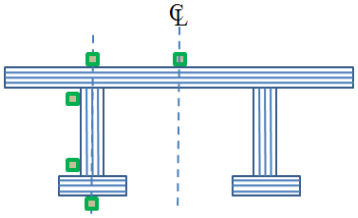

(c) Cross-section showing location of five accelerometers at mid span

Figure 4.7 Location of the accelerometers at different sections of the beams.

All beams were subjected to free vibration initiated by impact from an instrumented modal hammer (PCB model 086D20) as shown in Figure 4.8 (c). Impact force was applied on the top of top flange at mid span (node 3) to excite the first and third flexural modes and at 2/6 span (node 2) from pin support along its centreline to excite the second flexural mode. None of the first three flexural mode shapes has a node point at 1 or 5, but the hammer impact load was not applied at these nodes to minimize interference from the supports and for better excitation. The multi-channel signal conditioner (PCB model 483B03) as shown in Figure 4.8 (d) was used to amplify and condition the time history signals from the impact hammer and the accelerometers. The input and output channels from signal conditioners were connected to the data acquisition system through terminal block. Terminal block (model SCB - 68) as shown in Figure 4.8 (e) conveyed the time history signals acquired from signal conditioners to the acquisition system without any modification by integrating all channels into a single cable, which made possible to connect channels to the acquisition system. The acquisition system had two internally synchronised acquisition cards (model NI PCI - 6133) with resolution of 14 bit and sampling rate of 2.5 MS/sec, simultaneously.

For all tests, the sampling rate was set to 1000 Hz with 16,384 time domain data points recorded while this corresponds to a frequency bandwidth ranging from 0 to 500 Hz with 8,192 FRF data points giving a frequency resolution of 0.061 Hz in the frequency domain. The following features were integrated in the signal acquisition system to improve the quality of the input or excitation (impact hammer force) and output or response (accelerometer measurements) signals in the time domain (amplitude versus time).

- A pre-trigger delay was used to ensure that the entire impact excitation signal was captured.
- A force window was applied to the input channel to remove noise from the impulse signal and to thereby minimise spectral leakage.
- An exponential window was used for the output channels to ensure that the transient signals showed sufficient decay at the end of the sampling period (Dackermann 2010).

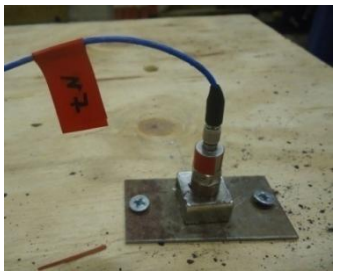

(a) Accelerometer model PCB 352C34

(b) Accelerometer model PCB 337A26

(c) Modal hammer

(d) Multi-channel signal conditioner

(d) Terminal block

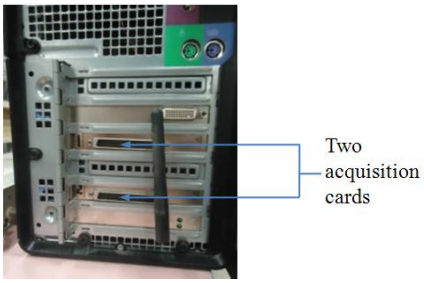

(e) Data acquisition system

Figure 4.8 Test instruments.

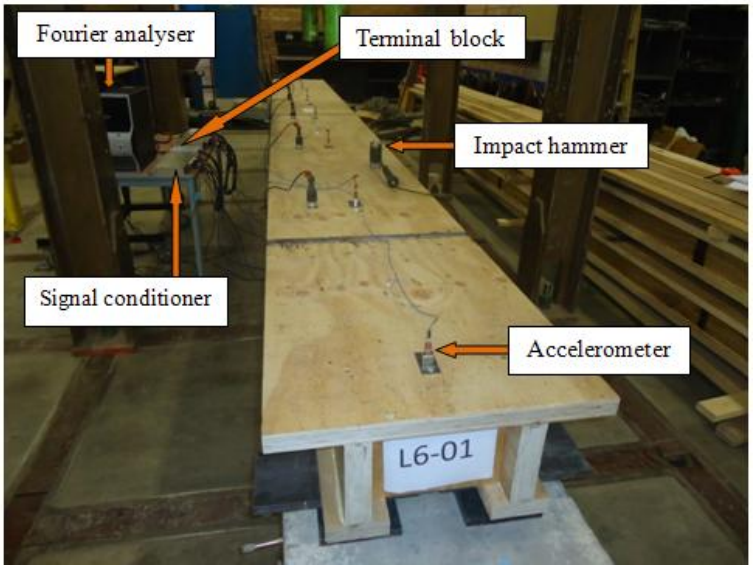

Figure 4.9 Instrumentation for a 6 m span timber beam.

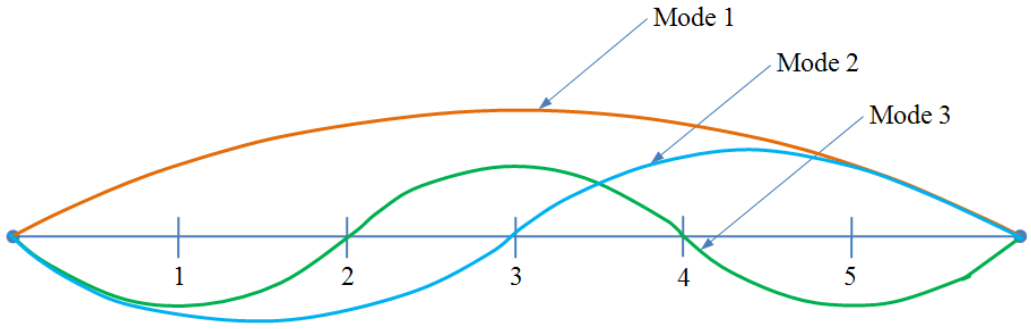

Figure 4.10 First three flexural mode shapes and their node points.

4.7 Data Processing and Analysis

MT and EMA was performed to identify the modal parameters (natural frequencies, damping ratios and mode shapes) of the 6 and 8 m span timber beams. The MT and EMA configuration is shown in Figure 4.11. The Fourier transformation was used to convert time history signals obtained from impact hammer and accelerometers into frequency spectra. The time history signals obtained from accelerometers attached at mid and 1/3rd span of the timber beam, L6-01, as a sample are shown in Figures B.1 and B.2 (Appendix B), respectively. The FRFs were obtained from the ratio of the Fourier transformed output and input signals. For each beam, 10 measurements were recorded for 10 different hammer hits at two different locations of the timber beam. The modal parameters of the timber beams were extracted from the FRFs with the use of post-processing module in CADA-X (1996) software package. The dynamic behaviour of the timber beams was assessed by evaluating their modal parameters and the results are presented in Section 4.8.

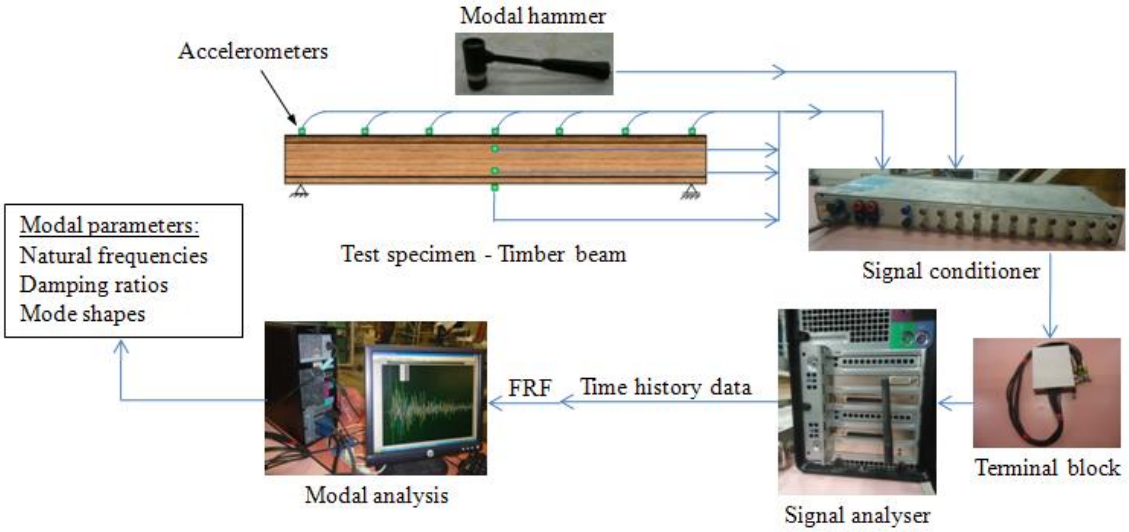

Figure 4.11 MT and EMA configuration.

4.8 Timber Floor Modules - Results

This section provides the results obtained from dynamic tests performed on three identical timber beams with 6 m span and three with 8 m span. The tests were aimed at comparing the fundamental frequencies, damping ratios and mode shapes of the 6 and 8 m span timber beams and to investigate the structural performance of a long spanning timber flooring system for both commercial and multi-storey residential applications under the application of impact action using modal parameters.

4.8.1 Modal Parameters

A summary of the captured three flexural natural frequencies and the corresponding damping ratios of the 6 and 8 m span timber beams is summarised in Table 4.4. In the same table mean value and CoV of the results for 6 and 8 m span timber beams is also presented. The results show discrepancies within 6 and 8 m span beams owing to a number of factors such as material properties, shear connectors (screws and glue), minor discrepancies in the geometry, moisture content, bouncing at supports and minor discrepancies in the boundary conditions. There was no major discrepancy within 6 m span beams as the CoV was only 1 to 2% for all modes, but for the 8 m span beams CoV was 2 to 9%. The discrepancies are expected mainly due to material properties variation and the sensitivity analysis performed on material properties variation is presented in Section 5.2.7.

The natural frequencies of the 6 m span beams have CoV of 1.02, 1.84 and 2.10% for modes 1 to 3, respectively. The 8 m span beams have CoV of 1.62, 4.64 and 8.50% for modes 1 to 3, respectively. For both 6 and 8 m span beams it is noted that the frequency discrepancies are larger when the mode is higher as local damage influence the higher modes compared to the fundamental mode. The fundamental mode is quite important from design point of view and higher modes to identify the local damage, and for health monitoring.

The damping ratios of the 6 m span beams have CoV of 6.07, 14.45 and 7.16% for modes 1 to 3, respectively. The 8 m span beams have CoV of 10.36, 14.10 and 17.01% for modes 1 to 3, respectively. There was no general trend between the damping ratios

and the natural frequencies. The damping ratio of the higher modes was lower compared to the fundamental mode.

The captured first three flexural modes of beam U8-01 are depicted in Figure 4.12. For all modes an uplifting motion is observed as expected for all tested beams as there was no restrain in the vertical direction at the supports owing to complexity of pin-roller arrangements. The bouncing at supports was observed higher for the higher modes.

Table 4.4 A summary of test results of the 6 and 8 m span timber beams

Beam	Natural frequencies (Hz)			Damping ratios (%)		
	Mode 1	Mode 2	Mode 3	Mode 1	Mode 2	Mode 3
L6-01	16.47	56.60	100.63	0.60	0.36	0.30
L6-02	16.16	54.61	97.05	0.68	0.28	0.34
L6-03	16.40	55.23	97.05	0.66	0.37	0.33
Mean	16.34	55.48	98.25	0.65	0.33	0.32
CoV (%)	1.02	1.84	2.10	6.07	14.45	7.16
U8-01	13.25	43.32	80.68	0.64	0.35	0.48
U8-02	12.89	42.52	71.47	0.58	0.46	0.43
U8-03	13.27	46.39	84.53	0.52	0.41	0.34
Mean	13.14	44.08	78.89	0.58	0.40	0.42
CoV (%)	1.62	4.64	8.50	10.36	14.10	17.01

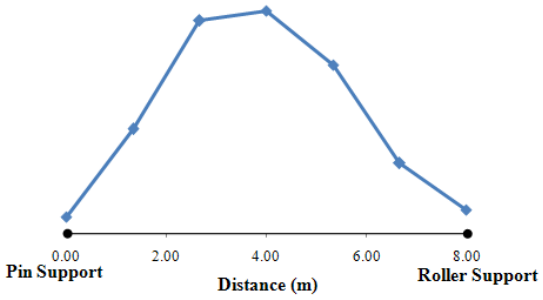

(a) Mode 1

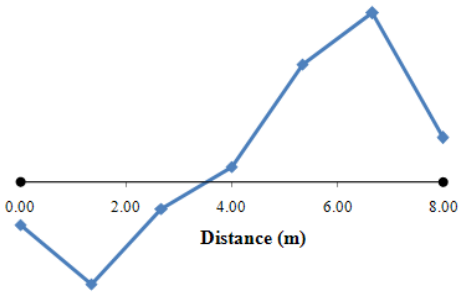

(b) Mode 2

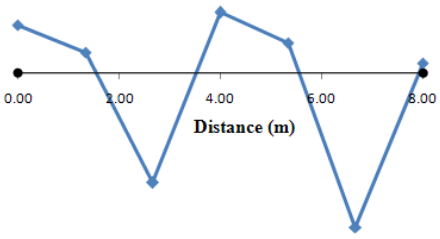

(c) Mode 3

Figure 4.12 First three flexural mode shapes of the timber beam U8-01.

4.9 Concluding Remarks

Dynamic tests were conducted on six timber beams, three with 6 m and three with 8 m clear span, to assess their dynamic performance based on the modal parameters. The following conclusions can be drawn based on the experimental results.

- The mean fundamental frequency of the 6 and 8 m span beams was 16.34 and 13.14 Hz, respectively and the damping ratio was 0.65% and 0.58%, respectively.
- For these floor modules the fundamental frequencies are all above 10 Hz as recommended by most codes of practice. However, some supplementary analysis and/or testing of full flooring systems consisting of several interconnected modules is required to establish whether or not the floor system frequency remains satisfactory.
- No general trend was found between the natural frequencies and damping ratios. The damping ratio of the higher modes was lower compared to the fundamental mode.

- The results showed discrepancies within 6 and 8 m span beams due to a number of factors such as material properties, shear connectors (screws and glue), minor discrepancies in the geometry, moisture content, bouncing at supports and minor discrepancies in the boundary conditions. For higher modes, the bouncing at supports was observed to be higher.

University of Technology, Sydney

CHAPTER 5

FINITE ELEMENT MODELLING

5 Finite Element Modelling

Finite element (FE) method is a numerical modelling technique to determine the behaviour of real structures to external and internal loads by dividing it into several elements. It describes the response of each element and the behaviour of the whole system can be obtained by reconnecting elements at nodes as if the nodes are glue holding elements together. It is one of the main computing tools for engineers due to its cost and time efficiency compared to the physical experiments. Some commercially available FE softwares are ANSYS, ABAQUS, SAP, LS-DYNA, ATENA, MICTROSTRAN, DIANA, ALGOR, and MFEAP. ANSYS can be used to solve linear and non-linear static and dynamic structural, acoustic, heat transfer, fluid flow and electromagnetic problems (ANSYS 2011).

Outputs from FE modelling are not necessarily 100% accurate, but can be obtained to a desired level of accuracy. The accuracy of the results from FE analysis depends upon the quality of the input data such as material properties, choice of element type, boundary conditions and mesh size, etc. The FE model is considered accurate when it is updated based on experimental results. The updated model can be used for the parametric study and to demonstrate the performance of the test sample under the application of various types of actions. Hence, a FE model needs to be calibrated against limited experiments to confirm whether results from it are acceptable.

In this thesis, ANSYS was used to develop FE models of TCC beams and timber floor modules presented in Chapters 3 and 4, respectively.

5.1 TCC Beams

5.1.1 Introduction

This chapter presents the numerical analysis of the tested TCC beams (details can be found in Section 3.4 of Chapter 3). The numerical analysis was performed by developing linear elastic FE models to simulate their behaviour. FE models for the TCC beams were created using ANSYS (2011) which is a commercially available FE analysis package. The FE models were used to obtain relevant modal parameters and to assess dynamic performance of the TCC beams. ANSYS was used for the FE modelling

due to the availability of high performance cluster nodes at computing resources of UTS, where multiple ANSYS models could be run simultaneously. Any other FE package can be used equally successfully provided that material models and boundary conditions can be properly simulated.

In this chapter, the fundamental principles and modelling approach in using the FE method are first discussed followed by the type of elements and material models used to model the different components of the beams. Further, verification of the ability of ANSYS to model the behaviour of the TCC beams is presented in this chapter. Deflection of the beams acquired from FE model is correlated with experimental result to verify the ability of ANSYS. The FE models of the four identical TCC beams tested with different connection systems were developed and then the models were calibrated and validated against the experimental results described in Section 3.4. The modal analysis was performed on the beams to acquire their modal parameters such as natural frequencies and mode shapes, and the results are discussed.

5.1.2 Layered Model for TCC Beams

The layered model represents behaviour of two materials model such as timber and concrete. Layered 2-D FE model was created and the model was then calibrated and validated with the static and impact hammer test results. The concrete topping was modelled without conventional reinforcement as minimal reinforcement was provided to control crack and minimal effect is expected due to its presence in the mechanical behaviour of the beams. Similar behaviour has been reported in Davison (2003).

The dimensions of the FE model were based on the measurements of the four tested TCC beams. The beams were T-shaped as shown in Figure 5.1 and had identical geometry with an overall length of 6 m and a clear span of 5.8 m. The LVL joists were 250 mm deep and had a thickness of 48 mm, while the concrete slab, which was cast on the top of LVL joist, had a depth of 75 mm and a width of 600 mm.

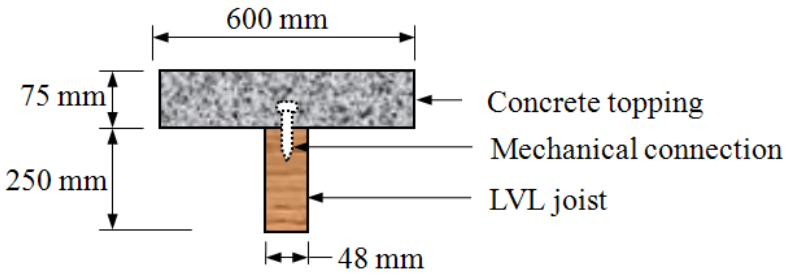

Figure 5.1 Cross-sectional view of the TCC beams.

5.1.2.1 Element Types

The elements for the models were selected from the ANSYS (2011) element library as they represent both static and dynamic response of the timber and concrete.

The 2-D element, namely, PLANE42 (four nodes) was utilized to model both LVL joist and concrete topping of the TCC beams. Higher order element PLANE182 also gives the same accuracy as PLANE42 element. PLANE42 element was used as a plane element with plane stress with thickness. It was defined by four nodes having translations in the x and y directions at each node as shown in Figure 5.2. It can also be defined by three nodes, however, not recommended for modelling. The main input properties of this element were elastic modulus, density and poisons ratio of the LVL and concrete topping. It has plasticity, creep, swelling, stress stiffening, large deflection, and large strain capabilities (ANSYS 2011).

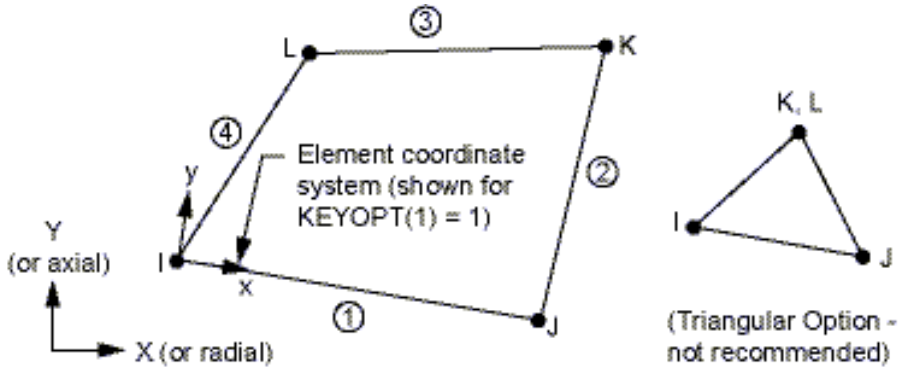

Figure 5.2 Geometric properties of PLANE42 (ANSYS 2011).

The interface between LVL joist and concrete topping was simulated utilizing contact and target elements to prevent the penetration of the joist and concrete topping elements to each other during deformation and for the stability of model. CONTA171 and

TARGE169 were chosen as contact and target elements, respectively. The bottom layer of the concrete topping was defined as contact surface while the top layer of timber joist was defined as target surface as shown in Figure 5.3. Therefore, contact elements were generated at the bottom layer of concrete topping and target elements were generated at the top layer of LVL joist. The contact element was used to represent contact and sliding between 2-D surfaces such as contact and target surfaces. The contact element is applicable to 2-D structural and coupled field contact analyses. This element is located on the surfaces of 2-D solid, shell, or beam elements without mid-side nodes such as PLANE42. It has the same geometric characteristics as the solid, shell, or beam element face with which it is connected to (see Figure 5.4). Contact occurs when the element surface penetrates one of the target segment elements such as TARGE169 on a specified target surface. Coulomb friction, shear stress friction, and user defined friction with the USERFRIC subroutine are allowed and therefore, friction between surfaces can be modelled using these contact and target elements. The interface delamination can also be simulated utilizing this element as it allows separation of bonded contact (ANSYS 2011). No separation was permitted at timber-concrete interface, but sliding was allowed.

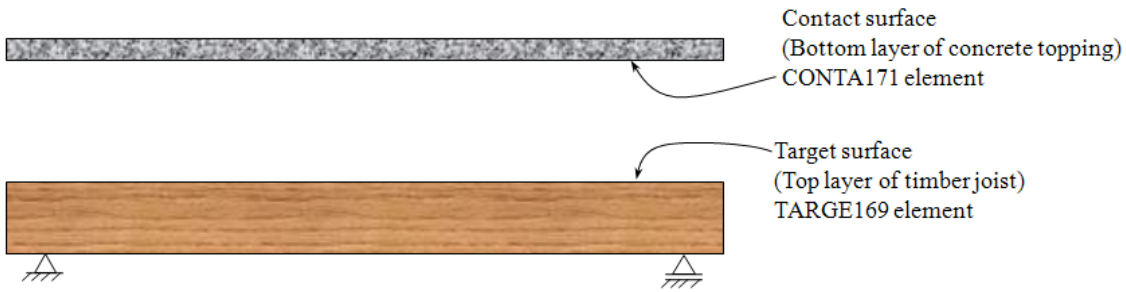

Figure 5.3 A schematic diagram of the TCC beams showing contact and target surfaces.

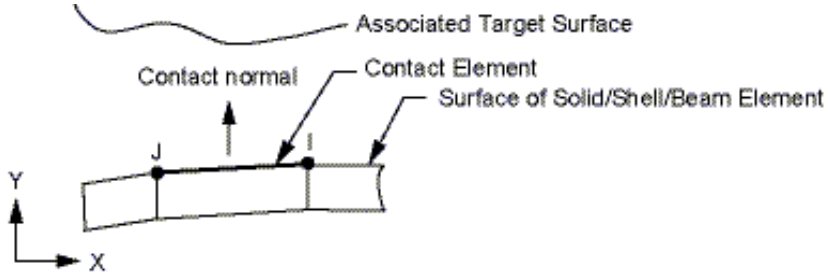

Figure 5.4 Geometric properties of CONTA171 (ANSYS 2011).

TARGE169 was utilized to represent various 2-D target surfaces for the associated contact elements such as CONTA171. The contact element itself overlays the solid elements describing the boundary of a deformable body and is potentially in contact with the target surface, defined by TARGE169. This target surface is discretised by a set of target segment element, namely TARGE169 and is paired with its associated contact surface having the same real constant set. Any translational or rotational displacement, temperature, voltage, and magnetic potential can be imposed on the target segment element. Moreover, forces and moments can be applied on target elements. For rigid targets, these elements can easily model complex target shapes. For flexible targets, these elements will overlay the solid elements describing the boundary of the deformable target body. The geometric properties of the TARGE169 are shown in Figure 5.5 (ANSYS 2011).

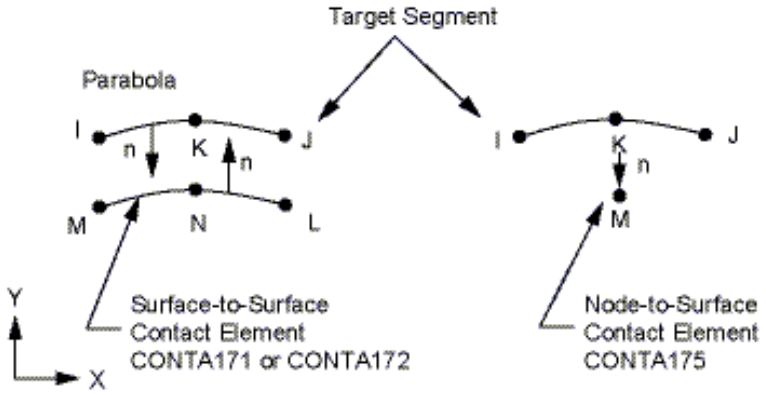

Figure 5.5 Geometric properties of TARGE169 (ANSYS 2011).

The shear connector of the beams was simulated using COMBIN39. This element is a unidirectional element with non-linear generalized force-deflection capability that can be used in any analysis. It is defined by two coincident nodes and a generalized force-deflection curve as shown in Figure 5.6. The serviceability stiffness of the shear connection systems acquired from push-out tests was used for this element and was defined by two coincident nodes, one node at timber and another at concrete. It has longitudinal or torsional capability in 1-D, 2-D, or 3-D applications. The longitudinal option is a uniaxial tension-compression (no bending or torsion considered) element with maximum three degrees of freedom at each node such as translations in the nodal x, y, and z directions. The torsional option is a purely rotational element, where bending and axial loads are not considered, with three degrees of freedom at each node like

rotations about the nodal x, y, and z axes. It has large displacement capability for which there can be two or three degrees of freedom at each node (ANSYS 2011).

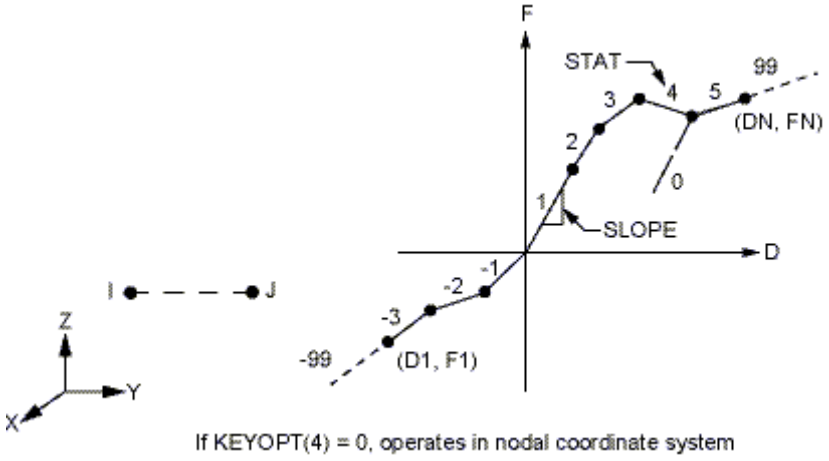

Figure 5.6 Geometric properties of COMBIN39 (ANSYS 2011).

5.1.3 Materials Properties

The properties of LVL joist, concrete and shear connectors are utilised in the FE model based upon their respective material tests. These properties include MOE (E_x), density (ρ) and Poisson's ratio (υ) of LVL joist and concrete and stiffness of shear connector. The sensitivity analysis of the orthotropic behaviour of the LVL joist showed similar results to isotropic behaviour. The material properties were assumed isotropic because it was deemed sufficient to represent the flexural stiffness in longitudinal direction along the span length as this is the major contribution to the overall stiffness of a TCC system. This is also acceptable considering that the modal analysis is within elastic range.

The material properties of LVL joists and concrete used for FE modelling are summarized in Table 5.1. The MOE values of LVL joists of individual TCC beams were found by conducting four point bending test on them before pouring concrete. The density of normal weight concrete was chosen as per AS 3600 (2001). The properties of shear connector of individual beams were characterised by conducting push-out tests on test samples (Refer to Section 3.1). The characteristic properties of the shear connector in the individual beams are presented in Table 5.2. The values of Poisson's ratio for LVL joist (pine timber) and concrete were approximated using Wood Handbook (General Technical Report FPF-GTR-113 1999) and AS 3600 (2001), respectively.

Table 5.1 Material properties of LVL joist and concrete topping of TCC beams

Beam	LVL joist			Concrete		
	MOE (E_x) (GPa)	Density (ρ) (kg/m^3)	Poisson's ratio (υ)	MOE (E_x) (GPa)	Density (ρ) (kg/m^3)	Poisson's ratio (υ)
Beam-1	14.75	620	0.3	35.9	2,400	0.3
Beam-2	14.88					
Beam-3	16.16					
Beam-4	15.77					

Table 5.2 Characteristics results for different connection systems in the TCC beams

Beam	Connection description	Connection		
		Strength (kN)	Stiffness (kN/mm)	
		Q_k	K_{serv}	K_u
Beam-1	SFS screw	30.3	58.0	34.0
Beam-2	Normal screw	9.6	49.0	7.0
Beam-3	6 Bird-mouth notches with coach screw	55.0	37.0	36.0
Beam-4	4 Bird-mouth notches with coach screw	55.0	37.0	36.0

5.1.4 Modelling Approaches and Assumptions

Modelling assumptions and techniques used in this study are presented in this section. Some assumptions and techniques are specific to ANSYS.

5.1.4.1 Boundary Conditions

The boundary conditions for the model were set as pin-roller, which was close to the real boundary conditions of the TCC beams as shown in Figure 5.7. Translations in global X and Y axis were restrained to simulate the pin support while translation in global Y axis was restrained for roller support at the other end. For both supports, rotation about global Z axis was allowed.

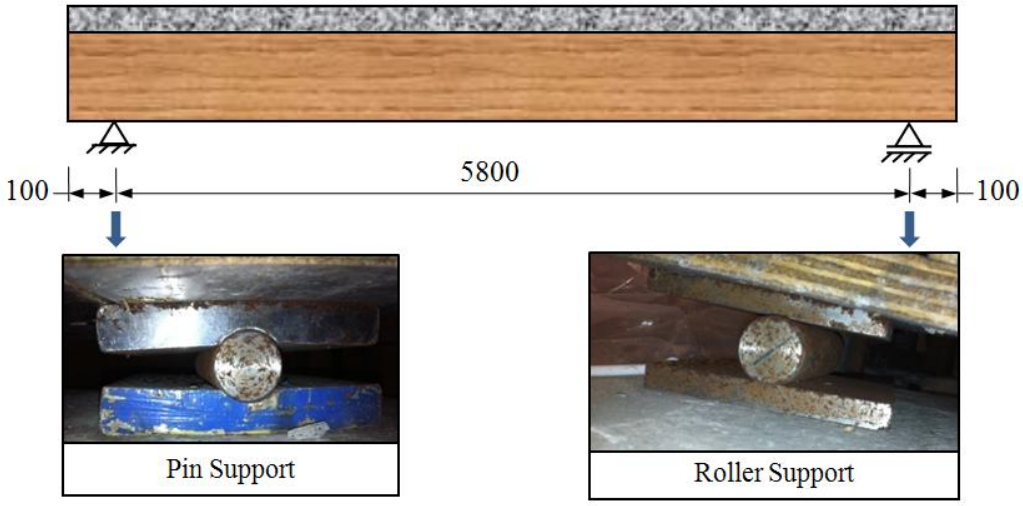

Figure 5.7 Experimental setup for the TCC beams (mm).

5.1.4.2 Mesh Size

To obtain sufficient accuracy in FE analysis, a sensitivity analysis was performed on the model for both static and free vibration analyses. FE mesh configurations with different size of elements were analysed to obtain mid span deflection for the static analysis and fundamental frequency (first natural frequency) for the free vibration analysis. The sizes of the elements in the longitudinal directions of the TCC beam chosen were 100, 50, 40, 25, 20, 12.5, 10 and 5 mm. The size of the elements was uniform throughout the span and aspect ratio of the elements was kept below 2. The timber-concrete interface was assumed to be fully composite for the sensitivity analysis. The results for the static and free vibration analyses are plotted against the number of elements in Figures 5.8 and 5.9, respectively. From the analyses it was observed that more than 12,480 elements having uniform size of 12.5 x 12.5 mm were appropriate to obtain for accurate results. The increment of total number of elements from about 19,800 to 78,000 merely increases the mid span deflection by about 0.2 %.

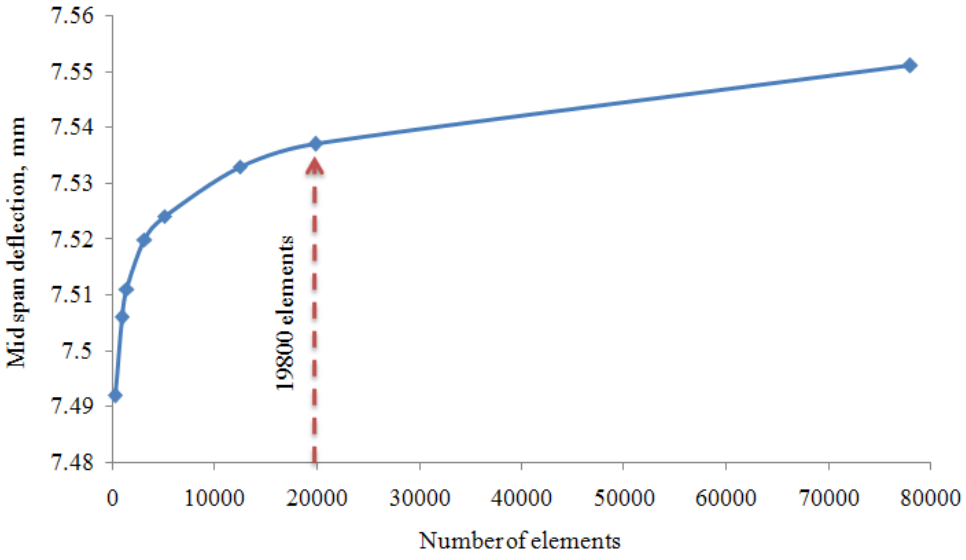

Figure 5.8 A sensitivity analysis for mesh density for static analysis.

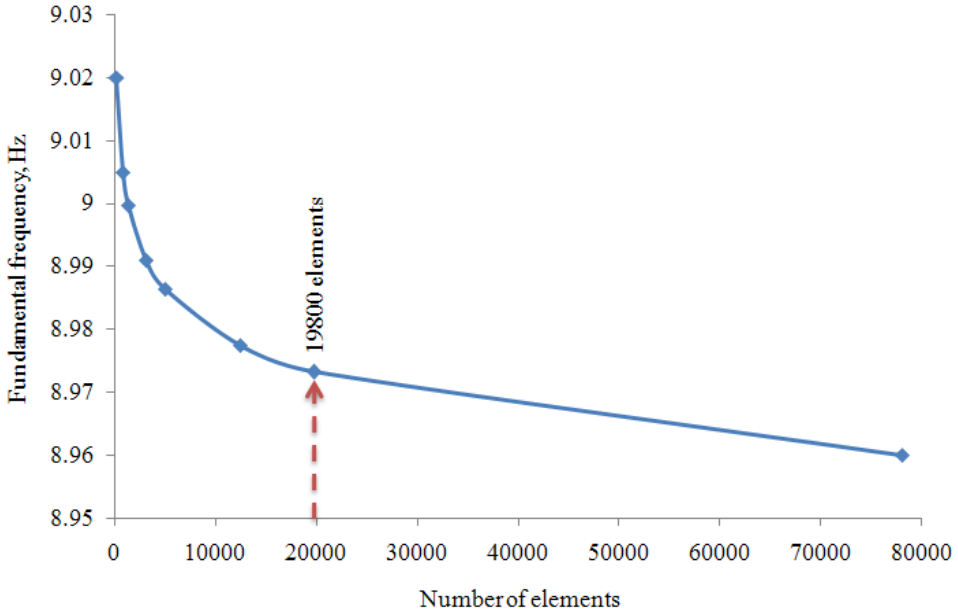

Figure 5.9 A sensitivity analysis for mesh density for dynamic analysis.

The size of the mesh in all the FE models was based on the mesh sensitivity. The size of the elements chosen for timber and concrete were 10 x 10 mm and 10.0 x 9.4 mm, respectively as shown in Figure 5.10. In total, the FE models of the beams consist of 21,016 elements. The contact pair was generated at timber and concrete interface.

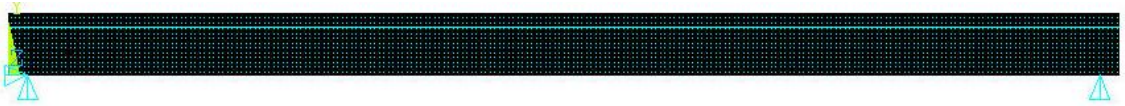

(a) Overall view of FE model of the TCC beams.

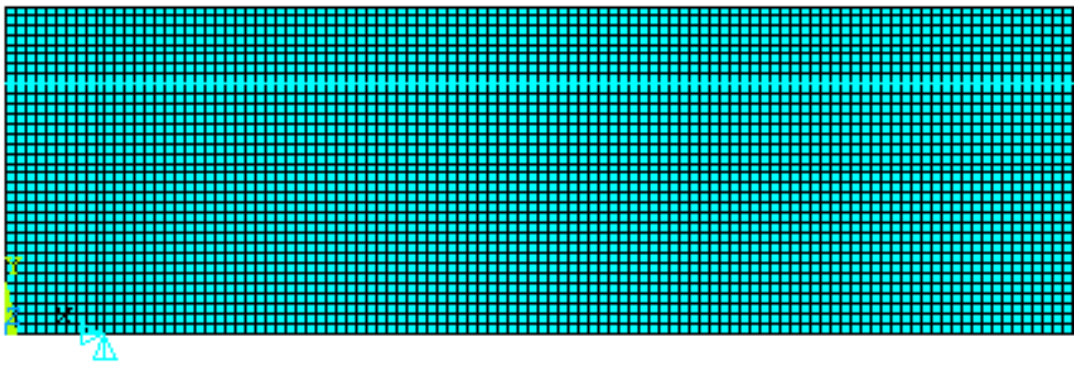

(b) Enlarged view of FE model of TCC beams from left end.

Figure 5.10 Nodes and elements for FE model of the TCC beams.

5.1.4.3 Dynamic Characteristics of the Beams

The first three flexural mode shapes of the beams were extracted from the FE model as shown in Figure 5.11 by solving the eigenvalue problem using the modal analysis module in ANSYS. The details of the mode shapes and their natural frequency from experiment and FE model are described in Tables 5.3 and 5.4. These mode shape data obtained from FE model were mass normalised, such that the modal vector satisfies Equation (5.1) (Farrar & Juaragui 1996).

$$\{\emptyset_n\}^T [m]\{\emptyset_n\} = 1 \tag{5.1}$$

where $\{\emptyset_n\}$ is the normalised modal vector and $[m]$ the mass matrix. Letting Ψ_n represent the original modal amplitudes obtained numerically or experimentally before the mass normalisation process, the normalised modal amplitude, φ_n, is formulated using Equation (5.2).

$$\{\emptyset_n\} = \frac{1}{\sqrt{M_n}}\{\Psi_n\} \tag{5.2}$$

where M_n is expressed as below;

$$M_n = \sum_{i=1}^{p} \Psi_{in}^2 m_i \tag{5.3}$$

In Equation (5.3), p represents the number of measured points and n is the mode shape number.

Table 5.3 Description of mode shape

Mode	Mode shape
1	First flexural mode
2	Second flexural mode
3	Third flexural mode

Table 5.4 Experimental and FE natural frequencies (Hz) of the TCC beams

Beam	Experiment, $f_{n(Exp)}$			FE, $f_{n(FE)}$		
	Mode 1	Mode 2	Mode 3	Mode 1	Mode 2	Mode 3
Beam-1	9.00	31.63	57.88	9.39	29.01	50.26
Beam-2	8.93	29.42	52.90	8.98	28.42	47.45
Beam-3	10.08	28.02	52.70	8.63	22.12	44.60
Beam-4	9.76	29.71	52.34	8.14	21.17	42.10

(a) Mode 1 of Beam-1

(b) Mode 2 of Beam-1

(c) Mode 3 of Beam-1

Figure 5.11 First three flexural mode shapes for the FE Beam-1 model.

5.1.4.4 Correlation between FE and Experimental Results

To validate the FE models, a correlation analysis between FE and experimental results of the TCC beams is conducted. In general, the correlation analysis is defined as a technique to examine quantitatively and qualitatively the correspondence and difference between analytically and experimentally acquired modal parameters such as natural frequencies and mode shapes (Brownjohan & Xia 1999). The correlation analysis is essential to validate or calibrate the FEM. The aim of validating or calibrating the FEM is to minimise the discrepancies between test and FE results such as natural frequency and mode shapes. In this section, natural frequency from FE models is correlated with test results. The discrepancy for natural frequency is defined as an error function *(NFerror)*. The error function *(NFerror)* for natural frequencies obtained from FEM and experimental work is given as:

$$NFerror = \frac{\left|\omega_{Exp} - \omega_{FE}\right|}{\omega_{Exp}} \, x \, 100 \tag{5.4}$$

where ω_{Exp} and ω_{FE} are the natural frequencies obtained from experiment and FEM, respectively. The values of the natural frequency for the first three flexural modes of the TCC beams and their *NFerror* values are listed in Table 5.5 and Figure 5.12. The correlation showed that the *NFerror* values are higher for higher modes due to their higher uplifting at supports and sensitivity to local defects. The values for mode 1 are below 5% for Beams- 1 and 2 while the values are about 15% for Beams- 3 and 4. These significant *NFerror* values for Beams- 3 and 4 are attributable to lower serviceability stiffness of their shear connector, namely bird-mouth notch with coach screw, acquired from push-out test than expected value. The stiffness of the connection was expected to be higher than normal screw shear connection. For Beams- 1 and 2 the results showed that the natural frequency obtained from the FEM match very well with the experimental results. Hence, the FEM for Beams- 1 and 2 can be used to predict their natural frequency with sufficient accuracy while for Beams- 3 and 4 calibration is needed by choosing the approximate but relevant serviceability stiffness values for bird-mouth notched connection to predict natural frequency with acceptable accuracy.

Table 5.5 Correlation between FEM and experimental results of TCC beams

Beam-1	Mode1	Mode 2	Mode 3
FEM (Hz)	9.39	29.01	50.26
Experiment (Hz)	9.00	31.63	57.88
Absolute difference (Hz)	0.39	2.62	7.62
NFerror (%)	4.33	8.28	13.17
Beam-2			
FEM (Hz)	8.98	28.42	47.45
Experiment (Hz)	8.93	30.23	52.90
Absolute difference (Hz)	0.05	1.81	5.45
NFerror (%)	0.56	6.00	10.30
Beam-3			
FEM (Hz)	8.63	22.12	44.60
Experiment (Hz)	10.08	28.02	52.70
Absolute difference (Hz)	1.45	5.9	8.1
NFerror (%)	14.38	21.06	15.37
Beam-4			
FEM (Hz)	8.14	21.17	42.1
Experiment (Hz)	9.76	29.71	52.34
Absolute difference (Hz)	1.62	8.54	10.24
NFerror (%)	16.60	28.74	19.56

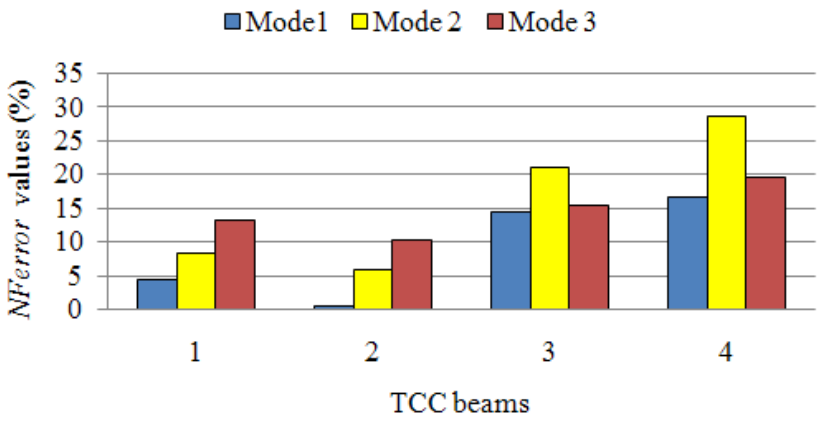

Figure 5.12 *NFerror* values of four TCC beams.

5.1.5 Calibration of FE Model

The FE models for Beams- 3 and 4 are calibrated to match the FE results with experimental results as *NFerror* values were significant or beyond acceptable range for these beams while these values were within acceptable range for Beams- 1 and 2. The Beams- 3 and 4 had identical shear connector, only the number of notches was different. They have similar *NFerror* values; therefore, the serviceability stiffness of the notched connections is increased, which reduces *NFerror* values, to calibrate the models against experimental results. To calibrate the models, the stiffness of 98 kN/mm was chosen for bird-mouth notched connection as thickness of LVL joist used in the beams was 48 mm. The stiffness value was derived from stiffness versus LVL joist thickness plot (acquired from Push-out test) as shown in Figure 5.13 (Gerber & Crews 2011). FE results for Beams- 3 and 4 with derived stiffness value of 100 kN/mm of bird-mouth notched connection are presented in Table 5.6 and shown in Figure 5.14. The correlation for calibrated FEM showed the *NFerror* values below 10% for first mode while the values are over 10% for other modes of Beams- 3 and 4, with the third mode of Beam-3 being an exception. The result showed that stiffness of the shear connector had no significant influence on second flexural mode of Beams- 3 and 4.

Table 5.6 Correlation between calibrated FEM and experimental results of Beams- 3 and 4

	Mode 1	Mode 2	Mode 3
Beam-3			
FEM (Hz)	9.41	22.78	47.51
Experiment (Hz)	10.08	28.02	52.70
Absolute difference (Hz)	0.67	5.24	5.19
NFerror (%)	6.65	18.70	9.85
Beam-4			
FEM (Hz)	8.94	21.48	44.82
Experiment (Hz)	9.76	29.71	52.34
Absolute difference (Hz)	0.82	8.23	7.52
NFerror (%)	8.40	27.70	14.37

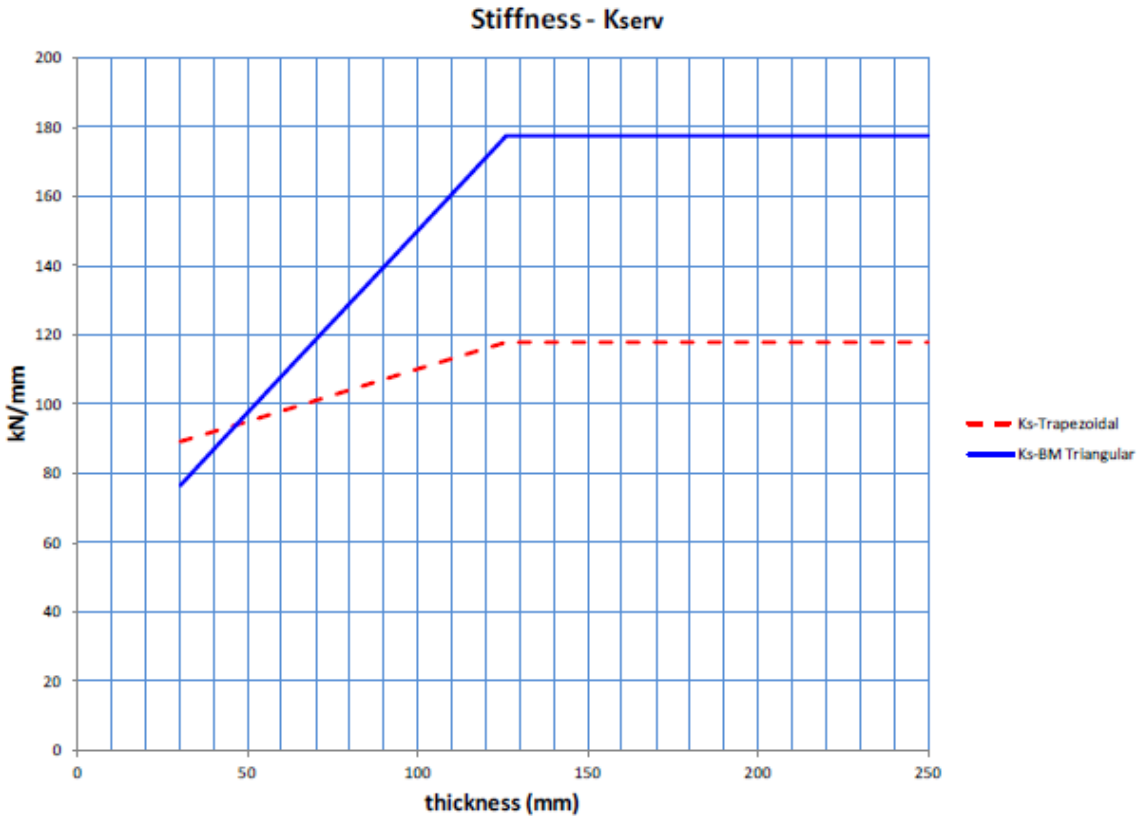

Figure 5.13 Serviceability stiffness (K_{serv}) of notched connections (Gerber & Crews 2011).

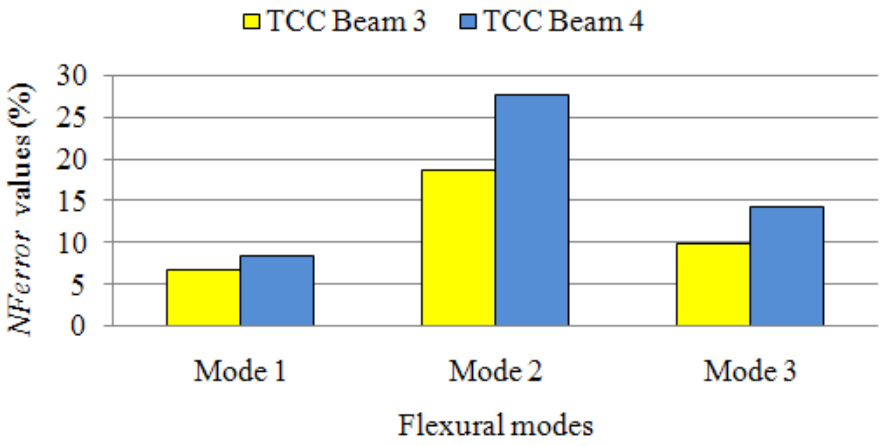

Figure 5.14 *NFerror* values of TCC Beams- 3 and 4 after calibration.

5.1.6 Validation of FE Model against Static Test

To validate the FE models for TCC beams, the results from FE model was also compared with static test results. Four point bending test was conducted on each TCC

beams. In the FE model the total static load, which was the summation of loads at 1/3rd span from each support and required to result in equivalent experimental mid span deflection of the beams, was found and correlated with the experimental total load producing the same deflections at mid span. The correlation of the FE and static test results of the beams is shown in Figures 5.15 to 5.18. The correlation showed the load error value below 10% for Beams- 1, 3 and 4, which was in the acceptable range. Beam-2, with normal screws, had relatively much higher load error values, which are shown in Figure 5.16.

In the FE model, no separation was allowed at timber-concrete interface, only sliding was permitted. However, timber and concrete tend to separate during static loading and the magnitude of separation depends upon the characteristic properties of the shear connector. Embedment strength of shear connector on LVL joist also influences the delamination tendency. The strength depends upon various factors such as embedment depth, diameter, type of thread and types of screw. Normal screw in Beam-2 had relatively low embedment depth compared to shear connectors in rest of the beams. Further, it had smaller diameter compared to coach screw. Hence, magnitude of separation in Beam-2 was expected to be higher, as a consequence, the correlation showed higher load error values, nevertheless, the model predicted natural frequency in modal analysis within acceptable accuracy. In dynamic analysis, the applied load was not as high as static load; therefore, separation in dynamic analysis was not expected to be as significant as in static analysis.

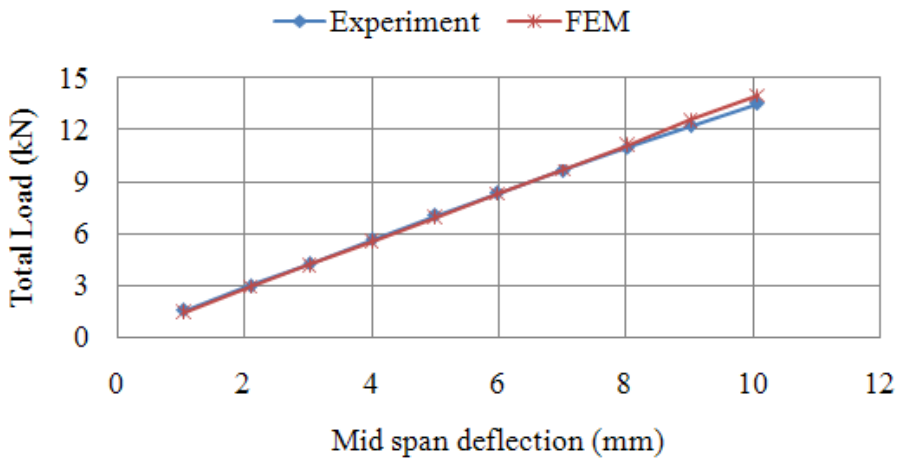

Figure 5.15 Validation of Beam-1 FE model with static deflection.

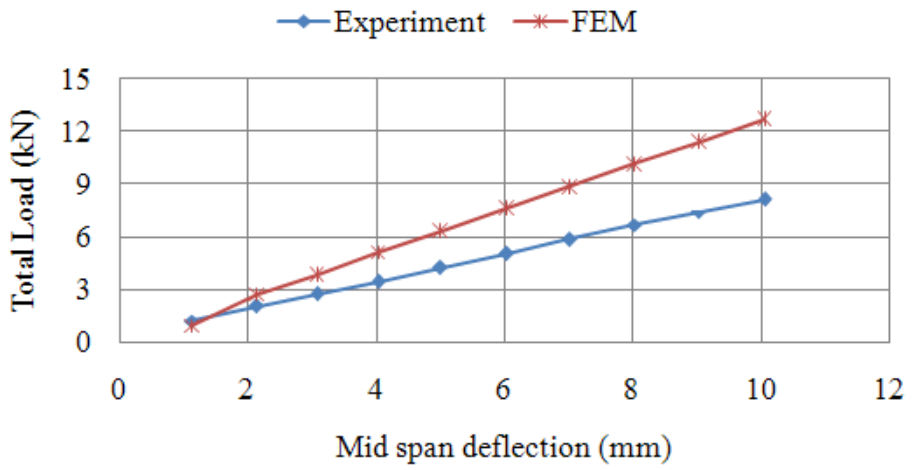

Figure 5.16 Validation of Beam-2 FE model with static deflection.

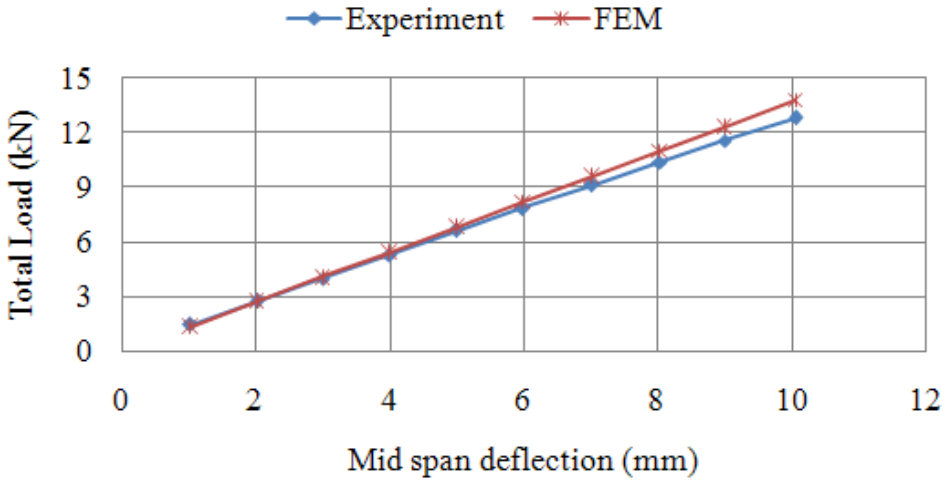

Figure 5.17 Validation of Beam-3 FE model with static deflection.

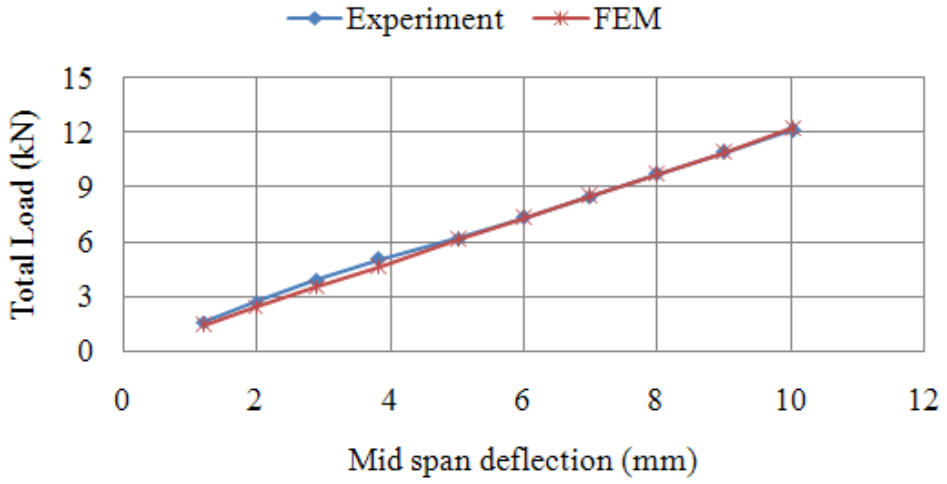

Figure 5.18 Validation of Beam-4 FE model with static deflection.

5.1.7 Concluding Remarks

A detailed description relating to the development of 2-D FE models of the four TCC beams using ANSYS was presented in Section 5.1. It included a description of elements used for modelling timber, concrete and shear connectors to simulate their behaviour. A correlation analysis was performed for all beams to validate the FE model results in terms of dynamic parameters against experimental results. Modal analysis was performed to acquire dynamic parameters such as natural frequencies and mode shapes. The following conclusions can be drawn based on the FE models results:

- Correlation between FE and experimental results showed that the NFerror values are higher for higher modes due to uplifting at supports and their sensitivity to local defects. The values for Beams- 1 and 2 were more consistent and within acceptable range compared to Beams- 3 and 4.
- For Beams- 1 and 2, the natural frequencies acquired from the FE model match very well with the experimental results. Hence, the FE model for Beams- 1 and 2 can be used to predict their natural frequency with sufficient accuracy.
- For Beams- 3 and 4, calibration was needed for their FE models as NFerror values were high, which were believed to be due to lower serviceability stiffness of the bird-mouth notched connection acquired from push-out tests. The stiffness of the connection was expected to be higher than the other two types of mechanical shear connectors. The models were calibrated by choosing approximate relevant serviceability stiffness values for bird-mouth notched connection to predict natural frequency with acceptable accuracy.
- For Beams- 3 and 4, the stiffness of the notched connection was chosen as 98 kN/mm as it was derived from the experimental parametric results obtained by performing push-out tests on a number of series of specimens. The correlation for calibrated FE model showed the NFerror values below 10% for first mode while the values were over 10% for other modes, with third mode of Beam-3 being an exception. The values were within acceptable range.
- The FE models for all beams were validated with static test results. The correlation between FE and experimental static load, expected to result in same mid span deflection of the beams, was below 10%, which was in the acceptable range, except for Beam-2 with normal screw. Beam-2 had relatively much

higher load error values due to relatively lower embedment strength of its shear connectors. The FE model of Beam-2 over-predicted the load. The serviceability stiffness of the normal screws acquired from the push-out tests also might be higher than expected, as a consequence, FE model becomes stiffer and predicted the higher load required to produce the same experimental deflections.

- Normal screw in Beam-2 had relatively low embedment strength compared to shear connectors than rest of the beams. Hence, magnitude of separation in Beam-2 was expected to be higher, as a consequence, the correlation showed higher load error values. Nevertheless, the model predicted natural frequency in modal analysis within acceptable range. In dynamic analysis, the applied load was not as high as static load; therefore, separation was not expected to be as significant in dynamic analysis than in static analysis.

5.2 Timber Floor Modules

This section presents the numerical analysis of the tested timber floor modules (timber beams) with 6 and 8 m span (Refer to Chapter 4) by developing 3-D linear finite element models to simulate their behaviour. The commercial FE analysis package ANSYS (2011) was used to simulate the beams. Modal analysis was performed on the models under pin-roller boundary conditions to obtain modal parameters such as natural frequency and mode shapes of the 6 and 8 m span beams. The models were calibrated and validated with the static and impact hammer test results. The dynamic performance of the beams was also assessed by evaluating their modal parameters.

5.2.1 Geometric Properties of the Models

The dimension of the FE model was based on the measurements of the tested timber beams. The overall length of the beams with 6 and 8 m clear span was 6.3 and 8.4 m, respectively. The cross-sectional dimensions of the 6 and 8 m span beams are shown in Figures 5.19 and 5.20, respectively (Zabihi et al. 2012).

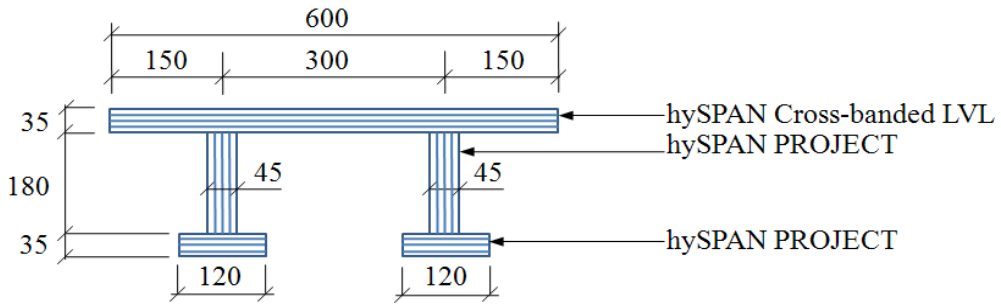

Figure 5.19 Dimensions of the 6 m span timber beams (mm).

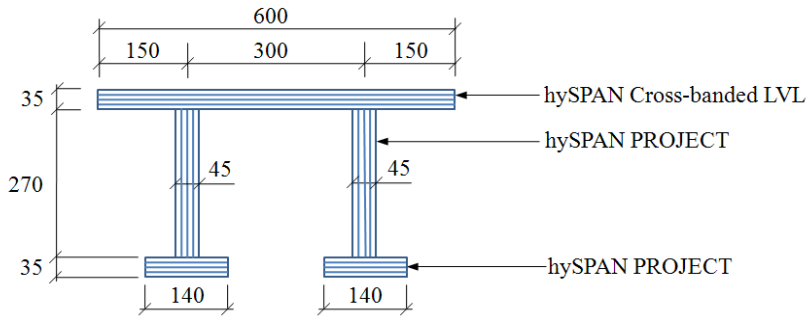

Figure 5.20 Dimensions of the 8 m span timber beams (mm).

5.2.2 Element Types

All LVL timber components such as top flange, webs and bottom flanges were modelled using SOLID45 element, which is an eight-node element used for 3-D modelling of solid structures and is capable of simulating plastic deformation, creep, large deflection and strain. The geometric properties of the element are shown in Figure 5.21 (ANSYS 2011). The interface between flanges and webs was assumed to be fully composite as no slip was observed during the four point bending tests under serviceability level loads. Bond between flanges and webs were not expected to be broken when tested under hammer impact load. To model a fully composite section, nodes at the interface between all components were coupled.

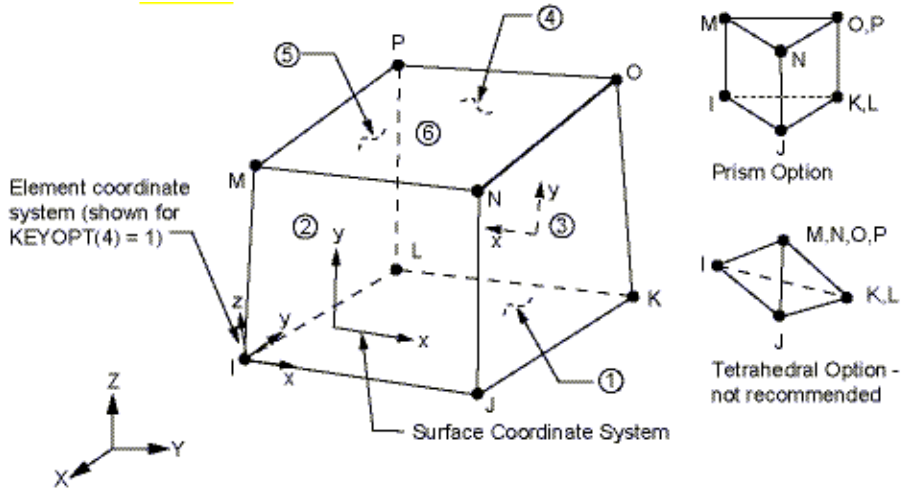

Figure 5.21 Geometric properties of SOLID45 (ANSYS 2011).

5.2.3 Material Properties

The three components of the beams such as top flange, webs and bottom flanges have different material properties. The properties from the tests were used in 3-D FE models. These properties include MOE (E_x), density (ρ) and Poisson's ratio (υ) of the components. The material properties were assumed isotropic for individual components, nevertheless, they were tested in the flat-wise and edge-wise direction, which replicate their orientation in the tested beams because it was deemed sufficient to represent the flexural stiffness in longitudinal direction along the span length as this is the major contribution to the overall stiffness of the beams.

The material properties of LVL components used for FE modelling are summarized in Table 5.7 (Refer to Chapter 4 for details). The MOE values of individual components were found by conducting four point bending tests on them (Zabihi et al. 2012). The value of Poisson's ratio of the LVL timber components (pine timber) was approximated using Wood Handbook (General Technical Report FPF-GTR-113 1999).

Table 5.7 Material properties of LVL components of timber beams

Component name	MOE	Density	Poisson's ratio
	E_x (GPa)	ρ (kg/m^3)	υ (%)
Top flange	9.6	607	
Webs	13.3	604	0.3
Bottom flanges	13.1	601	

5.2.4 Boundary Conditions

The boundary conditions for the model were set as pin-roller, which is close to the real boundary condition of the timber beams as shown in Figure 5.22. Translations in global X, Y and Z axis were restrained to simulate the pin support while translation in global Y and Z axis was restrained for roller support at the other end.

Figure 5.22 Experimental setup for 6 m span beam (mm).

5.2.5 Mesh Size

To obtain sufficient accuracy in FE analysis, a sensitivity analysis was performed on the model for both static and free vibration analyses. FE mesh configurations with different number of elements were analysed to obtain mid span deflection for the static analysis and fundamental frequency for the free vibration analysis. The interface between the components was assumed as full composite for the sensitivity analysis. The results for the static analysis and free vibration analysis are plotted against the number of elements in Figures 5.23 and 5.24, respectively. The size of the elements was uniform and aspect ratio was maintained below 2. The sizes of the elements in the longitudinal direction of the beams were chosen as 45, 25 and 10 mm for the sensitivity and the total number of elements in the beam for the corresponding element sizes was 3,528, 27,720 and 335,160, respectively. From the analysis it was observed that more than 27,720 elements were appropriate for accurate results. The increment from total number of elements of 27,720 to 335,160 merely increases the mid span deflection by 0.01% and fundamental frequency by about 0.02%.

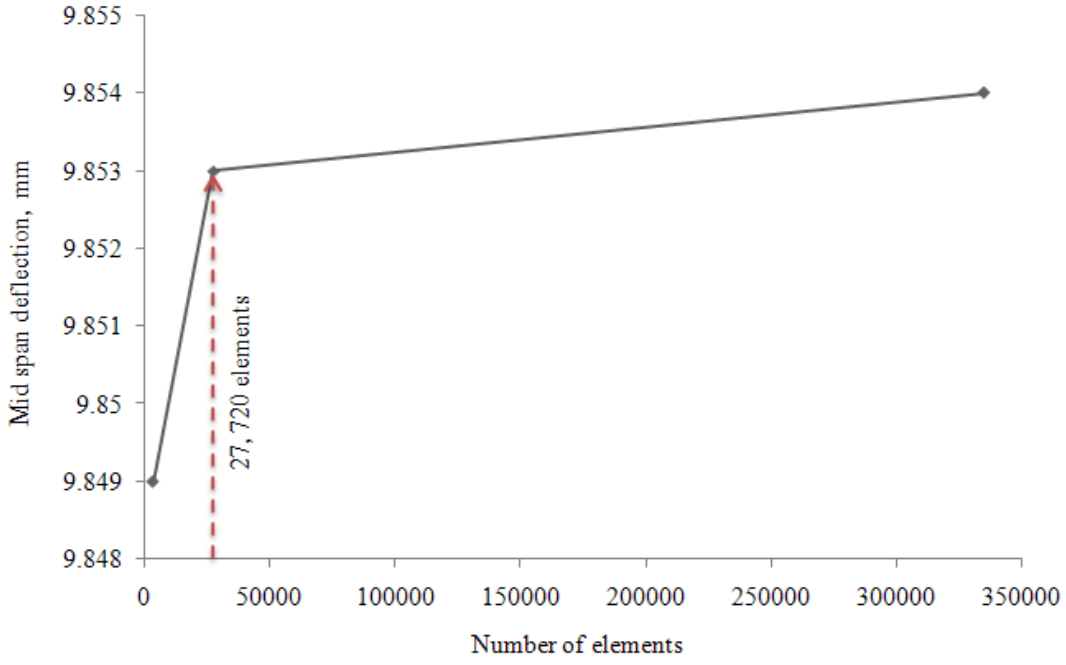

Figure 5.23 A sensitivity analysis for mesh density for static analysis of 6 m span beam.

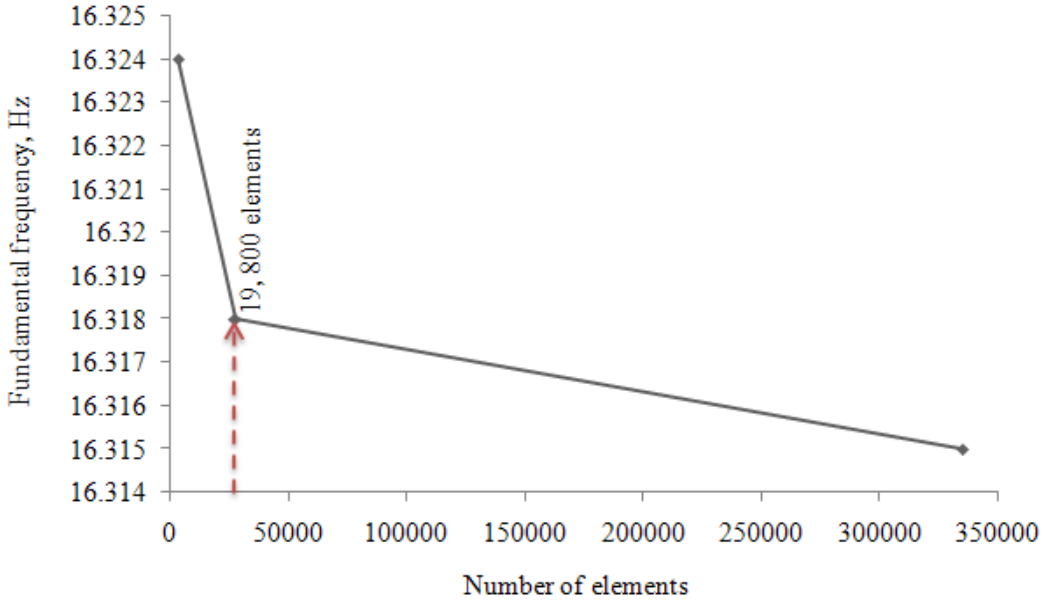

Figure 5.24 A sensitivity analysis for mesh density for dynamic analysis of 6 m span beam.

The size of the mesh in the FE models was based on the mesh sensitivity. For both 6 and 8 m span beams, the size of the elements in the longitudinal direction of the beams was chosen as 10 mm. The aspect ratio of the elements was below 2. In total, the FE models of the 6 and 8 m span beams had 335,160 and 535,920 elements, respectively. The overall view of FE model for the 6 m span beam is shown in Figure 5.25.

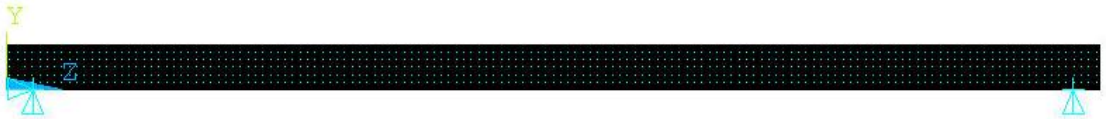

(a) Longitudinal view

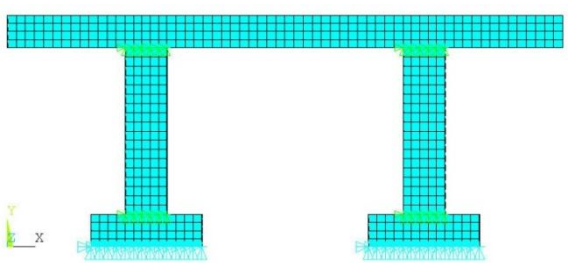

(b) Cross-sectional view

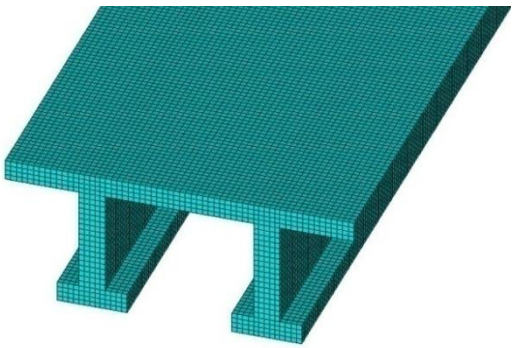

(c) Enlarged view of FE model from left end

Figure 5.25 Nodes and elements for FE model of 6 m span beam.

5.2.6 Modal Parameters of the Beams

The first three flexural mode shapes of the beams were extracted from the FE model as shown in Figure 5.26 by solving the eigenvalue problem using the modal analysis module in ANSYS. The details of the mode shapes are described in Table 5.8.

The natural frequency of the beams from experiment and FE model are presented in Table 5.9. The experimental fundamental frequency of the 6 m span beam was 16.34 Hz and for 8 m span beam it was 13.14 Hz while from FE model it was obtained as 16.45 and 12.93 Hz for 6 and 8 m beam, respectively.

Table 5.8 Description of mode shapes

Mode	Mode shape
1	First flexural mode
2	Second flexural mode
3	Third flexural mode

(a) Mode 1

(b) Mode 2

(c) Mode 3

Figure 5.26 First three flexural mode shapes of 8 m span beam FE model.

Table 5.9 Experimental and FE natural frequencies (Hz) of the beams

Beam	Experiment, $f_{n(Exp)}$			FE, $f_{n(FE)}$		
	Mode 1	Mode 2	Mode 3	Mode 1	Mode 2	Mode 3
6 m span	16.34	55.48	98.25	16.45	63.05	125.06
8 m span	13.14	44.08	78.89	12.93	49.64	98.27

5.2.7 Correlation between FE and Experimental Results

The values of the natural frequency for the first three flexural modes of the timber beams and their *NFerror* are listed in Table 5.10. The correlation showed that the *NFerror* values are higher for higher modes, which is shown in Figure 5.27, due to their higher uplifting at supports and sensitivity to local defects. The results from FE model for first mode is very close to the test results while they are higher than test results for higher modes for both spans as expected. The differences for mode 1 are below 2% for both 6 and 8 m span beams while the differences are about 13% and 25% for second and third modes, respectively. Hence, the FE models for the beams can be used to predict their first natural frequency with sufficient accuracy as this frequency is the main concern of the designer.

Table 5.10 Summary of results from FE model and comparison with test results

6 m span beam			
	Mode1	Mode 2	Mode 3
FEM (Hz)	16.45	62.05	125.06
Experiment (Hz)	16.34	55.48	98.25
Absolute difference (Hz)	0.11	7.57	26.81
NFerror (%)	0.70	13.65	27.29
8 m span beam			
FEM (Hz)	12.93	49.64	98.27
Experiment (Hz)	13.14	44.08	78.89
Absolute difference (Hz)	0.21	5.56	19.38
NFerror (%)	1.63	12.62	24.57

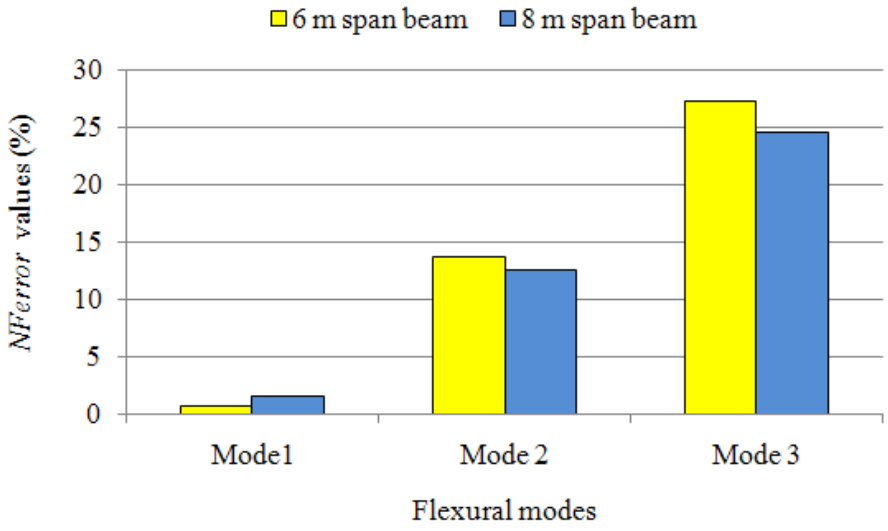

Figure 5.27 *NFerror* values of 6 and 8 m span beams.

For both 6 and 8 m beams, Modes 2 and 3 had *NFerror* values of about 13 and 25%, respectively, when the mean value of elastic modulus was used. Hence, a sensitivity analysis was performed to evaluate influence on natural frequency of the beams due to material properties variation, especially MOE. The average MOE values were varied by ±5 and ±10% and the natural frequencies of the 6 and 8 m span beams were extracted for the corresponding MOE values. Results for 6 and 8 m span beams are summarized in Tables 5.11 and 5.12, respectively. The *NFerror* values for three different modes of 6 and 8 m span beams with variation of the mean MOE values by ±5 and ±10% are shown in Figure 5.28.

Variation of the mean MOE by ±5 and ±10% changes *NFerror* values by about ±3 and ±6%, respectively and thus it is unlikely to have resulted in over-estimation of the natural frequency for these modes due to variation of material properties of the LVL timber. Further, *NFerror* values were negligible for Mode 1 for the mean value of elastic modulus. If the material properties variation was the cause of over estimation of the natural frequency, the Mode 1 would also have some *NFerror* values. The boundary conditions, material properties and connection between the flange and web of the model are more likely to have resulted in over-estimation of the frequency for higher modes from the FE model as these modes are highly sensitive to these factors.

Table 5.11 Correlation between FE model with "±5% of E_x" and test results of 6 m beam

6 m span beam with "–5% of Ex"			
Flexural mode	Mode1	Mode 2	Mode 3
FEM (Hz)	16.04	61.51	122.28
Experiment (Hz)	16.34	55.48	98.25
Absolute difference (Hz)	0.30	6.03	24.03
NFerror (%)	1.82	10.87	24.45
6 m span beam with "+5% of E_x"			
FEM (Hz)	16.87	64.67	128.66
Experiment (Hz)	16.34	55.48	98.25
Absolute difference (Hz)	0.53	9.19	30.41
NFerror (%)	3.22	16.56	30.95
6 m span beam with "–10% of E_x"			
FEM (Hz)	15.61	59.86	119.10
Experiment (Hz)	16.34	55.48	98.25
Absolute difference (Hz)	0.73	4.38	20.85
NFerror (%)	4.45	7.90	21.22
6 m span beam with "+10% of E_x"			
FEM (Hz)	17.26	66.18	131.67
Experiment (Hz)	16.34	55.48	98.25
Absolute difference (Hz)	0.92	10.70	33.42
NFerror (%)	5.64	19.28	34.01

Table 5.12 Correlation between FE model with "±10% of E_x" and test results of 8 m beam

8 m span beam with "–5% of E_x"			
Flexural Mode	Mode1	Mode 2	Mode 3
FEM (Hz)	12.60	48.42	96.11
Experiment (Hz)	13.14	44.08	78.89
Absolute difference (Hz)	0.54	4.34	17.22
NFerror (%)	4.10	9.84	21.83
8 m span beam with "+5% of Ex"			
FEM (Hz)	13.25	50.90	101.04
Experiment (Hz)	13.14	44.08	78.89
Absolute difference (Hz)	0.11	6.82	22.15
NFerror (%)	0.82	15.47	28.08
8 m span beam with "–10% of E_x"			
FEM (Hz)	12.26	47.12	93.53
Experiment (Hz)	13.14	44.08	78.89
Absolute difference (Hz)	0.88	3.04	14.64
NFerror (%)	6.67	6.89	18.56
8 m span beam with "+10% of E_x"			
FEM (Hz)	13.56	52.09	103.40
Experiment (Hz)	13.14	44.08	78.89
Absolute difference (Hz)	0.42	8.01	24.51
NFerror (%)	3.18	18.18	31.07

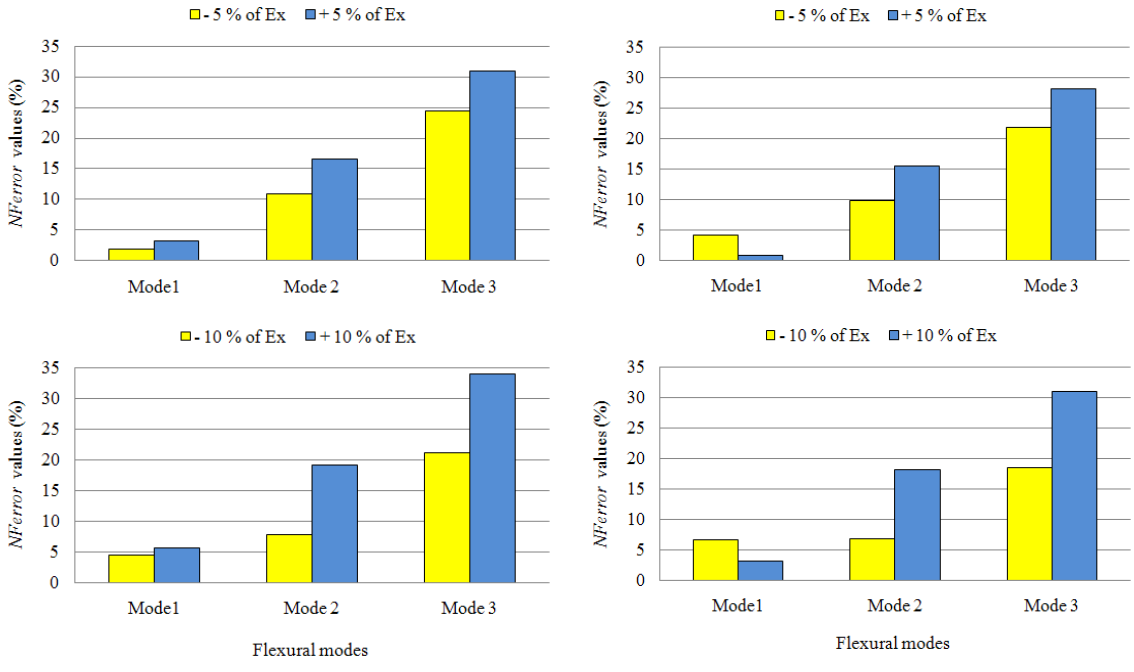

(a) (b)

Figure 5.28 *NFerror* values of (a) 6 m and (b) 8 m span beam for ±5% and ±10% of E_x.

5.2.8 Validation of FE Models against Static Test Results

To validate the FE models for 6 and 8 m span timber beams, the results from FE model is compared with static test results. The details of the static test results can be found in Zabihi et al. (2012). Four point bending tests were conducted on the beams and the tests were replicated in the FE models. In the FE models, different loads equal with experimental values were applied at each 1/3rd span from the supports and the mid span deflection was found. The mid span deflection was correlated with the experimental result caused by the same magnitude of point load at each 1/3rd span from the supports. The correlation analysis of the FE and static test results of 6 and 8 m span beams is shown in Figures 5.29 and 5.30, respectively. For both 6 and 8 m span beams, the deflection error values were below 10%, which were in the acceptable range.

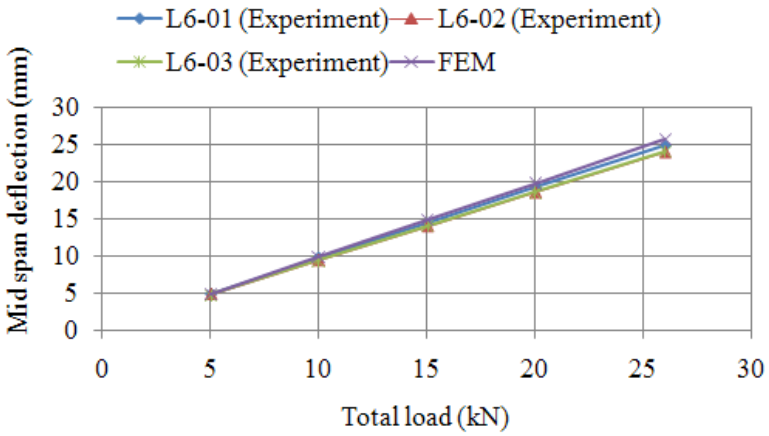

Figure 5.29 Validation of 6 m beam FE model with static deflection.

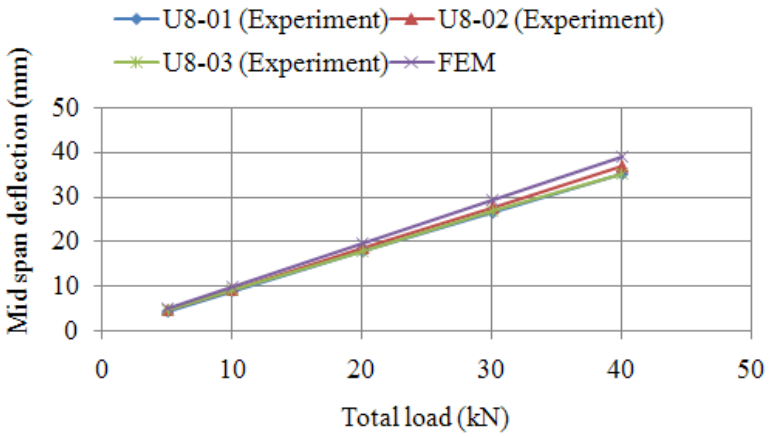

Figure 5.30 Validation of 8 m beam FE model with static deflection.

5.2.9 Concluding Remarks

This chapter presented a detailed description relating to the development of 3-D FE models of the timber beams with 6 and 8 m span, respectively, using ANSYS. It includes description of element used for modelling the beam components such as webs and flanges to simulate their behaviour. A correlation analysis was performed for both 6 and 8 m beams to validate the FE model results in terms of dynamic parameters against experimental results. Further, the results from FE model were validated with static test results. The following conclusions can be drawn based on the FE models results.

- Correlation between FE and experimental results showed that the *NFerror* values are higher for higher modes. The *NFerror* values were below 2% for first mode while they were about 13% and 25% for second and third modes, respectively. The values for both 6 and 8 m beams were consistent.
- For the beams, the natural frequency acquired from the FE models matched very well with the experimental results, especially for first mode. Hence, the FE models of the beams can be used to predict their natural frequency with sufficient accuracy.
- FE model over-predicted the natural frequency for higher modes by about 25% and it is unlikely to be due to only variation in material properties as frequencies for the first mode were very close. This should be due to uplifting of the beams at supports during experimental work as FE models were analysed under pure pin-roller boundary conditions which prevented bouncing at supports. Further, higher modes are more sensitivity to local defects within the timber material and at connections. In these models, interface at webs and flanges were assumed as fully composite.
- FE models for 6 and 8 m beams were validated with static test results. The correlation between FE and experimental mid span deflection caused by the same magnitude of load at each $1/3^{rd}$ span from the supports showed the deflection error below 10% for all beams. Deflection error was higher for higher mid span deflection. This should be due to discrepancies in the connection system.

University of Technology, Sydney

CHAPTER 6

COMPOSITE ACTION INVESTIGATION USING DYNAMIC-BASED METHOD

6 Composite Action Investigation using Dynamic-based Method

6.1 Introduction

This chapter presents the theory, background, methodology and results of two dynamic-based composite action identification schemes. The aim of both schemes is to evaluate the degree of composite action of a composite flooring system based on the Damage Index (DI) method. The two schemes analyse differences in modal strain energies obtained from mode shape measurements to identify the degree of composite action. The two proposed schemes are validated and tested on numerical and experimental composite beam structures with different degrees of composite action. The tested beam structures consist of two LVL components acting as flange and web. To simulate varying degrees of composite action, the two components are connected using different number of screws, i.e. '3', '5', '9', '17' and '33' screws, to generate five different states of composite actions. For the numerical and experimental beams of different screw connections, the structures are dynamically excited and through extraction of mode shapes and calculation of loss of composite action index (*LCAI*) values, the degree of composite action are determined.

6.2 Background

It is always desirable to have a high degree of composite action for better performance of a flooring system between its connected (or attached) components under both static and dynamic actions. In recent times, available flooring systems are TCC, steel-concrete composite, timber-mud composite and full timber flooring systems. The objective of this part of research work is to evaluate the efficiency and degree of composite action of an existing composite flooring system using only measurements acquired from non-destructive vibration testing.

For TCC flooring system, transfer of the shear force across the concrete-timber interface is critical to the design of the system. The composite interaction in timber-concrete beams is usually achieved with mechanical devices, such as shear connectors or plates driven into the materials. Effective bending stiffness is highly dependent on the shear

bond coefficient of the interface, γ. A flooring system with γ = 0 means the layers are acting totally independently and there is no shear transfer between the layers, and the system is known as "fully non-composite". This results in a large amount of slip between the layers and large deflection. A flooring system with γ = 1 represents a homogenous composite action with no slip in the interface and the smallest deflection possible, and the system is known as "fully composite" (Kuhlmann & Schänzlin 2007). The actual behaviour of a real structural composite system is "partially composite", i.e. it exhibits a deflection that lies between these two extremes. The degree of composite action is a measure of how close any interconnection comes to achieving the fully composite extreme. Pault (1977) quantified the degree of composite action (composite efficiency) based on static test results using the following equation:

$$CA\ (\%)\ = \frac{D_N - D_I}{D_N - D_C}\ \text{x}\ 100 \tag{6.1}$$

where *CA* (%) is the composite action in %, D_N is the theoretical fully non-composite deflection, D_I is the measured deflection for partial composite action, and D_C is the theoretical full composite deflection of the system (Gutkowski et al. 2011).

Failure of any shear connector of the composite flooring system influences its performance as deflection increases and natural frequencies decrease resulting in poorer performance. Furthermore, failure of the shear connectors reduces the degree of composite action of the system. This research deals with the loss of composite action of a composite system due to failure or deterioration of shear connectors. Very limited work has been conducted in the past in this specific research area. However, a wide range of research analogous to the field of this research project has been carried out. Such research is concerned with the delamination and damage detection of structural system, which are briefly summarized in the following sub-sections.

6.2.1 Delamination Detection

Delamination is a mode of failure of composite materials. Composite materials are engineered or naturally occurring materials made from two or more constituent materials with significantly different physical or chemical properties that remain separate and distinct within the finished structure. Delamination is increasingly an

aviation safety concern, especially in the tail sections of the airplanes due to increasing use of composite materials in aviation.

In laminated materials, operational conditions such as repeated cyclic stresses and impact can cause layers to separate, forming a mica-like structure of separate layers, with significant loss of mechanical toughness. Delamination also occurs in reinforced concrete structures subject to reinforcement corrosion, in which case the oxidized metal of the reinforcement is greater in volume than the original metal. The oxidized metal therefore requires greater space than the original reinforcing bars, which causes a wedge-like stress on the concrete. This force eventually overcomes the relatively weak tensile strength of concrete, resulting in a separation or delamination of the concrete above and below the reinforcing bars (Cantwell & Morton 1991).

The cause of delamination is weak bonding and thus, delamination is an insidious kind of failure as it develops inside of the material, without being obvious on the surface, much like metal fatigue (Kalpakjian & Schmid 2001).

Delamination failure may be detected in the material by its sound, as solid composites have sharp sounds while delaminated parts sound dull. As such, reinforced concrete sounds solid, whereas delaminated concrete will have a light drum-like sound when exposed to a dragged chain pulled across its surface. Bridge decks in cold climate countries, which use de-icing salts and chemicals, are commonly subject to delamination and as such are typically scheduled for annual inspection by chain-dragging as well as subsequent patch repairs of the surface. Other non-destructive testing methods include embedding optical fibres coupled with optical time domain reflectometer, testing with ultrasound, radiographic imaging and infrared imaging (Cantwell & Morton 1991; Kalpakjian & Schmid 2001).

6.2.2 Dynamic-based Damage Detection

Vibration-based damage detection methods are non-destructive testing techniques that have been developed to identify damage in mechanical and civil engineering structures. Damage is typically defined as changes to the material and/or geometric properties of a structural system, including changes to the boundary conditions and system connectivity, which adversely affect the system's performance. Vibration-based damage

detection techniques are based on the principle that changes of physical properties in a structure (i.e. stiffness, damping, mass and boundary conditions) reflect damage, which in turn will alter its dynamic characteristics (namely, natural frequencies, mode shapes and modal damping). Vibration-based methods examine changes in the structures dynamic characteristics to detect defects. Eventually, they are related to a certain form of pattern recognition problem. Over the past three decades, intensive research has been undertaken in the field of dynamic-based damage identification and many algorithms have been developed. Comprehensive literature reviews on vibration-based damage detection methods were published by Doebling et al. (1996) and Carden & Fanning (2004).

6.2.2.1 Modal Strain Energy-Based Damage Detection

Among various vibration-based techniques, especially those using modal parameters, the mode-shape-based DI method (Stubbs, Kim & Topole 1992) was found to be particularly promising. The DI method is based on changes in modal strain energy and utilises the relative differences in modal strain energy before and after damage. A mode shape stores an enormous amount of strain energy in a particular structural load path. The modal strain energy in the load path alters when damage occurs as frequency and shape of the mode are highly sensitive to changes in that load path. Therefore, changes in modal strain energy have been widely utilised as a damage indicator to locate and quantify damage. Several modifications of the algorithm, originally developed by Stubbs, Kim & Topole (1992), have been developed and verified by analytical and experimental studies. Two studies, both comparing the Modal Assurance Criterion (MAC), Coordinate Modal Assurance Criterion (COMAC), flexibility and modal strain energy approaches, concluded that the modal strain energy method was the most precise. The strain energy method was also the most stable technique in damage detection when different levels of noise and damage were present. However, this method has some limitations such as the identification of light damage (Barroso & Rodriguez 2004; Pereyra et al. 1999). Furthermore, the phenomenon of false positive damage identifications has been widely reported in Barroso & Rodriguez (2004). Another challenge is the sensitivity to noise, especially in the quantification of defects (Lee & Yun 2006; Shi, Law & Zhang 1998, 2000).

Kim & Stubbs (1995) presented a method that normalised the damage indicator derived from modal strain energy with respect to the standard space to locate and quantify damage from a few mode shapes of a structure. The method was verified experimentally using a two span aluminium plate girder model of 4.5 m length of each span. The model was supported on pin support at the left edge while roller supports were used to support the model at its midpoint and right edge. The model was set in motion by ambient forces from light-weight traffic and response of the model was measured using eleven accelerometers. Single crack damage was inflicted in the model. The results showed that the method clearly identified the damage location with relatively small localisation error. However, some relatively small false negative errors (missing detection of true damage locations) were present, along with a relatively large false positive error (prediction of locations that are not damaged). This method can be used to estimate damage severity with relatively large error.

Kim & Stubbs (2002) improved their damage index method presented in 1995 to improve accuracy of damage localisation and severity estimation. A two span aluminium plate girder model tested by these authors in 1995 was simulated numerically with ten different damage scenarios. First three modes of the numerical model before and after damage were utilized to locate and quantify damage. The improved method was able to locate damage and estimate its severity with better accuracy than the original damage index method. These conclusions were made based on purely numerical results. However, experimental results could not confirm these conclusions (Sánchez 2005).

Choi et al. (2007) further developed a Modified Damage Index (MDI) method to identify damage in a timber beam using modal strain energy. To perform mode shape reconstructions, a cubic spline data interpolation function was adopted to interpolate experimental mode shape data. The reconstructed mode shapes were then differentiated twice to acquire mode shape curvatures and the curvatures were normalised to evaluate DI. The MDI method was able to detect the damage locations from experimental results, however, with false positive errors. The authors reported that using higher modes proved to be more favourable for detecting multiple damage locations; nevertheless further investigation is needed to estimate damage severity.

Shi, Law & Zhang (1998; 2000) presented a damage indicator method that uses the ratio of changes in modal strain energy in each element. This method requires only the elemental stiffness matrix, the analytical mode shapes and incomplete measured mode shapes. The authors concluded that based on the results obtained from modal simulation and experiment with a two-storey partial steel frame, the presented method is effective in locating damage; however, the method was sensitive to noise in quantifying the damage severity. Shi, Law & Zhang (2002) improved the quantification of stiffness changes by reducing the modal truncation error in the process of damage detection.

Li, Yang & Hu (2006) proposed a modal strain energy decomposition method for damage localisation. The method incorporates the modal strain energy of each structural element by decomposing the energy into its axial and transverse coordinates. Therefore, for each element in the structure two damage indicators (axial damage indicator and transverse damage indicator) were formulated. From numerical and experimental results it was concluded that the axial damage indicator was able to locate damage occurring in horizontal elements and the transverse damage indicator was able to locate damage occurring in vertical elements with false positive errors. Nevertheless, the method could not estimate the damage severity.

Hu, Wang & Li (2006) presented a Cross-Modal Strain Energy (CMSE) method for estimating the damage severity. The authors used the structural cross modal strain energy between the i^{th} mode of the undamaged structure and the j^{th} mode of the damaged structure. The corresponding elemental CMSE for the stiffness matrix was also expressed mathematically. In the method, a parameter α_n was used to estimate the severity of damage. The method was verified by a numerical 3-D model of a five-storey frame structure. Damage in the model was simulated by the decrement of elemental stiffness. Results from the model showed that this method was able to estimate the damage severity under noise-free measurement conditions and without any numerical singularity problems; however, the method was unable to locate damage.

6.2.2.2 The Damage Index Method

Stubbs, Kim & Topole (1992) developed the Damage Index (DI) method. This method utilises an indicator based on modal strain energies, which are a function of relative changes in mode shape curvatures of a structure before and after damage, to detect,

locate and quantify damage. Considering a general Euler-Bernoulli beam, the strain energy stored in a system can be expressed as

$$U_i = \frac{1}{2}\int_0^L EI(w''(x))^2 dx \tag{6.2}$$

where *EI* is the flexural rigidity of the beam and *w* the beam deflection. Similarly, the energy in modal space associated with a particular i^{th} mode shape (ϕ_i) can be calculated using

$$U_i = \frac{1}{2}\int_0^L EI(\phi_i''(x))^2 dx \tag{6.3}$$

where ϕ_i'' is the second derivative or curvature of the i^{th} mode shape ϕ_i with respect to *x*.

If the beam is subdivided into *N* elements (see Figure 6.1), the modal strain energy associated with the j^{th} element for the i^{th} mode is given by

$$U_{ij} = \frac{1}{2}\int_j (EI)_j(\phi_i''(x))^2 dx \tag{6.4}$$

The fractional energy of the j^{th} element, denoted by F_{ij}, is therefore,

$$F_{ij} = \frac{U_{ij}}{U_i} = \frac{\frac{1}{2}\int_j (EI)_j(\phi_i''(x))^2 dx}{\frac{1}{2}\int_0^L EI(\phi_i''(x))^2 dx} \tag{6.5}$$

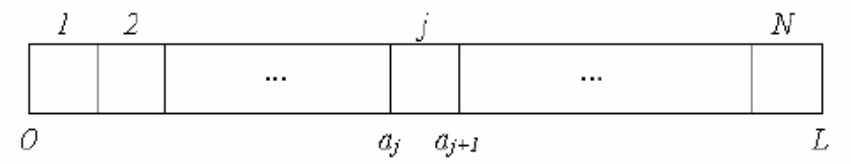

Figure 6.1 Schematic diagram showing subdivisions of a beam (Cornwell, Doebling & Farrar 1999).

Similarly, the expression of the fractional energy for the damaged beam (superscript * is used to denote the damaged state) can be obtained by assuming that the damage is located at a single subdivision and thus the fractional strain energy remains relatively

constant in the undamaged subdivision resulting in $F_{ij} \approx F^*_{ij}$. Assuming the fraction of modal energy is the same for damaged and undamaged structures, it is found that

$$\frac{\frac{1}{2}\int_j (EI)_j \, (\phi_i''(x))^2 dx}{\frac{1}{2}\int_0^L EI \, (\phi_i''(x))^2 dx} = \frac{\frac{1}{2}\int_j (EI)_j^* \, (\phi_i''^*(x))^2 dx}{\frac{1}{2}\int_0^L EI^* \, (\phi_i''^*(x))^2 dx} \tag{6.6}$$

When rearranging Equation (6.6), the damage indicator of mode *i* and member *j*, β_{ij}, is obtained from

$$\beta_{ij} = \frac{(EI)_j}{(EI)_j^*} = \frac{\int_j (\phi_i''^*(x))^2 dx \int_0^L (\phi_i''(x))^2 dx}{\int_j (\phi_i''(x))^2 dx \int_0^L (\phi_i''^*(x))^2 dx} \tag{6.7}$$

Here it is assumed that the flexural rigidity $(EI)_j$ of the damaged and undamaged modes is constant over the entire length of the element *j*. To establish a comparative basis for different modes, the index β_{ij} is transformed into the standard normal space, and the normalised damage indicator Z_{ij} is given by

$$Z_{ij} = \frac{\beta_{ij} - \mu_{\beta ij}}{\sigma_{\beta ij}} \tag{6.8}$$

with $\mu_{\beta ij}$ being the mean and $\sigma_{\beta ij}$ the standard deviation of the β_{ij} values for all *j* elements. The estimation of the damage severity for element *j* is expressed by

$$\alpha_{ij} = 1 - \frac{1}{\beta_{ij}} \tag{6.9}$$

with α_{ij} being the severity estimator.

Positive Z_{ij} and α_{ij} values indicate the possibility of damage and can therefore be utilised to locate and quantify defects, respectively. In the DI method, positive α values indicate the possibility of damage and thus can be utilised to quantify defects. There are a number of limitations of this method, which are summarized in Choi (2007) and Dackermann (2010). One of the limitations of this method is the existence of false damage indications, which can be resolved by summing up DI values of several modes and thereby enhancing the magnitude of the index at the actual damage site. In addition, the issue of spurious damage can be dealt with by introducing a threshold value, i.e. only DI values above a certain threshold value indicate damage.

In Dackermann (2010), a good example of the severity evaluation of damage using the damage indicator α_j is given and illustrated here in Figure 6.2. The damage indicator α_j was derived from the first mode of numerical beam simulations. The modelled beams were inflicted with damage at location '4' with three different severities of light, medium and severe extent. In the displayed figures, the horizontal axis shows the span of the beam with '1' to '7' indicating seven data measurement locations along the beam and the vertical axis presents the damage index, α_j. In the figures, clear indications of the different damage severities and the damage location are visible).

The ability of the damage index method to identify the severity of damage is used in this research as basis for the development of a vibration-based composite action index that can be used to evaluate the degree of composite action in a composite flooring system.

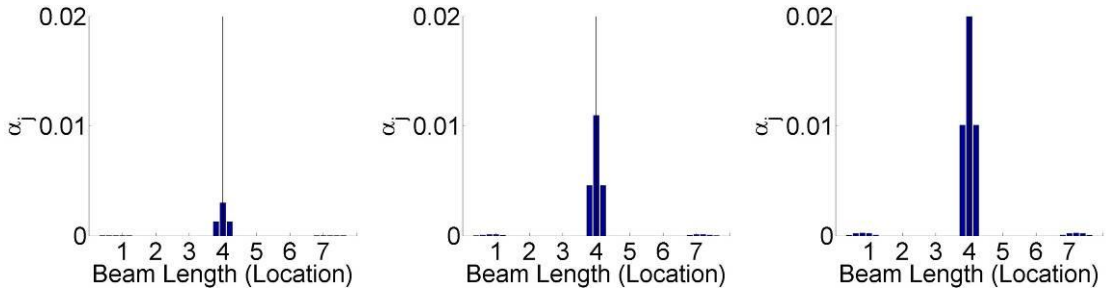

(a) *(b)* *(c)*

Figure 6.2 Severity estimator α_j derived from first mode of numerical beam simulations. Damage was situated at location '4' with (a) light, (b) medium and (c) severe damage severity (Dackermann 2010).

6.3 Proposed Methodology for Dynamic-based Composite Action Identification

For the identification of the composite action in a composite flooring system, such as the TCC system, a non-destructive method is proposed that uses derived mode shapes obtained from dynamic testing to determine the degree of composite action. As basis of this technique, the damage index method is used to calculate a damage severity index α_j, which indicates the loss of composite action (damage) along the flooring system. To

determine the overall loss of composite action, the severity index values along the flooring system are combined to form two types of "Loss of Composite Action Indices" (*LCAIs*). The first index, $LCAI_1$, calculates the summation of all positive α_j values along the flooring system; while the second index, $LCAI_2$, calculates the mean of the positive α_j values. The *LCAIs* are then factorised and subtracted from the value 100 to determine a "dynamic-based degree of composite action" that is comparable to the "static-based degree of composite action" defined in Equation (6.1).

6.3.1 Mode Shapes and Damage Severity Index α

The first step in the dynamic-based composite action identification of a composite flooring system is the determination of the mode shapes of the system. Therefore, for an in-service system or an experimental structure, Modal Testing and Experimental Modal Analysis (MT and EMA) must be performed to determine the modal parameters of the structure, i.e. natural frequencies, mode shapes and damping ratios. The procedures of MT and EMA are described in Section 3.3. As the accuracy of the calculated degree of composite action depends greatly on the quality and number of identified mode shapes, it is desirable to have a larger number of measurement sensors. The recommended minimum number of sensors along the span of a composite flooring system element is five, which allows the identification of the first five flexural mode shapes. For numerical simulations, the eigenvalue solution or transient analysis with subsequent EMA can be performed to derive the modal shapes.

Second, based on the damage index method, the damage severity estimator α_j is determined for each mode shape following Equations (6.8) and (6.9) described in Section 6.2.2. In the equations, the differences in modal strain energies between a flooring system of fully composite and partially composite states are calculated. For each identified mode shape, damage severity indices α_j are determined for each sensor location. In the DI method, positive α_j values indicate the possibility of damage and thus are utilised to quantify damage, while negative values are redundant. Accordingly, for the determination of the loss of composite action (damage), only positive α_j values indicate the loss of connection elements. Hence, negative α_j values (or those below a determined threshold value) are discarded and set to zero. As an example, α values of the first flexural mode of an experimental composite beam structure dynamically tested with seven sensors are shown in Figure 6.3 (a). In the figure, the horizontal axis shows

the length of the beam, with '1' to '7' indicating seven sensor locations and the vertical axis the damage index, α. These values are positive for sensors at locations '3' and '4', while they are negative for other locations. Figure 6.3 (b) depicts only the positive α values at locations '3' and '4' and all other values are set to zero.

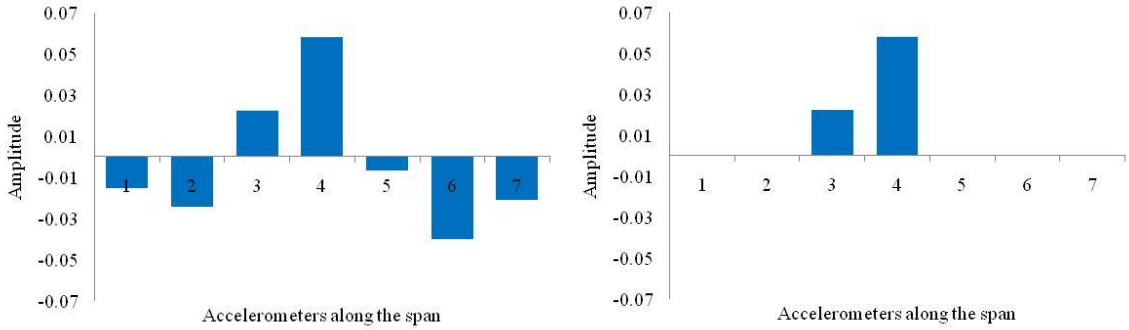

(a) All α values (b) Only positive α values

Figure 6.3 Severity estimator α derived from first mode of an experimental composite beam.

6.3.2 Loss of Composite Action Indices $LCAI_1$ and $LCAI_2$

6.3.2.1 $LCAI_1$

For the determination of the first loss of composite action index ($LCAI_1$), at first, all positive values (or amplitudes) of the damage severity estimator α_j are added up for each mode. Then, the mean of the summarised positive α_j values are determined for all considered modes, M. This can mathematically be expressed as

$$LCAI_1 = \left(\sum_{i=1}^{M}\sum_{j=1}^{n}\alpha_{ij}\right)/M \qquad for\ \alpha_{ij} > 0 \ \text{ and } \ n \leq N \tag{6.10}$$

where n is the number of positive α_j values and M the total number of modes. Further, the number n of positive α_j values must be smaller or equal to the total number of measurement locations with N being the total number of measurement locations. The value of n can be different for different modes, but it cannot be greater than N. In the example displayed in Figure 6.3, the value of n is 2 while N is 7.

6.3.2.2 $LCAI_2$

To calculate the second loss of composite action index ($LCAI_2$), first, the mean of all positive α_j is computed for each mode. Then, similar to $LCAI_1$, the mean of the averaged positive α_j values are determined for all considered modes, M. $LCAI_2$ can mathematically be expressed as:

$$LCAI_2 = \left\{\sum_{i=1}^{M}\left(\sum_{j=1}^{n}\alpha_{ij}\ /n\right)\right\}\Big/_{M} \qquad for\ \alpha_{ij} > 0 \ \text{ and } \ n \le N \tag{6.11}$$

The reason for introducing $LCAI_2$ is explained in the following example. Figures 6.4 (a) and 6.5 (a) illustrate positive α_j values obtained from composite structures of two different composite states (Case 1 and Case 2). While the loss of connectivity is much greater in Case 2 (the maximum amplitude is 0.7 for Case 2, in contrast to 0.1 for Case 1), the calculated $LCAI_1$ value is the same for both cases ($LCAI_1$ = 0.7), see Figures 6.4 (b) and 6.5 (b). The second proposed method, however, considers such discrepancy, and the corresponding $LCAI_2$ values of the two cases give appropriate values of 0.1 and 0.7 (see Figures 6.4 (c) and 6.5 (c)). Hence, the loss of composite action derived from the second proposed index ($LCAI_2$) is expected to deliver better results than those determined with $LCAI_1$.

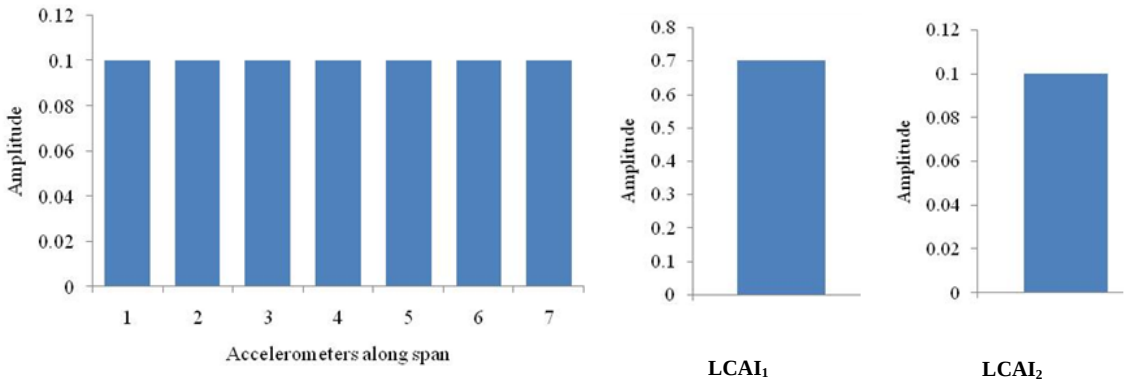

(a) α values (b) $LCAI_1$ value (c) $LCAI_2$ value

Figure 6.4 Case1: (a) α values, (b) $LCAI_1$ value and (c) $LCAI_2$ value.

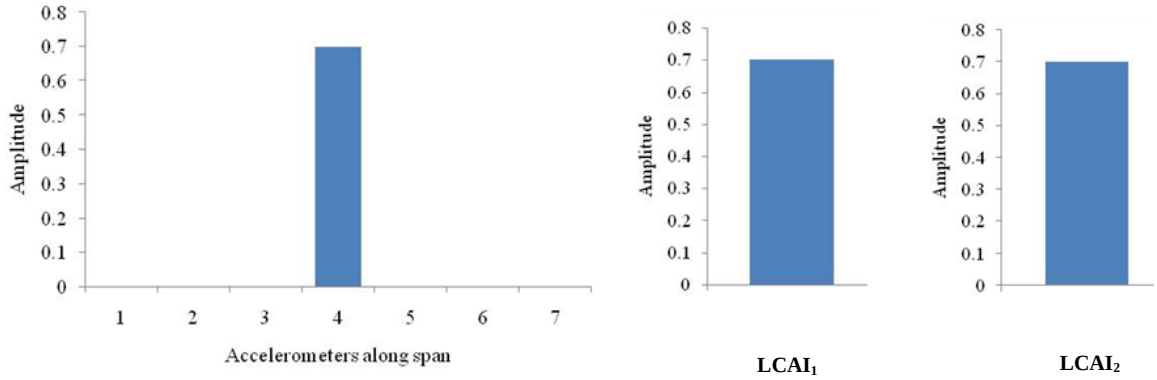

(a) α values (b) $LCAI_1$ value (c) $LCAI_2$ value

Figure 6.5 Case2: (a) α values, (b) $LCAI_1$ value and (c) $LCAI_2$ value.

6.3.3 Dynamic-based Degree of Composite Action

To correlate the dynamically derived loss of composite action indices to the static-based degree of composite action, the indices are first multiplied with a calibration factor to derive the actual loss of composite action, and then subtracted from the value 100 to obtain the actual degree of composite action (in percentage). To derive the corresponding calibration factors, the static-based degree of composite action must be determined for the investigated composite structure according to Equation (6.1).

For the composite timber beam structure, used to validate the proposed composite action identification methods of this research, the derived "degree of composite action" and "loss of composite action" values determined from static deflection are illustrated in Figure 6.6 (a) and (b), respectively. For the tested structure, five degrees of composite action were simulated by connecting the composite beam with '3', '5', '9', '17' and '33' screws, respectively. The degree of composite action of the beam was calculated using Equation (6.1), where deflections of the beam for fully composite and non-composite sections were derived analytically, while FE models were used to calculate deflections for partial composite sections with different number of screws. Details of the FE modelling and analysis are presented in Section 6.4. The degree of composite action of the beam increases with an increase in the number of screws resulting in higher stiffness. The beam with '3' and '33' screws had a composite action of 75% and almost 100%, respectively. The loss of composite action of the beam is shown in Figure 6.6 (b). Here, the maximum loss of composite action was obtained as 25% for '3' screws while there was no loss for '33' screws. These statically derived composite action

values are used as targets for the calculation of calibration factors that correlate the dynamically determined $LCAI_1$ and $LCAI_2$ values to the statically derived degrees of composite action.

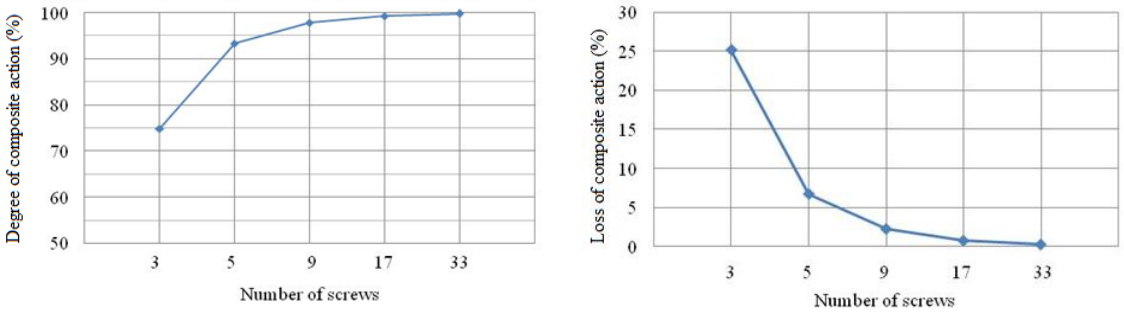

(a) Degree of composite action. (b) Loss of composite action.

Figure 6.6 Static-based degree of composite action and (b) loss of composite action of FE composite beam structure with different number of screw connections.

Note: For the experimental composite beam structure, only dynamic and no static tests were performed. In comparison to dynamic testing, heavier and more expensive instrumentations are needed for experimental static tests to identify deflections for partial composite systems. In addition, static load testings are time consuming and have the potential of damaging the test structure. In this study, it is assumed that the degrees of composite action of the experimental structure equal the ones of the numerical structure. However, the connection stiffness of the experimental structure can be slightly lower than those of the corresponding FE model. Nevertheless, the results should be within acceptable range since a composite action of 100% for '33' screws is expected. Usually FE models are stiffer than specimens to be tested and thus can over-predict the degree of composite action of the beam resulting in under-predictions of the loss of composite action.

6.3.4 Methodologies' Flow Chart

The methodology proposed in this research to determine the degree of composite action for composite flooring systems is described in this section. Figures 6.7 and 6.8 depict the procedures to determine the composite action using the two proposed dynamic-based methods $LCAI_1$ and $LCAI_2$, respectively.

First, the modal parameters (natural frequencies, mode shapes and damping ratios) are obtained from both EMA and numerical analysis procedures. Details on the determination of the modal parameters using EMA are described in Section 3.3. Second, the number of modes (*M*) that give good identification results are selected. The mode shape of the fundamental mode alone cannot give good composite action results as the curvature of the first flexural mode is low resulting in a low sensitivity for identifying the composite action. Hence, mode shape results of higher modes need to be considered along with the fundamental mode. Third, for each mode shape, α values are calculated following the DI method as described in Section 6.2.2. These values indicate the severity of damage along a structure. In a composite beam, failure of screw connections is considered as the damage, which changes the performance of the systems. In the DI method, positive α values indicate the possibility of damage and thus can be utilised to quantify damage while negative values need to be discarded. Fourth, for the $LCAI_1$ method, all positive α values are summed up for each mode giving α_{sum1}. For the $LCAI_2$ method, the mean of all positive α values is calculated giving α_{sum2}. Fifth, the loss of composite action indices, $LCAI_1$ and $LCAI_2$, are computed by calculating the mean of the summed and averaged α values of the total number of modes (*M*), respectively. Sixth, the dynamic-based Loss of Composite Action (*LCA*) of a composite flooring system in percentage is obtained by multiplying the indices $LCAI_1$ and $LCAI_2$ with their corresponding calibration factors, λ_1 and λ_2, respectively. These calibration factors are obtained from the ratio of maximum possible static-based loss of composite action value to the corresponding dynamic-based loss of composite action indices (*LCAIs*) of a composite system. And at last, the degree of composite action in percentage is determined by subtracting the *LCA* value from 100.

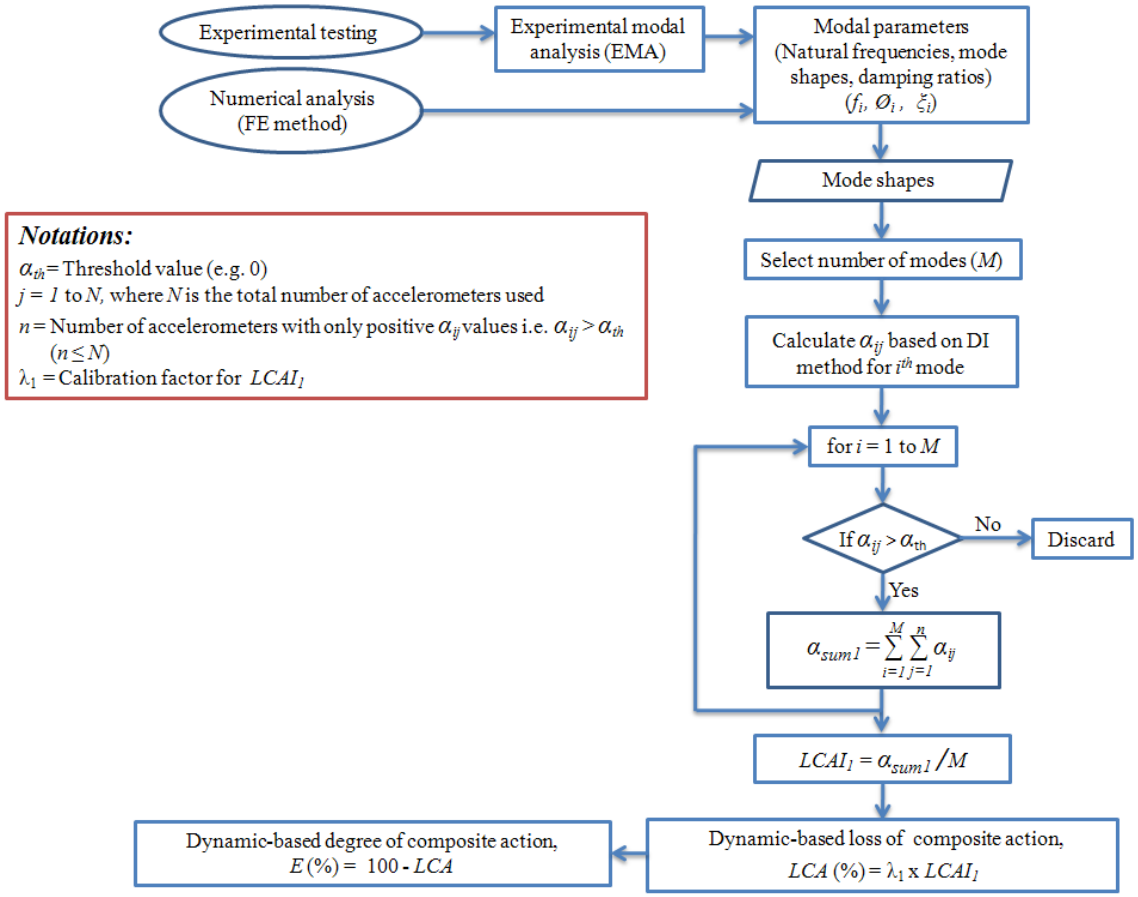

Figure 6.7 Flow chart for first composite action method ($LCAI_1$).

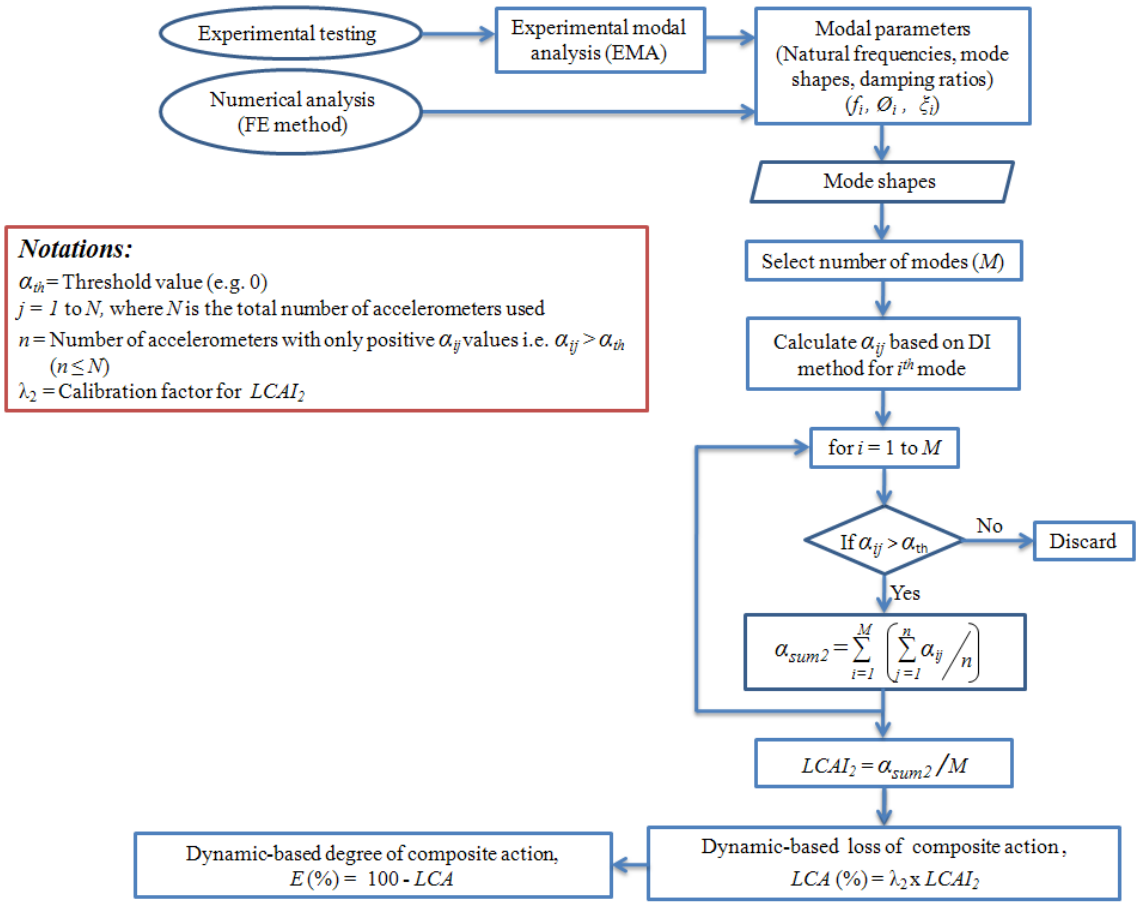

Figure 6.8 Flow chart for second composite action method ($LCAI_2$).

6.4 Numerical Analysis

This section presents the validation of the two proposed dynamic-based composite action methods applied to a numerical structure. As test structure, a 3.6 m long composite timber beam structure is used with different numbers of screw connections (‘3’, ‘5’, ‘9’, ‘17’ and ‘33’ screws) simulating different degrees of composite action. The beam structure is based on an experimental structure presented in Section 6.7. The numerical beam structure is simulated in 2-D with the commercial FE analysis package ANSYS (2011). Presented are the details of the numerical modelling including the element type selection, flange-web interface modelling and mesh size sensitivity study, the determination of the degree of composite actions and the discussion of the results.

6.4.1 Numerical Model

The test structure consisted of two LVL beams with an overall length of 3.6 m that are connected to form a T-shaped cross-section via screw-type connections (see Figures 6.9 and 6.10). The flange element of the composite beam was 90 mm wide and 45 mm thick, while the web element had a depth of 90 mm and a width of 35 mm. The flange and web elements were connected using shear connectors. Five different FE models were created having identical beam dimensions but different connection systems, i.e. five different shear connector configurations with '3', '5', '9', '17' and '33' screw connections. A summary of the number of screws and their spacing is presented for the different beam models.

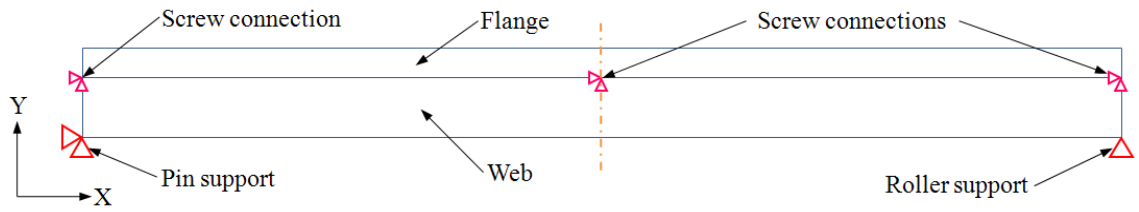

Figure 6.9 A numerical beam model with three screw connections (mm).

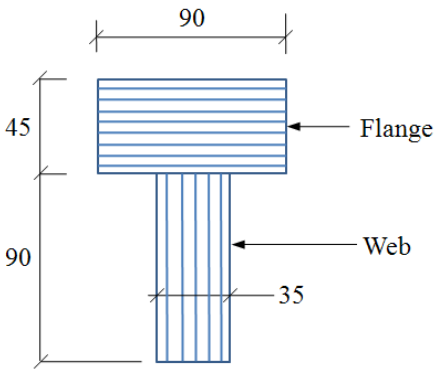

Figure 6.10 Cross-section and dimensions of the numerical timber beam models (mm).

Table 6.1 A summary of different screw configurations

No. of screws	Screw spacing (mm)
'33'	110
'17'	219
'9'	438
'5'	875
'3'	1750

The boundary conditions of the beam models were set as pin-roller as shown in Figure 6.9. Translations in global X and Y axes were restrained to simulate the pin support while the translation in global Y axis was restrained for roller support at the other end. For both supports, rotation in the global Z axis was allowed.

Note: The experimental beam was tested with a special type of pin-pin boundary conditions as shown in Figure 6.31 owing to the small thickness of the web and light-weight of the beam. The experimental pin supports had an offset of 75 mm from the bottom of the web. For the numerical models, a pin-roller support system was modelled with the support connections located at the bottom of the web. This resulted in a FE structure with good correlation in the natural frequencies and mode shapes to the experimental beam structure.

6.4.2 Element Types

The 2-D element PLANE42 was utilized to model both, the LVL flange and web of the composite beam structure. The PLANE42 element can be used either as a plane element such as for plane stress or plane strain or as an axisymmetric element. It is defined by four nodes having translations in the X and Y directions at each node as shown in Figure 6.11. The element has plasticity, creep, swelling, stress stiffening, large deflection and large strain capabilities (ANSYS 2011).

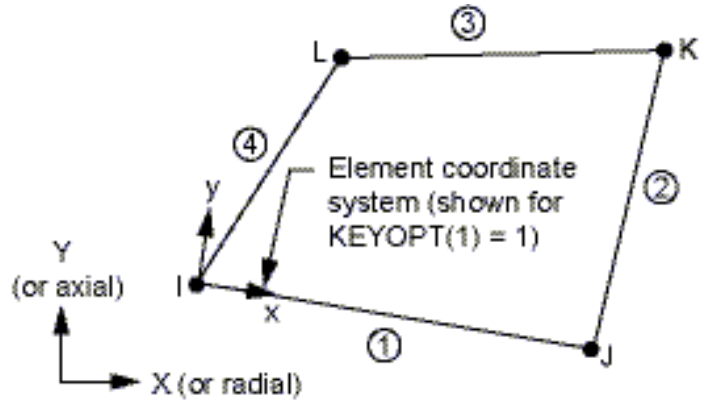

Figure 6.11 Geometric properties of PLANE42 (ANSYS 2011).

6.4.3 Flange-web Interface

To simulate different degrees of composite action, five FE beam models with identical dimensions but different number of screw connections (‘3’, ‘5’, ‘9’, ‘17’ and ‘33’) were created. Two nodes, one at the top of the web and another at the bottom of the flange, were coupled for each screw location to simulate a screw connection (see Figure 6.9). The coupling of nodes constrains both, horizontal and vertical displacements. While it is more accurate to undertake push-out tests on the experimental composite structure to determine correct shear connection properties, a contact connection of two nodes is deemed accurate enough for the numerical modelling of a screw connection. To prevent the penetration of the flange and web elements during deformation, the interface between the LVL flange and web was simulated utilizing contact and target elements. CONTA171 and TARGE169 were chosen as contact and target elements, respectively. The bottom layer of the flange was defined as contact surface while the top layer of the web was defined as target surface as shown in Figure 6.12.

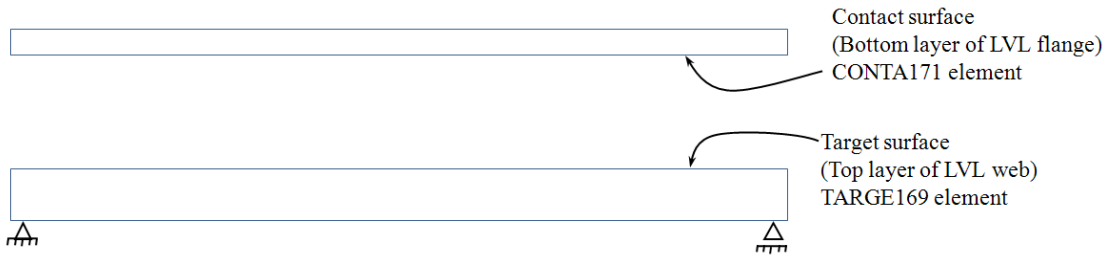

Figure 6.12 Schematic diagram of the composite beam showing contact and target surfaces.

CONTA171 was used to represent contact and sliding action between 2-D surfaces such as contact and target surfaces. The contact element is applicable to 2-D structural and coupled field contact analyses. It is located on the surfaces of 2-D solid, shell, or beam elements without midpoint nodes such as PLANE42. CONTA171 has the same geometric characteristics as the solid, shell, or beam element face to which it is connected to (see Figure 6.13). Contact occurs when the element surface penetrates one of the target segment elements such as TARGE169 on a specified target surface. Coulomb friction, shear stress friction, and user defined friction with the USERFRIC subroutine are allowed. The interface delamination can also be simulated utilizing this

element as it allows separation of bonded contact. No separation was permitted at flange-web interface while sliding was allowed (ANSYS 2011).

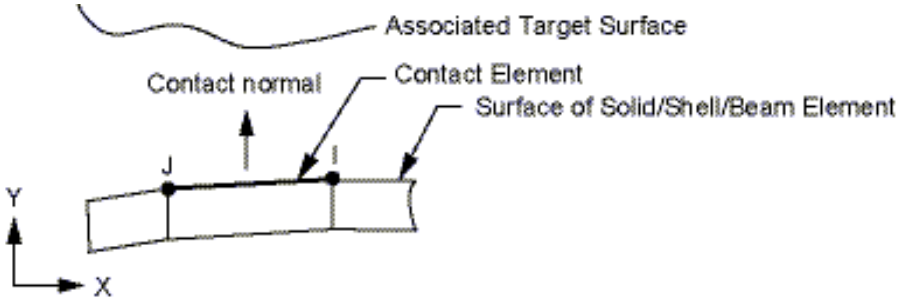

Figure 6.13 Geometric properties of CONTA171 (ANSYS 2011).

TARGE169 was utilized to model the 2-D target surfaces for the associated contact element CONTA171. The contact element itself overlays the solid elements describing the boundary of a deformable body and is potentially in contact with the target surface, defined by TARGE169. This target surface is discretised by a set of target segment element, namely TARGE169 and is paired with its associated contact surface having the same real constant set. Any translational or rotational displacement, temperature, voltage, and magnetic potential can be imposed on the target segment element (ANSYS 2011). The geometric properties of the TARGE169 are shown in Figure 6.14.

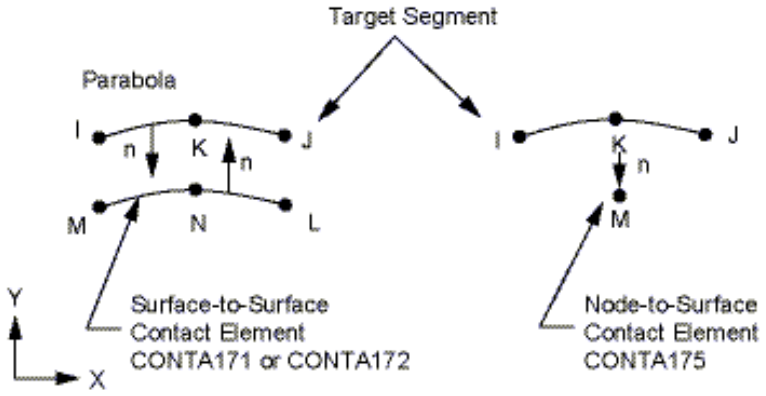

Figure 6.14 Geometric properties of TARGE169 (ANSYS 2011).

6.4.4 Material Properties

The material properties of the beam components (flange and web) were determined for the experimental LVL elements from different tests including bending, shear, compression and tension tests (Zabihi et al. 2012). The material properties relevant for

the 2-D FE modelling were MOE (E_x), density (ρ) and Poisson's ratio (υ). The assigned material properties were assumed isotropic for individual components because it was deemed sufficient to represent the flexural stiffness in longitudinal direction along the span length as this is the major contribution to the overall stiffness of the beam. However, the flange and web elements were experimentally tested in the flat-wise and edge-wise directions. The material properties used for the LVL components in the FE modelling are summarized in Table 6.2. The full set of material properties determined through experimental testing is presented in Section 6.7.3. More details on the experimental testing can be found in Zabihi et al. (2012).

Table 6.2 Material properties of LVL components of composite beam used for FE modelling

Component name	MOE	Density	Poisson's ratio
	E_x (GPa)	ρ (kg/m^3)	υ (%)
Flange	13.1	601	0.3
Web	13.3	604	0.3

6.4.5 Mesh Size

To identify the optimal mesh size for the numerical beam models, a sensitivity analysis was performed for both, static and modal analysis, to determine the optimum size of the elements resulting in sufficient accuracy. The optimisation parameters were the mid span deflection and first natural frequency, which were extracted from the FE models using static and modal analyses for different mesh sizes. The interface between the web and flange components was assumed fully composite for the sensitivity analysis. Five different element sizes were chosen, i.e. 45 × 45 mm, 22.5 × 22.5 mm, 15 × 15 mm, 10 × 10 mm and 5 × 5 mm. The total numbers of elements in the composite beam models for the corresponding element sizes were 234, 936, 2,106, 4,900 and 18,900. The results for the static and modal analyses are shown in Figures 6.15 and 6.16, respectively. From this sensitivity analysis, it was found that an element size of not greater than 10 x 10 mm (4,900 elements) is appropriate for the accurate modelling of the composite beam structure. Hence, in all the FE models, the size of the elements chosen for both, flange

and web components, was 5 x 5 mm. In total, the FE models of the beam had 18,900 elements.

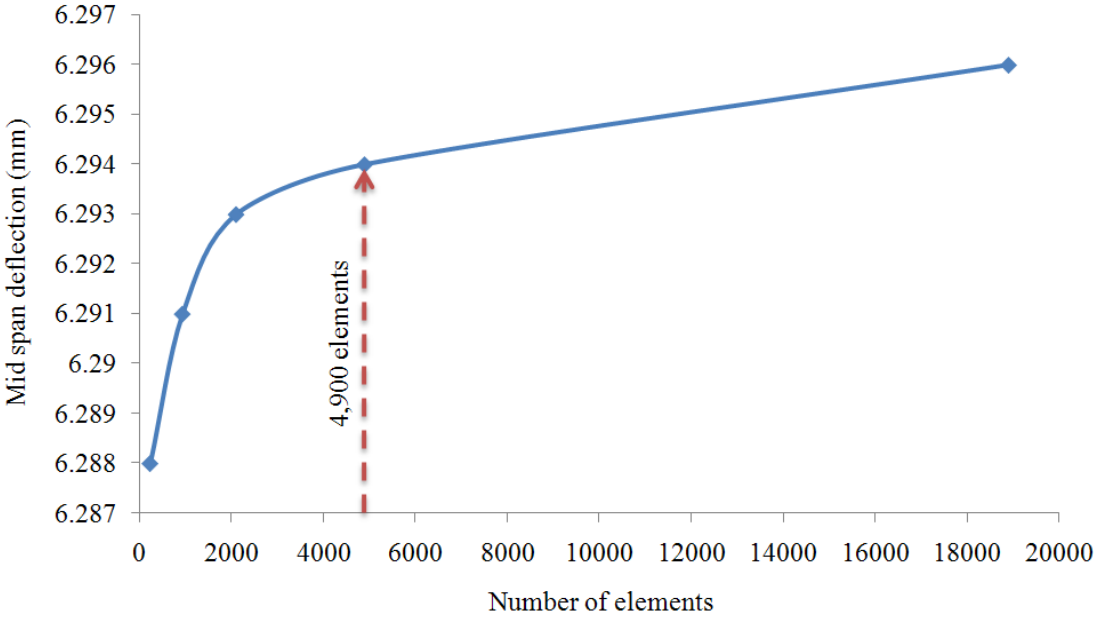

Figure 6.15 Mesh density sensitivity study of numerical timber composite beam for static analysis.

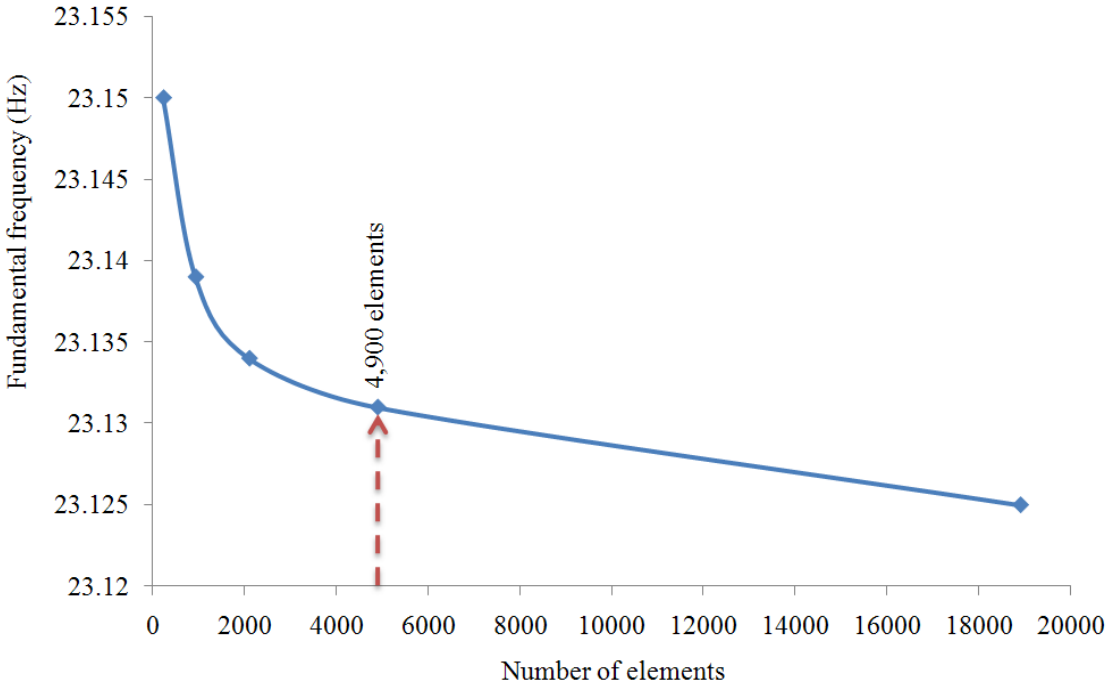

Figure 6.16 Mesh density sensitivity study of numerical timber composite beam for modal analysis.

6.5 Results of Numerical Analysis

6.5.1 Modal Parameters

For each composite beam model (with various numbers of screw connections), the natural frequencies and mode shapes of the first five flexural modes (*M1* to *M5*) were identified using the eigenvalue solution. Table 6.3 presents the determined natural frequencies of all numerical composite beam models along with the frequencies of the corresponding experimental beam structure. For the fundamental mode, the numerical composite beam connected with '33' screws had a natural frequency of 23.1 Hz. While for '9' and '17' screw connections, the frequency decrease was only minor, for '5' screws, there was a significant drop of about 21% in the first natural frequency. For '3' screws the natural frequency had a value of 18.1 Hz. For the higher modes, the frequency differences were higher for a reduced number of screw connections when compared to the fundamental frequency.

The errors between the natural frequencies of the numerical models and the experimental structures are presented in Table 6.4. In the table, the error is given in percentage for five different number of screw connections. The correlation showed that the FE results are fairly accurate as errors are below 10% for most cases. The second mode of the composite beam with '3' screw connections had a relatively larger error of 20.8%.

Table 6.3 Natural frequencies of numerical and experimental composite beam structures with different number of connection screws

No. of screws	Natural frequencies of numerical composite beam models (Hz)					Natural frequencies of experimental composite beam structure (Hz)				
	M1	*M2*	*M3*	*M4*	*M5*	*M1*	*M2*	*M3*	*M4*	*M5*
'33'	23.1	88.3	175.9	240.3	352.0	24.1	85.8	161.4	256.3	350.6
'17'	22.9	86.1	170.0	231.8	326.9	23.8	83.9	154.9	240.3	336.0
'9'	22.4	80.8	156.7	215.1	282.4	23.0	80.4	139.0	222.1	318.7
'5'	21.1	69.8	131.7	189.1	275.2	22.1	76.7	133.0	207.6	269.1
'3'	18.1	69.7	109.2	156.1	226.4	19.3	57.7	118.4	156.9	213.4

Table 6.4 Correlation between numerical and experimental natural frequencies (error in %)

No. of screws	*M1*	*M2*	*M3*	*M4*	*M5*
'33'	4.2	2.9	9.0	6.3	0.4
'17'	3.7	2.6	9.7	3.5	2.7
'9'	2.4	0.5	12.7	3.2	11.4
'5'	4.5	9.0	1.0	8.9	2.2
'3'	6.4	20.8	7.7	0.5	6.1

The mode shapes of the first five flexural modes of the numerical composite beam model with '33' screws are shown in Figure 6.17. In the figure, the horizontal axis shows the span of the beam, with '1' to '7' indicating seven data points along the beam, which correspond to sensor measurement locations in the experimental beam. The vertical axis presents scaled amplitudes of the mode shapes. The amplitude of the two data points at the ends of the beam was set to zero as no deformation was expected at the supports. The details of the first five flexural mode shapes of a timber composite beam from FE models with different number of screws are presented in Figures C.1 to C.3 (Appendix C). These figures show that the general shape of flexural modes of the beam is not affected due to increase in number of screws; however, there are slight differences in amplitude.

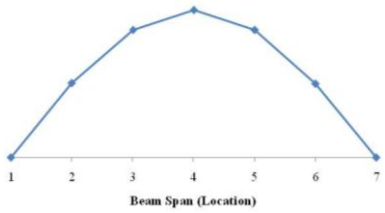

(a) Mode 1

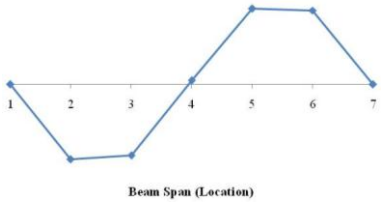

(b) Mode 2

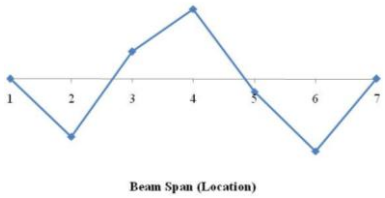

(c) Mode 3

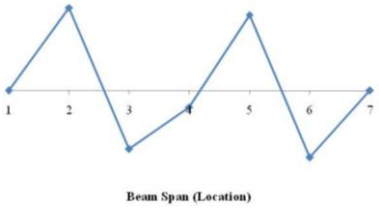

(d) Mode 4

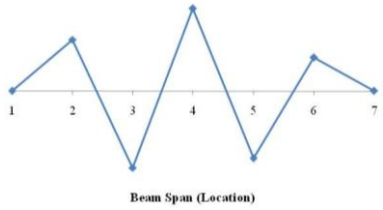

(e) Mode 5

Figure 6.17 First five flexural mode shapes of timber composite beam from FE model with '33' screw connections.

6.5.2 Indices $LCAI_1$ and $LCAI_2$

From the determined mode shapes, the DI method was applied to calculate the differences in modal strain energy between the beam models of different composite states, i.e. '33' connection screws represented the "undamaged"/"fully composite" state while '17', '9', '5' and '3' screws presented the various "damaged"/"partially composite" states. The severity estimator α was calculated for each of the first five mode shapes of the four partially composite states ('17', '9', '5' and '3' screws) using Equations (6.7) and (6.9). All determined α values are presented in Figures C.4 to C.7 (Appendix C). Next, from the α values, indices $LCAI_1$ and $LCAI_2$ were calculated according to Equations (6.10) and (6.11), respectively, to determine the loss of composite action of the beam models with reduced number of screw connections from '33' to '17', '9', '5' and '3' screws. The indices $LCAI_1$ and $LCAI_2$ were determined for two sets of modes, i.e. modes 1 to 3 and modes 1 to 5. This was done in order to study the effects of inclusion of mode shapes from higher modes in the composite action

analysis. This is of special importance for experimental structures, as with experimental modal analysis, it is generally very difficult to determine mode shapes of higher modes.

The results of the first index, $LCAI_1$, are shown in Figure 6.18 (a) and (b) for the mode shape sets of modes 1 to 3 and modes 1 to 5, respectively. Higher amplitudes of the index indicate a higher loss of composite action. As it was anticipated, the results show the smallest index amplitude for '17' screws while the amplitude increases with a decrease in the number of screw connections. The amplitudes obtained from modes 1 to 5 were slightly higher compared to the results from modes 1 to 3.

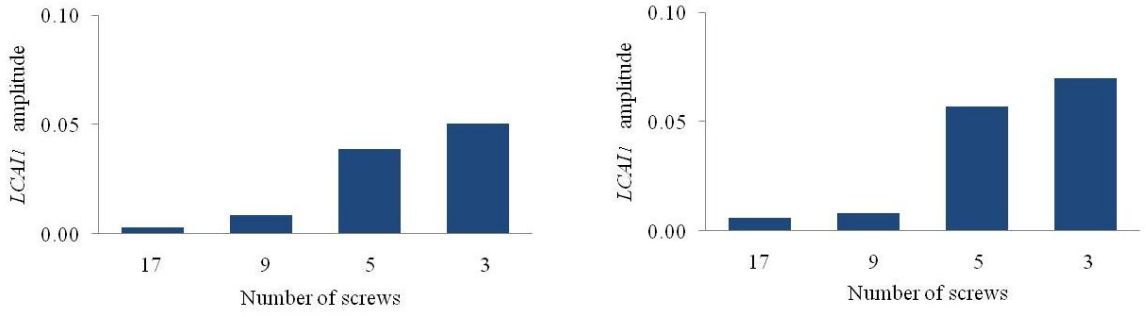

(a) (b)

Figure 6.18 $LCAI_1$ values of numerical timber composite beam for (a) modes 1 to 3 and (b) modes 1 to 5.

Figure 6.19 (a) and (b) present the results of the second index, $LCAI_2$, for modes 1 to 3 and modes 1 to 5, respectively. For $LCAI_2$, a similar trend of the results was found as for $LCAI_1$. Due to calculation differences in deriving $LCAI_1$ and $LCAI_2$, amplitudes of $LCAI_2$ are lower than of $LCAI_1$.

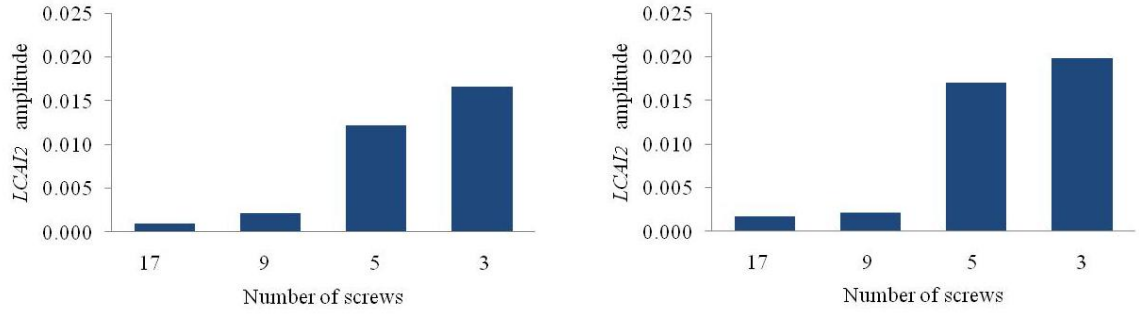

(a) (b)

Figure 6.19 $LCAI_2$ values of numerical timber composite beam for (a) modes 1 to 3 and (b) modes 1 to 5.

The results of $LCAI_1$ and $LCAI_2$ clearly show the capability of these indices to indicate the composite state of a structure. The full set of outcomes of $LCAI_1$ and $LCAI_2$ for the first five flexural modes of the numerical composite beam is shown in Figures C.8 and C.9 (Appendix C).

6.5.3 Loss of Composite Action

To correlate the determined indices $LCAI_1$ and $LCAI_2$ to the static-based loss of composite action, calibration factors must be applied. These factors were obtained by scaling the dynamic-based indices to the static-based loss of composite action values based on the amplitudes of the maximum loss of composite action, i.e. connection with '3' screws. These calibration factors, λ_1 and λ_2, were determined as 496 and 1,508 for $LCAI_1$ and $LCAI_2$, respectively. By multiplying the indices $LCAI_1$ and $LCAI_2$ with these corresponding factors, the dynamic-based loss of composite action, *LCA*, is identified.

The results of the determined dynamic-based *LCA* values compared to the static-based *LCA* values are depicted for $LCAI_1$ and $LCAI_2$ in Figures 6.20 and 6.21, respectively. In the figures, results are presented for (a) mode shape set of modes 1 to 3 and (b) mode shape set of modes 1 to 5. When compared to the static-based *LCA* values, good results are obtained for the composite beam models of '17', '9' and '3' screws with errors below 10%; while for '5' screws, the error is significant. It is assumed that the high error for '5' screws is due to the fact that the location of the two quarter-point screws is close to the location of node points of modes 3, 4 and 5. This causes a singularity issue, which results in increased α values for these modes, and subsequently in an increase in *LCA* values. Due to this error, the outcomes of the beam model with '5' screw connections are poorer for the mode set of modes 1 to 5 than for modes 1 to 3. It is further observed that the outcomes derived from $LCAI_2$ are slightly better than those obtained from $LCAI_1$, which highlights the superiority of using $LCAI_2$ instead of $LCAI_1$. Overall, a good correlation between the dynamically derived *LCA* and the static-based *LCA* is obtained, which demonstrates the effectiveness of the proposed composite identification method.

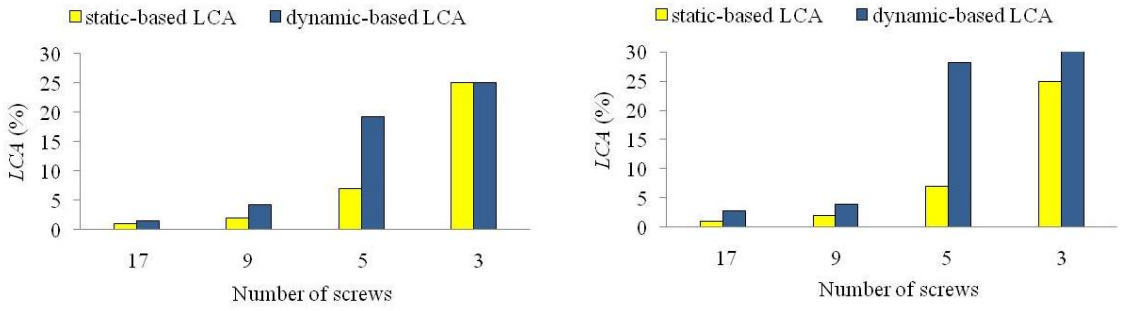

(a) (b)

Figure 6.20 Dynamically derived *LCA* based on $LCAI_1$ and static-based *LCA* of numerical timber composite beam for (a) modes 1 to 3 and (b) modes 1 to 5.

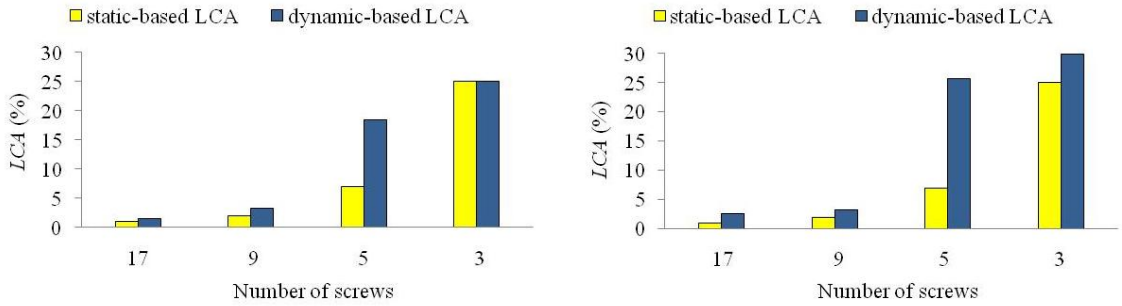

(a) (b)

Figure 6.21 Dynamically derived *LCA* based on $LCAI_2$ and static-based *LCA* of numerical timber composite beam for (a) modes 1 to 3 and (b) modes 1 to 5.

6.6 Exploration

6.6.1 Study of Mode Shape Reconstruction

This section studies the effect of mode shape reconstruction on the results of the proposed dynamic-based composite action method. It is investigated if it is beneficial to reconstruct mode shapes of a structure derived from a limited number of sensors using interpolation techniques. In particular, the cubic spline function is used to reconstruct mode shapes from a 7 point to a 31 point data array.

The reliability and accuracy of damage/composite action identification is greatly influenced by the density of measurement points (or sensors), especially for modal-based methods (Stubbs & Park 1996; Wang & Zong 2002). The diagnosis of

damage/composite action can be done more accurately with the use of more sensors. However, it is important for both, cost and practicality, to be able to obtain reliable results using only a few number of measurement sensors. If the acquired data are below a certain quantity, the results inevitably become unreliable. Hence, an optimal procedure is able to give more reliable and precise identification results from a minimal number of sensors. For mode-shape-based methods, one way of achieving improved identification results from a minimal number of measurement points is to refine mode shape vectors utilising data interpolation techniques. For the DI method, the approach of mode shape reconstruction for improved damage detection has been discussed in several publications. Park & Stubbs (1995) and Stubbs & Park (1996) utilised Shannon's sampling theorem combined with the DI method to locate damage with fewer sensor data points. Worden, Manson & Allman (2001) applied a cubic convolution polynomial interpolation to refine mode shapes for strain-energy-based damage detection. Choi (2007) compared cubic spline interpolation techniques against Shannon's sampling theorem techniques for mode shape reconstruction and subsequent damage identification based on the DI method. Choi concluded that utilising cubic spline interpolation for mode shape refinement is more effective in improving damage identification results than using Shannon's sampling theorem.

In this study, the experimental testing of the timber composite beam was performed utilising a number of five accelerometers (see Section 6.7) and two data points at the supports were set to zero. To obtain comparable results for the numerical investigation, data was also only acquired from five measurement point with the beam ends being set to zero. Hence, for both studies, the mode shape vectors had seven data points. To enhance the quality and effectiveness of the composite action identification, a reconstruction of the mode shape vectors from 7 to 31 points is performed. Based on the results and recommendations of Choi (2007), the cubic spline technique is used for interpolation. MATLAB (The MathWorks 2007) provides an easy access to data interpolation using the spline function. In the operation, a tri-diagonal linear system is solved to describe the coefficients of various cubic polynomials, which make up the interpolating spline. From the seven-point mode shapes and the reconstructed mode shape vectors (containing 31 data points), first, α values were calculated for the various numerical composite beam models. The results of the derived 7-point and 31-point α values of the first five flexural mode shapes are shown in Figures C.4 to C.7 (Appendix

C). Second, the loss of composite action indices, $LCAI_1$ and $LCAI_2$, were determined based on the 7-point and 31-point α values. The full set of results of $LCAI_1$ and $LCAI_2$ from 7 and 31 point mode shapes are shown in Figures C.8 to C.10 (Appendix C). Third, the dynamic-based *LCA* values were determined by multiplying indices $LCAI_1$ and $LCAI_2$ with unique calibration factors for reconstructed mode shape vectors with 31 data points, i.e. 285 and 4,787, respectively. The resulting dynamic-based *LCA* values compared to the static-based *LCA* values are shown for $LCAI_1$ and $LCAI_2$ derived values in Figures 6.22 and 6.23, respectively. In the figures, the dynamic-based *LCA* values obtained from combinations of (a) modes 1 to 3 and (b) modes 1 to 5 are presented. From the results it was found that for '17', '9' and '3' screws, the accuracy of the loss of composite action predictions were very similar for 7-point and reconstructed 31-point modes shapes. For the beam model with '5' connection screws, the obtained errors were even larger for dynamic-based *LCA* values of 31-point mode shapes compared to 7-point mode shapes. The reason for this increased error is assumed to be related to the accumulation of the singularity error as discussed above. To conclude, a reconstruction of mode shapes using cubic spline interpolation techniques for improved composite action identification is not recommended.

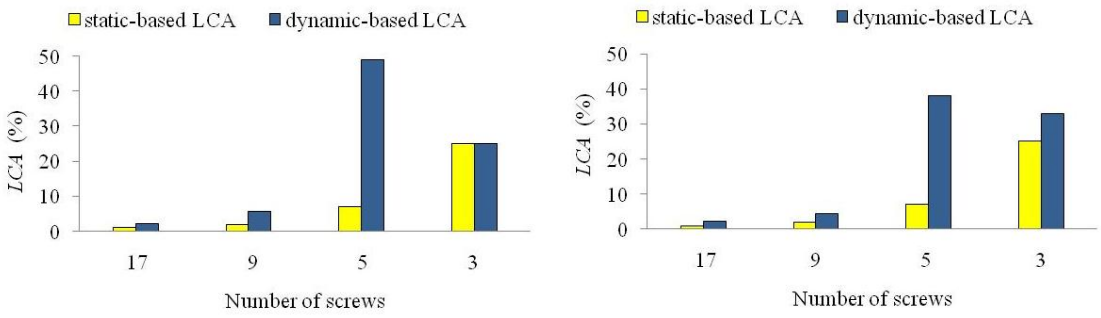

(a) (b)

Figure 6.22 Dynamically derived *LCA* based on $LCAI_1$ and static-based *LCA* of numerical timber composite beam for (a) modes 1 to 3 and (b) modes 1 to 5 from reconstructed 31-point mode shapes.

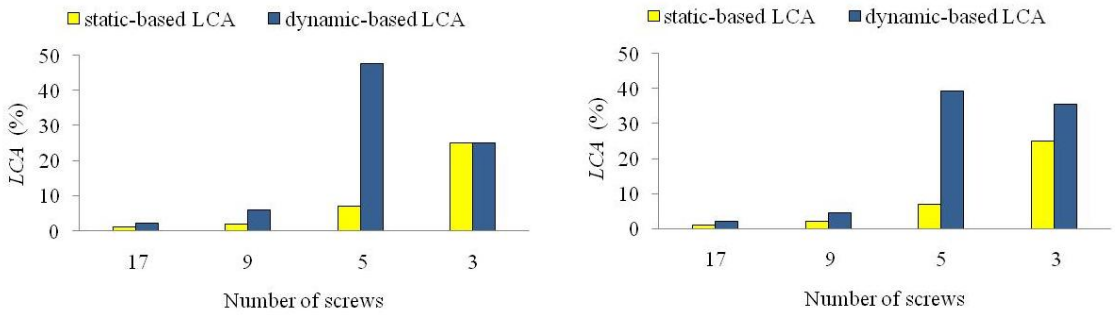

(a) (b)

Figure 6.23 Dynamically derived *LCA* based on $LCAI_2$ and static-based *LCA* of numerical timber composite beam for (a) modes 1 to 3 and (b) modes 1 to 5 from reconstructed 31-point mode shapes.

6.6.2 Study on the Effect of the Shear Connection Plane to the Neutral Axis

To investigate the applicability of the proposed composite action identification method, to flooring systems of various cross-sections (with special focus on the neutral axis), the method was applied to timber composite beam models of different cross-section dimensions. In particular, the effect of the distance of the neutral axis to the shear connection plane was studied.

In total, numerical composite beam models of five different cross-sections (Cases 1 to 5) were created and analysed. All beam models had a span of 3.5 m. The different cross-sections of the various composite beam structures including the position of the neutral axis are shown in Figure 6.24. Case 1 represents the composite beam structure that was studied in the previous sections and that was also experimentally tested and analysed as presented in later sections. The neutral axis of Case 1 was located 7 mm from the shear connection plane. For Cases 2, 4 and 5, the neutral axis was in the same location as the shear connection plane (0 mm distance). Case 3 represents a composite beam structure characteristic of a typical composite flooring section with the neutral axis having a distance from the shear connection plane of 15 mm. The neutral axis of these sections was determined based on fully composite section.

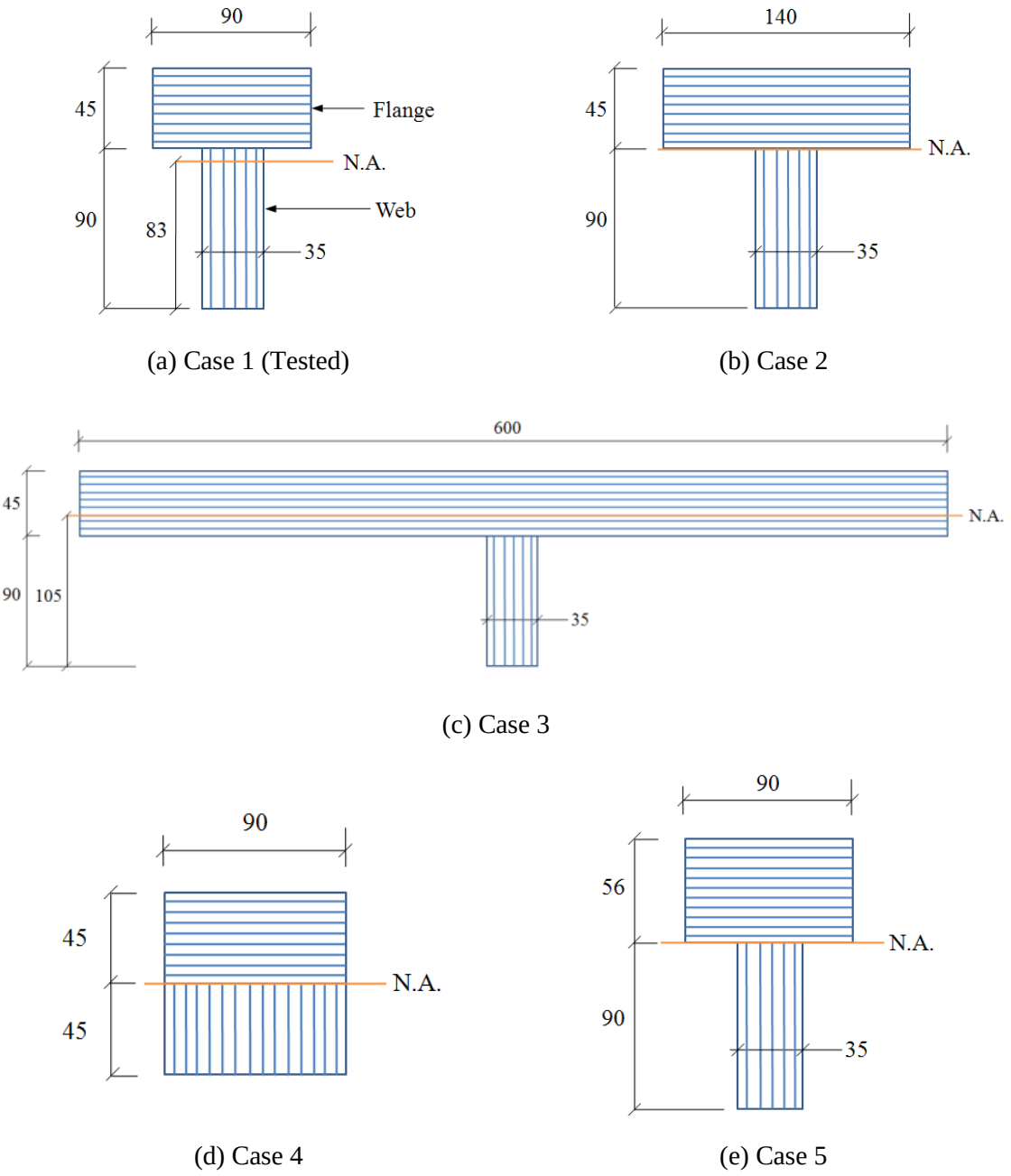

(a) Case 1 (Tested)

(b) Case 2

(c) Case 3

(d) Case 4

(e) Case 5

Figure 6.24 Five different cross-sectional dimensions of investigated timber composite beam structures (mm).

For each case, the first five flexural modes including natural frequencies and mode shapes were determined. From the mode shapes, α values were calculated and subsequently the indices $LCAI_1$ and $LCAI_2$ were derived. By multiplying $LCAI_1$ and $LCAI_2$ with individual calibration factors, the dynamic-based *LCA* values were determined. For Case 2, the derived dynamic-based *LCA* values were correlated against the static-based *LCA* values and depicted in Figures 6.25 and Figure 6.26. The *LCA*

results of all other cases are shown in Figures C.11 to C.13 (Appendix C). From the presented outcomes it is observed that the proposed composite action method delivers very comparable results for composite beam structures of different cross-sections. Further, it is found that the distance of the neutral axis to the shear connection plane does not have any significant effect on the composite action identification results. Hence, it is concluded that the proposed method is applicable to composite flooring systems of any cross-sectional dimensions.

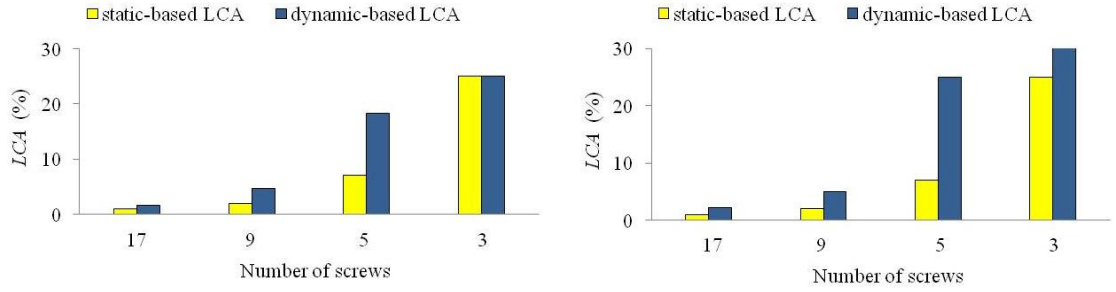

(a) (b)

Figure 6.25 Dynamically derived *LCA* based on $LCAI_1$ and static-based *LCA* of numerical timber composite beam of Case 2 for (a) modes 1 to 3 and (b) modes 1 to 5.

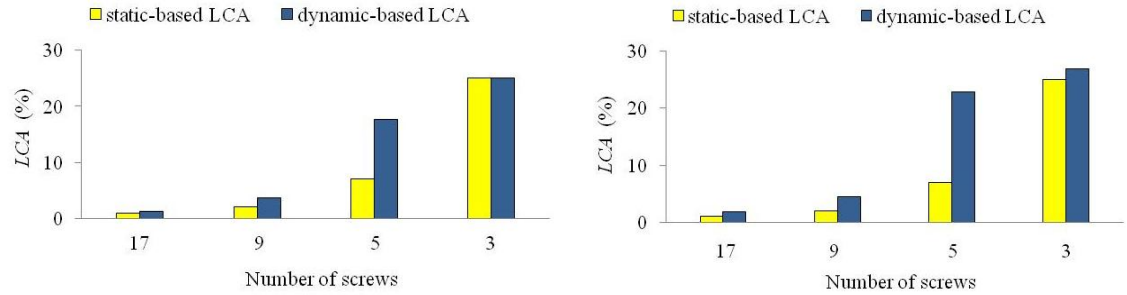

(a) (b)

Figure 6.26 Dynamically derived *LCA* based on $LCAI_2$ and static-based *LCA* of numerical timber composite beam of Case 2 for (a) modes 1 to 3 and (b) modes 1 to 5.

6.7 Experimental Investigation

6.7.1 Experimental Test Structure

To validate the proposed dynamic-based composite action identification method, it was tested on a laboratory structure. As test structure, a timber composite beam consisting of

two hySPAN PROJECT LVL elements with pin-pin support conditions and a span length of 3.5 m was used. The two LVL web and flange elements were connected with different numbers of screws to simulate various degrees of composite action. The dimensions of the experimental beam were the same as for the numerical timber composite beam structure (Case 1) that was discussed in the previous sections. The test setup of the laboratory composite beam is illustrated in Figure 6.27. The cross-sectional dimensions of the flange and web elements were 90 × 45 mm and 90 × 35 mm, respectively (see Figure 6.28).

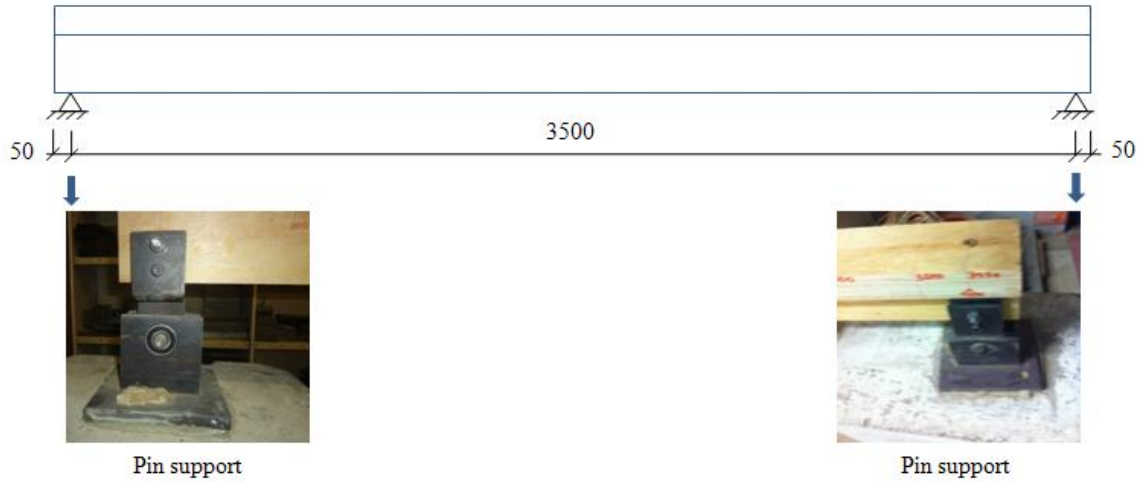

Figure 6.27 Experimental test setup of laboratory timber composite beam (mm).

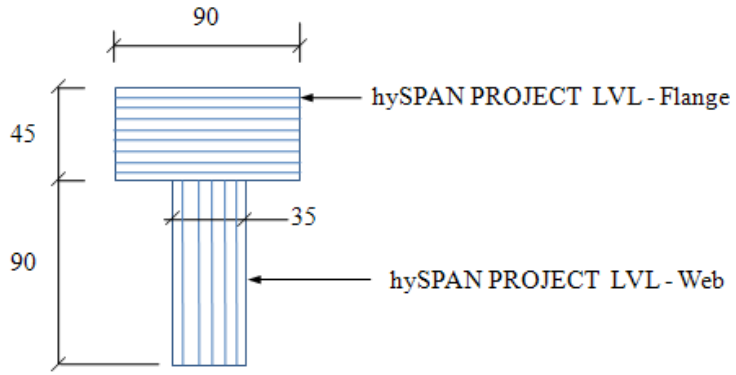

Figure 6.28 Cross-sectional dimensions of laboratory timber composite beam (mm).

As shear connector, a normal wood screw (Type 17) was used to connect the flange to the web element as illustrated in Figure 6.29. The total length of the screw was 75 mm and the threaded length was 50 mm. The measured shank diameter was 5 mm. The screw was inserted from the top of the flange, with about 30 mm length of the screw being driven into the web element as shown in Figure 6.30. The laboratory beam

structure was tested with five different screw connection conditions, i.e. '3', '5', '9', '17' and '33' screws. The spacing between the screws for all five composite conditions is presented in Table 6.5.

Figure 6.29 Dimensions of the wood screw used to connect the elements of the experimental timber composite beam (mm).

Table 6.5 Number of screw connections and their spacing for different composite test stages

Experimental test order	No. of screws	Screw spacing (mm)
1	'3'	1750
2	'5'	875
3	'9'	438
4	'17'	219
5	'33'	110

For the first tested composite condition, only three screws were used to connect the two LVL elements; two were inserted at the pin supports and one at mid span with equal spacing of 1,750 mm as shown in Figure 6.30. For the succeeding four composite conditions, the number of connection screws was increased to '5', '9', '17' and '33' screws. The additional screws were inserted in-between the screws of the previous configuration. Hence, the spacing between the screws in the succeeding configurations was halved from previous ones.

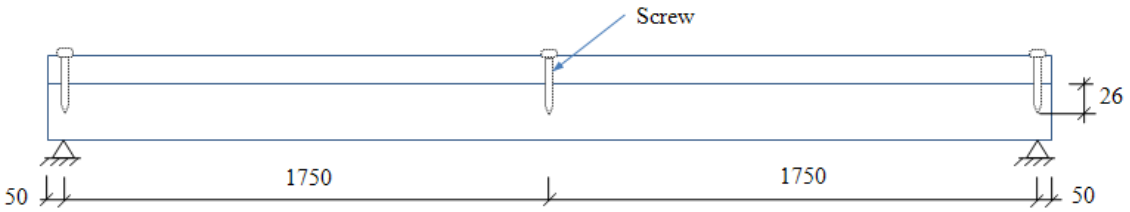

Figure 6.30 Setup of first experimental test with '3' screws (mm).

6.7.2 Fabrication of Test Structure

To install the laboratory test structure, first, the two pin supports were glued to concrete blocks as shown in Figure 6.31 (a). Then, the two concrete blocks were bonded rigidly to the floor using plaster of paris with a distance between the pin support centres of 3.5 m. Second, for the LVL web element, two holes of 10 mm diameter were drilled. The holes were located at beam each with an offset of 50 mm from both ends of the beam (see Figure 6.31 b). The holes were used to connect the web to the pin supports as shown in Figure 6.31 (c). Third, the flange was placed on top of the web and clamped at three locations as illustrated in Figure 6.31 (d). Fourth, for the first testing stage, three screws were drilled from the top of flange element (two at the supports and one at mid span) as shown in Figure 6.31 (e).

(a) Pin support

(b) Hole in web

(c) Web element connected to supports

(d) Clamping of flange and web before screwing

(e) Installation of screw

Figure 6.31 Fabrication of the experimental timber composite beam.

6.7.3 Material Properties

The two timber components of the laboratory beam structure, i.e. flange and web, were made from HySpan PROJECT LVL (supplied by Carter Holt Harvey). The orientation of the LVL components in the composite beam structure was different since the flange was installed in a flat-wise (or horizontal) direction while the web was installed in edge-wise (or vertical) direction. To characterise the properties of the LVL components, a number of bending, shear, compression and tension tests were conducted at UTS. The material properties were tested in flat-wise and edge-wise directions as these replicate the orientation of the flange and web elements in the tested composite beam. Details of the conducted tests can be found in Zabihi et al. (2012). A summary of the determined material properties (mean values) for the individual components of the timber composite beam is presented in Table 6.6.

Table 6.6 Material properties of LVL timber elements (*Courtesy of Zhinus Zabihi as part of a concurrent PhD study*)

Component name	MOE	Density	Bending	Shear	Compression	Tension	MoR
	E_x (GPa)	ρ (kg/m^3)	f_b (MPa)	f_v (MPa)	f_c (MPa)	f_t (MPa)	G (MPa)
Web	13.3	603.7	66.1	6.7	51.1	37.4	554.3
CoV (%)	4.0	1.3	9.8	4.2	7.6	13.5	16.0
Flange	13.1	601.1	65.5	5.8	51.4	36.4	239.5
CoV (%)	12.3	1.8	17.1	15.0	8.2	4.7	25.5

Moisture content (MC) of the tested beam elements was measured on the day of testing in accordance with the AS/NZS 1080.1 (1997) using the oven dry method. The MC value of the LVL used in the beam was found to be 10.2%. Three small LVL timber blocks (test piece) were used to measure the MC of the LVL components of the beam. The size of these pieces was 100 × 100 × 50 mm. The test pieces were placed on the top of the beam a week before testing. On the day of testing, the weight of the test pieces was measured by weighing them with a digital scale and subsequently they were put in the drying oven for 24 hours at a temperature range from 102^{o}C to 105^{o}C. The weight of the test pieces was measured after 24 hours and they were placed in the oven for a further 24 hours to make sure that the moisture was completely removed. The MC values were calculated using the weight of the test pieces before (initial weight) and after (dry weight) oven drying.

6.7.4 Instrumentation and Testing Procedure

To measure the dynamic response of the experimental timber composite beam, five uniaxial accelerometers were mounted on the test structure. The sensors were located on the centre line on top of the flange element with even spacing. The actual locations (1/6th, 2/6th, 3/6th, 4/6th and 5/6th of the span length) are shown in Figures 6.32 and 6.33.

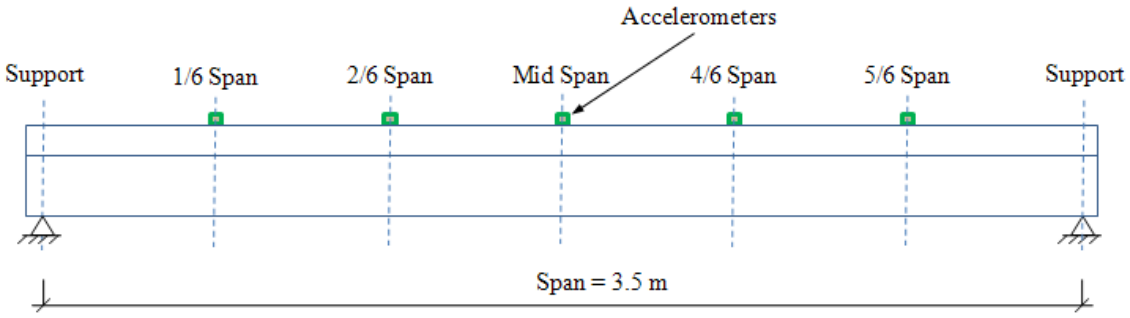

Figure 6.32 Arrangement of the accelerometers along the span at 1/6th, 2/6th, 3/6th, 4/6th and 5/6th span.

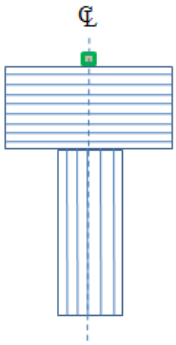

Figure 6.33 Location of accelerometers at the cross-section.

The equipment used for the experimental testing is shown in Figure 6.34. The accelerometers were of ICP type (model 352C34) having a sensitivity of 100 mV/g. The beam was dynamically excited with an impact using a modal hammer (model HP 086C05). The impact force was applied on top of the beam at two impact locations, i.e. at 1/3rd of the span and mid span. A multi-channel signal conditioner (PCB model 483B03) was used to amplify and condition the time history signals from the impact hammer (input signal) and the accelerometers (output signal). From the signal conditioner, the input and output channels were connected to a data acquisition system through a terminal block (model SCB - 68). The acquisition system had two internally synchronised acquisition cards (model NI PCI - 6133) with a resolution of 14 bit and a sampling rate of 2.5 MS/sec, simultaneously. The full instrumentation of the test beam is shown in Figure 6.35.

For all tests, the sampling rate was set to 1,000 Hz with 16,384 time domain data points recorded, which corresponds to a frequency bandwidth ranging from 0 to 500 Hz with 8,192 FRF data points giving a frequency resolution of 0.061 Hz in the frequency domain. The software LMS CADA-X was used for operating the modal testing. For each screw connection stage, five test measurements (five different hammer hits) were recorded each for the two different impact locations (1/3rd of the span and mid span).

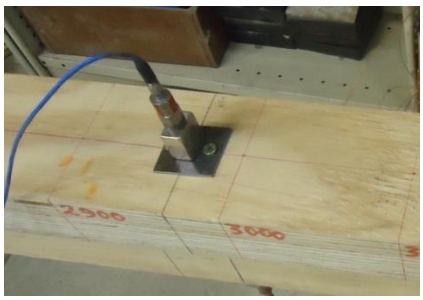

(a) Accelerometer model PCB 352C34

(b) Modal hammer

(c) Terminal block

(d) Multi-channel signal conditioner

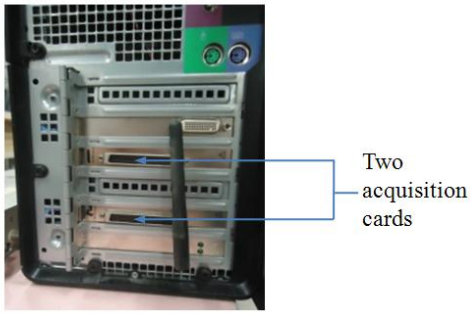

(e) Data acquisition system

Figure 6.34 Dynamic test equipment.

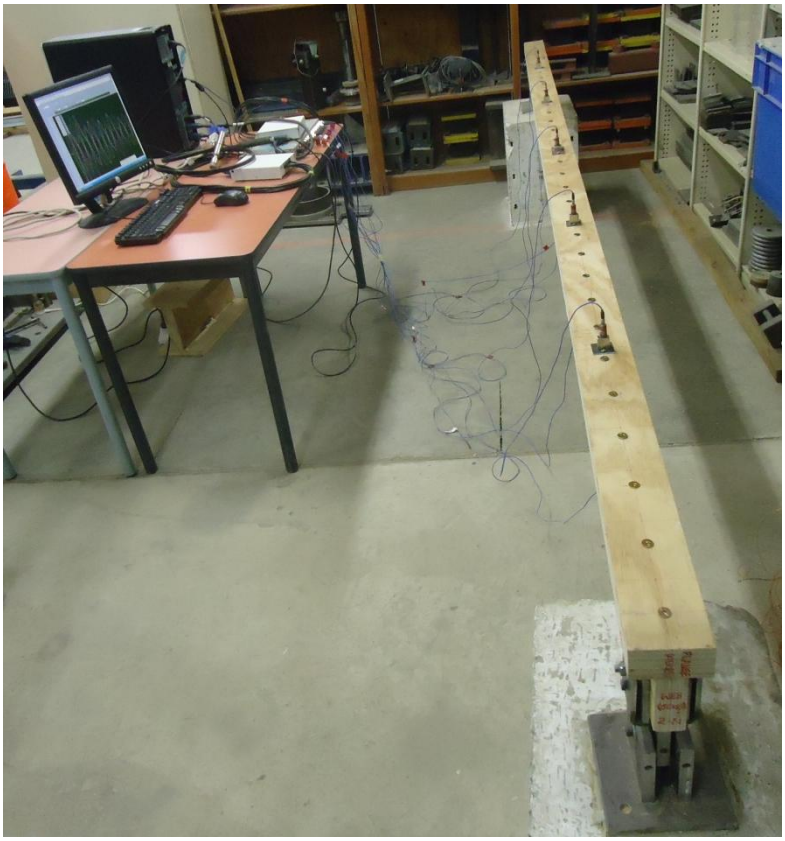

Figure 6.35 Instrumentation of the experimental timber composite beam.

6.7.5 Data Processing and Analysis

MT and EMA was performed to determine the modal parameters of the experimental timber composite beam such as natural frequency, damping ratio and mode shapes. The MT and EMA configuration is shown in Figure 6.36. Fourier transformation was used to convert the time history signals acquired from input and output channels into frequency spectra. The modal parameters of the beam were extracted from the FRFs with the use of the post-processing module in LMS CADA-X software. A maximum of five modes were determined for the experimental beam structure of various connection configurations. The acquired mode shapes consisted of seven data points resulting from five accelerometer measurements and the values on the beam supports set to zero.

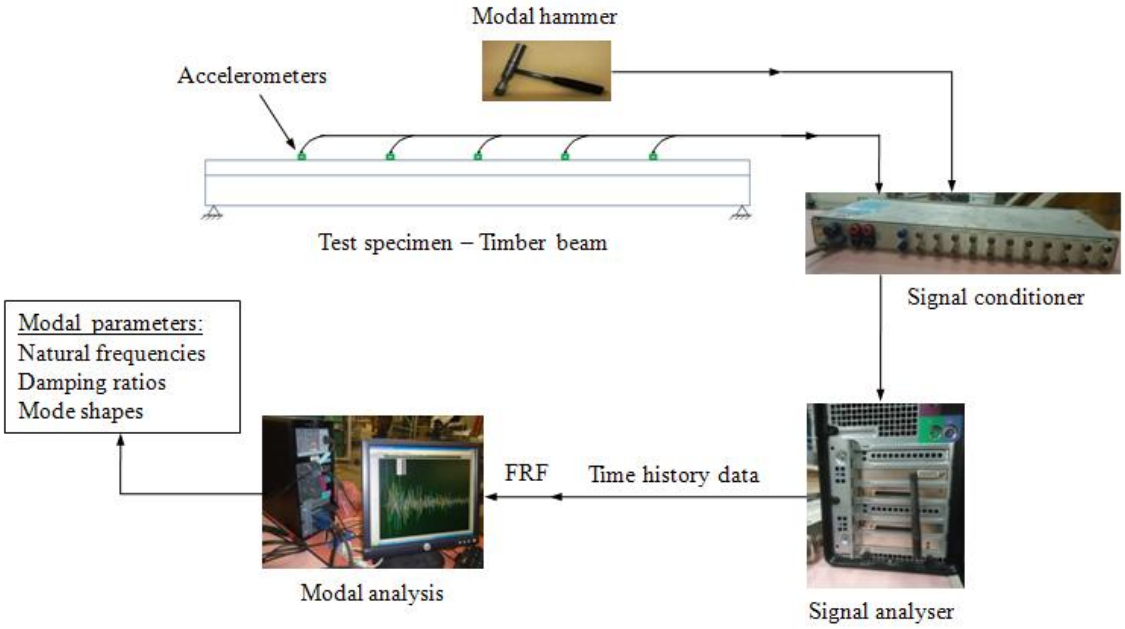

Figure 6.36 MT and EMA configuration.

6.8 Results of Experimental Investigation

In this section, the results of the dynamic testing along with the identification of the composite action of different connection configurations of the laboratory beam structure are presented. First, the identified modal parameters are discussed, second, the indices $LCAI_1$ and $LCAI_2$ are presented, third, the determined *LCA* values are analysed and fourth, the results of mode shape reconstructions are discussed.

6.8.1 Modal Parameters

The natural frequencies and the corresponding damping ratios of the first five modes, identified through MT and EMA, are presented in Table 6.7 and Table 6.8, respectively. The listed values are mean values of five sets of testing data resulting from five different hammer hits. Along with the actual frequency and damping values, CoV are given in brackets. The full set of identified natural frequencies and damping ratios for all tests including statistical values of mean and CoV are listed in Tables C.1 and C.2 (Appendix C).

From Table 6.7, it can be seen that the determination of the natural frequencies is more reliable compared to the damping ratios as CoV values for the frequencies are below 5% while values for the damping ratios are up to 56%. The stiffness of the beam increases with an increase in the number of shear connectors, as a consequence, the natural

frequency also increases. This phenomenon can clearly be seen in the presented table. For the fundamental frequency, there was a large increase of about 15% from the composite stage of '3' screws to '5' screws, while for the preceding stages of '9', '17' and '33' screws, the increments were only 4.0%, 3.5% and 1.3%, respectively. This shows that an almost fully composite state was achieved for '33' screws and there will only be a minimal increment in natural frequency and stiffness with a further increase in the number of connection screws. For damping ratios, no general trend was observed.

Table 6.7 Natural frequencies of the first five flexural modes of the experimental timber composite beam for different screw connection stages

Stage	No. of screws	Natural frequencies (Hz)				
		f_1	f_2	f_3	f_4	f_5
1	'3'	19.3 (1.3%)	57.7 (0.4%)	118.4 (0.3%)	156.9 (1.2%)	213.4 (0.4%)
2	'5'	22.1 (0.5%)	76.7 (2.2%)	133.0 (2.3%)	207.6 (1.8%)	269.1 (3.8%)
3	'9'	23.0 (0.8%)	80.4 (0.8%)	139.0 (0.9%)	222.1 (0.9%)	318.7 (1.3%)
4	'17'	23.8 (0.2%)	83.9 (0.9%)	154.9 (1.3%)	240.3 (0.9%)	336.0 (1.7%)
5	'33'	24.1 (0.2%)	85.8 (0.2%)	161.4 (1.0%)	256.3 (0.6%)	350.6 (2.9%)

Note: in bracket (%) = CoV

Table 6.8 Damping ratios of the first five flexural modes of the experimental timber composite beam for different screw connection stages

Stage	No. of screws	Damping ratio (%)				
		ξ_1	ξ_2	ξ_3	ξ_4	ξ_5
1	'3'	2.1 (6.8%)	1.9 (6.7%)	1.4 (13.5%)	2.1 (53.7%)	1.0 (13.6%)
2	'5'	2.4 (13.6%)	1.1 (32.1%)	2.4 (50.2%)	2.8 (19.9%)	3.0 (22.3%)
3	'9'	2.6 (13.8%)	3.3 (23.5%)	4.0 (17.6%)	3.1 (30.9%)	0.4 (41.4%)
4	'17'	1.9 (1.0%)	2.0 (28.9%)	2.1 (31.5%)	2.6 (22.1%)	0.8 (40.1%)
5	'33'	1.6 (8.8%)	1.7 (5.5%)	1.6 (34.4%)	1.2 (18.1%)	0.1 (55.9%)

Note: in bracket (%) = CoV

The captured mode shapes of the first five flexural modes of the experimental beam with '33' screw connections are shown in Figure 6.37. The horizontal axis presents the span of the beam with locations '1' and '7' being the two support ends, which were set to zero, and locations '2' to '6' representing the positions of the measurement sensors.

The vertical axis displays the amplitudes of the mode shapes. The captured mode shapes were as expected and comparable to the results from the numerical simulations. For modes 4 and 5, however, it was difficult to extract reliable mode shape results due to uncertainties in the stabilisation diagram. In MT and EMA, the issue of reliable extraction of higher modes is however unavoidable due to the limited number of sensors. The details of the first five flexural mode shapes of the experimental timber composite beam, with different number of screws, are presented in Figures C.14 to C.16 (Appendix C). These figures show that the general shape of flexural modes of the beam is not affected by the increase in number of screws, however, there are significant differences in amplitude of beam with '3' screws compared to '5', '9', '17' and '33' screws for higher modes.

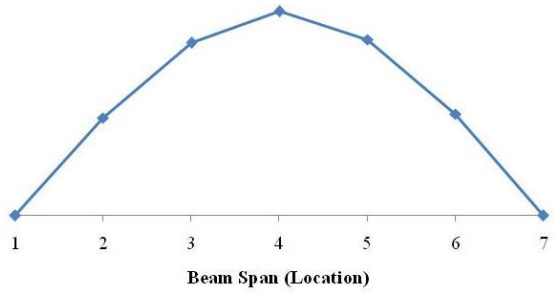

(a) Mode 1

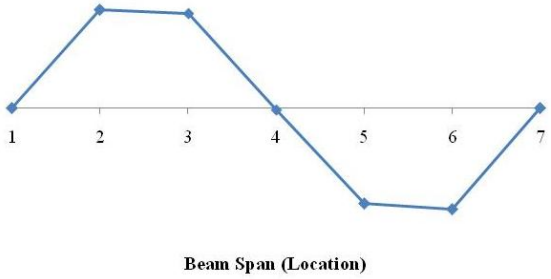

(b) Mode 2

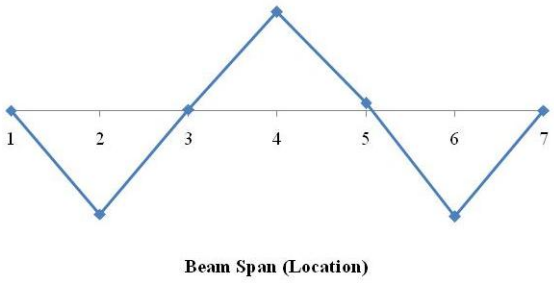

(c) Mode 3

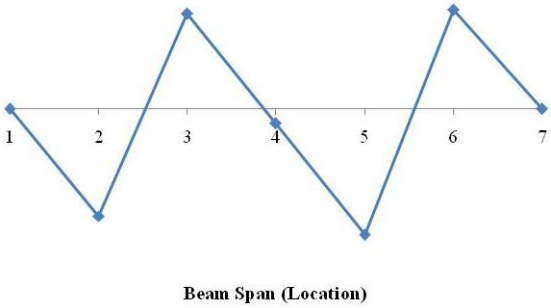

(d) Mode 4

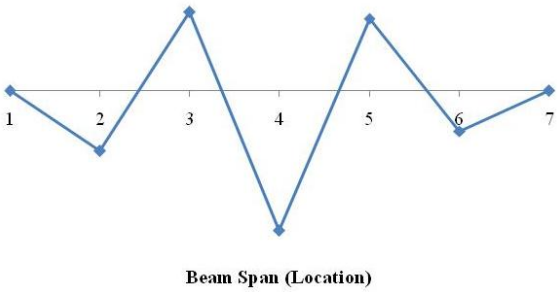

(e) Mode 5

Figure 6.37 Mode shapes of first five flexural modes of the experimental timber composite beam with '33' screws.

6.8.2 Indices $LCAI_1$ and $LCAI_2$

From the determined mode shapes, the severity estimator α was calculated for the different partially composite stages by following the DI method and applying Equations (6.7) and (6.9). The connection stage with '33' screws was regarded as "fully composite state" (no loss of screws/undamaged) and the "partial composite stages" of '17', '9', '5' and '3' screws were regarded as damaged states. From the α values, the indices $LCAI_1$ and $LCAI_2$ were determined following Equations (6.10) and (6.11). As with the numerical simulations, two sets of modes were considered for the calculation of $LCAI_1$ and $LCAI_2$, i.e. modes 1 to 3 and modes 1 to 5. This was particularly important for the experimental investigation, as it was difficult to reliably extract mode shapes of higher modes, especially modes 4 and 5.

The results of the first index, $LCAI_1$, are shown in Figure 6.38 (a) and (b) for modes 1 to 3 and 1 to 5, respectively. Higher amplitude of the index indicates a larger loss of composite action. As anticipated, the outcomes show the smallest amplitude for '17' screws with an increase in amplitude for a smaller number of screw connections. The amplitudes of the composite beam with '3' screws were similar for both mode combinations (modes 1 to 3 and modes 1 to 5), while amplitudes for '5', '9' and '17' screws were significantly higher for the mode set of modes 1 to 5.

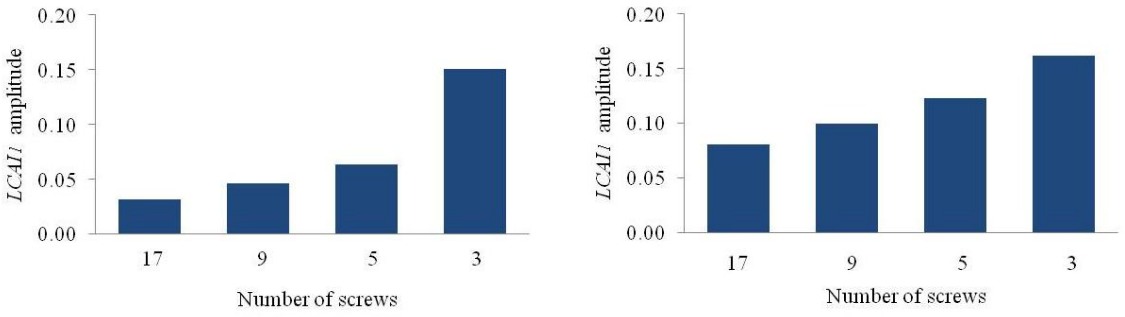

(a) (b)

Figure 6.38 $LCAI_1$ values of experimental timber composite beam for (a) modes 1 to 3 and (b) modes 1 to 5.

The outcomes of the second index, $LCAI_2$, are shown in Figure 6.39 (a) and (b) for modes 1 to 3 and modes 1 to 5, respectively. The results of $LCAI_2$ show a similar trend as for $LCAI_1$, i.e. significantly larger amplitudes for mode combinations of modes 1 to 5 compared to modes 1 to 3. The reason for the increase in amplitude for modes 1 to 5 is

the unreliability of modes 4 and 5. Since the severity estimator α indicates differences in two mode shapes, with the increase in mode shape reliability and variability, the amplitudes of α values increase and subsequently the indices $LCAI_1$ and $LCAI_2$ give incorrectly increased amplitude values.

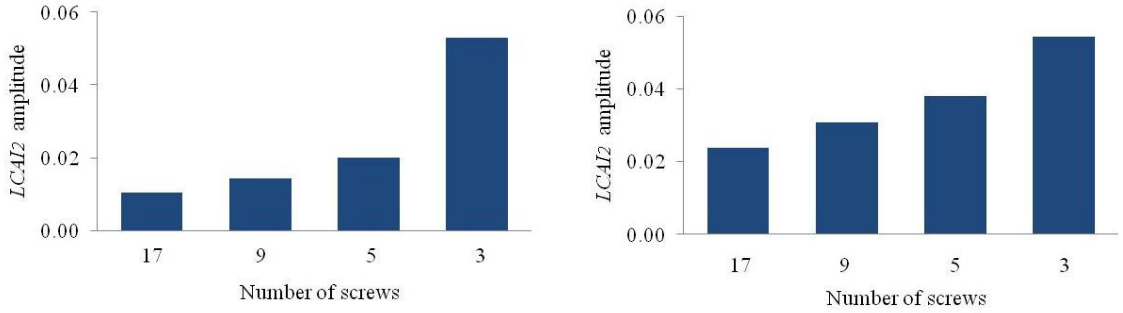

(a) (b)

Figure 6.39 $LCAI_2$ values of experimental timber composite beam for (a) modes 1 to 3 and (b) modes 1 to 5.

6.8.3 Loss of Composite Action

Based on $LCAI_1$ and $LCAI_2$, the dynamic-based loss of composite action was derived. The calibration factors λ_1 and λ_2 were identified for $LCAI_1$ and $LCAI_2$, respectively, to convert the indices into loss of composite action values in percentage. The calibration factors were identified by scaling the index amplitudes for '3' screw connections to the corresponding static-based loss of composite action. The determined calibration factors, λ_1 and λ_2, for $LCAI_1$ and $LCAI_2$ were 166 and 472, respectively. The loss of effectiveness of the beam acquired from the dynamic tests was correlated against static results.

Figure 6.40 shows the results of the determined dynamic-based *LCA* values derived from $LCAI_1$ plotted against the static-based *LCA* values. Figure 6.40 (a) displays the outcomes from combining modes 1 to 3, while Figure 6.40 (b) illustrates the results from modes 1 to 5. The results showed a significantly better agreement with the static-based *LCA* for modes 1 to 3 (maximum error is 5.7%) than for modes 1 to 5 (maximum error is 14.5%). The larger errors for modes 1 to 5 are related to the unreliability of extracting modes 4 and 5 from experimental modal testing data, as explained above.

The dynamic-based *LCA* values derived from $LCAI_2$ are shown in Figure 6.41 (a) and (b) for mode combinations 1 to 3 and 1 to 5, respectively. These results show improved errors for $LCAI_2$ when compared to the outcomes of $LCAI_1$. This confirms the findings from the numerical investigation and showcases the advantages of using $LCAI_1$ over $LCAI_2$. Again, the results of modes 1 to 3 were noticeably better than those of modes 1 to 5. This stresses the importance of evaluating the reliability of mode shapes and of adapting the composite action calculations accordingly. In general, it must be highlighted that errors from mode shape uncertainties lead to overestimations of the loss of composite action, which are conservative predictions on the safe side.

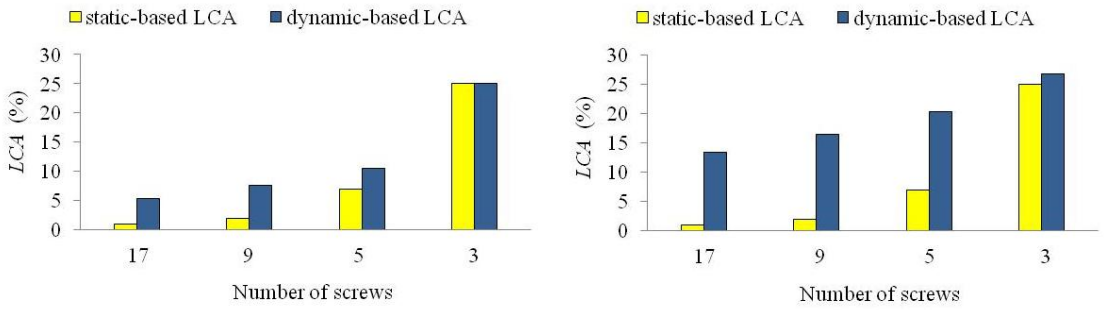

(a) (b)

Figure 6.40 Dynamically derived *LCA* based on $LCAI_1$ and static-based *LCA* of experimental timber composite beam for (a) modes 1 to 3 and (b) modes 1 to 5.

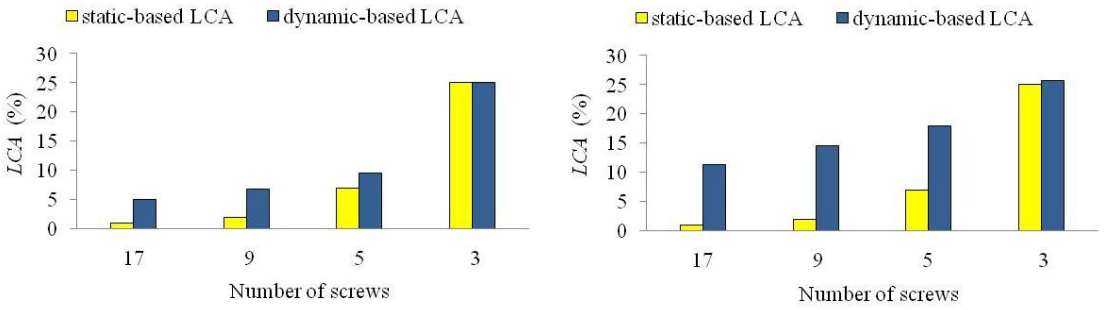

(a) (b)

Figure 6.41 Dynamically derived *LCA* based on $LCAI_2$ and static-based *LCA* of numerical timber composite beam for (a) modes 1 to 3 and (b) modes 1 to 5.

6.8.4 Study of Mode Shape Reconstruction

As for the numerical analysis, the approach of mode shape reconstruction for better composite action estimation was investigated. The cubic spline method was applied to the experimental mode shape data for interpolation. The original data of 7-point mode shape arrays was interpolated to obtain 31-point mode shape vectors. By applying the proposed composite action identification method, the dynamic-based *LCA* values were calculated for different connection stages of the experimental beam structure. The results are displayed in Figures 6.42 and 6.43, showing the dynamic-based *LCA* values derived from $LCAI_1$ and $LCAI_2$ plotted against the static-based *LCA* values obtained from numerical simulation. For the mode combination of modes 1 to 3 (shown in figures (a)), the results obtained from 7-point mode shape data were better than for 31-point mode shape data. For the mode shape combination of modes 1 to 5 (shown in figures (b)), the outcomes from 31-point mode shapes delivered better results, however, the errors were still significant due to the inaccuracies of modes 4 and 5. These outcomes confirm the findings of the numerical investigation concluding that a mode shape reconstruction using cubic spline interpolation does not provide any advantage over using the original mode shape data for dynamic-based composite action determination.

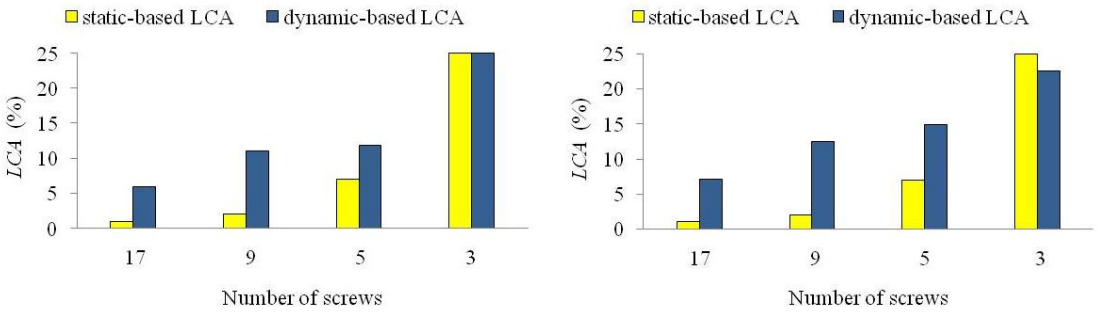

Figure 6.42 Dynamically derived *LCA* based on $LCAI_1$ and static-based *LCA* of experimental timber composite beam for (a) modes 1 to 3 and (b) modes 1 to 5 from reconstructed 31-point mode shapes.

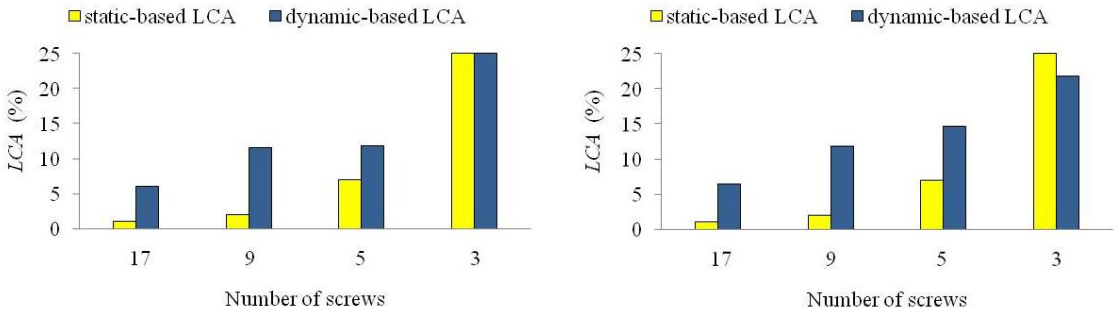

Figure 6.43 Dynamically derived *LCA* based on $LCAI_2$ and static-based *LCA* of experimental timber composite beam for (a) modes 1 to 3 and (b) modes 1 to 5 from reconstructed 31-point mode shapes.

6.9 Concluding Remarks

This chapter presented a dynamic-based method for the identification of the composite action (efficiency) of a composite flooring system. Traditionally, the composite action of a system is determined from static load testing using deflection measurements. However, static load testing is expensive, time consuming and inappropriate for existing flooring system. Hence, the main objective of this research was to develop a method based on dynamic measurements for the identification of the composite action (degree and loss of composite action) of a composite flooring system due to failure of shear connectors. The results acquired from the proposed dynamic-based method were calibrated to make them comparable to traditional static-based composite action results.

Two novel methods were proposed with this research work for the determination of the composite action of a timber composite flooring system are only based on mode shape measurements obtained from dynamic testing. The core of both methods is the use of the Damage Index (DI) method to derive the indices $LCAI_1$ and $LCAI_2$ that evaluate the degree of composite action. The proposed methods were successfully tested and validated on a numerical and experimental timber composite beam consisting of two LVL components. To create different degrees of composite action, the beam was modelled/tested with different numbers of shear connectors to simulate the failure of connection screws. The results from the proposed dynamic-based composite action method were correlated against outcomes from the traditional static-based method. From the findings, the following conclusions can be drawn.

- The proposed vibration-based method is capable of determining the composite action of a composite structure using only mode shape measurements obtained from dynamic testing.
- The parameters, $LCAI_1$ and $LCAI_2$, clearly indicate the loss of composite action due to the removal of screw connectors. The calculated loss of composite action indices of the tested beam structure were of increased amplitude for a smaller number of connection screws.
- To correlate the dynamic-based composite action outcomes to static-based values, the indices $LCAI_1$ and $LCAI_2$ are multiplied with the calibration factors λ_1 and λ_2. Due to laboratory and time constraints, static-based composite action results from deflection measurements were only obtained from numerical simulations. This resulted in differences in the calibration factors for the numerical and experimental investigations. In the FE model, nodes at the location of the screws were rigidly coupled to simulate the screw connections. Such rigid modelling of the shear connection might not represent the real experimental situation. To correctly simulate the shear connections, experimental push-out tests need to be performed on small scale screw connector specimens to characterize the properties of the connector. Alternatively, four point bending testing is to be performed on the experimental composite beam structure. To identify a generic solution, more tests need to be performed to derive calibration factors for multiple types of composite flooring systems with different types of shear connectors.
- The accuracy of the composite action predictions greatly depends on the reliability of the mode shape measurements. For the experimental investigation, mode shapes of higher modes (modes 4 and 5) contained a high degree of error due to the limited number of sensors used and thus resulted in erroneous composite action outcomes. Therefore, only reliable mode shapes should be considered in the calculation of the loss of composite action indices $LCAI_1$ and $LCAI_2$. In general, a larger number of sensors will increase the accuracy of mode shape measurements and thereby reduce the error in the prediction of the composite action.

- The investigation on mode shape reconstruction using cubic spline interpolation techniques for improved composite action results showed that such approach does not have any advantage over the use of the original mode shape vectors.
- The numerical study on various composite beams with different cross-sections with particular focus on the neutral axis revealed that the proposed method is generically applicable including for composite structures where the neutral axis coincides with the shear plane of the structure.
- For both, numerical and experimental investigations, results of dynamic-based loss of composite actions over-predicted the actual loss of composite action resulting in errors that are conservative, which is of great importance for design engineers.
- For the investigated composite timber beam, the connection screws were equally spaced for all five composite stages. Hence, more testing are needed to apply this method to composite flooring systems with non-uniform spacing of the screws and different types of shear connectors.
- The calibration factors determined in this chapter are unique for a specific test set up and type of beam. The factors are a function of degree of composite i.e., it is not a linear relationship. This is a relatively novel idea and therefore, further investigations are needed to develop general solutions for calibration factors so that this method would have potential for general implementation.

University of Technology, Sydney

CHAPTER 7

NATURAL FREQUENCY PREDICTION

7 Natural Frequency Prediction

An accurate prediction of the fundamental frequency to be used in the design criteria against floor vibrations is required to assess dynamic performance of the flooring systems. A number of analytical prediction models can be found in the design standards and literature to determine the fundamental frequency, particularly with flooring systems.

This chapter presents a summary of available natural frequency prediction methods and use of these methods to estimate the fundamental frequency of the tested TCC beams with 5.8 m and timber floor modules (timber beams) with 6 and 8 m span. Further, the predicted fundamental frequency of these TCC and timber beams are correlated with experimental results presented in Chapters 3 (Section 3.5) and 4, respectively.

7.1 Simplified Natural Frequency Prediction Models

The prediction models are essentially based on the natural frequency prediction relationship for a simple spring-mass system as expressed in Equation (7.1) and it is also expressed in terms of elastic deflection of the system due to its self-weight and imposed action as in Equation (7.2). A summary of each analytical prediction model is presented under sub-headings of this section.

$$f_1 = {}^1\!/_{2\pi}\sqrt{{}^k\!/_m} \tag{7.1}$$

where k is the stiffness of the system and m is the mass of the system.

$$f_1 = {}^1\!/_{2\pi}\sqrt{{}^g\!/_\Delta} \tag{7.2}$$

where g is the acceleration due to gravity (9.81 m/s^2) and Δ is the elastic deflection of the system (m).

7.1.1 Wyatt (1989)

Wyatt (1989) has presented four methods to evaluate natural frequencies of the beams and floors. In this section only the first two analytical methods will be discussed as the other two methods needed software packages such as iterative application of static

analysis using common static analysis software at the desk-top and dynamic analysis software packages including FE method of the structure to predict the natural frequencies.

The first method predicts the fundamental frequency of the systems based on the self-weight deflection approach using Equation (7.3).

$$f_1 = {}^{1}/_{2\pi}\sqrt{{}^{g}/_{y_w}} \tag{7.3}$$

where y_w is the weighted average value of the static deflection (m) due to self-weight of a slab or floor beam system and g is the acceleration due to gravity (m/s^2).

Considering that in many plate and beam problems, the weighted average value of the deflection, y_w, is expressed in terms of maximum deflection, y_0, due to the self-weight of the system in millimetre (mm) as $y_w = (3/4)y_0$ and the Equation (7.3) is rewritten in the simpler form for convenience as below.

$$f_1 = 18/\sqrt{y_0} \tag{7.4}$$

This method can be used to estimate the fundamental frequency of a slab and floor beam system on main beams. This method does not consider long-term deflection due to shrinkage and creep effects, and the appropriate assumptions should be made on boundary conditions, MOE of materials and the contribution of live loads for continuous beams. This method is one of the basic design approaches for flooring systems, but the resistance to floor vibration for joist floor systems is not only due to the slab itself but also due to the beams on girders supported by columns or walls. Allen (1990) modified Equation (7.3) to take this into account (Refer to Section 7.1.2).

The second method is based on the Equivalent Beam Method (EBM) that can be used to predict the fundamental frequency of single span beams with different types of boundary conditions and continuous beams having maximum of three spans, but this method is generally preferable for regular continuous beams. The analytical solution is given in Equation (7.5). Wyatt (1989) presents the values for frequency coefficient, C_B for a single span with different boundary conditions as presented in Table 7.1. The coefficient for both ends pinned is 1.57; for one end fixed and the other end pinned is 2.45; for both ends fixed is 3.56 and for cantilever beam is 0.56. The coefficient is the

same for both pin-pin and pin-roller boundary conditions where a higher frequency is expected for pin-pin compared to pin-roller boundary conditions. For continuous beams, Wyatt (1989) recommended to use Figure 7.1 to identify the coefficient. This is known as the component frequency approach.

$$f_1 = C_B\sqrt{EI/mL^4} \tag{7.5}$$

where m is the mass per unit length (t/m if EI is in kNm^2, or kg/m if EI is in Nm^2), L is the span (for continuous beams take the longest span) (m) and C_B is the frequency factor which depends upon the number of spans and boundary conditions (see Table 7.1 and Figure 7.1).

Table 7.1 Values of C_B for a single span

No. of spans	End conditions	Values of C_B
Single	pinned/pinned (simply supported)	1.57
	fixed/pinned	2.45
	fixed both ends	3.56
	fixed/free (cantilever)	0.56

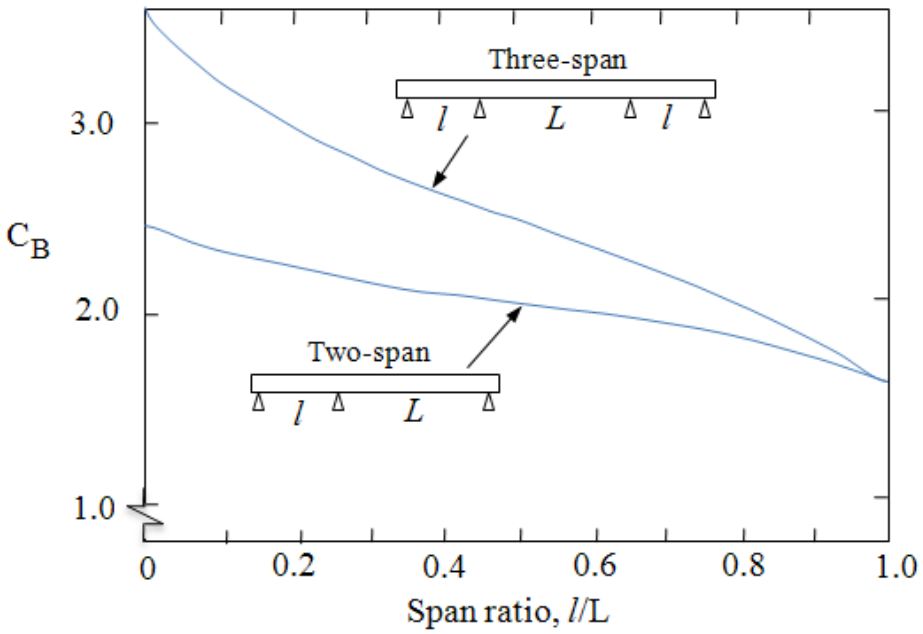

Figure 7.1 Frequency factor, C_B for continuous beams (Wyatt 1989).

7.1.2 Allen (1990)

Generally the deflection based prediction models estimate the natural frequency of the beams and floor system from the flexural deflection of the beam; however, the deflection due to shear deformation and flexibility of supports influence the flexibility of the floor system significantly and ultimately reduce the natural frequency obtained from solely beam flexure. The shear deformation is important for deep beams, girders and trusses. Allen (1990) modified Equation (7.3) to predict the fundamental frequency, f_1, considering elastic deflection of a beam and girder flooring system due to all factors as,

$$f_1 = {}^1\!/_{2\pi}\sqrt{\frac{g}{\frac{\Delta_B+\Delta_G}{1.3}+\Delta_S}} \tag{7.6}$$

where Δ_B is the mid span deflection of the floor beam due to flexure and shear, Δ_G is the deflection of the girder at the beam support due to flexure and shear, Δ_S is the deflection of the supports such as column or wall due to axial strain.

All deflections are consequence of self-weight of the member and other imposed actions, including weight of people. In regards to flexibility of supports, the most flexible one from two supports is considered in the prediction. The factor 1.3 in Equation (7.6) can be used for most beam-floor systems while the factor should be increased to 1.5 in the case of fixed cantilevers and two-way slabs.

The deflection Δ_B and Δ_G should be determined based on the complete mode shape of the systems if beams or girders are continuous over supports. The deflection of adjacent spans is in the opposite directions without change in slope over the supports and the weight carried by the individual span acts in the deflected direction.

7.1.3 Murray, Allen & Ungar (2003)

Murray, Allen & Ungar (2003) provided a similar approach to second method of Wyatt (1989) prediction model to predict the fundamental frequency of the simply supported beam or joist and girder panel under uniformly distributed permanent and imposed action as given in Equation (7.7).

$$f_1 = \frac{\pi}{2}\sqrt{{gEI}/{wL^4}} \tag{7.7}$$

where *E* is the modulus of elasticity of the transformed system, *I* is the transformed moment of inertia of the system, *w* is the uniformly distributed load per unit length and *L* is the span. For a partial composite flooring systems, such as TCC flooring systems, the equivalent bending stiffness, EI, can be determined using Gamma method as described in Eurocode 5 (2008). The equation was further simplified in terms of mid span deflection of a simply supported beam as;

$$f_1 = 0.18\sqrt{{g}/{\Delta}} \tag{7.8}$$

where Δ is the mid span deflection of a beam due to the uniformly distributed load and can be determine from $5wl^4/384EI$.

7.1.4 Eurocode 5 (2008)

Eurocode 5 (2008) also presents a similar approach to second method of Wyatt (1989) prediction model to predict the fundamental frequency of the rectangular floors simply supported along all four edges using Equation (7.9). It also presents a "Gamma method" to determine the equivalent bending stiffness of the systems having partial composite action such as TCC floor system, but transformed section method can be used for fully composite systems.

$$f_1 = {\pi}/{2l^2}\sqrt{{(EI)_l}/{m}} \tag{7.9}$$

where $(EI)_l$ is the equivalent bending stiffness of the floor in the perpendicular to the beam direction (Nm^2/m), *l* is the floor span (m) and *m* is the mass per unit area (kg/m^2). The mass includes self-weight of the floor and other permanent actions.

7.2 Natural Frequency Prediction of the TCC Beams

This section presents an overview of natural frequency, especially fundamental frequency prediction of the tested TCC beams using three prediction models and the predicted results are correlated with experimental results (Refer to Section 3.5).

7.2.1 Scope

The serviceability design of TCC floor solutions requires an assessment of the first natural frequency in order to check the vibration behaviour of the floor and occupant comfort. The following frequency ranges must be avoided:

- Frequency below about 3 Hz to prevent walking resonance.
- Frequency range of 5-8 Hz to prevent human discomfort.

For residential/office floors, a natural frequency greater than 10 Hz shall be targeted (Hanes 1970). A special investigation is needed if the predicted fundamental frequency of the floors is less than 8 Hz. Hence, the prediction of natural frequency, especially fundamental frequency is the main concern of the designer for the dynamic assessment of the flooring systems.

7.2.2 Fundamental Frequency Prediction

The fundamental frequency of the TCC beams was predicted using 1st and 2nd methods of Wyatt (1989) models using Equations (7.4) and (7.5), respectively. In addition, the frequency of the beams was estimated using Equations (7.6) and (7.8) of Allen (1990) and Murray, Allen & Ungar (2003) prediction models, respectively.

The effective bending stiffness, $(EI)_{ef}$ of the section of the beams was calculated using the Gamma coefficient method in accordance with Eurocode 5 (2008) as the sections were partially composite, using Equation (7.10). The parameters with subscript *t* and *c* correspond to timber and concrete, respectively. Further details about the calculation of the stiffness, $(EI)_{ef}$ and connection properties are presented in Gerber & Crews (2011).

$$(EI)_{ef} = E_c I_c + E_t I_t + \gamma_c E_c A_c a_c^2 + \gamma_t E_t A_t a_t^2 \quad (7.10)$$

Material properties of the LVL joist and concrete topping of the TCC beams used in the fundamental frequency prediction are presented in Table 7.2. The serviceability stiffness of the connection system adopted in the corresponding beams obtained from push-out tests on shear connector samples (Refer to Section 3.1) required for the determination of the bending stiffness, $(EI)_{ef}$ is summarised in Table 7.3. The stiffness, $(EI)_{ef}$ was determined using Equation (7.10). The self-weight of the beams was 1.13 kN/m. The mid span deflection of the beams based on their self-weight and the stiffness, $(EI)_{ef}$ of the corresponding beams was determined and presented in the same Table 7.3.

Table 7.2 A summary of material properties of concrete and LVL timber

Beam	LVL joist		Concrete	
	MOE (E_x) (GPa)	Density (ρ) (kg/m^3)	MOE (E_x) (GPa)	Density (ρ) (kg/m^3)
Beam-1	14.8	620	35.9	2,400
Beam-2	14.9			
Beam-3	16.2			
Beam-4	15.8			

Table 7.3 A summary of connection stiffness and deflection of TCC beams

Beam	Beam-1	Beam-2	Beam-3	Beam-4
Serviceability stiffness, K_{serv} (kN/mm)	58	49	37	37
Bending stiffness, $(EI)_{ef}$ (Nmm^2)	4.84E+12	4.70E+12	3.89E+12	3.63E+12
Mid span deflection, y_0 (mm)	3.45	3.55	4.28	4.59

A summary of fundamental frequency predicted using five different methods and correlation of predicted values against test results is presented in Table 7.4. Figure 7.2 depicts that all these methods over-predicted the values for Beams- 1 and 2, and under-predicted for Beams- 3 and 4. In the figure, horizontal bold line at frequency ratio 1.00 shows the ideal matching of the predicted and tested frequency of the beams. The predicted values from all these methods were similar for corresponding beams. For the

similar values, correlation with test results showed discrepancies below 8% for Beams-1 and 2, while for Beams- 3 and 4 the values had significant deviation of about 15% from experimental values. For Beams- 3 and 4, the correlation between experimental and FE results had also similar *NFerror* values for first mode (Refer to Section 5.1). Hence, predicted frequency of Beams- 1 and 2 using all of these methods were fairly accurate and the discrepancies may be due to variation in material properties.

This significant deviation of predicted values of Beams- 3 and 4 using all of these methods might be due to lower characteristic stiffness, K_{serv} of the bird-mouth notched connection as these beams had notched connection. The stiffness of the notched connection was expected higher than other connections without notches, but the experimental result was significantly lower. This might be one of the causes of significant variation of predicted values. Additional push-out test on bird-mouth notch connection would be essential to develop more confidence in the stiffness of the connection. However, fundamental frequency of Beams- 3 and 4 with higher stiffness derived from a series of push-out tests is presented in Section 7.2.3.

Table 7.4 A summary of correlation of predicted values against test results

Beam	Prediction, $f_{1(model)}$, Hz					Experiment
	Wyatt (1989)		Allen (1990)	Murray, Allen & Ungar (2003)	Eurocode5 (2008)	$f_{1(exp)}$ (Hz)
	1st method	2nd method				
Beam-1	9.69	9.56	9.68	9.60	9.56	9.00
$f_{1(model)}/f_{1(exp)}$	1.08	1.06	1.08	1.07	1.06	
Beam-2	9.56	9.42	9.54	9.46	9.42	8.90
$f_{1(model)}/f_{1(exp)}$	1.07	1.06	1.07	1.06	1.06	
Beam-3	8.70	8.57	8.66	8.61	8.58	10.10
$f_{1(model)}/f_{1(exp)}$	0.86	0.85	0.86	0.85	0.85	
Beam-4	8.40	8.28	8.38	8.32	8.28	9.80
$f_{1(model)}/f_{1(exp)}$	0.86	0.84	0.85	0.85	0.85	

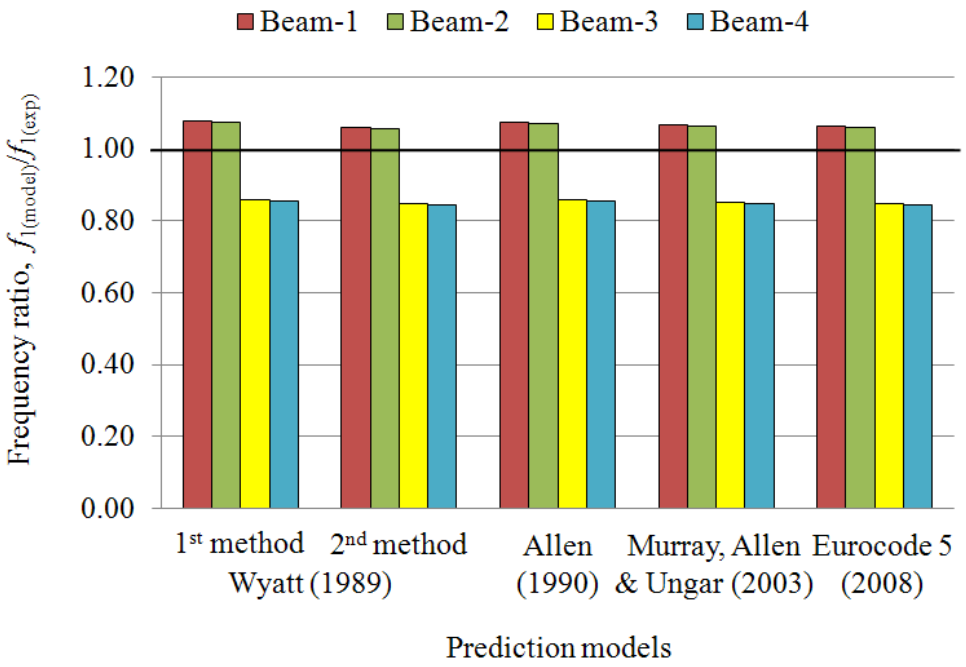

Figure 7.2. Correlation of predicted values and test results of TCC beams.

7.2.3 Frequency Prediction of Beams- 3 and 4 using Derived Stiffness

Beams- 3 and 4 had identical bird-mouth notched connection and all of the prediction models in previous sub-section predicted the frequency of these beams with the same order of significant error. Therefore, the relevant stiffness value (98 kN/mm) for this notched connection was used to minimize error. The relevant stiffness value for 48 mm thick LVL joist used in these beams was derived from a plot as shown in Figure 7.3 presented by Gerber & Crews (2011). This plot was also used to calibrate FE models of these beams (Refer to Section 5.1.5).

Predicted results of these beams with derived stiffness value of 98 kN/mm of bird-mouth notched connection are presented in Table 7.5 and Figure 7.4. In the figure, horizontal bold line at frequency ratio 1.00 shows the ideal frequency prediction of the tested beams. The correlation of all prediction models showed the frequency error below 5%. Hence, these predicted values are fairly accurate and the remaining discrepancies should be due to variation in material properties of LVL joist and concrete topping. A sensitivity analysis was performed on the material properties of LVL joist as its properties variation is higher than concrete topping, and details are presented in Section 7.2.4.

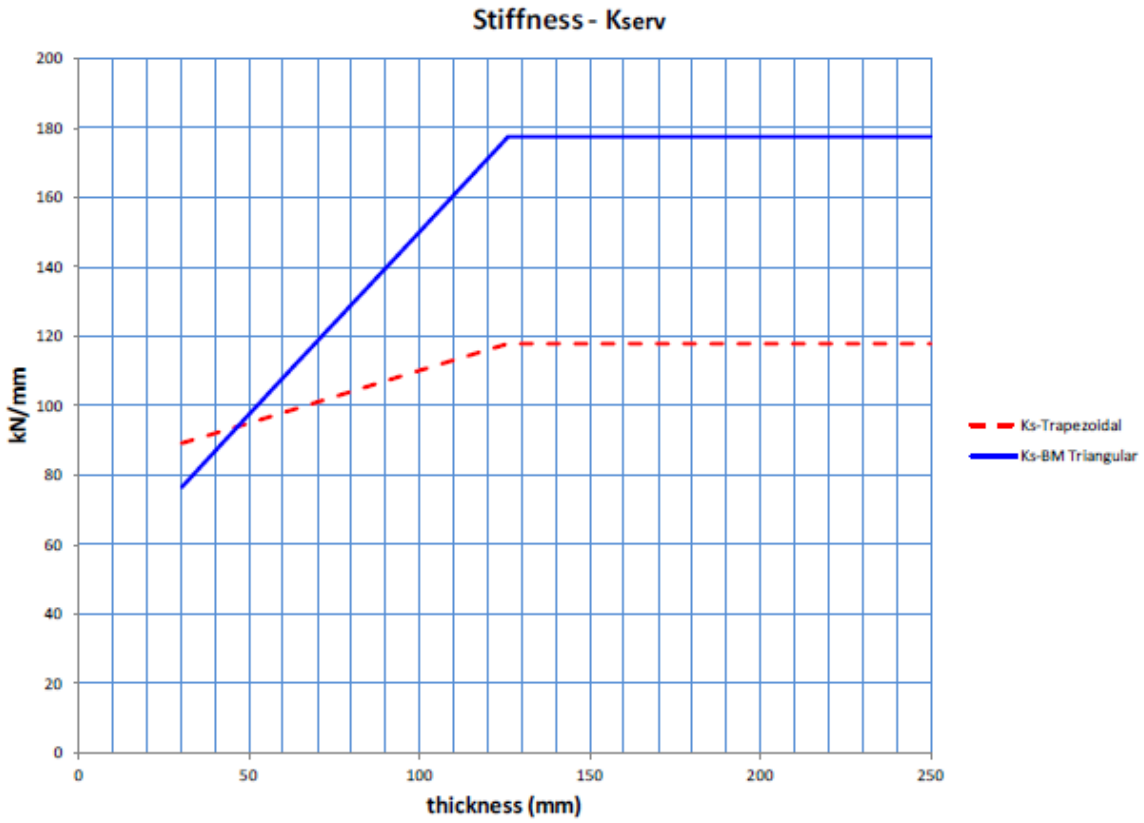

Figure 7.3 Serviceability stiffness (K_{serv}) of notched connections (Gerber & Crews 2011).

Table 7.5 Correlation between predicted values against test results of Beams- 3 and 4

Beam	Prediction, $f_{1(model)}$, Hz					Experiment
	Wyatt (1989) 1st method	Wyatt (1989) 2nd method	Allen (1990)	Murray, Allen & Ungar (2003)	Eurocode5 (2008)	$f_{1(exp)}$ (Hz)
Beam-3	9.79	9.65	9.78	9.70	9.66	10.10
$f_{1(model)}/f_{1(exp)}$	0.97	0.96	0.97	0.96	0.96	
Beam-4	9.54	9.40	9.52	9.45	9.41	9.80
$f_{1(model)}/f_{1(exp)}$	0.97	0.96	0.97	0.96	0.96	

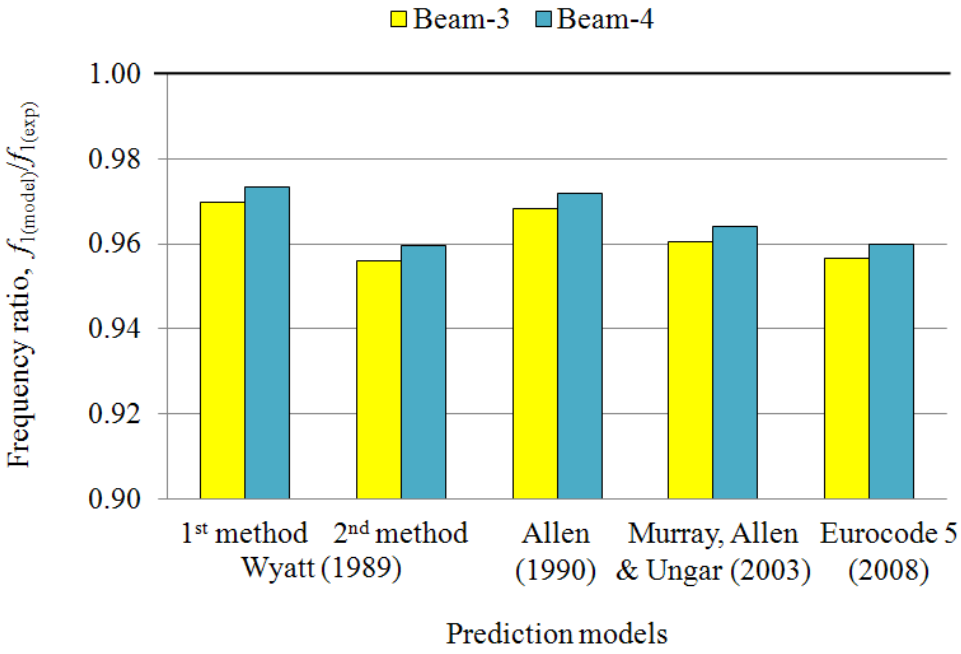

Figure 7.4 Correlation of predicted values and test results of TCC Beams- 3 and 4.

7.2.4 Sensitivity Analysis

A sensitivity analysis on material properties of LVL joists of TCC beams was performed using 2nd method of Wyatt (1989) prediction model as expressed in Equation (7.5). The MOE values of LVL joists of each beam were varied by ±5% and the predicted values were correlated with test results. A typical correlation analysis of Beam-3 is shown in Figure 7.5, where the ratio of predicted fundamental frequency for three different combinations and experimental results i.e. $f_{1(model)}/f_{1(exp)}$ is plotted against combinations. In the figure, bold black line at frequency ratio 1.00 represents ideal matching of predicted values with experimental results. The figure showed that the ratio of predicted and experimental frequency changes by ±2% when MOE value varies by ±5%. Sensitivity analyses on density variation of LVL joist by ±5% showed minimal effect in the predicted values while effect of concrete density variation was significant as density and volume of concrete topping was significantly higher than LVL joist. Hence, it can be concluded that the discrepancies between experimental and predicted natural frequency of the beams was mainly due to the material properties variation of LVL and concrete topping.

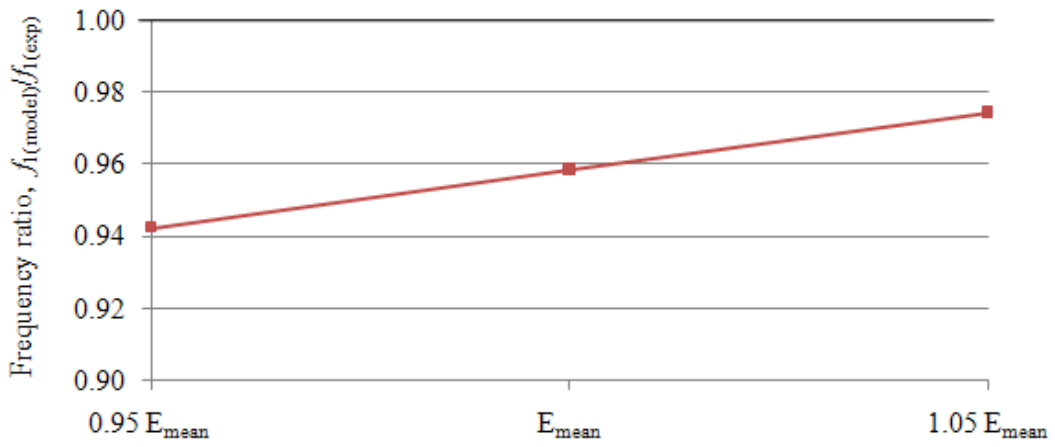

Figure 7.5 A typical sensitivity analysis on MOE of LVL joist of Beam-3 using 2nd Wyatt (1989) model.

7.2.5 Concluding Remarks

The fundamental frequency of the TCC beams was predicted using five analytical methods and the predicted values were correlated with test results. The following conclusions can be drawn based on the correlation:

- Fundamental frequency of Beams- 1 and 2 without notched connection was predicted accurately within 8% of test results while there was under-prediction of about 15% for Beams- 3 and 4 with notched connection.
- All prediction models predicted frequency of Beams- 1 and 2 within acceptable range. However, all models can predict natural frequency of the TCC beams accurately if the inputs of the models are accurate.
- Significant under-prediction of the fundamental frequency of Beams- 3 and 4 with notched connection could be a consequence of two major causes such as variation in the material properties of LVL joist and concrete topping, and stiffness of the connections. A sensitivity analysis on material properties showed that predicted values were sensitive to MOE of LVL joist and concrete density.
- Material properties of the LVL joists and concrete topping, and stiffness of connections from push-out tests should be found accurately in order to develop confidence in the use of the simplified analytical models and thus more tests need to be carried out.

7.3 Timber Floor Modules

This section presents a summary of fundamental frequency prediction of the tested timber floor modules (timber beams) with 6 and 8 m spans using three prediction models and the predicted results are correlated with experimental results (Refer to Section 4.8).

7.3.1 Fundamental Frequency Prediction

The fundamental frequency of the timber beams was predicted using 1st and 2nd methods of Wyatt (1989) models using Equations (7.4) and (7.5). In addition, the frequency was also estimated using Equations (7.6), (7.8) and (7.9) from Allen (1990); Murray, Allen & Ungar (2003) and Eurocode 5 (2008) prediction models, respectively. The deflections Δ_G and Δ_S was discarded in Allen (1990) prediction model for the tested beams.

A summary of the parameters that were used as input to the prediction models to predict fundamental frequency of the timber beams is summarized in Table 7.6, where mass corresponds to the self-weight of the beams. Bending stiffness, $EI_,$ of the beams' section, was calculated using the transformed section method as the section was assumed to be fully composite and the material properties (as relevant) from the experimental tests were used to predict the fundamental frequency. The mid span deflection due to the self-weight of the beams was also calculated.

Table 7.6 A summary of the parameters used to predict the fundamental frequency

Span	Bending stiffness	Mass	Mid span deflection
L (m)	EI (Nm^2)	m (kg/m)	y_o (m)
6	4.03E+06	28.0	1.15E-03
8	9.47E+06	34.4	1.90E-03

A summary of the predicted values from each prediction model for the beams and their correlation with experimental results is given in Table 7.7. The results show that the fundamental frequencies predicted from all models are fairly accurate as values are within ±5% of those measured experimentally. The predicted values from Wyatt's (1989) 1st method; Allen (1990) and Murray, Allen & Ungar (2003) prediction models are similar as all models are based on the mid span deflection of the systems. Allen

(1990) model is more advanced compared to the 1st method and Murray, Allen & Ungar (2003) as it incorporates the deflections Δ_G and Δ_S of the systems (if applicable). The results from Wyatt's (1989) 2nd method and Eurocode 5 (2008) are identical as the latter model was originally derived from the 2nd method. Comparison of the models against planned additional experimental studies will give more confidence in the results obtained from the prediction models.

Table 7.7 A summary and comparison of the predicted values against the test results

Span	Prediction, $f_{1(model)}$, Hz					Experiment
	Wyatt (1989)		Allen (1990)	Murray, Allen & Ungar (2003)	Eurocode5 (2008)	$f_{1(exp)}$ (Hz)
	1st method	2nd method				
6 m	16.79	16.55	16.76	16.63	16.56	16.34
$f_{1(model)}/f_{1(exp)}$	1.03	1.01	1.03	1.02	1.01	
8 m	13.06	12.88	13.04	12.94	12.88	13.14
$f_{1(model)}/f_{1(exp)}$	0.99	0.98	0.99	0.98	0.98	

A sensitivity analysis was performed on variation of LVL material properties such as mean MOE (E) and density (ρ) for 6 and 8 m timber beams using 2nd method of Wyatt (1989) prediction model as expressed in Equation (7.5). The properties were varied by ±5% in six different combinations as shown in Figures 7.6 and 7.7, respectively, where the ratio of predicted fundamental frequency for different combinations and experimental results i.e. $f_{1(model)}/f_{1(exp)}$ is plotted against combinations. A bold black line in the graphs shows an ideal matching of predicted values with test results with unit frequency ratio. The results showed that the experimental fundamental frequency was within the range of ±5% variation of MOE and density. Hence, it can be concluded that the discrepancies between experimental and predicted natural frequency of 6 and 8 m timber beams was mainly due to the material properties variation of LVL as it had up to 12.3% CoV.

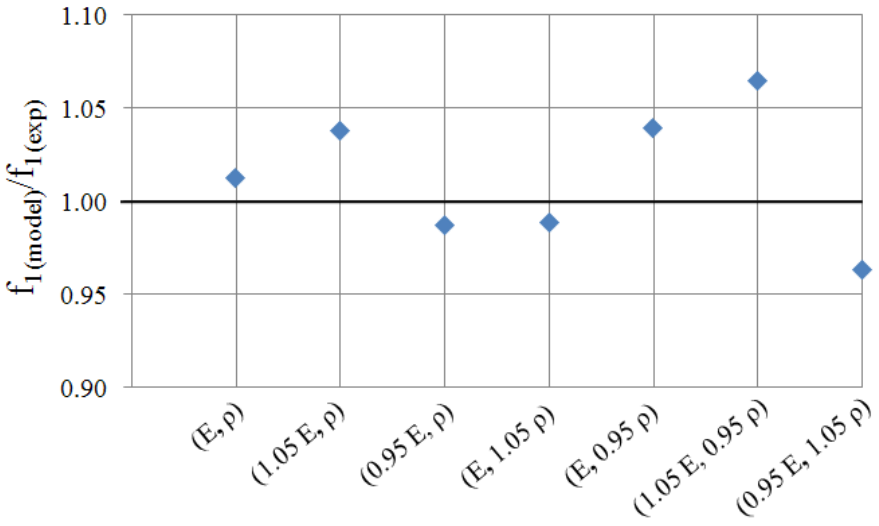

Figure 7.6 A summary of sensitivity analysis on 6 m span timber beam.

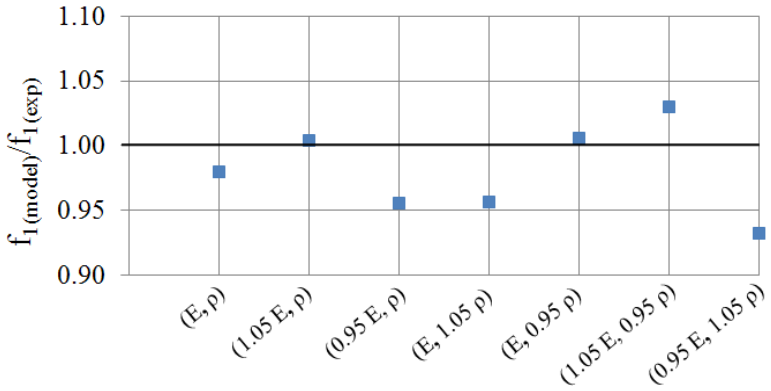

Figure 7.7 A summary of sensitivity analysis on 8 m span timber beam.

7.3.2 Concluding Remarks

The fundamental frequency of the timber beams with 6 and 8 m span was predicted using five analytical methods and the frequency was correlated with the test results. The following conclusions can be drawn based on these predicted results:

- Predicted values among the models have minor discrepancies. The correlation showed that the fundamental frequency can be predicted with satisfactory results as the predicted values were fairly accurate as they were within ±5% of the test results while there was 12.3% of CoV in MOE of LVL timber.
- A sensitivity analysis on material properties such as MOE and density variation of LVL timber showed the deviation of ±5% from experimental results was mainly due to properties variation.

7.4 Conclusions

This section presents the overall conclusions of the prediction models and correlation of their results with test results presented in Sections 7.2 and 7.3 for TCC beams and timber beams, respectively.

- Five analytical prediction methods were summarized in this chapter. The last two analytical prediction models such as Murray, Allen & Ungar (2003) and Eurocode 5 (2008) were basically derived from Wyatt (1989) models in different forms. 1st prediction method of Wyatt (1989) was modified by Allen (1990) considering the effect of girder and supports deflections.
- All models predicted fundamental frequency of the timber beams accurately. Obviously, TCC beams had higher number of variables compared to timber beams as the TCC beams had two different materials connected using different connection systems without any glue resulting in partially composite sections. Hence, the predicted values for TCC beams were less accurate compared to the timber beams.
- Material properties of the timber have higher variation compared to the steel and concrete. The material properties of the beam's components such as webs and flanges should be determined accurately in order to have more confidence in the predicted values as the natural frequency is highly sensitive to MOE and density of the materials used in the beams. In order to develop confidence in the use of the simplified analytical models more tests need to be carried out.
- Wyatt (1989) prediction models (both methods) can be used to estimate the fundamental frequency of the beams accurately if the inputs such as material properties, geometry and boundary conditions, etc. provided are accurate. Other methods also give the same order of accuracy.
- These models may under-predict natural frequency of the narrow floors supported on all four sides since they are based on a beam model.

University of Technology, Sydney

CHAPTER 8

PARAMETRIC ANALYSES

8 Parametric Analyses

This chapter presents the parametric study performed on the tested TCC beams with 5.8 m and timber floor modules with 6 and 8 m spans. Experimental results of these beams can be found in Section 3.5 and Chapter 4, respectively. For TCC beams, the study was performed on different cross-sectional dimensions, where depth of concrete and, width and depth of LVL joist were varied. Maximum allowable span for the cross-sectional dimensions of the beams were found based on natural frequency criteria of 8 Hz to generate the span table. For timber floor modules, calibrated FE models of the modules were utilised to assess dynamic performance of different size of the floors based on natural frequency. In addition, maximum allowable span, which satisfy the frequency criteria, was found for different cross-sectional dimensions of the modules to generate span table. Depth of flanges and, width and depth of webs were varied for the study. Detail of these studies is presented in the following sub-headings.

8.1 TCC Beam

Parametric study was conducted on the cross-section of four identical TCC beams with different connection systems. The connection systems were SFS and normal wood screws, bird-mouth notch with coach screw. Details of shear connector and their configuration in the individual beam can be found in Section 3.4. In the study, thickness of concrete topping and both dimensions (width and depth) of LVL joist were varied. Span was found for corresponding cross-sectional dimensions of the beams resulting in 8 Hz fundamental frequency. From previous findings it has been concluded that a flooring system with fundamental frequency above 8 Hz will not have any dynamic issues and thus this frequency was chosen as baseline to generate span table.

A natural frequency prediction analytical model, which is given in Equation (8.1) presented by Wyatt (1989), was used to identify span for different cross-sectional dimensions of the beams for 8 Hz natural frequency limit.

$$f_1 = C_B\sqrt{EI/_{mL^4}} \tag{8.1}$$

where m is the mass per unit length (t/m if EI is in kNm^2, or kg/m if EI is in Nm^2), L is the span of beam (m) and C_B is the frequency factor which depends upon the number of spans and boundary conditions. Magnitude of C_B for simply supported boundary condition is 1.57.

Width of concrete topping (B_c), which is 600 mm, was kept constant while its thickness (T_c) was varied from 25 to 200 mm with increments of 25 mm in the study. For LVL joist, both thickness (T_w) and depth (D_w) were changed. Depth of LVL web was varied for a range of 100 to 500 mm with increment of 25 mm while thicknesses were 35, 45, 63 and 75 mm as these are standard thicknesses of LVL produced by manufacturer. Cross-section of the beams with variables used in the study is shown in Figure 8.1.

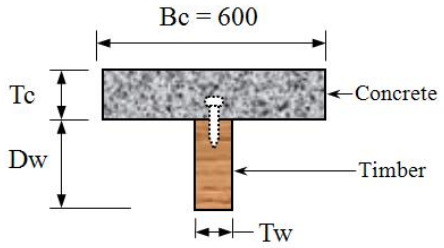

Figure 8.1 Parametric study on cross-section of the TCC beams (mm).

Span tables of the beams with different connection systems are presented in the following sub-headings. Trend of the results for all beams is similar and thus it can be concluded that increasing the concrete thickness will increase the stiffness of the floor but the additional mass may have a more prominent effect in reducing the fundamental frequency of the floor. In contrast, increase in thickness (T_w) and depth (D_w) of the joist will increase the frequency of the floor as additional mass of the webs have less prominent effect on reducing the frequency of the floor. The given sections in the span tables only fulfil the limit of vibration but not necessarily the required strength and the deflection limit. Therefore, the structural engineer still has to check whether these limits are met. In addition, the developed tables are for specific set of material properties, shear connectors and simply supported boundary conditions. However, such tables can be developed easily for any set of material properties and shear connectors if their properties are available, using any frequency prediction models.

8.1.1 Beam-1 with SFS Screw

Span tables for different cross-sectional dimensions of TCC Beam-1 are shown in Figures 8.2 to 8.9. The number of SFS screws was changed with change in span of the beams as the spacing of screws was kept constant throughout the span. The effective spacing (S_{ef}) of the screws was 413 mm. The spacing was determined based on spacing of the screws in tested Beam-1, where minimum (S_{min}) and maximum (S_{max}) spacing of the screws were 350 and 600 mm, respectively. The effective spacing of the screws is the sum of 75% of minimum and 25% of maximum spacing of the screws. The procedure to find the effective spacing was followed as mentioned in Gerber & Crews (2011). These span tables can be used to determine maximum span of the beams, which satisfy vibration limit, to be designed if the beams have similar shear connection system and spacing of the screws in Beam-1 with corresponding geometry provided in the tables. If the spacing of screws in the beams to be designed is closer than in Beam-1, the span determined from these tables will be conservative; otherwise the span will be over-estimated. Such tables can be developed for any spacing of the screws easily using one of the frequency prediction models as described in Section 7.1.

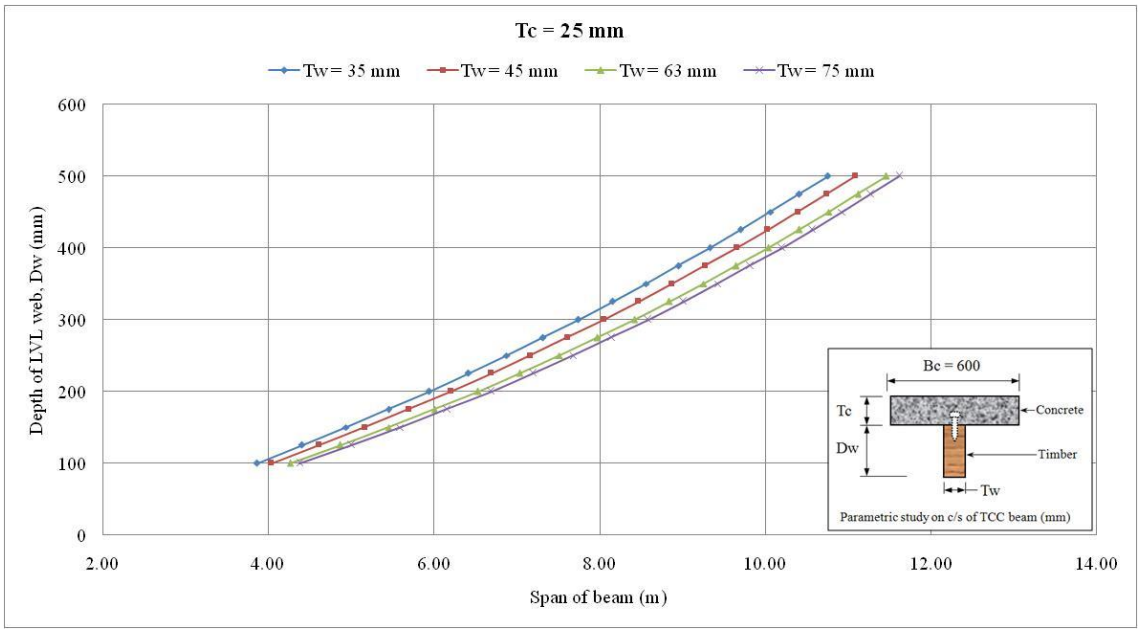

Figure 8.2 A span table of TCC Beam-1 with 25 mm thick concrete topping.

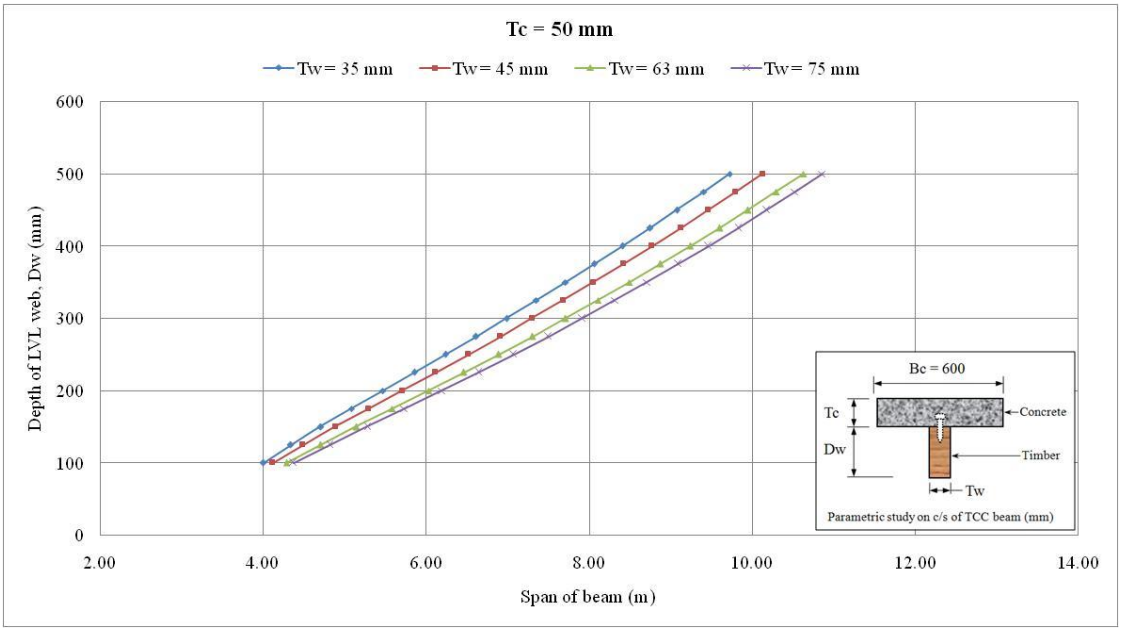

Figure 8.3 A span table of TCC Beam-1 with 50 mm thick concrete topping.

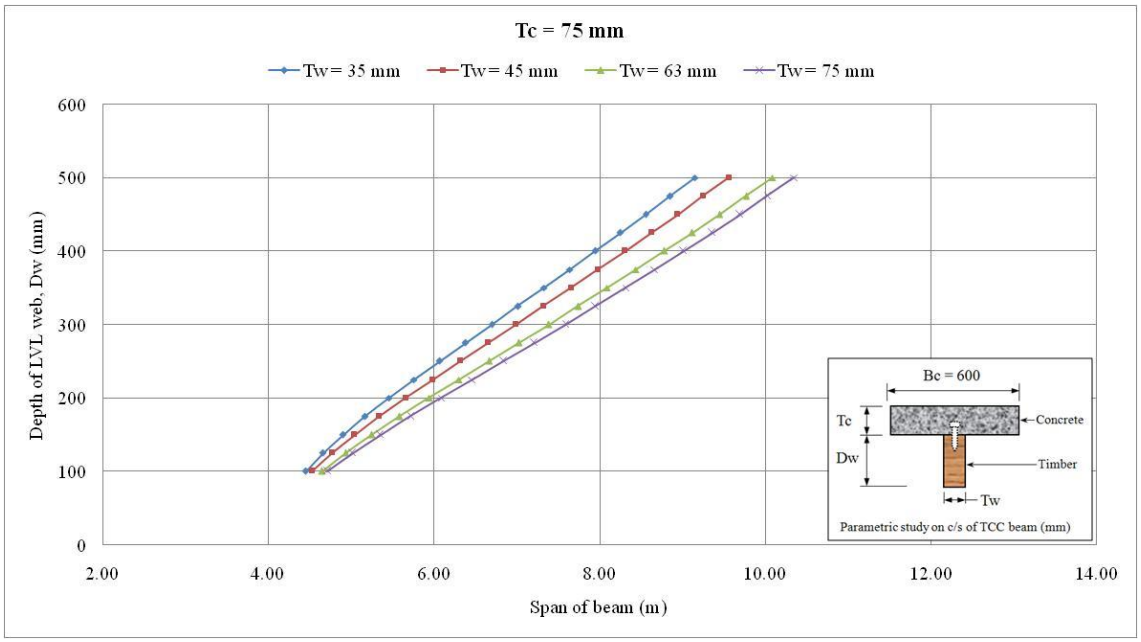

Figure 8.4 A span table of TCC Beam-1 with 75 mm thick concrete topping.

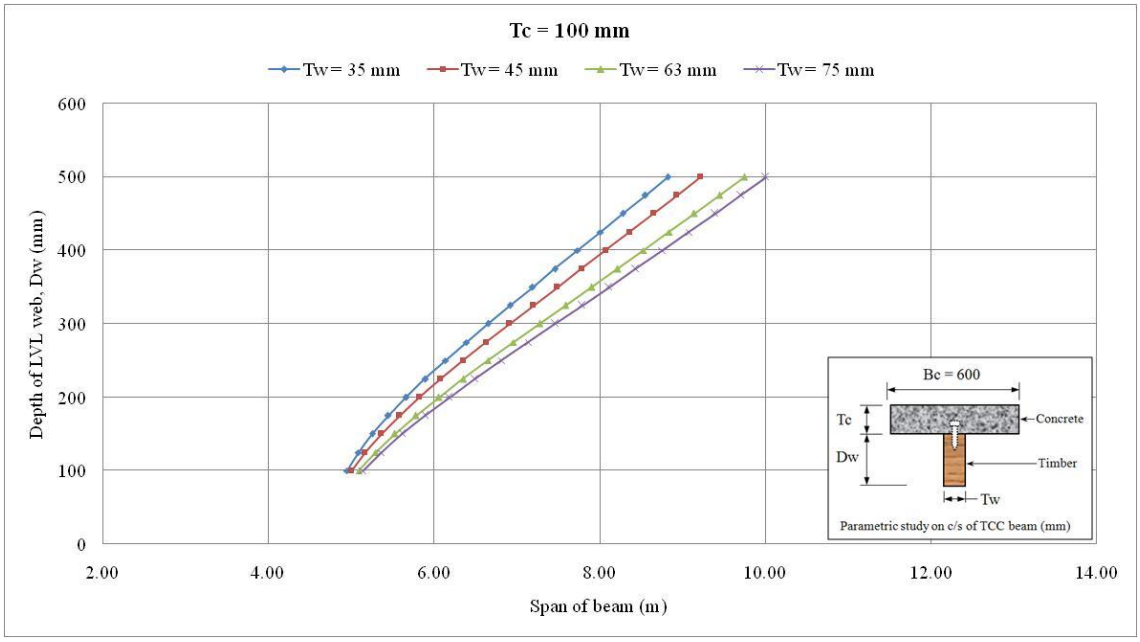

Figure 8.5 A span table of TCC Beam-1 with 100 mm thick concrete topping.

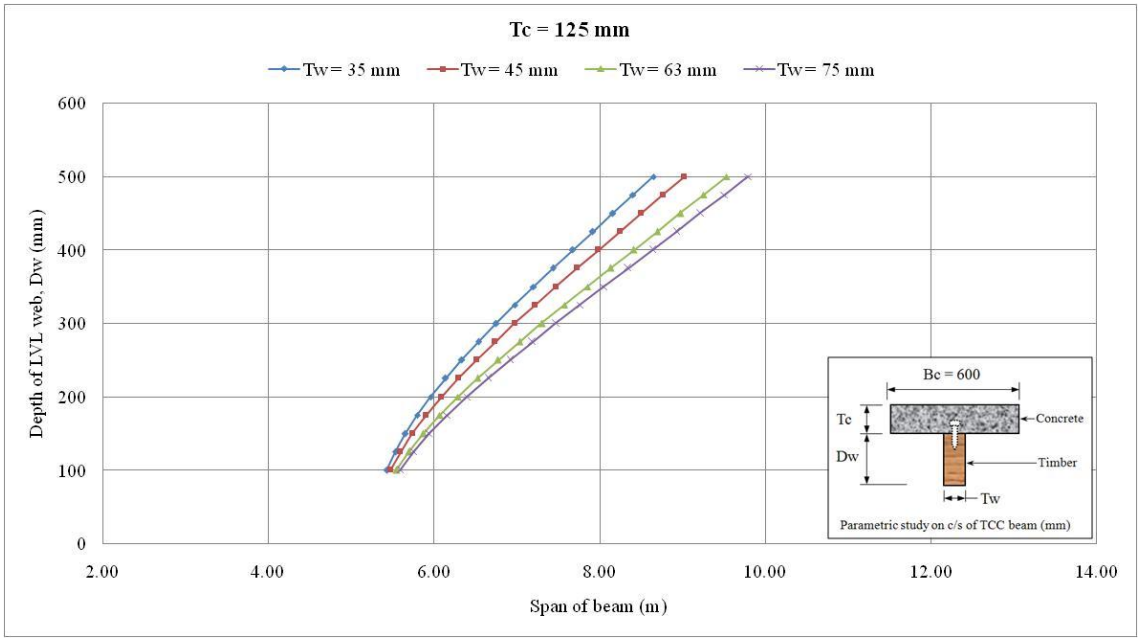

Figure 8.6 A span table of TCC Beam-1 with 125 mm thick concrete topping.

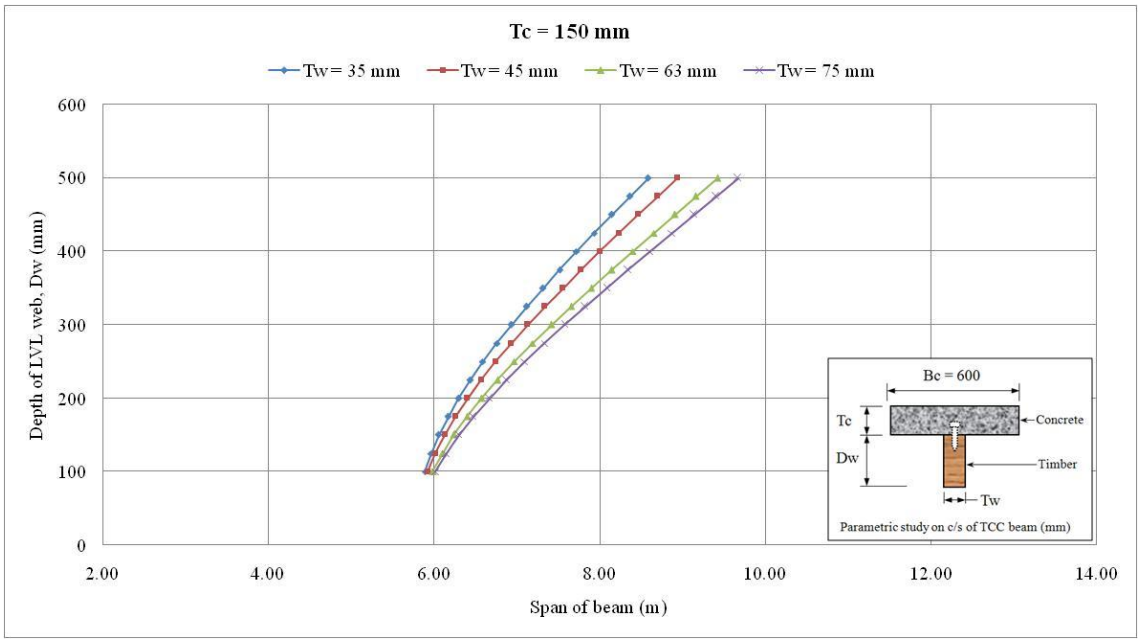

Figure 8.7 A span table of TCC Beam-1 with 150 mm thick concrete topping.

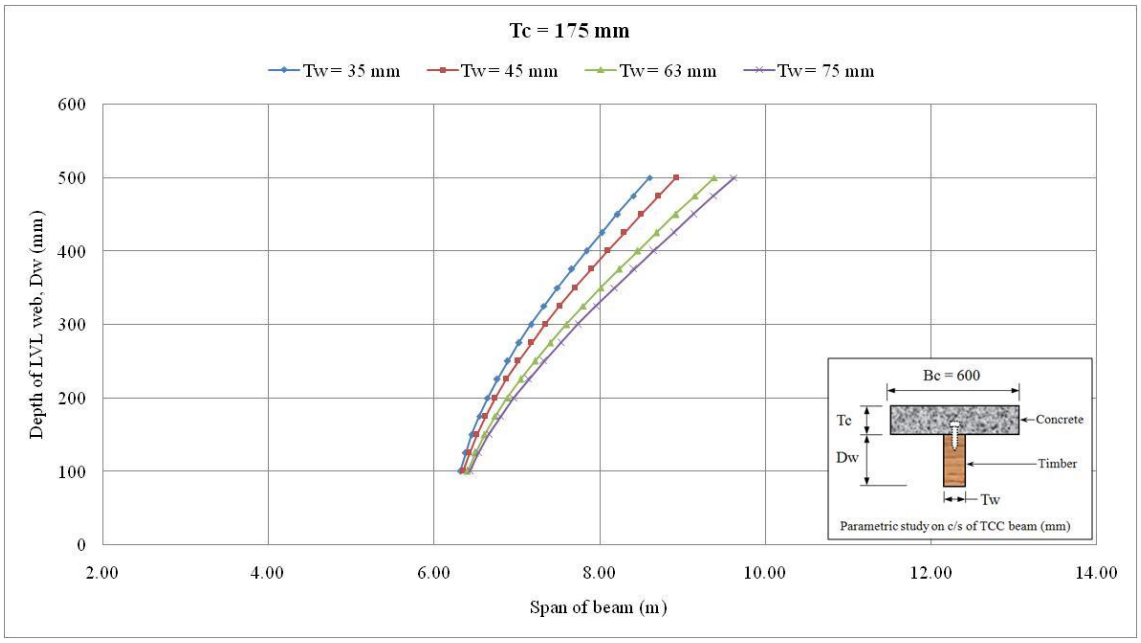

Figure 8.8 A span table of TCC Beam-1 with 175 mm thick concrete topping.

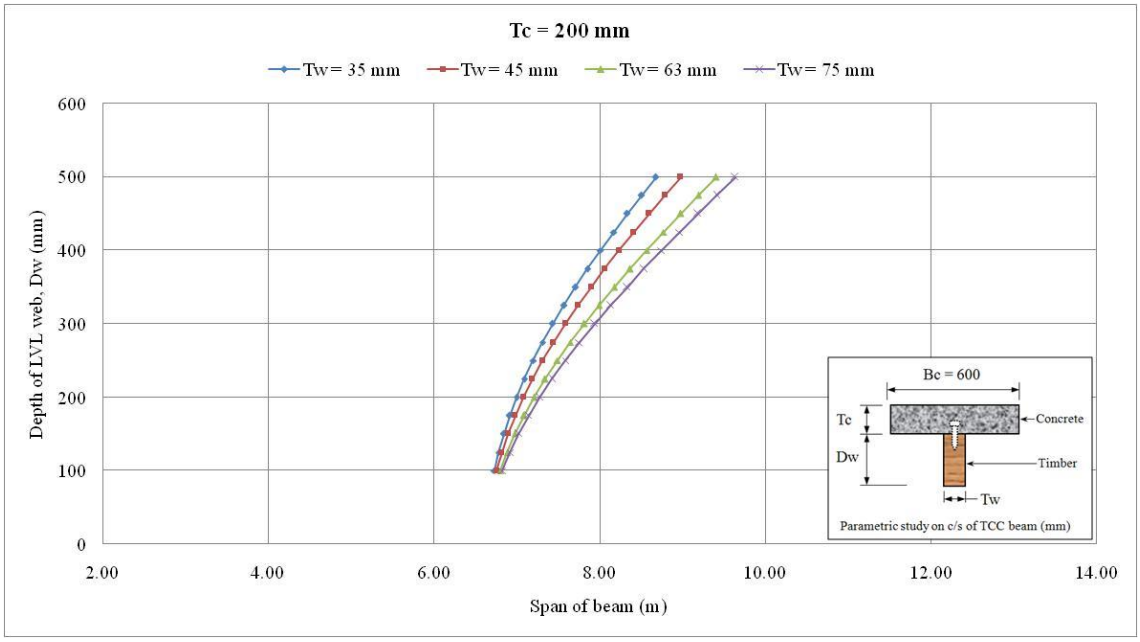

Figure 8.9 A span table of TCC Beam-1 with 200 mm thick concrete topping.

8.1.2 Beam-2 with Normal Screw

Span tables for different cross-sectional dimensions of TCC Beam-2 are shown in Figures 8.10 to 8.17. The number of normal screws was changed with change in span of the beams as the spacing of screws was kept constant throughout the span. The effective spacing (S_{ef}) of the screws was 425 mm. The spacing was determined based on spacing of the screws in tested TCC Beam-2, where minimum (S_{min}) and maximum (S_{max}) spacing of the screws were 400 and 500 mm, respectively.

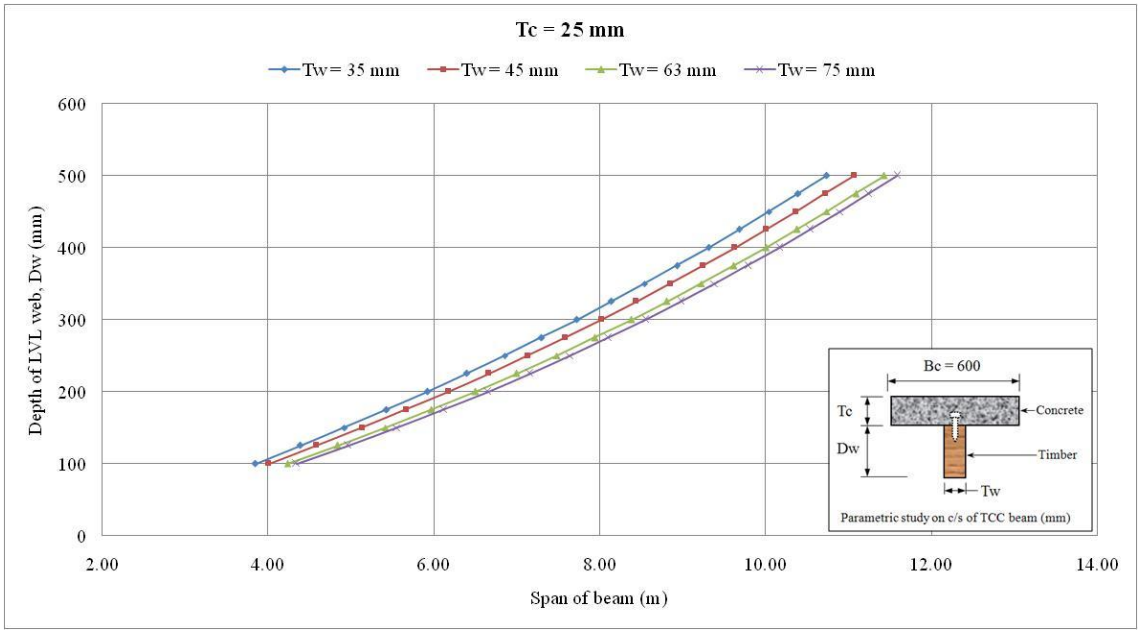

Figure 8.10 A span table of TCC Beam-2 with 25 mm thick concrete topping.

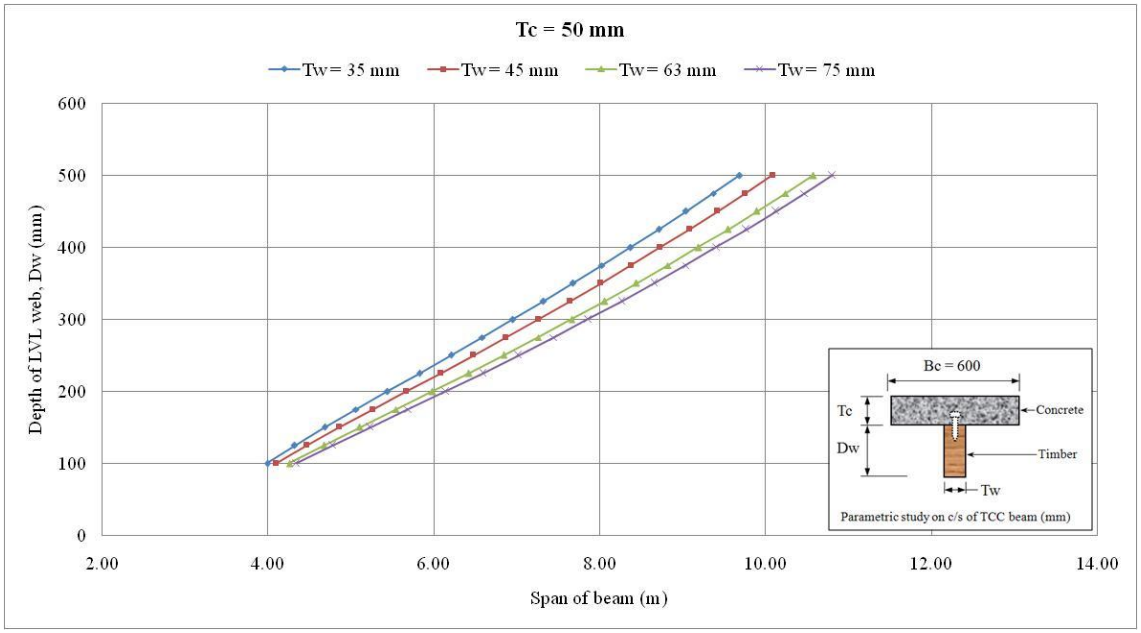

Figure 8.11 A span table of TCC Beam-2 with 50 mm thick concrete topping.

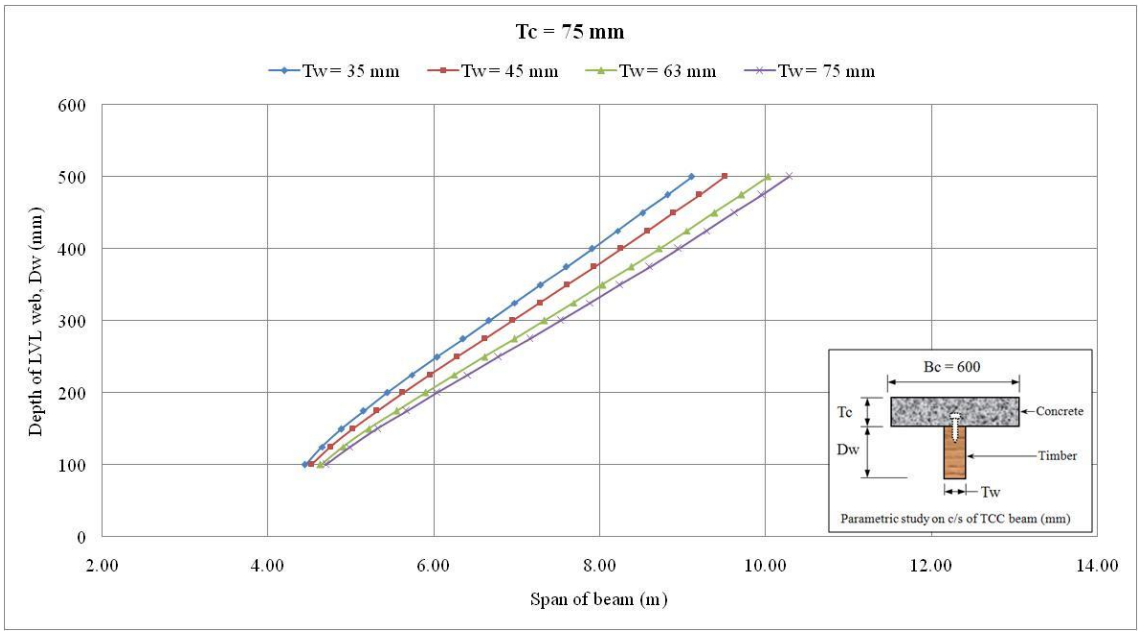

Figure 8.12 A span table of TCC Beam-2 with 175 mm thick concrete topping.

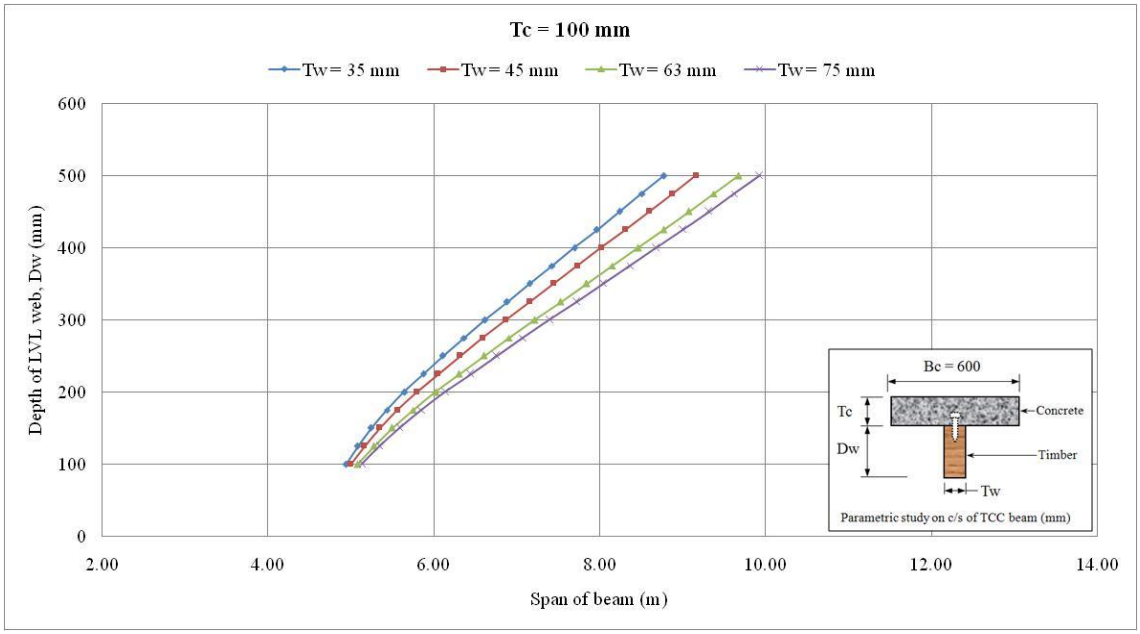

Figure 8.13 A span table of TCC Beam-2 with 100 mm thick concrete topping.

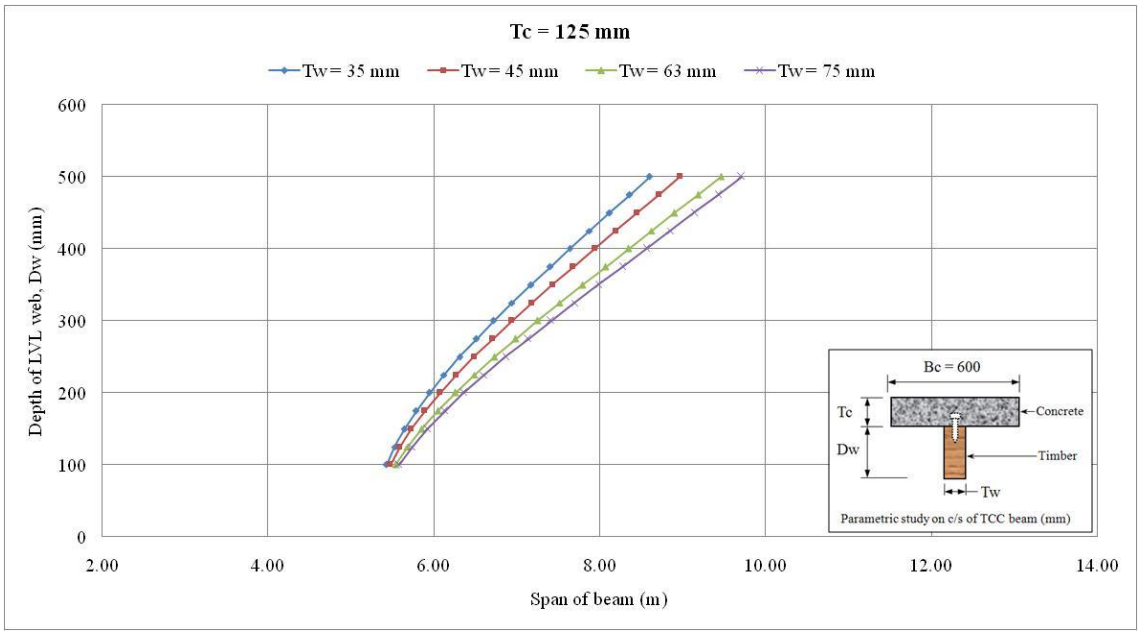

Figure 8.14 A span table of TCC Beam-2 with 125 mm thick concrete topping.

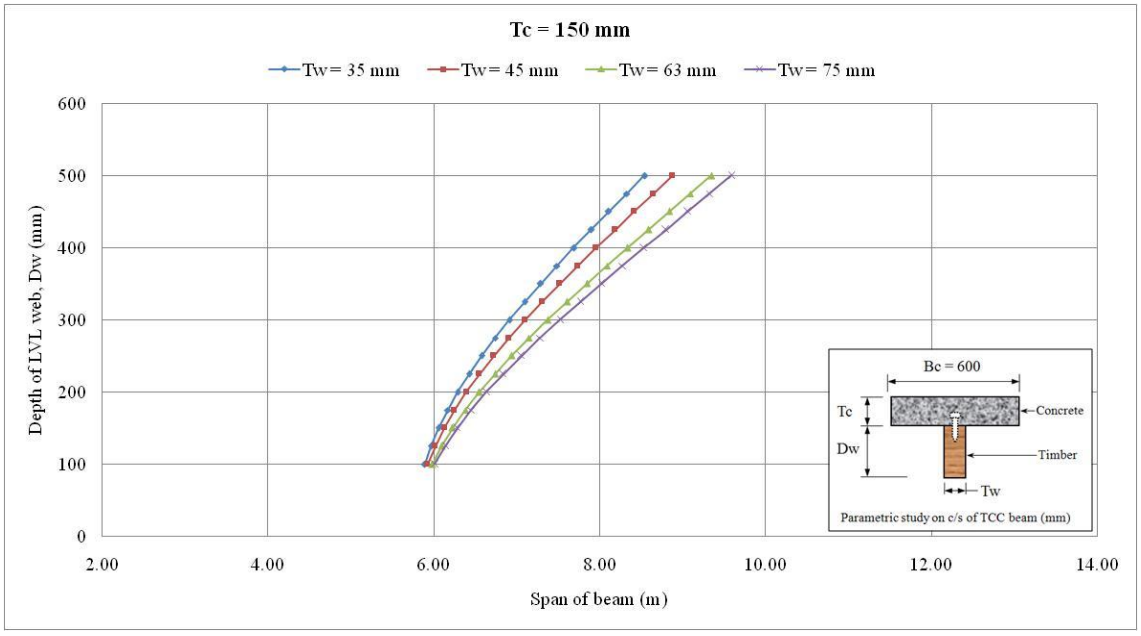

Figure 8.15 A span table of TCC Beam-2 with 150 mm thick concrete topping.

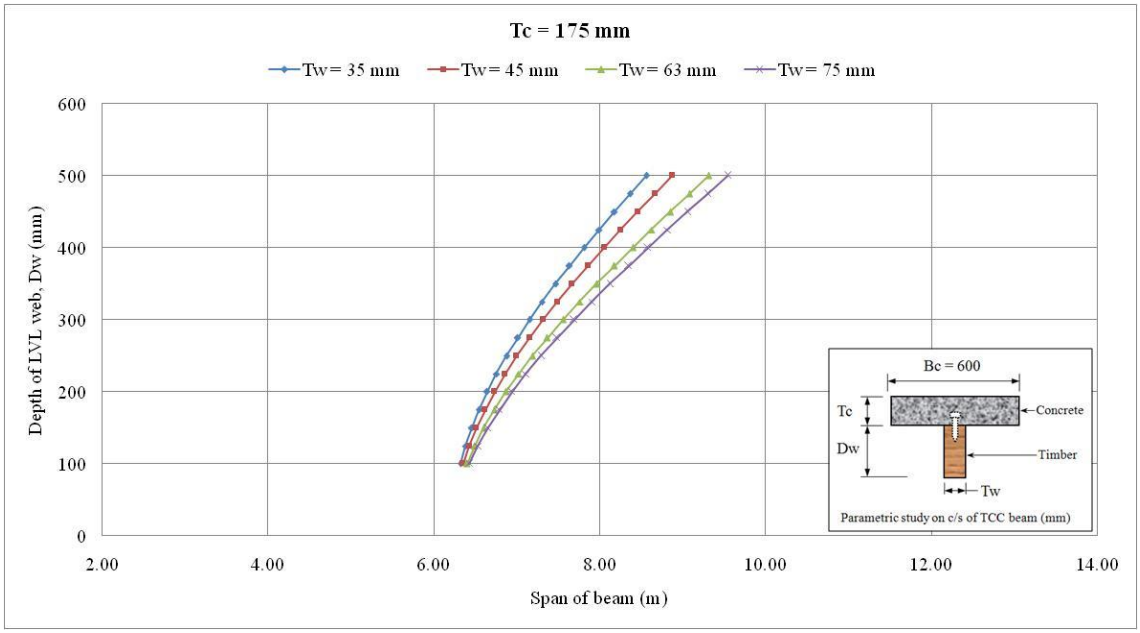

Figure 8.16 A span table of TCC Beam-2 with 175 mm thick concrete topping.

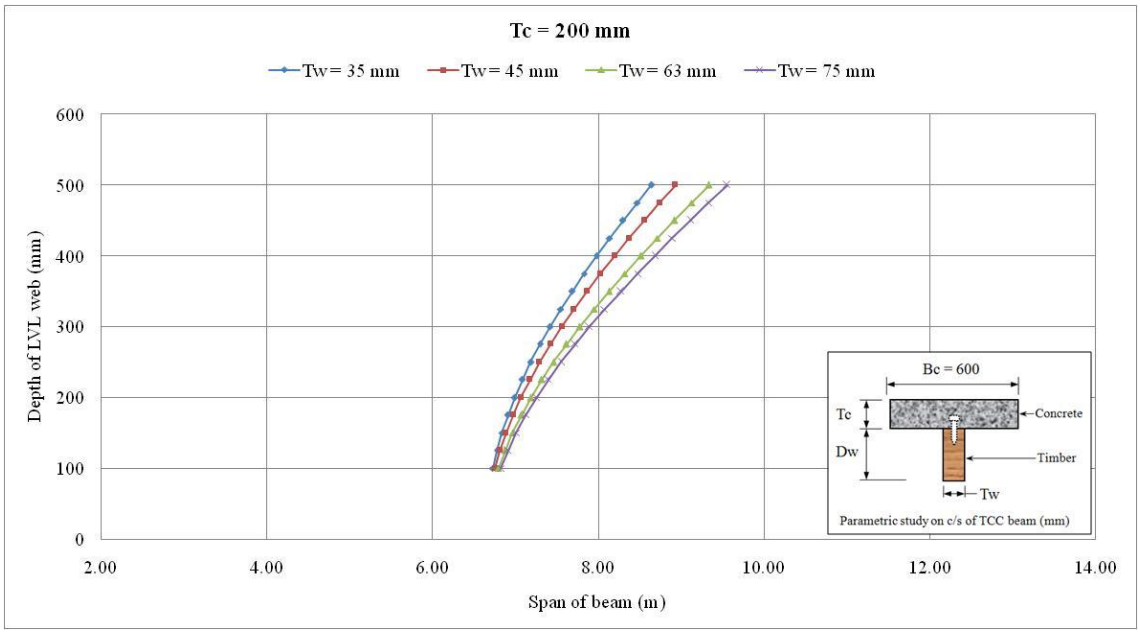

Figure 8.17 A span table of TCC Beam-2 with 200 mm thick concrete topping.

8.1.3 Beam-3 with Six Bird-mouth Notches

Span tables for different cross-sectional dimensions of TCC Beam-3 are shown in Figures 8.18 to 8.25. The number of bird-mouth notches was constant for all span tables, however their spacing was different for each span as the minimum and maximum spacing of the notches was a function of span of the beams. There were three notches at each end of the beams. The effective spacing (S_{ef}) of the notches was different for different spans. The method described in Gerber & Crews (2011) was utilised to determine minimum (S_{min}) and maximum (S_{max}) spacing of the notches. For six notches, minimum and maximum spacing of the notches were 10 and 30% of the span, respectively.

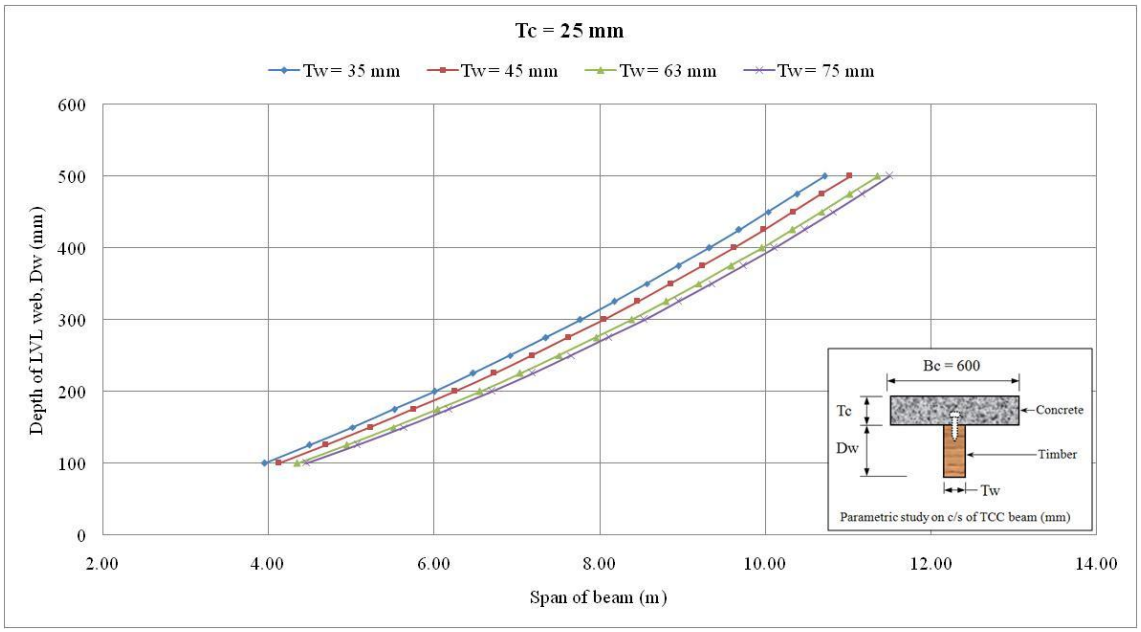

Figure 8.18 A span table of TCC Beam-3 with 25 mm thick concrete topping.

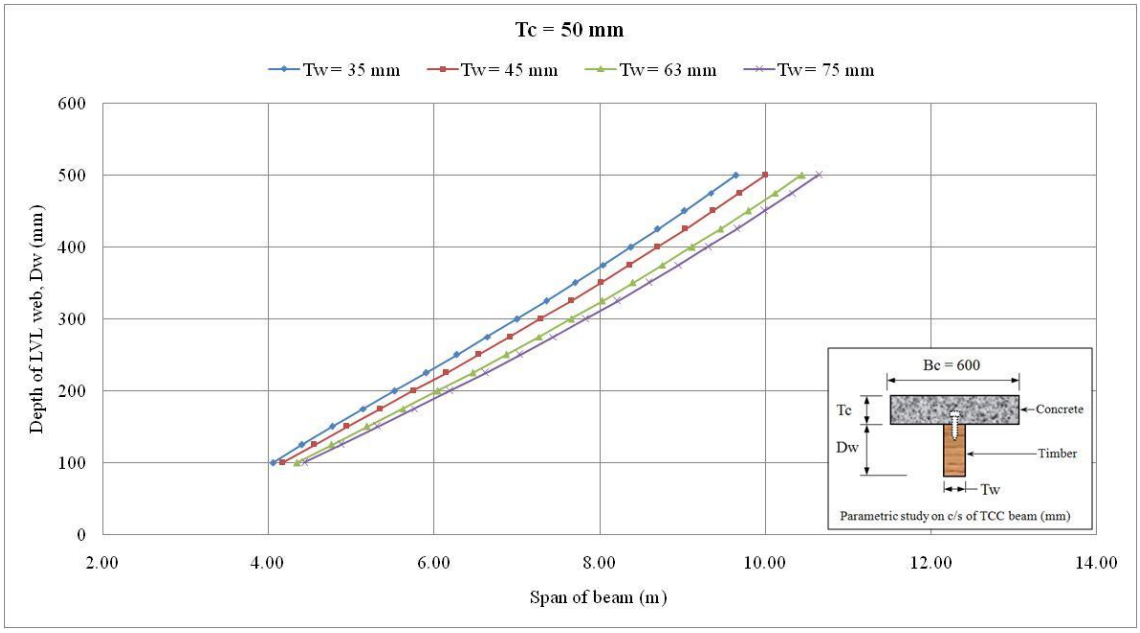

Figure 8.19 A span table of TCC Beam-3 with 50 mm thick concrete topping.

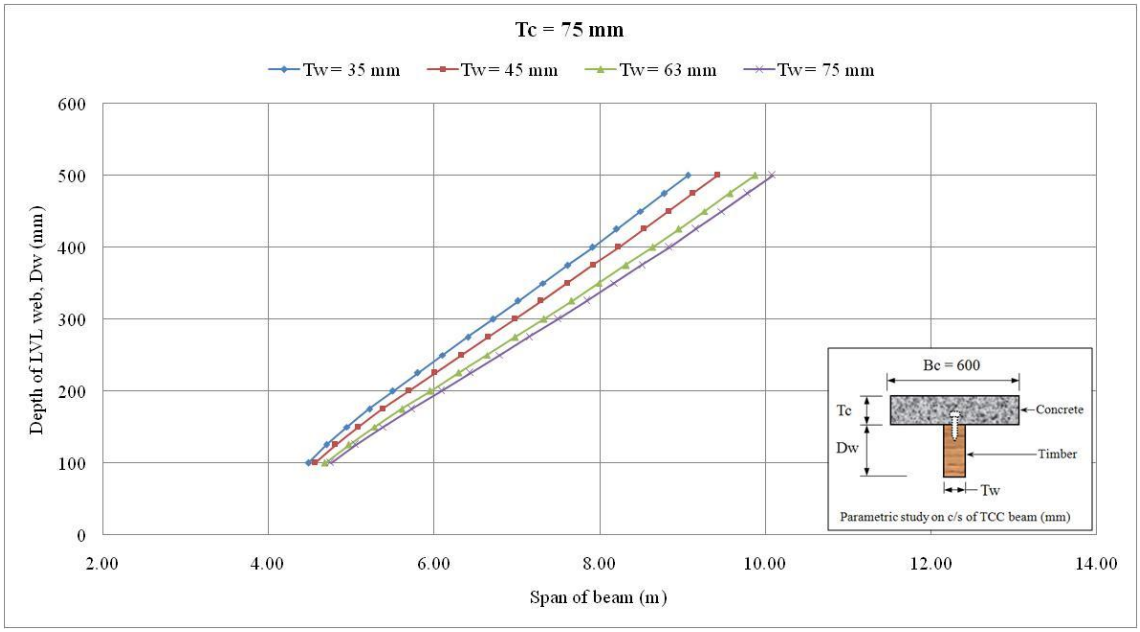

Figure 8.20 A span table of TCC Beam-3 with 75 mm thick concrete topping.

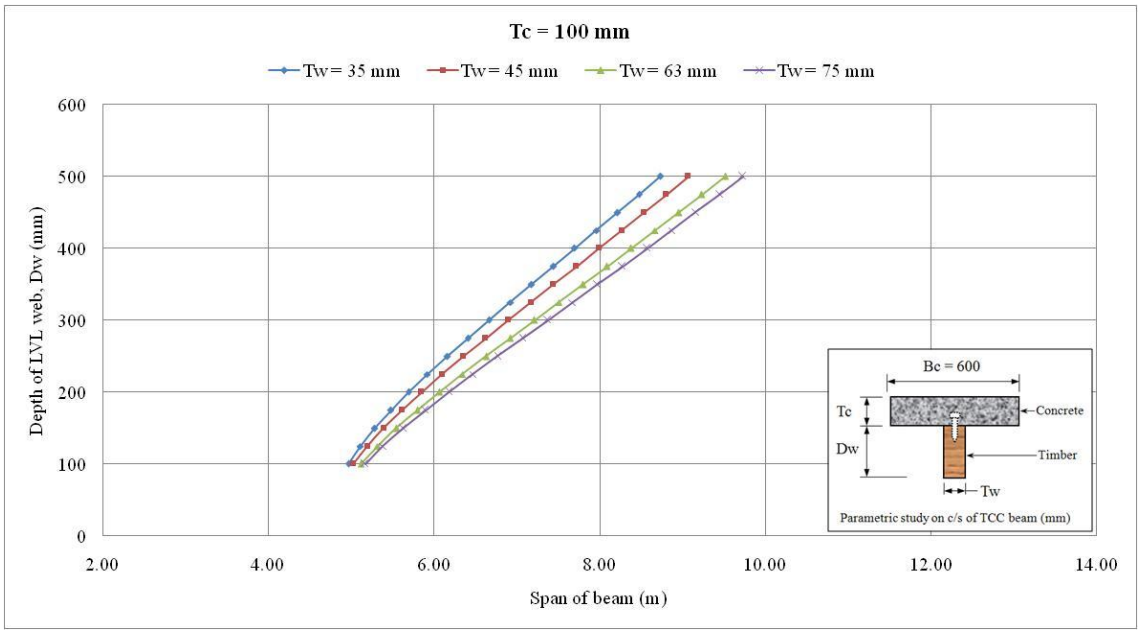

Figure 8.21 A span table of TCC Beam-3 with 100 mm thick concrete topping.

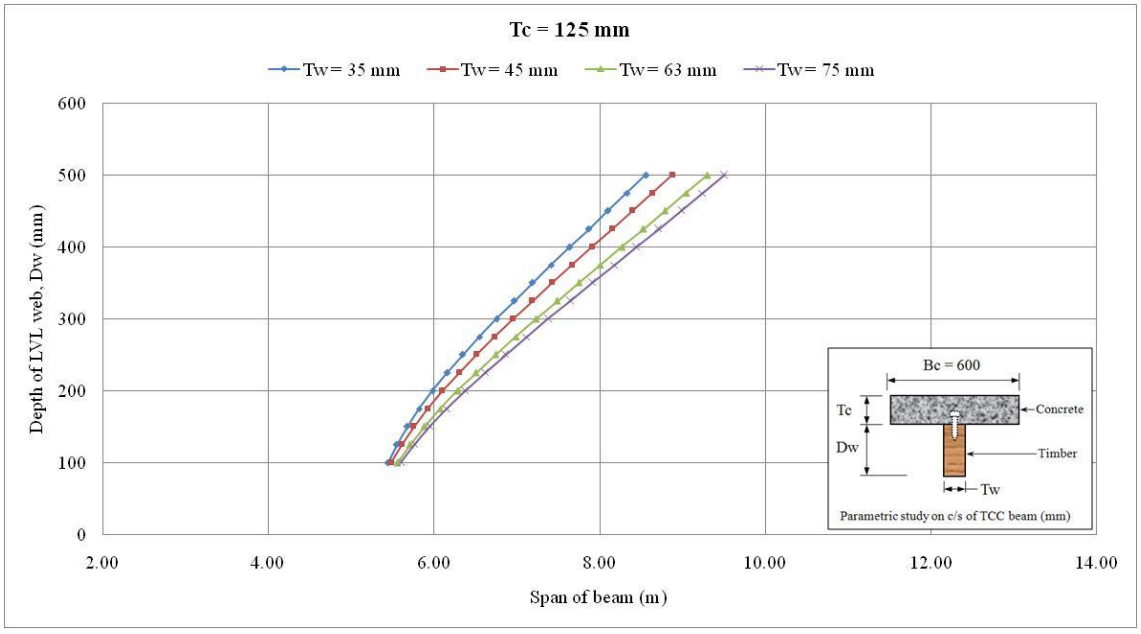

Figure 8.22 A span table of TCC Beam-3 with 125 mm thick concrete topping.

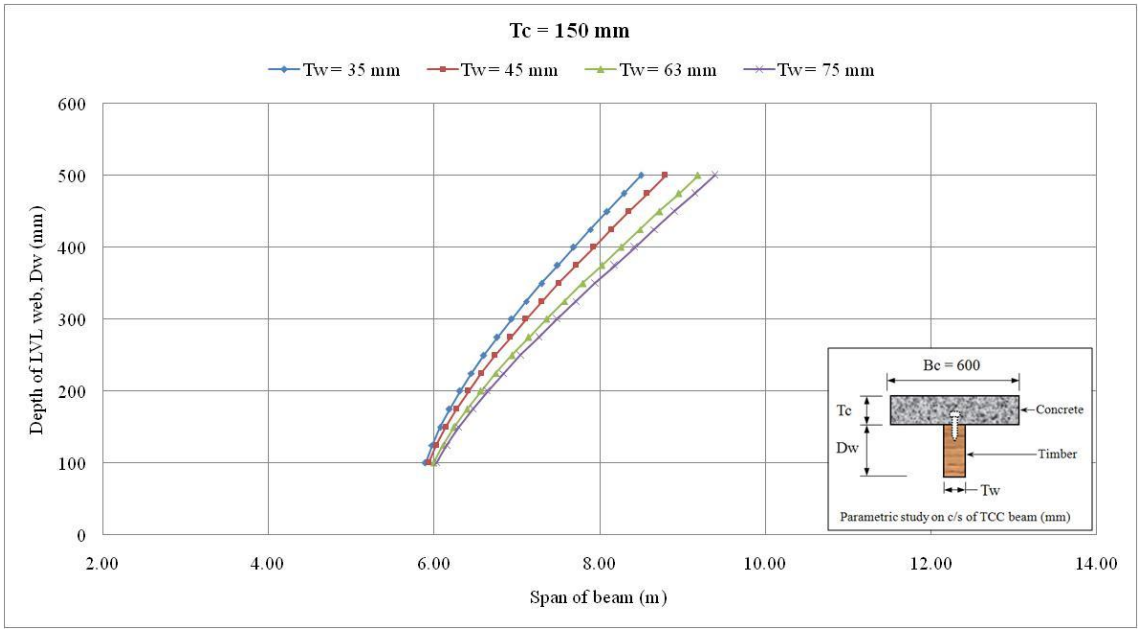

Figure 8.23 A span table of TCC Beam-3 with 150 mm thick concrete topping.

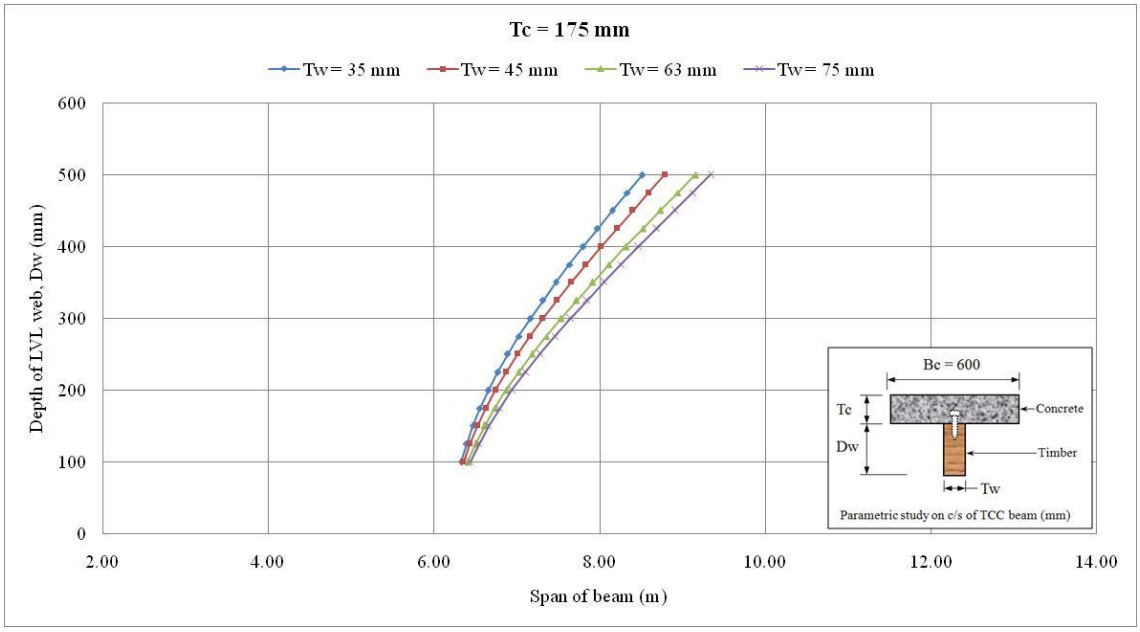

Figure 8.24 A span table of TCC Beam-3 with 175 mm thick concrete topping.

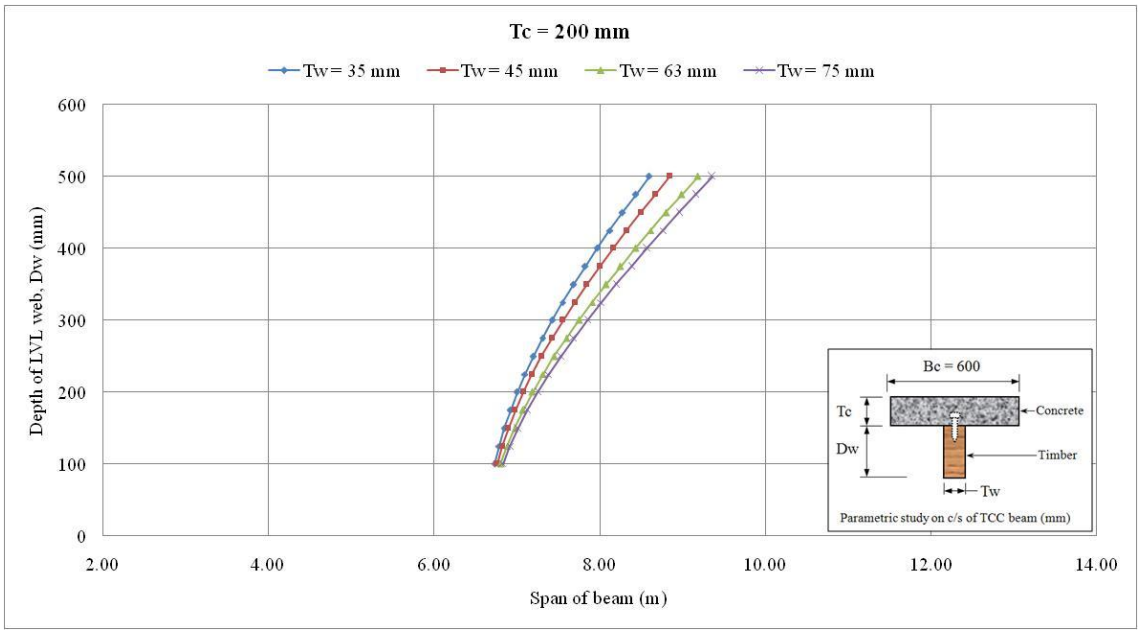

Figure 8.25 A span table of TCC Beam-3 with 200 mm thick concrete topping.

8.1.4 Beam-4 with Four Bird-mouth Notches

Span tables for different cross-sectional dimensions of TCC Beam-4 are shown in Figures 8.26 to 8.33. The number of bird-mouth notches was constant for all span tables which were four. However, their spacing was different for each span as the minimum and maximum spacing of the notches was a function of span of the beams. There were two notches at each end of the beams. The effective spacing (S_{ef}) of the notches was different for different spans. The method described in Gerber & Crews (2011) was utilised to determine minimum (S_{min}) and maximum (S_{max}) spacing of the notches. For four notches (two at each end of the beams), minimum and maximum spacing of the notches were 17% and 33% of the span, respectively.

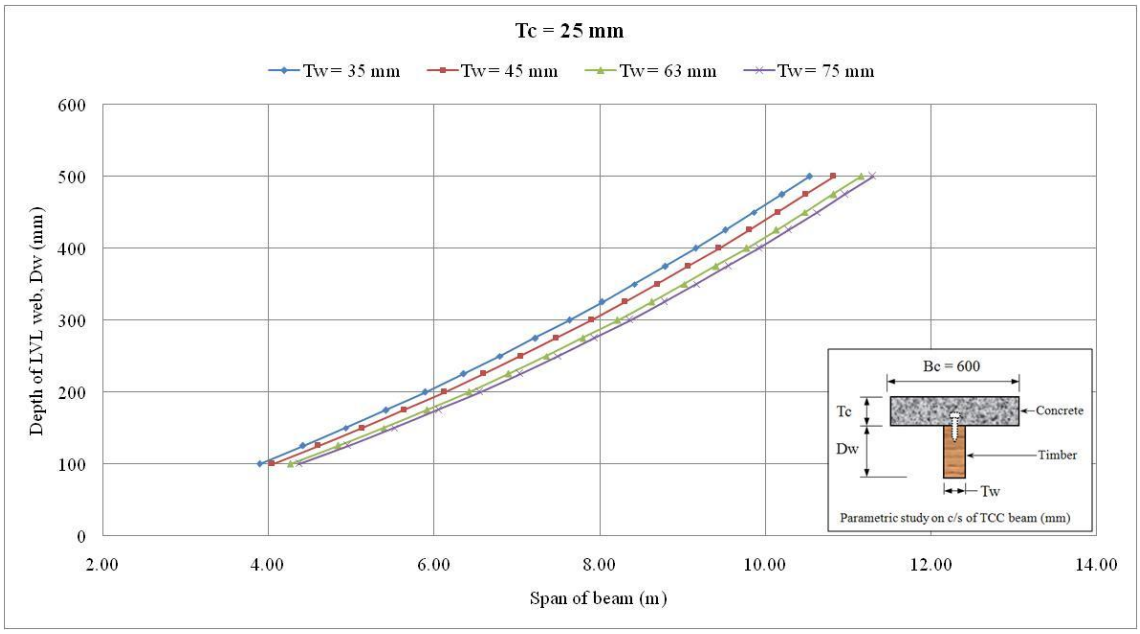

Figure 8.26 A span table of TCC Beam-4 with 25 mm thick concrete topping.

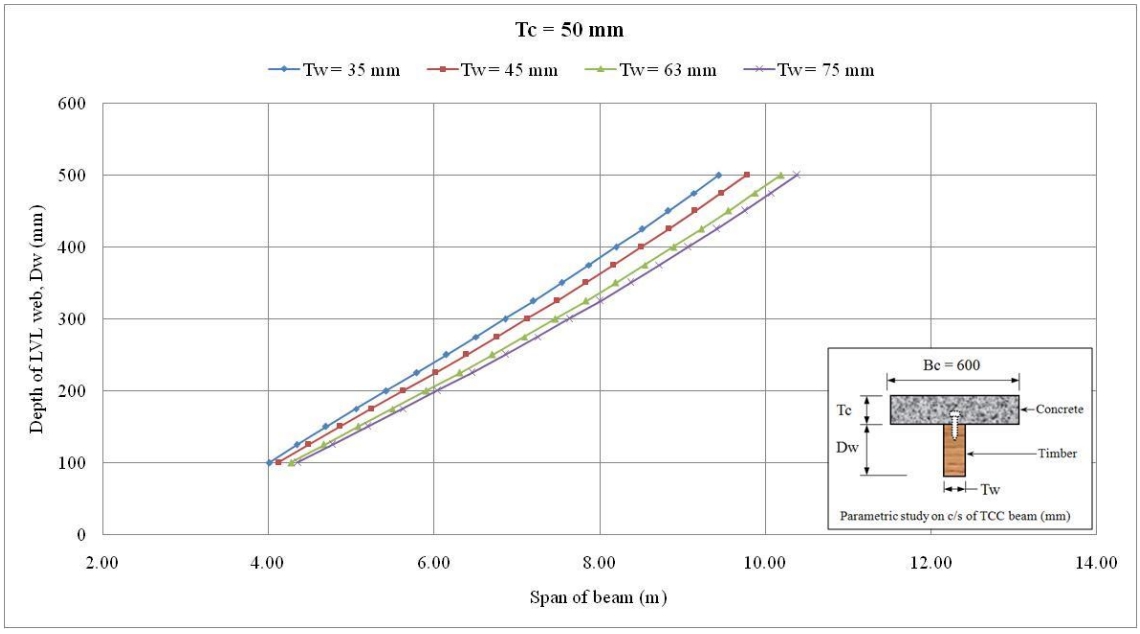

Figure 8.27 A span table of TCC Beam-4 with 50 mm thick concrete topping.

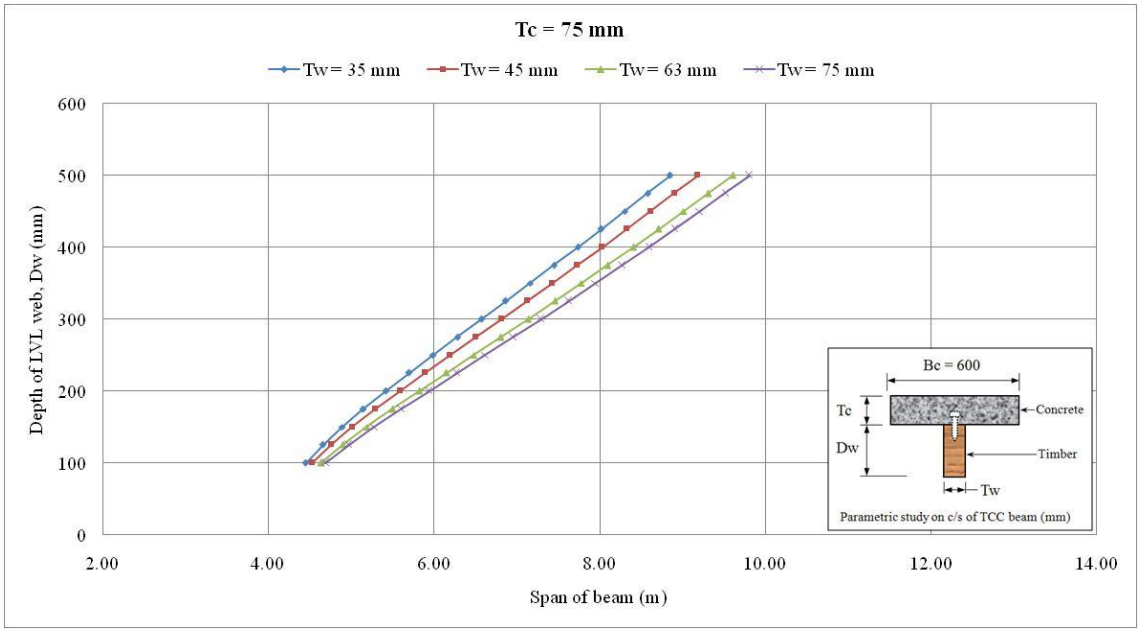

Figure 8.28 A span table of TCC Beam-4 with 75 mm thick concrete topping.

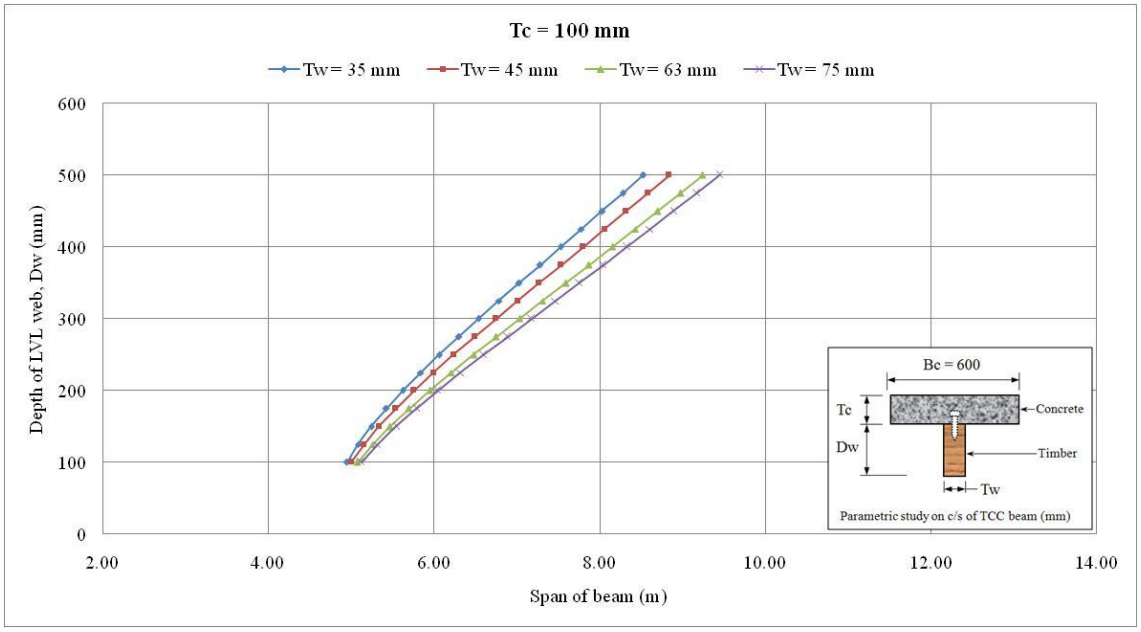

Figure 8.29 A span table of TCC Beam-4 with 100 mm thick concrete topping.

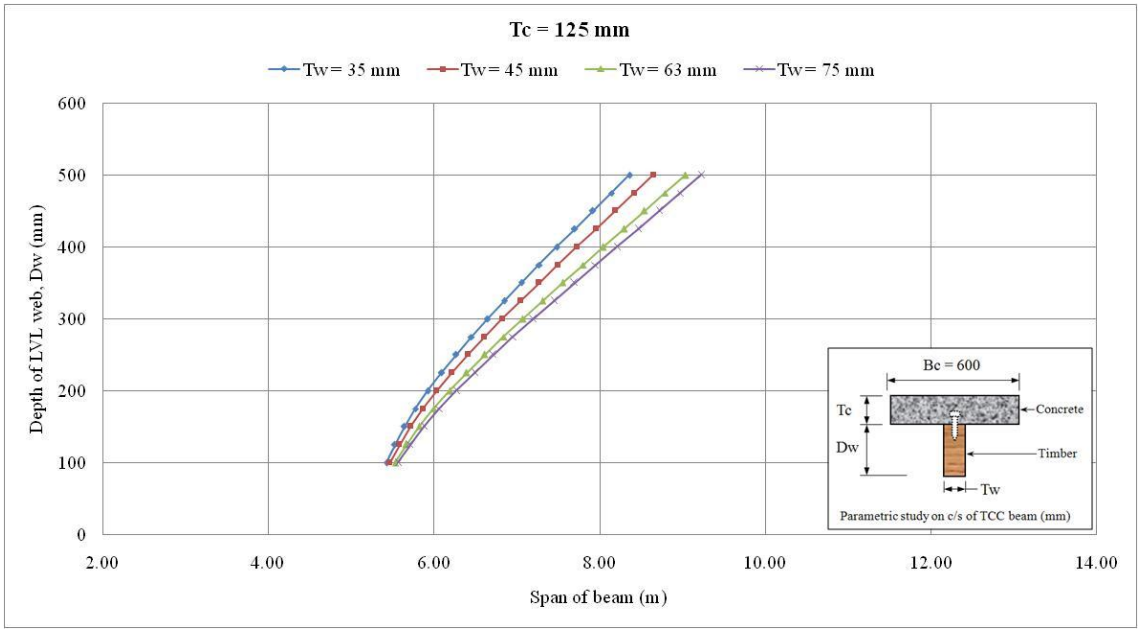

Figure 8.30 A span table of TCC Beam-4 with 125 mm thick concrete topping.

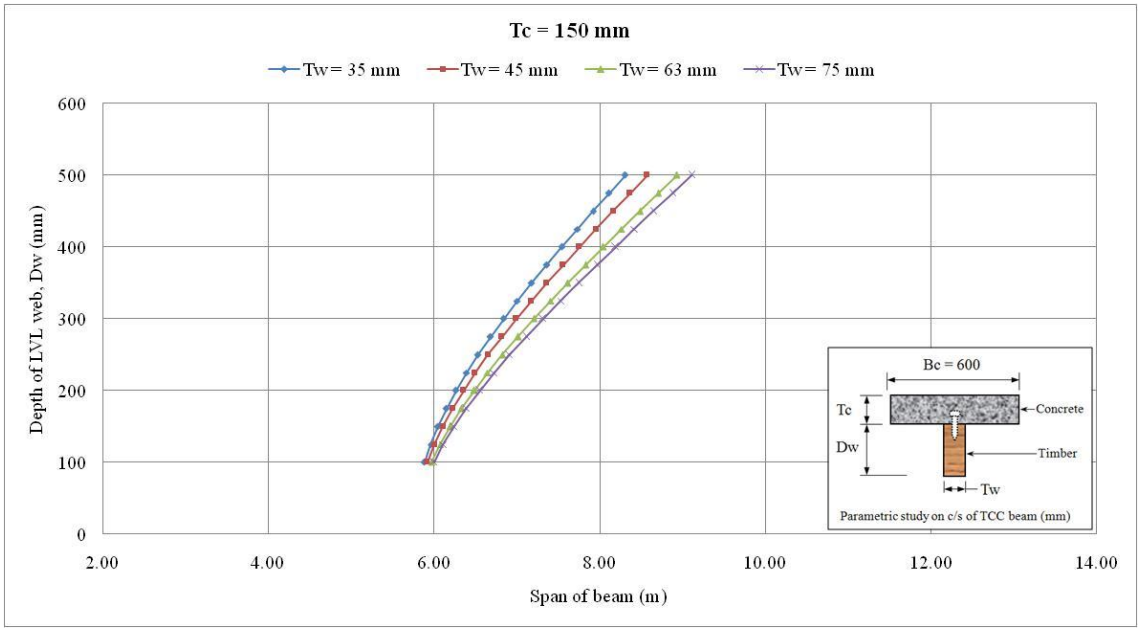

Figure 8.31 A span table of TCC Beam-4 with 150 mm thick concrete topping.

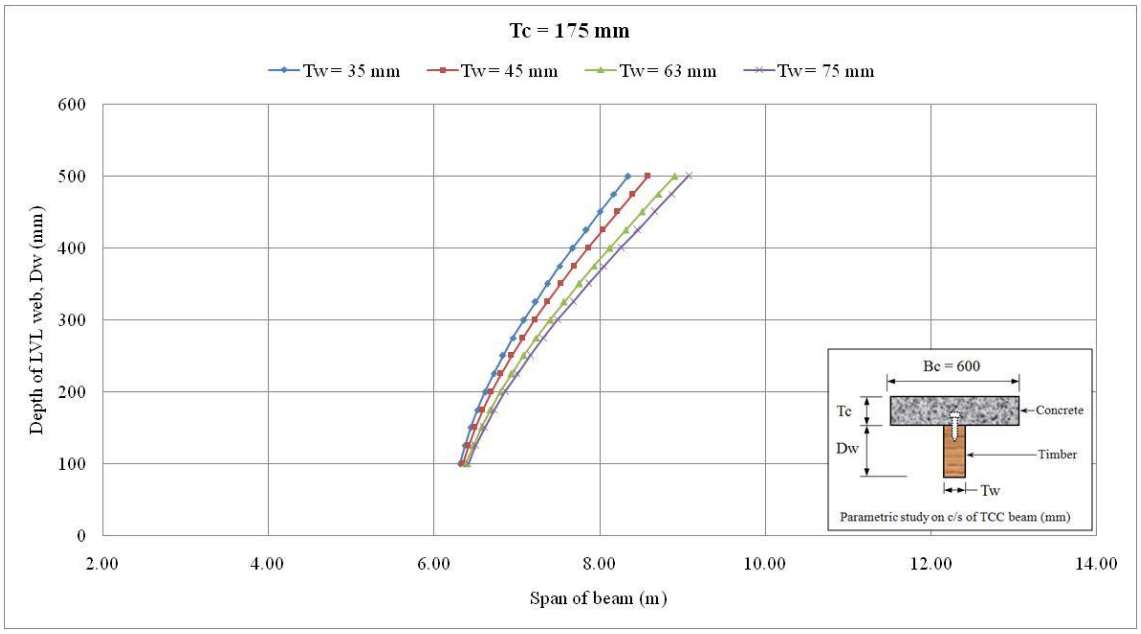

Figure 8.32 A span table of TCC Beam-4 with 175 mm thick concrete topping.

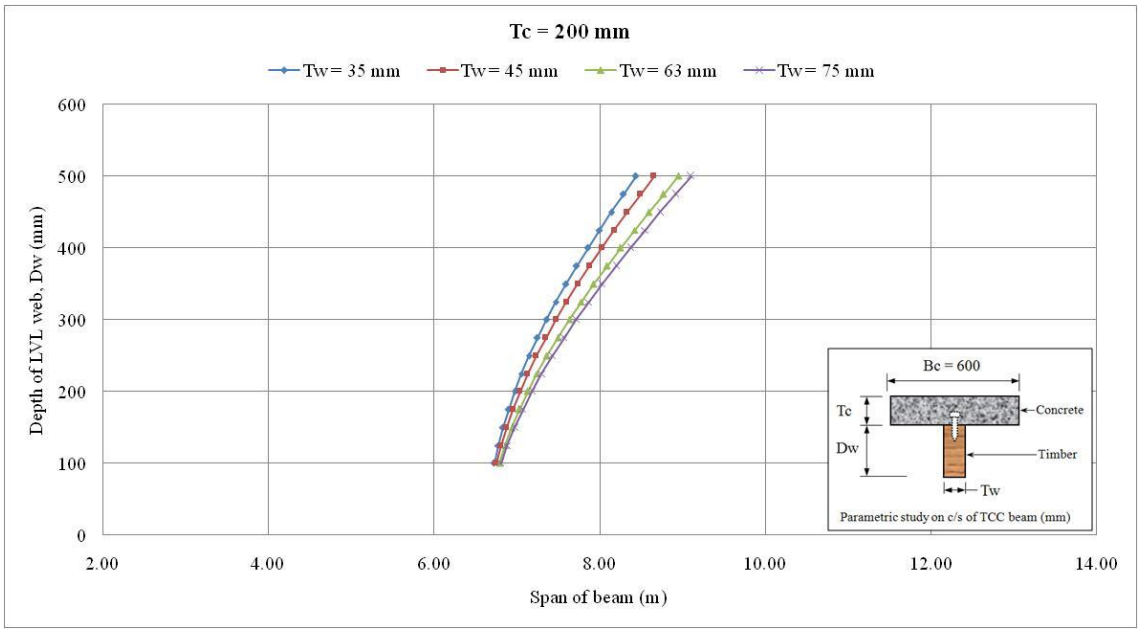

Figure 8.33 A span table of TCC Beam-4 with 200 mm thick concrete topping.

8.2 Timber Floor Module

Parametric study was also conducted on different size floors modelled using calibrated FE models of the tested timber floor modules with 6 and 8 m span (Zabihi et al. 2012). Details of experimental and FE results of these modules can be found in Chapter 4 and Section 5.2, respectively. Cross-sections of these modules are shown in Figure 8.34. The identical FE models of 6 and 8 m span modules were repeated side by side to create floors. In addition, an analytical frequency prediction model presented by Wyatt (1989) was used to generate span table for different cross-sectional dimensions of geometry of 8 m span module. Details of these studies are presented in the following sub-headings.

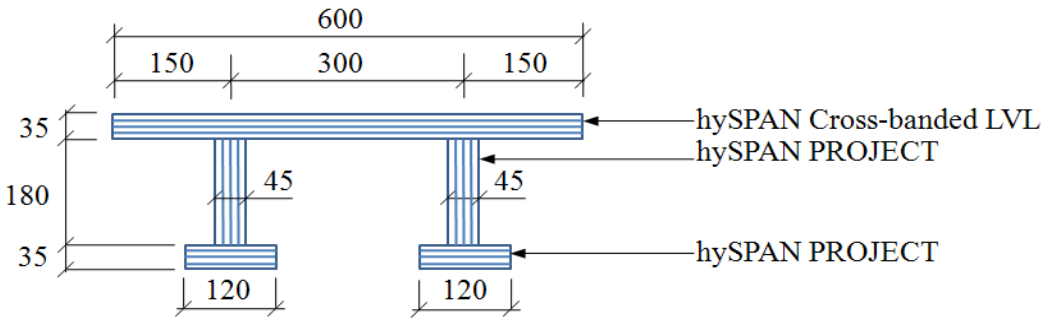

(a) Cross-sectional dimensions of 6 m timber floor module

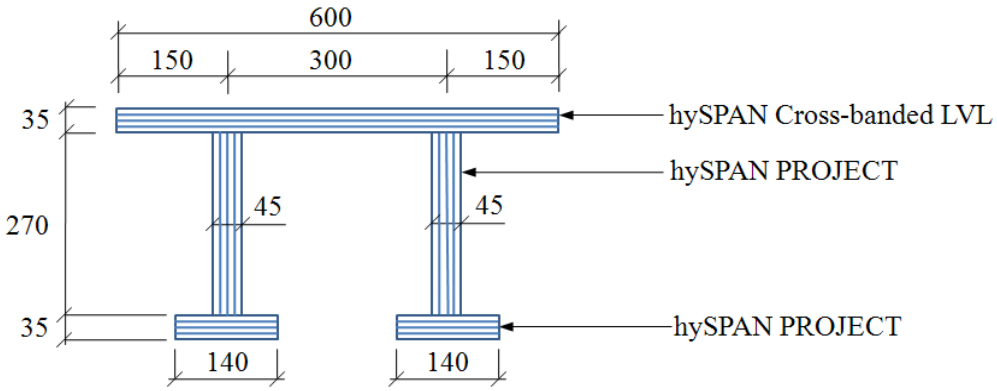

(b) Cross-sectional dimensions of 8 m timber floor module

Figure 8.34 Cross-sectional dimensions of timber floor modules (mm).

8.2.1 Parametric Study on Floors

In this study, calibrated FE models of the timber floor modules were used to model a floor of different sizes using different number of timber floor modules. Sizes of the floors modelled using 6 m span timber floor modules were 6.0 x 1.8 m, 6.0 x 3.6 m and 6 x 6 m. For 8 m timber floor modules, sizes of the floors were 8.0 x 1.8 m, 8.0 x 3.6 m and 8.0 x 7.8 m. Cross-sectional dimensions and span of 6 and 8 m span modules were unchanged throughout this study, only the width of floors was increased. The main objective of this study was to investigate the dynamic performance of all these floors by assessing their natural frequencies. Details of FE model of each floor and their results is presented in the following sub-sections.

8.2.1.1 Using Three Identical Timber Floor Modules

This section presents results from FE models of the timber floors with 6.0 x 1.8 m and 8.0 x 1.8 m dimensions and these floors were modelled using calibrated FE models of timber floor modules with 6 and 8 m spans, respectively. The overall length of 6 and 8 m span floor modules was 6.3 and 8.4 m and their top flange had a 0.6 m width. FE model of each floor had three identical models of the corresponding timber floor modules joined side by side as shown in Figure 8.35.

Figure 8.35 A FE model of 8.0 x 1.8 m floor.

Based on mesh sensitivity analyses, the size of element in these models was chosen as 25 x 25 x 22.5 mm and 25 x 25 x 17.5 mm for webs and flanges, respectively. In total, FE models of 6.0 x 1.8 m and 8.0 x 1.8 m floors had 83,160 and 122,976 elements, respectively. These floors had coarser mesh compared to mesh used in the timber floor modules, nevertheless, the mesh sensitivity showed that results for mesh size up to 25 x 25 x 25 mm were fairly accurate. The mesh size was optimized for the floor to minimize FE model processing time with sufficient accuracy.

The interface between the top flanges of the floor modules were modelled as fully composite. The nodes at the interface were coupled in all three directions to generate fully composite interface.

Boundary conditions of the floors were pin-roller support identical with the FE model of the timber floor modules on its two opposite ends. These floors behave like a beam, also known as one way floor.

First three flexural mode shapes and their corresponding natural frequencies of the floors were extracted from the FE models. The frequencies of the floors are presented in Table 8.1 and flexural modes of 6.0 x 1.8 m floor are shown in Figure 8.36. Fundamental frequency of the 6.0 x 1.8 m and 8.0 x 1.8 m floors was 16.46 and 12.93 Hz, respectively. The results showed that the natural frequency of the floors had minor discrepancies with corresponding single timber floor modules. Therefore, natural frequency of the simply-supported floors will be similar to the single beam with identical boundary conditions if the beams were connected side by side rigidly during fabrication of the floor.

Table 8.1 Natural frequencies of the floors

Floor	Natural frequencies (Hz)		
	f_1	f_2	f_3
6.0 x 1.8 m	16.46	63.16	125.70
8.0 x 1.8 m	12.93	49.69	98.65

(a) Mode 1 (b) Mode 2 (c) Mode 3

Figure 8.36 First three flexural mode shapes of 6.0 x 1.8 m floor.

These FE models of the floors were also analysed for different boundary conditions, namely pin support along four bottom edges of the floors. First natural frequency of 6.0 x 1.8 m and 8.0 x 1.8 m floors were 58.44 and 48.85 Hz, respectively. These frequencies were significantly higher (almost four times) than the corresponding frequencies of the floors with pin-roller support at two opposite ends. The deformed shape for fundamental mode of the 8.0 x 1.8 m floor with pin support along four edges is shown in Figure 8.37. In the figure, vertical deflection contour is shown in order to visualize the shape. Maximum deflection contour plot is toward the centre of the floor and minimum is towards the edges. Contours with red and blue colour show the maximum and minimum deflections, respectively. A scale at the bottom of the figure depicts contours with different deflections in meters.

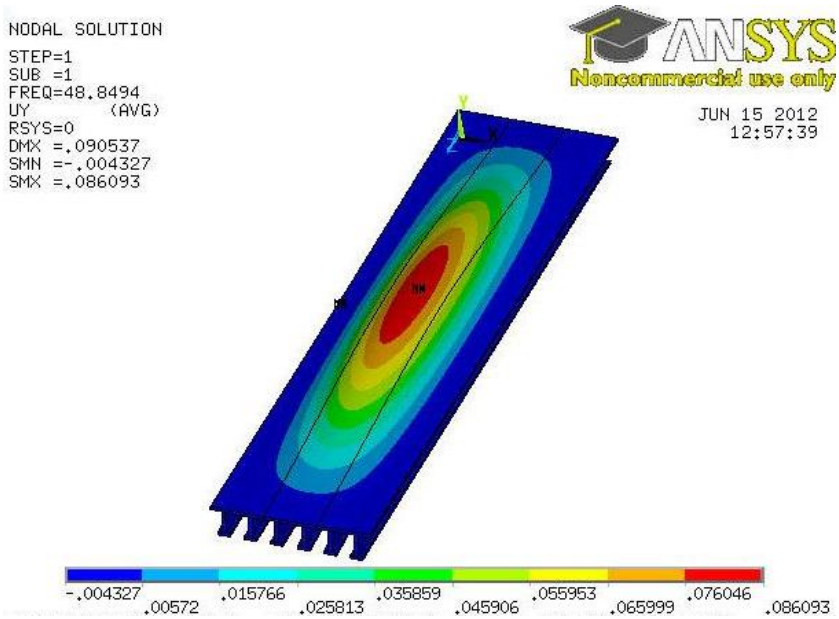

Figure 8.37 Fundamental deformed shape of 8.0 x 1.8 m floor with pin support along four edges.

8.2.1.2 Using Six Identical Timber Floor Modules

In this section results from FE models of the 6.0 x 3.6 m and 8.0 x 3.6 m floors are presented. The FE model of each floor had six identical calibrated models of the corresponding timber floor modules joined side by side as shown in Figure 8.38 for 6.0 x 3.6 m floor. Size of the elements in these models was chosen as 25 x 25 x 22.5 mm and 25 x 25 x 17.5 mm for webs and flanges, respectively. In total, the FE models of 6.0 x 3.6 m and 8.0 x 3.6 m floors had 166,314 and 245,952 elements, respectively. The interface between the top flanges of the floor modules were modelled as fully composite. Pin support was used along four sides of the floors.

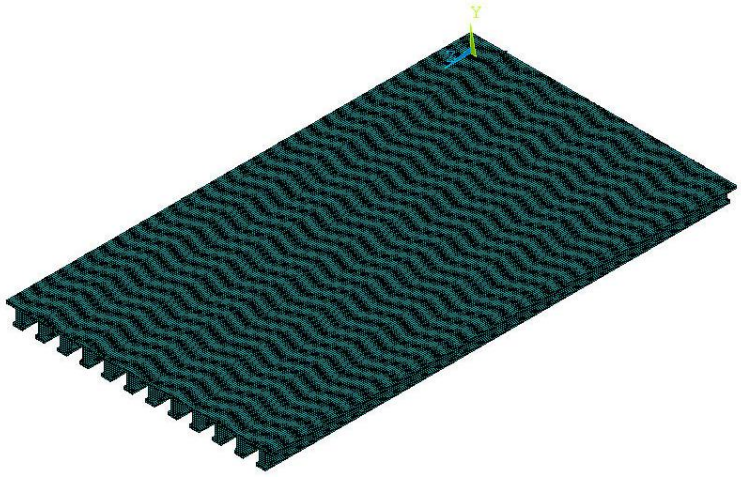

Figure 8.38 A FE model of 6.0 x 3.6 m floor.

The first four natural frequencies of the floors are presented in Table 8.2. The first natural frequency of 6.0 x 3.6 m and 8.0 x 3.6 m floors were 31.44 and 26.25 Hz, respectively. This result showed about 50% reductions in first natural frequency of the floors with identical boundary conditions when their dimensions were increased from 6.0 x 1.8 m and 8.0 x 1.8 m to 6.0 x 3.6 m and 8.0 x 3.6 m, respectively.

Deformed shapes of 6.0 x 3.6 m floor corresponding to first four natural frequencies are shown in Figures 8.39 and 8.40. In the figures, vertical deflection contour is shown in order to visualize the shapes. A scale at the bottom of the each figure depicts contours with different deflections in meters. Positive magnitude of deflection in the scale shows upward deflection and negative magnitude represents downward deflection from the undeformed position of the floor. Maximum upward and downward deflections are shown by red and blue contours in the figures.

Table 8.2 Natural frequencies of the floors

Floor	Natural frequencies (Hz)			
	f_1	f_2	f_3	f_4
6.0 x 3.6 m	31.44	44.87	64.75	74.54
8.0 x 3.6 m	26.25	37.05	53.10	55.38

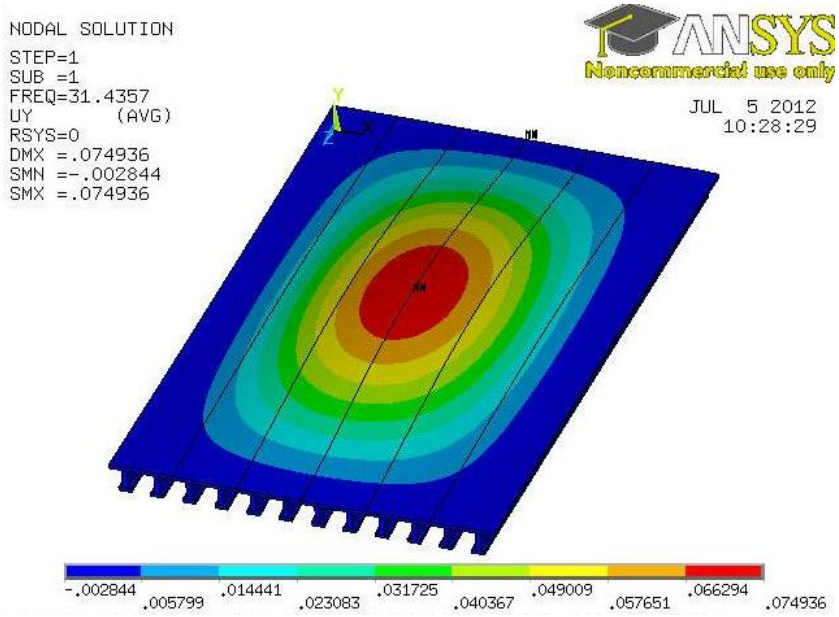

(a) First mode shape

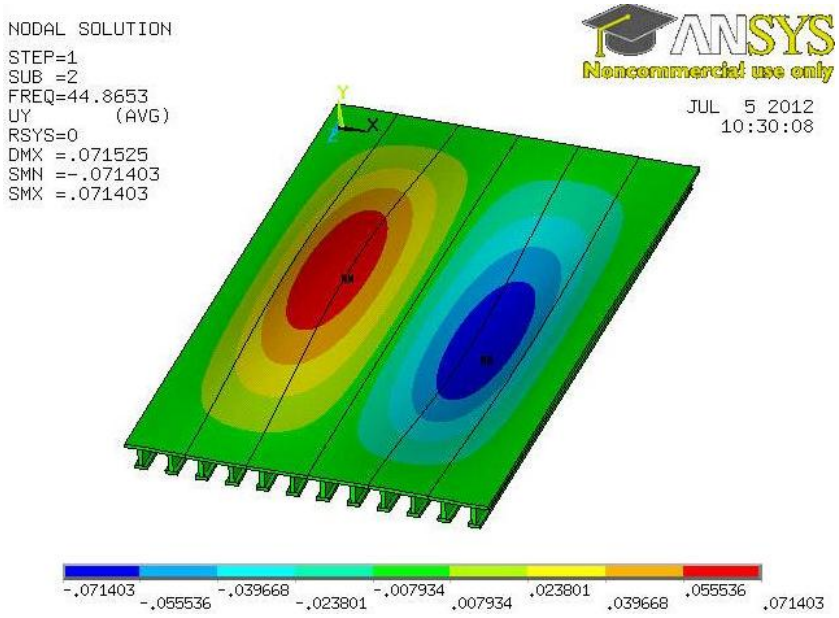

(b) Second mode shape

Figure 8.39 Two deformed shapes of 6.0 x 3.6 m floor corresponding to the first two natural frequencies.

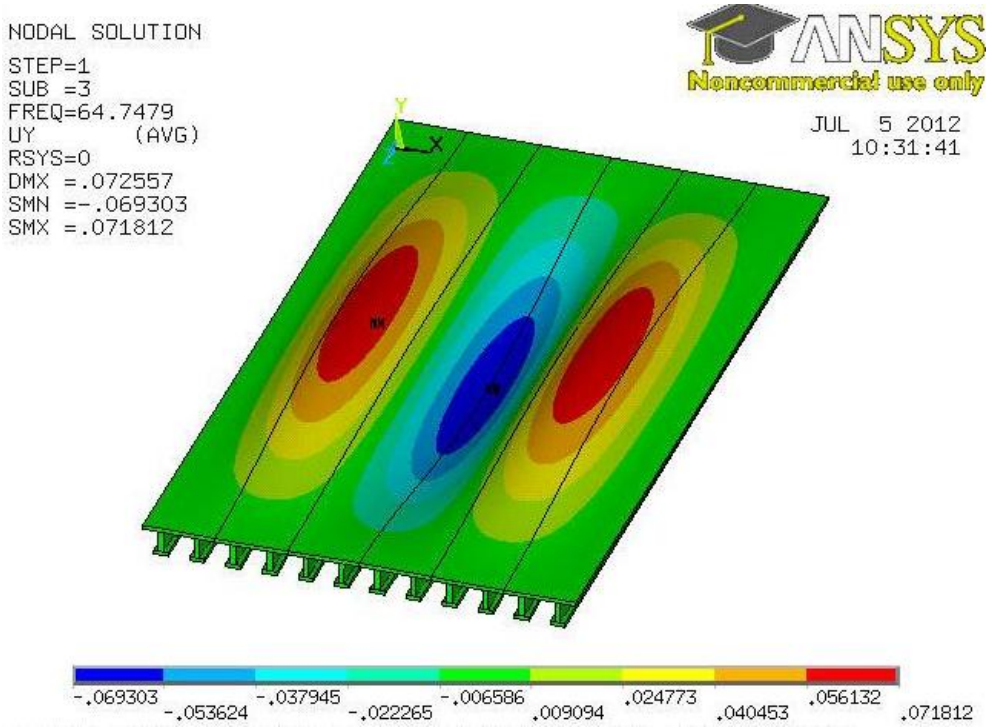

(c) Third mode shape

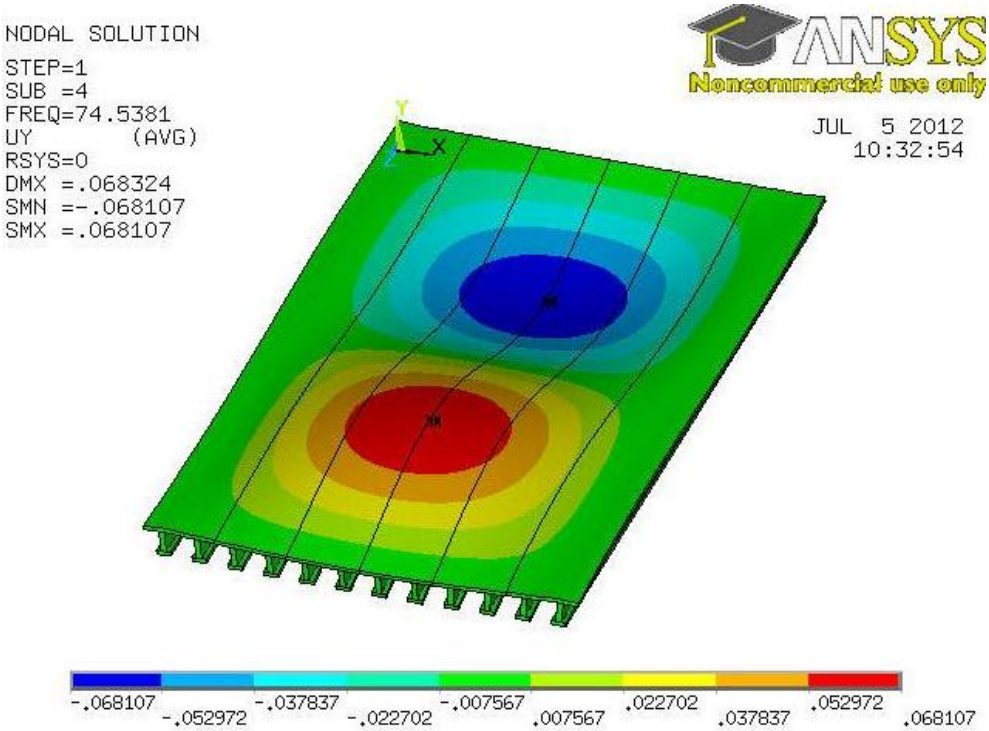

(d) Fourth mode shape

Figure 8.40 Two deformed shapes of 6.0 x 3.6 m floor corresponding to the third and fourth natural frequencies.

8.2.1.3 Square Floors

This section presents results from FE models of 6 x 6 m and 8.0 x 7.8 m floors. These floors had 10 and 13 identical calibrated FE models of the corresponding 6 and 8 m floor modules joined side by side, respectively. A FE model of 6 x 6 m floor is shown in Figure 8.41. The size of element in the models was chosen as 25 x 25 x 22.5 mm and 25 x 25 x 17.5 mm for webs and flanges, respectively. In total, FE models of 6 x 6 m and 8.0 x 7.8 m floors had 277,200 and 532,896 elements, respectively. The interface between the top flanges of the floor modules were modelled as fully composite. Pin support was used along four sides of the floors.

Figure 8.41 A FE model of 6 x 6 m floor.

First four natural frequencies of the floors are presented in Table 8.3. First natural frequency of 6 x 6 m and 8.0 x 7.8 m floors were 26.60 and 20.18 Hz, respectively. This result showed about 15 and 23% reductions in first natural frequency of the floors with identical boundary conditions when their dimensions were increased from 6.0 x 3.6 m and 8.0 x 3.6 m to 6 x 6 m and 8.0 x 7.8 m, respectively.

Deformed shapes of 6 x 6 m floor corresponding to first four natural frequencies are shown in Figures 8.42 and 8.43. In the figures, different colours show vertical deflection contour and a scale at the bottom of the each figure depicts contours with different deflections in meters. Positive magnitude of deflection in the scale shows upward deflection and negative magnitude represents downward deflection from the undeformed position of the floor.

Table 8.3 Natural frequencies of the floors

Floor	Natural frequencies (Hz)			
	f_1	f_2	f_3	f_4
6 x 6 m	26.60	32.47	40.27	48.39
8.0 x 7.8 m	20.18	24.15	29.17	33.70

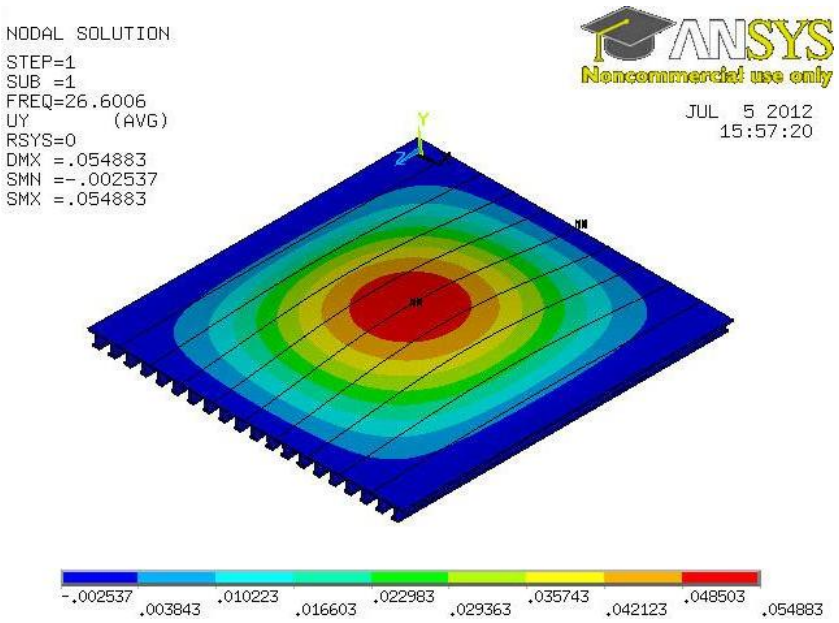

(a) First mode shape

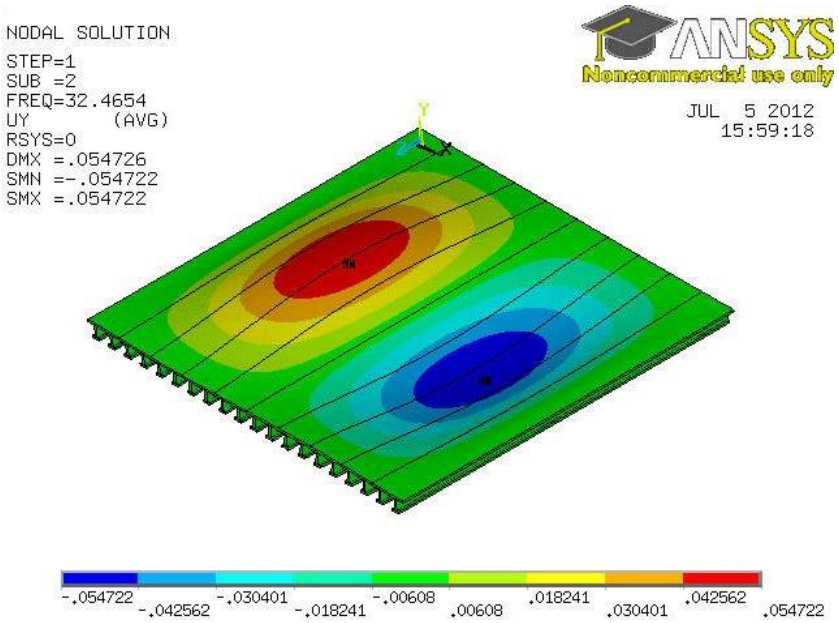

(b) Second mode shape

Figure 8.42 Two deformed shapes of 6 x 6 m floor corresponding to the first two natural frequencies.

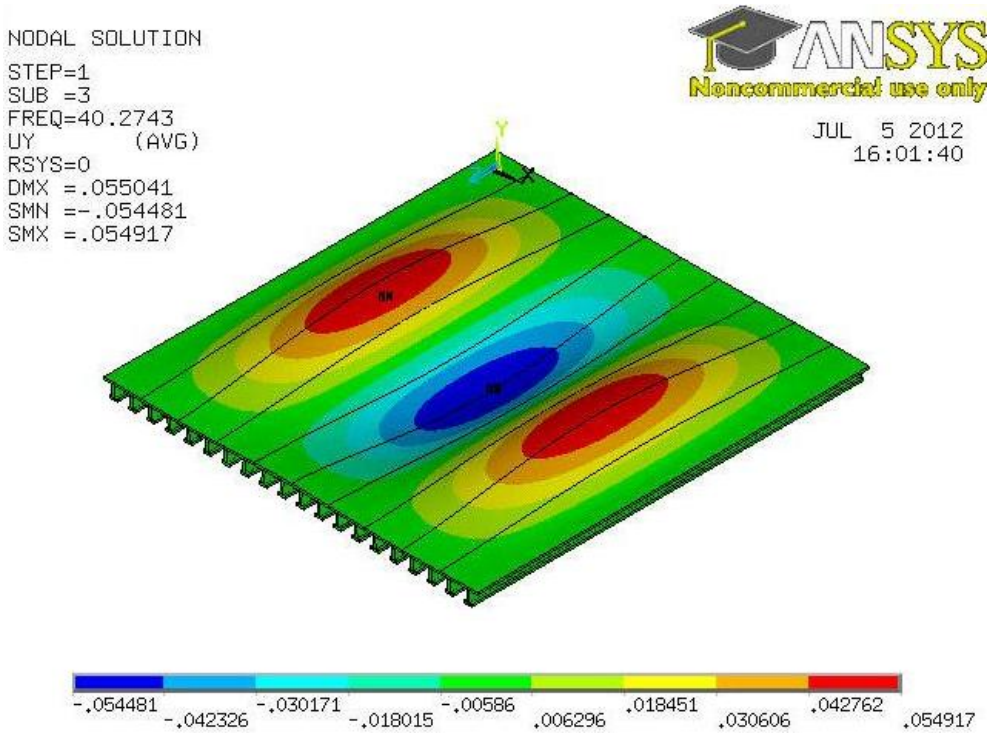

(c) Third mode shape

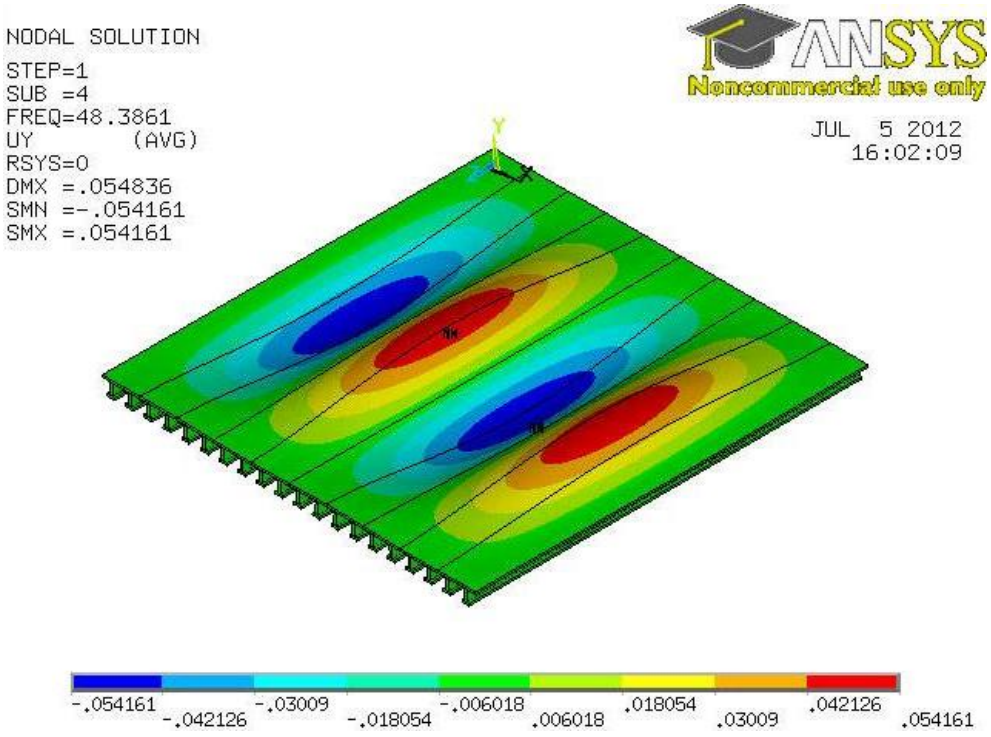

(d) Fourth mode shape

Figure 8.43 Two deformed shapes of 6 x 6 m floor corresponding to the third and fourth natural frequencies.

8.2.2 Span Table using Analytical Model

A parametric study was performed using the same natural frequency prediction analytical model presented by Wyatt (1989) as described in Section 8.1 to identify span for different cross-sectional dimensions of a timber floor module that satisfy 8 Hz natural frequency limit. Cross-sectional geometry as shown in Figure 8.44 was adopted from 8 m span floor module for the study. For top and bottom flanges, their widths at 600 and 140 mm, respectively, were kept constant throughout the study. However, thickness (T_f) of top and bottom flanges was identical and the thicknesses chosen in the study were 35, 45, 63 and 75 mm as these are standard thicknesses of LVL. For webs, both thickness (T_w) and depth (D_w) were varied. Depth was varied for a range of 100 and 500 mm with increments of 25 mm while thicknesses chosen were 35, 45, 63 and 75 mm.

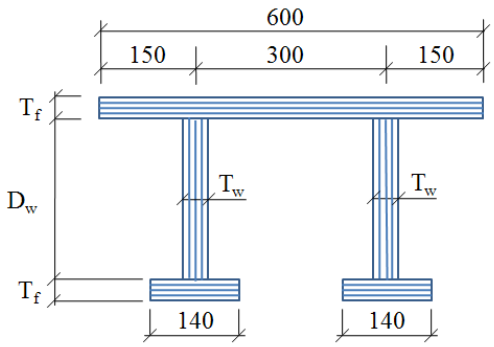

Figure 8.44 A cross-sectional geometry for the parametric study (mm).

Results for different cross-sectional dimensions against depth of webs (D_w) is shown in Figures 8.45 to 8.48. The results showed that the natural frequency is more sensitive to the thickness of flanges (T_f) and webs depth (D_w) rather than webs thickness (T_w). Hence, it can be concluded that increasing the flange thickness and web depth will increase the natural frequency. In contrast, increasing the web thickness will decrease the frequency as the additional mass of the webs may have an adverse effect on the frequency.

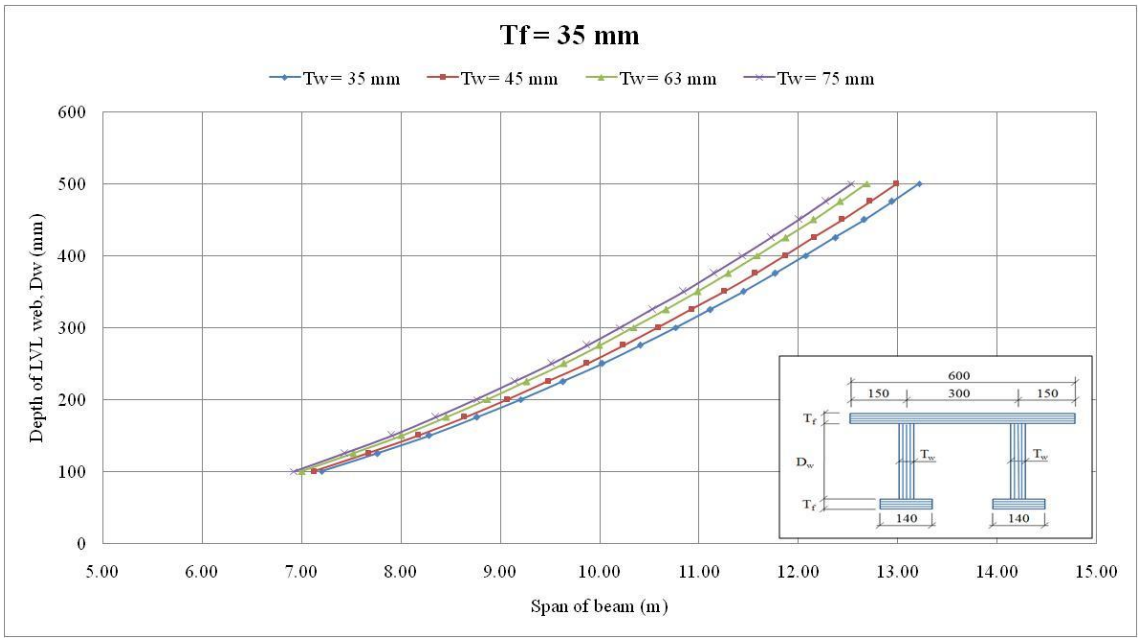

Figure 8.45 A span table of 8 m span timber floor module with 35 mm thick flanges.

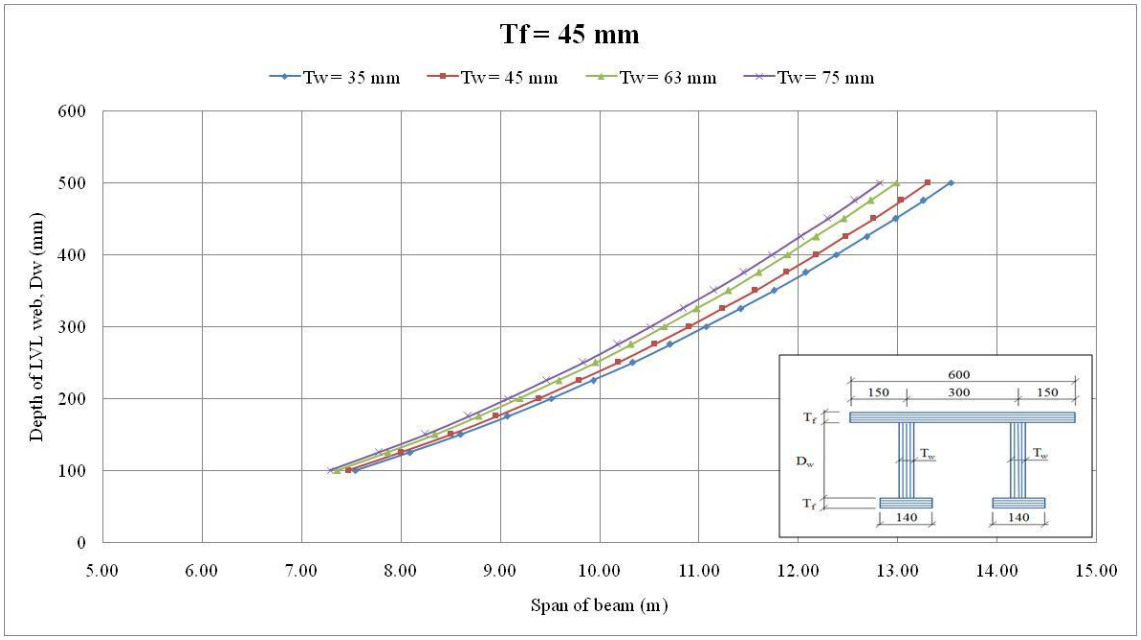

Figure 8.46 A span table of 8 m span timber floor module with 45 mm thick flanges.

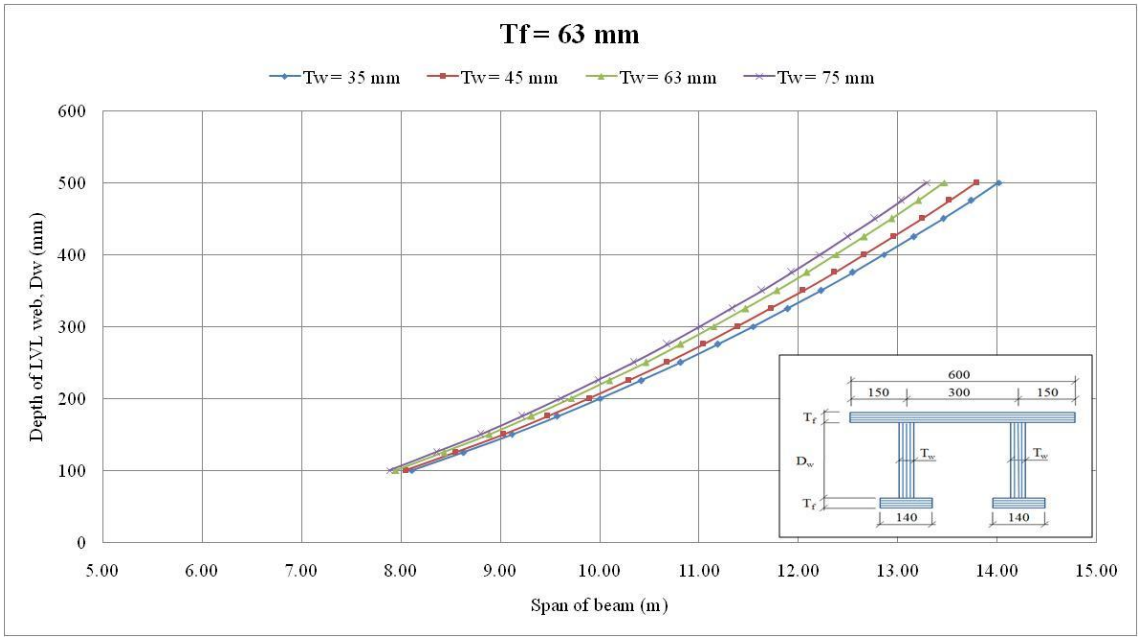

Figure 8.47 A span table of 8 m span timber floor module with 63 mm thick flanges.

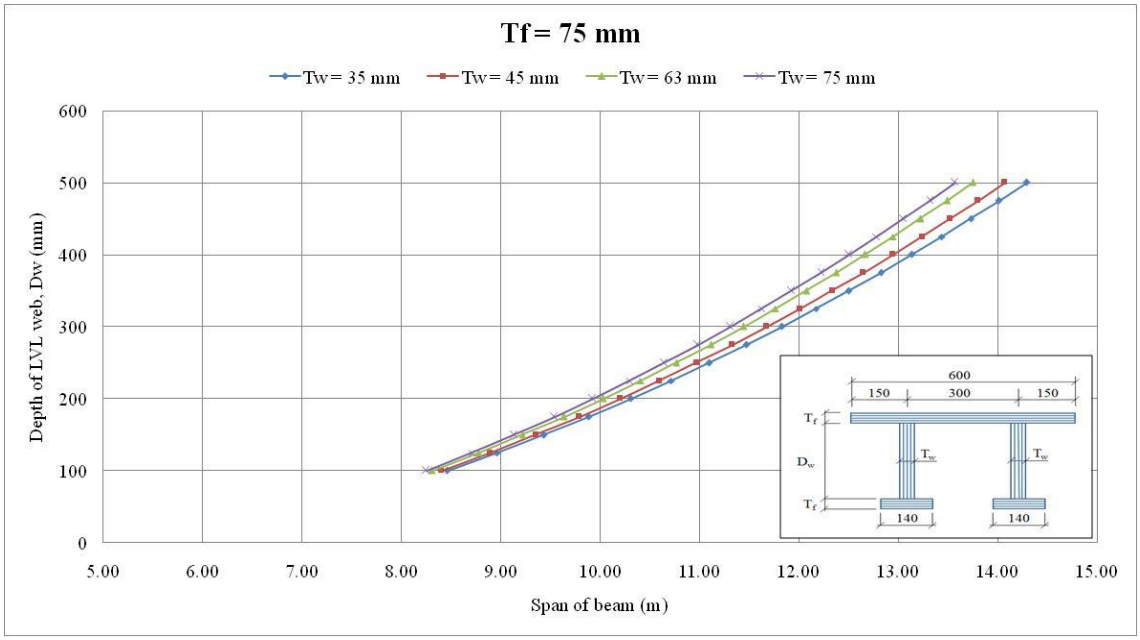

Figure 8.48 A span table of 8 m span timber floor module with 75 mm thick flanges.

8.3 Concluding Remarks

This chapter presented a detailed description of a parametric study performed on tested TCC beams with 5.8 m span and timber floor modules with 6 and 8 m span. Span tables were generated for both TCC beams and timber floor modules using an analytical natural frequency prediction model. To generate span tables, the required span was found for different cross-sectional dimensions resulting in 8 Hz fundamental frequency using the prediction model. These tables can be used to identify span of the beams for particular cross-sectional dimensions or vice versa that satisfy dynamic serviceability requirement of 8 Hz fundamental frequency, nevertheless, selected dimensions must satisfy other serviceability requirements such as deflection, acoustic and fire, and ultimate strength design criteria as well.

Parametric analyses were performed on different size floors using calibrated FE model of 6 and 8 m span timber floor modules. Floors with 6.0 x 1.8 m and 8.0 x 1.8 m dimensions were analysed for two boundary conditions such as pin-roller at their two opposite ends and pin along four edges of the floors while other floors were analysed with pin support only along four edges. The following conclusions can be drawn based on results for all these floors.

- A floor with pin-roller boundary conditions at two opposite ends of the floors in the longitudinal direction of the timber floor modules have similar response to the single module if the connection between top flanges of the identical modules is fully composite.
- The fundamental frequency of the floors (6.0 x 1.8 m and 8.0 x 1.8 m) with pin support along four sides is significantly higher, i.e., about four times larger than the floors with pin-roller support at two opposite ends.
- The first natural frequency of the floors with 6.0 x 3.6 m and 8.0 x 3.6 m dimensions decreased by about 50% from the frequency of the floors with 6.0 x 1.8 m and 8.0 x 1.8 m dimensions, respectively when they were provided pin support along four sides.
- The first natural frequency of the square floors with 6 x 6 m and 8.0 x 7.8 m dimensions reduced by about 15 and 23% from the frequency of the floors with 6.0 x 3.6 m and 8.0 x 3.6 m dimensions, respectively.

- Design is conservative in terms of dynamic serviceability design criterion because simply supported boundary conditions are considered in the design, whereas in reality fixity of the floor supports fall in the range between pinned and fixed, resulting in higher fundamental frequency.
- FE model can replicate the experimental results and thus this tool can be used to predict natural frequency, especially fundamental frequency of the single module and floor to be used in the dynamic serviceability design.

University of Technology, Sydney

CHAPTER 9

CONCLUSIONS & RECOMMENDATIONS

9 Conclusions and Recommendations

9.1 Summary and Conclusions

In recent times, timber and TCC flooring systems are more popular, nevertheless they are susceptible to vibrations under human-activity and operation of machinery. Some limited prior studies have been conducted on the serviceability assessment for dynamic/vibration properties of long-span and light-weight flooring systems. Normally, flooring systems are designed against the static actions, but the dynamic actions are also of great importance as they have also been the cause of many structural failures. The main objectives of this research project have therefore been to (a) understand the floor vibration characteristics of these flooring systems under action of impact load induced using modal hammer and (b) assessment of composite action using dynamic properties.

The research information was used to provide an assessment of vibration response of these flooring systems and to evaluate their compliance with the serviceability and comfort criteria. Vibration characteristics, especially natural frequency was utilised to assess dynamic performance of these flooring systems. Furthermore, the reliability of the available empirical methods to predict natural frequency is checked.

The development of dynamic-based method to identify loss of composite action (LCA) of the composite flooring systems due to failure of shear connectors and deterioration due to passage of time is essential as static-based method is more expensive, time consuming and difficult to perform static test in an existing flooring system at different intervals of time. The performance of the composite flooring systems depends upon the degree of composite action of the systems and it is closely related to the type of connection system used at interface of the flooring systems to transfer shear force from one component to another. Hence, methodologies of two novel dynamic-based composite action identification schemes named $LCAI_1$ and $LCAI_2$ were developed. The core of both schemes is the use of Damage Index (DI) method. The proposed methods were tested on a numerical and experimental timber beam consisting of two LVL components with 3.5 m span.

This chapter summarises the research which has been reported in this dissertation followed by suggested future research needs.

9.1.1 Dynamic Performance of TCC Flooring Systems

A series of push-out tests were carried out to characterise the shear connectors used in the TCC beams and dynamic tests were conducted on the beams to assess their performance. In addition, the tested beams were also analysed numerically by developing their 2-D FE models using ANSYS.

- *For dynamic test:* Beam-3 with six bird-mouth notched connection had maximum fundamental frequency of 10 Hz and Beam-2 with normal wood screws had minimum fundamental frequency of 8.93 Hz. The damping ratio of Beam-3 was about 1.9% while the other three beams had about 1% for the fundamental mode. Hence, the connection type and its configuration for Beam-3 was superior.
- The fundamental frequency of the beams with notch connection was higher than the beams without any notches by about 1 Hz as expected. Furthermore, increase in the number of notches from four to six as Beam-4 had four notches while Beam-3 had six notches had minimal effect on the fundamental frequency of the beams, but had significant effect on the damping ratio. The fundamental frequency of Beam-3 was only 3% higher than Beam-4 frequency.
- *For FE models:* Correlation between FE and experimental results showed that the *NFerror* values are higher for higher modes due to uplifting at supports and their sensitivity to local defects. However, the error was below 10% for the first mode. Hence, the FE models can be used to predict their natural frequencies with sufficient accuracy.

Long-term Dynamic Test: The following conclusions can be drawn based on the results from three dynamic tests performed on the beams for long-term investigation:

- Moisture content variation of the LVL timber has significant effect on dynamic performance as natural frequency varies with variation in moisture content of LVL timber. The natural frequency increases with decrease in moisture content and vice versa.
- Creep effects in the beams also influence the dynamic performance as percentage of increment and decrement of natural frequency of corresponding beams was not identical for the same decrement and increment of moisture content in the LVL timber.

9.1.2 Dynamic Performance of Timber Floor Modules

Dynamic test was performed on the timber floor modules to assess their performance. Numerical investigation was also performed using 3-D FE models. Furthermore, parametric analysis was carried out on different size of floors using calibrated FE models of these modules. The following conclusions can be drawn based on all these investigations.

- *For test:* fundamental frequency of the 6 and 8 m span beams was 16.34 and 13.14 Hz, respectively and the corresponding damping ratio was 0.65 and 0.58%. Hence, the fundamental frequencies were above 10 Hz as recommended by most codes of practice. However, some supplementary analysis and/or testing of full flooring systems consisting of several interconnected modules is required to establish whether or not the floor system frequency remains satisfactory.
- No general trend was found between the natural frequencies and damping ratios. The damping ratio of the higher modes was lower compared to the fundamental mode.
- The results showed discrepancies within three 6 and 8 m span beams due to a number of factors such as material properties, shear connectors (screws and glue), minor discrepancies in the geometry, moisture content, bouncing at supports and minor discrepancies in the boundary condition. For higher modes, the bouncing at supports was observed to be higher.
- *For FE models:* Natural frequencies acquired match very well with the experimental results, especially for first mode as the *NFerror* values were below 2%. Hence, the FE models can be used to predict fundamental frequency, which is the main interest of the designer, of the beams with sufficient accuracy.
- The FE model over-predicted the natural frequency for higher modes by about 25% and it is unlikely due to only variation in material properties. This should be due to uplifting of the beams at supports during experimental work as FE models were analysed under pin-roller boundary conditions which prevented bouncing at supports. Further, higher modes are more sensitive to local defects within the timber material and at connections.

- *For parametric study:* Floor with pin-roller boundary conditions at two opposite ends of the floors in the longitudinal direction of the timber floor modules had similar fundamental frequency to the single module. Hence, the frequency of the floors will be similar to the beam if the connection between the identical beams is fully composite.
- The frequency of 6.0 x 3.6 m and 8.0 x 3.6 m floors was dropped by about 50% from the frequency of 6.0 x 1.8 m and 8.0 x 1.8 m floors, respectively when they were provided pin support along four sides.
- FE model can replicate the experimental results and thus this tool can be used to predict natural frequency of the beams and floors to be analysed for dynamic serviceability assessment.

9.1.3 Dynamic-based Composite Action Identification

A timber beam with 3.5 m span with different number of screws was tested to validate the two novel vibration-based composite action identification schemes, $LCAI_1$ and $LCAI_2$. Numerical analysis was also performed on the beam using 2-D FE model. The following conclusions can be drawn from the findings:

- The proposed dynamic-based method is capable of determining the composite action of a composite structure utilising only mode shape measurement obtained from dynamic testing.
- For both, numerical and experimental investigations, results of dynamic-based LCAs over-predicted the actual loss of composite action resulting in errors that are on the safe side, which is of great importance for design engineers.
- To correlate the dynamic-based composite action results to static-based values, the indices $LCAI_1$ and $LCAI_2$ are multiplied with the calibration factors λ_1 and λ_2. Due to laboratory and time constraints, static-based composite action results from deflection measurements were only obtained from numerical simulations. This resulted in differences in the calibration factors for the numerical and experimental investigations. In the FE model, nodes at the location of the screws were rigidly coupled to simulate the screw connections. Such rigid modelling of the shear connection might not represent the real experimental situation. To correctly simulate the shear connections, experimental push-out tests need to be

performed on small scale screw connector specimens to characterize the properties of the connector. Alternatively, four point bending testing is to be performed on the experimental composite beam structure. To identify a generic solution, more tests need to be performed to derive calibration factors for multiple types of composite flooring systems with different types of shear connectors.

- The accuracy of the composite action predictions greatly depends on the reliability of the mode shape measurements. For the experimental investigation, mode shapes of higher modes (modes 4 and 5) contained a high degree of error and thus resulted in erroneous composite action outcomes. Therefore, only reliable mode shapes should be considered in the calculation of the loss of composite action indices $LCAI_1$ and $LCAI_2$.

Limitations:

- For the investigated composite timber beam, the connection screws were equally spaced for all five composite stages. Hence, more testing are needed to apply this method to composite flooring systems with non-uniform spacing of the screws and different types of shear connectors.
- Dynamic-based method can not distinguish the damage of materials such as timber and concrete of the flooring system and shear connectors. Hence, this method gives the loss of composite action due to failure of shear connectors along with material damage if any.
- At least two dynamic tests are needed to identify loss of composite action of the system. This gives relative LCA of succeeding test from initial test and thus initial test acts as baseline.
- The determined calibration factors are unique for a specific test set up and type of beam. The factors are a function of degree of composite, i.e. it is not a linear relationship. This is a relatively novel idea and therefore, further investigations are needed to develop general solutions for calibration factors so that this method would have potential for general implementation.

9.1.4 Natural Frequency Prediction using Analytical Models

Five analytical models were utilised to predict fundamental frequency of the tested TCC beams and timber floor modules (beams). In addition, parametric study was performed on these beams to generate span tables using one of these analytical models, namely Wyatt (1989). These tables can be used to identify span of the beams for different cross-sectional dimensions, which satisfy the fundamental frequency requirement of 8 Hz.

- *For TCC beams:* Fundamental frequency of Beams- 1 and 2 with SFS and normal wood screws connection, respectively, was predicted accurately within 8% of over-prediction by all these models except Allen (1990), which significantly over-predicted the frequency by about 23%. While for Beams- 3 and 4 with six and four bird-mouth notched connection, respectively, the frequency was under-predicted by 15% of test results from the models except Allen (1990) where under-prediction was just 2%.
- A sensitivity analysis on material properties showed that predicted values were sensitive to MOE of LVL joist and concrete density. Stiffness of connections from push-out tests should be found accurately in order to develop confidence in the use of the simplified analytical models and thus more tests need to be carried out.
- *For timber floor modules:* The correlation showed that the frequency can be predicted using these models with satisfactory values as the predicted values were fairly accurate as values were within ±5% of the test results.
- Two models presented by Wyatt (1989) can be used to estimate the fundamental frequencies of all these beams accurately. Other methods also give the same order of accuracy if the inputs provided are accurate. Tested TCC beams had higher number of variables compared to timber beams as these beams had two different materials connected using different connection systems without any glue resulting in partially composite sections. Hence, the predicted values for TCC beams were less accurate compared to the timber beams.

9.2 Recommendations and Future Works

Further work and some refinements are required to make findings of this research work more practical. Hence, the purpose of this section is to focus on the issues that should be addressed by future researchers to make use of these methods as a viable and practical tool for composite action identification in the composite flooring systems, especially TCC. In the past research very limited investigation can be found to establish problematic natural frequency range and thus further investigation is suggested in this regards. Recommendations and future works are listed as:

- For composite action investigation of a 3.5 m span timber beam, static results were acquired from FE models. Usually FE models under-predict the deflection as the models are stiffer than the beam to be tested and thus loss of composite action of the beam can be under-predicted. Hence, static four point bending test on the beam need to be performed to establish the reliability of static results.
- The screws in the tested beam were equally spaced for all five stages of testing. Therefore, more tests are needed to apply this method on the composite flooring systems with non-uniform spacing of the screws and different type of shear connectors. In addition, further investigations are needed to develop general solutions for calibration factors so that dynamic-based loss of composite action estimation method would have potential for implementation.
- From automobile and aircraft study it was concluded that humans are sensitive to vibrations in the 5 to 8 Hz natural frequency range. Murray (1991) investigated more than 100 problematic floors and the frequency of most of these floors was found in the range of 5 to 8 Hz. However, further investigation is needed whether this is problematic or not for the flooring systems.

University of Technology, Sydney

REFERENCES

References

ABD. Ghafar, N.H. 2008, 'Forced vibration testing on LVL-concrete composite floor systems', *7th Fib PhD Symposium in Stuttgart*, Germany, pp. 1-6.

ABD. Ghafar, N.H., Deam, B., Fragiacomo, M. & Buchanan, A. 2008, 'Susceptibility to vibrations of LVL-concrete composite floors', pp. 1-9.

Abdul Rahman, A.G. 1999, *Notes of signal processing*, Mechanical Engineering Department, Faculty of Engineering, University of Malaya.

Agilent Technologies 2000, *The fundamental of modal testing*, Agilent Technologies, Application Note 243-3.

Ahmadi, B.H. & Saka, M.P. 1993, 'Behavior of composite timber-concrete floors', *Journal of Structural Engineering*, vol. 119, no. 10, pp. 3111-3130.

Allemang, R.J. 1999, *Experimental modal analysis*, Report Number UC-SDRL-RJA, University of Cincinnati, Cincinnati, OH, US.

Allen, D.E. 1990, 'Building vibrations from human activities', *American Concrete Institute, Concrete International: Design and Construction*, vol. 12, no. 6, pp. 66-73.

Allen, D.E. & Murray, T.M. 1993, 'Vibration of composite floors', *Structural Engineering in Natural Hazards Mitigation*, American Society of Civil Engineers, California.

Allen, D.E. & Pernica, G. 1998, 'Control of floor vibration', *Construction Technology*, no. 22.

Al-Sanad, H., Aggour, M.S., & Yang, J.C.S. 1983, 'Dynamic shear modulus and damping ratio from random loading tests', *Geotechnical Testing Journal*, GTJODJ, vol. 6, no. 3, pp. 120-127.

ANSYS Inc 2011, ANSYS, release 12.1.

AS 1012.9 1999, Methods of testing concrete, Determination of the compressive strength of concrete specimens, *Australian Standard*, Sydney, Australia.

AS 1012.17 1997, Methods of testing concrete, Determination of the static chord modulus of elasticity and Poisson's ratio of concrete specimens, *Australian Standard*, Sydney, Australia.

AS 1720.1 2010, Timber Structures, Part 1: Design Methods, *Australian Standard*, Sydney, Australia.

AS 3600 2001, Concrete Structures, *Australian Standard*, Sydney, Australia.

AS/NZS 1080.1 1997, Timber - Methods of test, Moisture content, *Australian/New Zealand Standard*.

AS/NZS 4357.2 2006, Structural Laminated Veneer Lumber (LVL), Part2: Determination of structural properties - Test methods, *Australian/New Zealand Standard*, Incorporating Amendment No. 1.

Bachmann, H. & Ammann, W. 1987, 'Vibrations in structures induced by man and mechanics', *IABSE – AIPC – IVBH*, Switzerland.

Barroso, L.R. & Rodriguez, R. 2004, 'Damage detection utilizing the damage index method to a benchmark structure', *Journal of Engineering Mechanics*, vol. 130, no. 2, pp. 142-151.

Bathon, L. 2000, viewed 8 December 2009, http://www.hbv-systeme.de/HBV-Systeme/Geschichte_e.htm.

Bathon, L.A. & Clouston, P. 2004, 'Experimental and numerical results on semi prestressed wood-concrete composite floor systems for long span applications', pp. 1-6.

Bernard, S. 2004, 'Vibration of composite timber and concrete flooring', Prepared for the Forest and Wood Products Research and Development Corporation, Project No: PN03.1211, 3.

Blakeborough, A. & Williams, M.S. 2003, 'Measurement of floor vibrations using a heel drop test', *Structures and Buildings*, vol. 156, pp. 367-371.

Boice, M.D. 2003, 'Study to improve the predicted response of floor systems due to walking', *Civil Engineering*, Polytechnic Institute and State University, Virginia.

Brincker, R., Krenk, S. & Jensen, J.L. 1991, 'Estimation of correlation functions by the random decrement technique', *Proceedings of the Florence Modal Analysis Conference*, Held under the Auspices of the Consiglio Nationale Delle Ricerche Florence, pp. 783-788.

Brownjohn, J.M.W. 2001, 'Energy dissipation from vibrating floor slabs due to human-structure interaction', *Shock and Vibration*, vol. 8, pp. 315-323.

Brownjohn, J.M.W. & Xia, P. 1999, 'Finite element model updating of a damaged structure', *Proceedings of the 17th International Modal Analysis Conference*, Society for Experimental Mechanics, Inc., Hyatt Orlando Hotel, Kissimmee, Florida, US, pp. 457-462.

Brunner, M., Romer, M. & Schnuriger, M. 2006, 'Timber-concrete composite with an adhesive connector (wet on wet process)', vol. 40, pp. 119-126.

BSI 1991, *Timber Structures, Joints made with mechanical fasteners, General principles for the determination of strength and deformation characteristics*, BS EN 6891:1991, BSI British Standards, London, UK.

CADA-X 1996, *Modal analysis manual*, LMS International, Belgium.

Cantwell, W.J. & Morton, J. 1991, 'The impact resistance of composite materials - A review', *Composites*, vol. 22, no. 5, pp. 347–362.

Carden, P.E. & Fanning, P. 2004, 'Vibration based condition monitoring: a review', *Structural Health Monitoring*, vol. 3, no. 4, pp. 355-377.

Ceccotti, A. 2002, 'Composite concrete-timber structures', *Prog. Struct. Engng Mater*, vol. 4, pp. 264-275.

Chien, E.Y.L. & J. Richie, K. 1984, 'Design and construction of composite floor systems', *Canadian Institute of Steel Construction*, Toronto.

Choi, F.C. 2007, 'Assessment of the structural integrity of bridges using dynamic approaches', PhD thesis, University of Technology Sydney (UTS), NSW, Australia.

Choi, F.C., Li, J., Samali, B. & Crews, K. 2007, 'An experimental study on damage detection of structures using a timber beam', *Journal of Mechanical Science and Technology - MOVIC Special Edition*, vol. 21, pp. 903-907.

Chopra, A.K. 2005, *Dynamics of structures - Theory and applications to earthquake engineering*, 2nd edn, Pearson Education.

Clough, R.W. & Penzien, J. 1993, *Dynamics of structures*, McGraw-Hill.

Cornwell, P., Doebling, S.W. & Farrar, C.R. 1999, 'Application on the strain energy damage detection method to plate-like structures', *Journal of Sound and Vibration*, vol. 224, no. 2, pp. 359-374.

Da Silva, J.G.S., da S. Vellasco, P.C.G., de Andrade, S.A.L., da Soeiro, F.J.C.P. & Werneck, R.N. 2003, 'An evaluation of the dynamical performance of composite slabs', *Computers and Structures*, vol. 81, no. 18-19, pp. 1905-1913.

Dackermann, U. 2010, 'Vibration-based damage identification methods for civil engineering structures using artificial neural networks', PhD Thesis, University of Technology Sydney (UTS), NSW, Australia.

Dallard, P., Fitzpatrick, A.J., Flint, A., Le Bourva, S., Low, A., Ridsdill, S.R.M. & Willford, M. 2001a, 'The Millennium Bridge, London: problems and solutions', *The Structural Engineer*, vol. 79, no. 8, pp. 15-17.

Dallard, P., Fitzpatrick, A.J., Flint, A., Le Bourva, S., Low, A., Ridsdill, S.R.M. & Willford, M. 2001b, 'The London Millennium footbridge', *The Structural Engineer*, vol. 79, no. 22, pp. 17-33.

Davison, J.B. 2003, 'Composite floors', *Composite Construction*, D. A. Nethercot, London, Spon Press.

De Silva, C.W. 2007a, 'Vibration damping, Control and design', *Taylor & Francis*, Boca Raton.

De Silva, S.S. 2007b, 'Vibration characteristics of steel-deck composite floor systems under human excitation', PhD thesis, Queensland University of Technology, Australia.

Dias, A.M.P.G. 2005, 'Mechanical behaviour of timber-concrete joints', *Technical University Delft*.

Doebling, S.W., Farrar, C.R., Prime, M.B. & Shevitz, D.W. 1996, *Damage identification and health monitoring of structural and mechanical systems from changes in their vibration characteristics: A literature review*, Report Number Report LA-13070-MS, Los Alamos National Laboratory, New Mexico.

Dolan, J.D., Murray, T.M., Johnson, H., Runte, D. & Shue, B.C. 1999, 'Preventing annoying wood floor vibrations', *J. Struct Eng*., ASCE, vol. 15, no. 1, pp. 19-24.

Ebrahimpour, A. & Sack, R.L. 2005, 'A review of vibration serviceability criteria for floor structures', *Computers and Structures*, vol. 83, pp. 2488-2494.

Elnimeiri, M. & Iyengar, H. 1989, 'Composite floor vibrations: Predicted and measured', *Steel Structures*, San Francisco, CA, USA, American Society of Civil Engineers.

Eurocode 5 2008, *Design of Timber Structures, Serviceability Limit States*.

Farrar, C.R. & Juaragui, D. 1996, Damage detection algorithms applied to experimental and numerical modal data from the I-40 Bridge, Los Alamos National Laboratory, Los Alamos, New Mexico, US.

Fragiacomo, M., Amadio, C., ASCE, M. & Macorini, L. 2004, 'Finite-element model for collapse and long-term analysis of steel-concrete composite beams', *Journal of Structural Engineering*, ASCE, vol. 130, no. 3, pp. 489-497.

General Technical Report FPL-GTR-113 1999, *Wood handbook – wood as an engineering material*, Forest Products Laboratory, United States Department of Agriculture, Madison MI US.

Gerber, C. & Crews, K. 2011 'Development of design procedures for timber-concrete composite floors in Australia and New Zealand', *New Zealand Timber Design Journal*, vol. 9, no. 2, pp. 6-15.

Gerber, C., Crews, K. & Sigrist, C. 2005, 'Investigation of the ultimate behaviours and FEA of wood stressed-skin panels', *Third international structural engineering and construction conference*, Shunan, Japan.

Gutkowski, R., Brown, K., Shigidi, A. & Natterer, J. 2007, 'Laboratory tests of composite wood-concrete beams', *Construction and Building Materials*, vol. 22, pp. 1059-1066.

Gutkowski, R., Miller, N., Fragiacomo, M., and Balogh, J. 2011. 'Composite wood-concrete beams using utility poles: Time-dependent behavior', *Journal of Structural Engineering*, vol. 137, no. 6, pp. 625-634.

Hailu, M., Gerber, C., Shrestha, R. & Crews, K. 2012, 'Interim report on long-term test on timber-concrete composite beams', *World Conference on Timber Engineering*, WCTE 2012, Auckland, New Zealand.

Hanes, R.M. 1970, 'Human sensitivity to whole-body vibration in urban transportation systems: A literature review', *Applied Physics Laboratory*, the John Hopkins University, Silver Springs, MD.

Haritos, N. 1993, 'The equivalent area method for estimating damping levels', *13th Australasian Conference on Mechanics of Structures and Materials (ACMSM13)*, Wollongong, Australia, pp. 341-348.

Hicks, S. 2004, 'Vibration characteristics of steel-concrete composite floor systems', *Prog. Struct. Engineering Materials*, vol. 4, pp. 21-38.

Howard, C.Q. 2005, 'An inexpensive DIY impact hammer for vibration analysis of buildings', *Acoustics Australia*, vol. 33, pp. 1-24.

Hu, L.J., Chui, Y.H. & Onysko, D.M. 2001, 'Vibration serviceability of timber floors in residential construction', *Progress in Structural Engineering and Materials*, vol. 3, no. 3, pp. 228-237.

Hu. S.J., Wang, S. & Li, H. 2006, 'Cross-modal strain energy method for estimating damage severity', *Journal of Engineering Mechanics*, vol. 132, no. 4, pp. 429-437.

Hunadidi, O. 2000, 'Traffic vibrations in buildings', *Institute for Research in Construction,* Construction Technology Update no. 39.

Hveem, S. 1990, 'Vibration of lightweight floors', Building Research and Practice, *Journal of CIB*, no. 1.

ISO 2631-2 1989, 'Evaluation of human exposure to whole-body vibration, Part 2: Continuous and shock-induced vibration in buildings', *International Organization for Standardization*, Switzerland.

John, S., Nebel, B., Perez, N. & Buchanan, A. 2008, *Environmental impacts of multi-storey buildings using different construction materials*, Research Report.

Kalpakjian, S. & Schmid, S.R. 2001, *Manufacturing engineering and technology*, 4th edn, Prentice Hall.

Kim, J.T., & Stubbs, N. 1995, 'Model-uncertainty and damage-detection accuracy in plate girder', *Journal of Structural Engineering*, vol. 121, no. 10, pp. 1409-1417.

Kim, J.T. & Stubbs, N. 2002, 'Improved damage identification method based on modal information', *Journal of Sound and Vibration*, vol. 252, no. 2, pp. 223-238.

Kolb, J. 2008, *Systems in timber engineering*, 2nd edn, Switzerland.

Kuhlmann, U. & Schänzlin, J. 2007, 'A timber-concrete composite slab system for use in tall buildings', *Structural Engineering International*, pp. 174-178.

Kullaa, J. & Talja, A. 1999, 'Vibration performance test for light-weight steel-joist floors', *Fourth international conference on steel and aluminium structures*: *Light-weight steel and aluminium structures*, Espoo, Finland, Elsevier science Ltd.

Küng, R. 1987, 'Composite floor timber-lightweight concrete', TU Graz, Austria.

LabVIEW 2009, Software package.

Lam, F. 2009, 'Timber products and manufacturing processes', *ICE Manual of Construction Materials – Institution of Civil Engineers*.

Lee, J.J. & Yun, C.B. 2006, 'Damage diagnosis of steel girder bridges using ambient vibration data', *Engineering Structures*, vol. 28, no. 6, pp. 912-925.

Li, H., Yang, H. & Hu, S.L.J. 2006, 'Modal strain energy decomposition method for damage localization in 3D frame structures', *Journal of Engineering Mechanics*, vol. 132, no. 9, pp. 941-951.

Linden, M.V.D. 1999, 'Timber-concrete composite beams', *HERON*, vol. 44, no. 3, pp. 25.

Lukaszewska, E., Johnsson, H. & Fragiacomo, M. 2008, 'Performance of connections for prefabricated timber-concrete composite floors', *Materials and Structures*, vol. 41, pp. 1533-1550.

Mahrenholtz, O. & H. Bachmann 1995, Appendix C: Damping, Vibration problems in structures: *Practical guidelines*. Berlin, Germany.

Maia, N.M.M., Silva, J.M.M., He, J., Lieven, N.A.J., Lin, R.M., Skingle, G.W., To, W.M. & Urgueira, A.P.V. 1997, *Theoretical and experimental modal analysis*, Research Studies Press, Baldock, Hertfordshire, England.

Maurenbrecher, P.M. 1997, 'Induced vibrations from buildings: from people to earthquakes', Delft, Delft University of Technology, Faculty of Applied Earth Sciences: 1-1.

Murray, T.M. 1981, 'Acceptability criterion for occupant-induced floor vibrations', *Engineering Journal*, American Institute of Steel Construction Inc., vol. 18, no. 2.

Murray, T.M. 1990, 'Floor vibration in buildings-design method', *Australian Institute of Steel Construction*.

Murray, T.M. 1991, Building floor vibrations, *T.R. Higgins lectureship paper presented at the AISC National Steel Construction Conference*, Washington, D.C.

Murray, T.M., Allen, D.E. & Ungar, E.E. 2003, *Steel Design Guide Series 11: Floor vibrations due to human activity*, American Institute of Steel Construction (AISC), Chicago, USA.

Naeim, F. 1991, 'Design practice to prevent floor vibrations', *Steel Tips*, S.S.E. Council.

NBC 1990, *Serviceability criteria for deflections and vibration, Chapter 4: Commentaries on Part 4, Commentary A*, National Building Code of Canada, National Research Council of Canada, Ottawa.

Nor Hayati, A.G., Deam, B. & Fragiacomo, M. 2009, 'Dynamic measurements of LVL-concrete composite floors', *13th Asia Pacific Vibration Conference*, University of Canterbury, New Zealand, pp. 1-8.

Ollgard, J.G., Slutter, R.G., & Fischer, J.W. 1971, 'Shear strength of stud connectors in lightweight and normal concrete', *AISC Eng. J.*, vol. 8, pp. 55-64.

Olmos, B.A. & Roesset, J.M. 2010, 'Evaluation of the half-power bandwidth method to estimate damping in systems without real modes', *Earthquake Engineering and Structural Dynamics*, vol. 39, no. 14, pp. 1671-1686.

Osborne, K.P. & Ellis, B.R. 1990, 'Vibration design and testing of a long-span lightweight floor', *The Structural Engineer*, vol. 68, no. 15, pp. 181-186.

Papagiannopoulos, G.A. & Hatzigeorgiou, G.D. 2011, 'On the use of the half-power bandwidth method to estimate damping in building structures', *Soil Dynamics and Earthquake Engineering*, vol. 31, no. 7, pp. 1075-1079.

Park, S. & Stubbs, N. 1995, 'Reconstruction of mode shapes using Shannon's Sampling Theorem and its application to the non-destructive damage localization algorithm', *Proceedings of Smart Structures and Materials: Smart Systems for Bridges, Structures, and Highways*, vol. 2446, Society of Photo-Optical Instrumentation Engineers, San Diego, CA, US, pp. 280-292.

Pault, J. (1977). 'Composite action in Glulam timber bridge systems', M.S. thesis, Colorado State Univ., Fort Collins, CO.

Pereyra, L.R., Osegueda, R.A., Carrasco, C.J. & Ferregut, C.M. 1999, 'Damage detection in a stiffened plate using modal strain energy differences', *Proceedings of the Non-destructive Evaluation of Aging Aircraft, Airports, and Aerospace Hardware III*, vol. 3586, Society of Photo-Optical Instrumentation Engineers, Newport Beach, CA, US, pp. 211-222.

Planinc, I., Schnabl, S., Saje, M., Lopatic, J. & Cas, B. 2008, 'Numerical and experimental analysis of timber composite beams with interlayer slip', *Engineering Structures*, vol. 30, pp. 11.

Ramsey, K.A. 1982, 'Experimental modal analysis, structural modifications and FEM analysis on a desktop computer', *Proceedings of the 1st International Modal Analysis Conference*, Society for Experimental Mechanics, Orlando, FL, US.

Ratcliffe, C.P. 1998, Correcting a significant and consistent error in the modal damping obtained using transient vibration data.

Reiher, H. & Meister, F.J. 1931 'The effect of vibration on people', Translated from *Forsch. Geb.Ing*. Wes: vol. 2, no. 11, pp. 381-386, by U. S. Air Material Command. Translation F-TS- 616-RE.Wright Field, Ohio, AMC, 1946.

Rijal, R., Samali, B. & Crews, K. 2010, 'Dynamic performance of the timber-concrete composite flooring systems', *Australasian Conference on the Mechanics of Structures and Materials (ACMSM) 21*, Melbourne, Australia.

Rodrigues, J. & Brincker, R. 2005, 'Application of random decrement technique in operational modal analysis', *Proceedings of the 1st International Operational Modal Analysis Conference (IOMAC)*, Copenhagen, Denmark.

Ronca, P., Gelfi, P. & Giuriani, E. 1991, 'The behaviour of a wood-concrete composite beam under cyclic and long term loads', *International Conference STREMA*, Seville, vol. 2, pp. 263-275.

Saidi, I., Haritos, N., F Gad, E. & Wilson, J.L. 2006, 'Floor vibrations due to human excitation - Damping perspective', *Earthquake Engineering in Australia*, pp. 257-264.

Sánchez, J.C.H. 2005, 'Evaluation of structural damage identification methods based on dynamic chracteristics', PhD thesis, University of Puerto Rico, Mayagüez.

Schwarz, B.J. & Richardson, M.H. 1999, 'Experimental modal analysis', *CSI Reliability Week*, Orlando, FL, USA, p. 12.

Shi, Z.Y., Law, S.S. & Zhang, L.M. 1998, 'Structural damage localization from strain energy change', *Journal of Sound and Vibration*, vol. 218, no. 5, pp. 825-844.

Shi, Z.Y., Law, S.S. & Zhang, L.M. 2000, 'Damage localization by directly using incomplete mode shapes', *Journal of Engineering Mechanics*, vol. 126, no. 6, pp. 656-660.

Shi, Z.Y., Law, S.S. & Zhang, L.M. 2002, 'Improved damage quantification from elemental modal strain energy change', *Journal of Engineering Mechanics*, vol. 128, no. 5, pp. 521-529.

Smith, I. & Chui, Y.H. 1988, 'Design of lightweight wooden floors to avoid human discomfort.', *Can J Civ Eng*., vol. 15, pp. 254-262.

Soltis, L.A., Wang, X., Ross, R.J. & Hunt, M.O. 2002, 'Vibration testing of timber floor systems', *Forest Products Journal*, vol. 52, pp. 75-81.

Steinberg, E., Selle, R. & Faust, T. 2003, 'Connectors for timber-lightweight concrete composite structures', *Journal of Structural Engineering*, vol. 129, no. 11, pp. 1538-1545.

STIC Ltd 2009, *Structural Timber Innovation Company (STIC)*, viewed 19 April 2011, <http://www.stic.co.nz/company>.

Structural Dynamic Research Laboratory 1999, *Experimental modal analysis*, Report Number UC-SDRL-RJA, University of Cincinnati, Cincinnati, Ohio, US.

Stubbs, N., Kim, J.T. & Topole, K. 1992, 'An efficient and robust algorithm for damage localization in offshore platforms', *Proceedings of the 10th Structures Congress*, ASCE, Antonio, LA, USA, pp. 543-546.

Stubbs, N. & Park, S. 1996, 'Optimal sensor placement for mode shapes via Shannon's Sampling Theorem', *Microcomputers in Civil Engineering*, vol. 11, no. 6, pp. 411-419.

The MathWorks, I. 2007, *Matlab 2007b*.

Uchiyama, Y., Mukai, M. & Fujita, M. 2009, 'Robust control of electrodynamic shaker with 2DOF control using H∞ filter', *Journal of Sound and Vibration*, vol. 326, pp. 75-87.

Vu Lam, P. 2010, *Final report: Testing analyses and discussion for TCC beams*, Report 2, In partial fulfilment of STIC, Faculty of Engineering and IT, University of Technology, Sydney.

Wang, T.L., & Zong, Z. 2002, *Improvement of evaluation method for existing highway bridges*, Research Report No. FL/DOT/RMC/6672-818, Florida International University, Tallahassee, FL, US.

Williams, M.S. & Waldron, P. 1994, 'Evaluation of methods for predicting occupant-induced vibrations in concrete floors', *The Structural Engineer*, vol. 72, no. 20, pp. 334-340.

Worden, K., Manson, G. & Allman, D. 2001, 'An experimental appraisal of the strain energy damage location method', *Proceedings of the International Conference on Damage Assessment of Structures*, Cardiff, UK, pp. 35-46.

Wyatt, T.A. 1989, 'Design guide on the vibration of floors', *SCI Publication 076: Steel construction Institute*, Construction Industry Research and Information Association, UK.

Zabihi, Z., Samali, B., Shrestha, R, Gerber, C. & Crews, K. 1012, 'Serviceability and ultimate performance of long span timber floor modules', *12th WCTE Conference*, Auckland, New Zealand.

University of Technology, Sydney

APPENDICES

Appendices

Appendix A (Chapter 3)

Table A.1 Test data for compressive strength of concrete used in NS and SFS series

	Specimen 1	Specimen 2	Specimen 3
Minimum diameter (mm)	99.4	99	99.5
Maximum diameter (mm)	99.8	99.9	100.1
Mean diameter (mm)	99.6	99.45	99.8
Height (mm)	204	204	203
Peak load (kN)	231.7	287.3	283.7
Area (mm^2)	7791	7767	7822
f'c (MPa)	29.7	36.9	36.3
W (gram)	3728.2	3739.8	3730.4
Mean *f'c* (MPa)	36.6*		
Density (kg/m^3)	2346	2360	2349
Mean density (kg/m^3)	2351.6		
*Notes: * – based on last two specimens only*			

Table A.2a Test data for MOE of concrete used in NS and SFS series

Specimen No			**1**	
e_g (mm)			95	
e_r (mm)			92.5	
Compressometer factor ($e_r/(e_r+e_g)$)			0.4933	
Cross section (mm^2)			18247	
	Load	Stress	Gauge	Strain
	(kN)	(MPa)	x0.001 mm	(mm)
1	30.1	1.6495	15	5E-05
2	265	14.523	180	0.0006
MOE (MPa)				23722
	Load	Stress	Gauge	Strain
	(kN)	(MPa)	x0.001 mm	(mm)
	28	1.5345	15	5E-05
	265	14.523	180	0.0006
MOE (MPa)				23934

Table A.2b Test data for MOE of concrete used in NS and SFS series

Specimen No			**2**	
e_g (mm)			92	
e_r (mm)			95	
Compressometer factor ($e_r/(e_r+e_g)$)			0.5080	
Cross section (mm^2)			18240	
	Load	Stress	Gauge	Strain
	kN	MPa	x0.001 mm	mm
1	38	2.0833	15	5E-05
2	265	14.528	162	0.0005
MOE (MPa)				24997
	Load	Stress	Gauge	Strain
	kN	MPa	x0.001 mm	mm
	36	1.9737	15	5E-05
	265	14.528	162	0.0005
MOE				25217
Specimen No			**3**	
e_g (mm)			98	
e_r (mm)			94	
Compressometer factor ($e_r/(e_r+e_g)$)			0.4896	
Cross section (mm^2)		18224		
	Load	Stress	Gauge	Strain
	(kN)	(MPa)	x0.001 mm	(mm)
1	30	1.6462	15	5E-05
2	265	14.542	175	0.0006
MOE (MPa)				24693
	Load	Stress	Gauge	Strain
	(kN)	(MPa)	x0.001 mm	(mm)
	27	1.4816	15	5E-05
	265	14.542	175	0.0006
MOE (MPa)				25009

Table A.3 Summary of push-out test results for NS and SFS Series

Specimen	Load	Serviceability stiffness	Ultimate stiffness	Remarks
	Peak load	Centre	Centre	
	PL (kN)	k_{sls} (kN/mm)	k_C (kN/mm)	
SFS1	32.1	41.8	28.1	
SFS2	32.3	50.1	33.5	
SFS3	33.1	62.2	36.0	
SFS4	34.5	49.6	32.7	
SFS5	32.7	54.6	31.2	
SFS6	33.7	79.3	40.1	
SFS7	31.9	70.1	43.5	
SFS8	31.3	66.8	32.7	
SFS9	30.8	47.6	29.7	screw did not break
SFS10	33.5			Centre LVDT malfunctioned
NS1	9.4	55.4	4.9	
NS2	11.3	72.4	4.8	
NS3	10.3	33.9	5.7	
NS4	11.0	92.9	87.8	
NS5	10.7	34.2	8.4	
NS6	12.3	100.5	93.2	
NS7	12.0	48.0	11.9	
NS8	19.1	108.6	107.2	
NS9	10.5	338.9	292.1	
NS10	10.9	91.7	4.3	
4NS50-1	42.7	37.6	6.2	
4NS50-2	30.5	31.3	15.3	
4NS50-3	42.4	46.5	6.8	
4NS100-1	33.1	71.5	14.2	
4NS100-2	42.6	84.6	4.3	
4NS100-3	43.0	32.2	7.6	
4NS150-1	43.6	41.4	9.1	
4NS150-2	39.9	53.7	6.8	One screw did not break and remained in the concrete
4NS150-3	43.1	33.9	5.5	

Table A.4 Summary of push-out test results for bird-mouth notched connection series

Specimen	Peak load	Stiffness	
	PL (kN)	K_{serv} (kN/mm)	K_{ult} (kN/mm)
B2-1	54.9	136.7	33.1
B2-2	55.3	82.1	67.7
B2-3	62.7	91.2	25.8
B2-4	59.1	35.2	25.3
B2-5	63.6	122.4	33.2
B2-6	52.9	88.4	79.7
B2-7	58.5	179.3	31.8
B2-8	67.3	99.1	32.7
B2-9	57.4	156.8	30.4
B2-10	66.6	130.9	103.8
B3-1	83.3	99.1	44.3
B3-2	69.8	97.1	98.1
B3-3	79.0	123.9	53.7
B3-4	81.2	87.2	54.0
B3-5	78.6	89.3	73.6
B3-6	78.6	110.1	81.3
B3-7	70.4	79.2	64.1
B3-8	88.5	106.7	94.3
B3-9	73.0	99.6	88.6
B3-10	73.0	91.6	83.1
B4-1	90.3	112.1	115.3
B4-2	104.3	124.7	104.8
B4-3	105.8	138.0	114.8
B4-4	108.3	204.6	172.3
B4-5	104.2	158.9	125.2
B4-6	103.1	180.2	119.2
B4-7	96.3	124.4	99.6
B4-8	104.2	179.4	134.9
B4-9	97.1	171.5	77.9
B4-10	104.4	164.0	120.3
B5-1	129.3	135.6	91.6
B5-2	137.2	223.2	162.4
B5-3	147.1	207.9	183.4
B5-4	158.3	161.4	121.3
B5-5	187.6	203.1	166.0
B5-6	166.3	162.8	135.2
B5-7	129.3	471.5	178.2
B5-8	157.4	202.4	149.8
B5-9	152.4	187.9	184.2
B5-10	157.9	184.6	126.9

Table A.5 Summary of push-out test results for trapezoidal notched connection series

Specimen	Peak load	Stiffness	
	PL (kN)	K_{ser} (kN/mm)	K_{ult} (kN/mm)
T1-1	50.6	76.8	59.4
T1-2	56.8	71.8	58.7
T1-3	61.7	85.3	51.7
T1-4	52.7	113.7	70.8
T2-1	54.2	121.5	89.3
T2-2	57.0	89.2	74.8
T2-3	53.0	102.2	95.4
T2-4	50.5	118.0	100.4
T2-5	47.5	122.4	106.6
T2-6	50.9	82.5	62.4
T2-7	56.7	91.8	72.2
T2-8	57.5	106.5	80.6
T2-9	48.8	119.2	96.2
T2-10	52.9	362.8	167.1
T3-1	92.7	113.7	61.3
T3-2	97.5	104.5	97.9
T3-3	91.2	104.4	77.3
T3-4	82.1	70.4	68.8
T3-5	82.2	96.0	89.7
T3-6	92.4	110.2	102.2
T3-7	83.6	128.1	64.5
T3-8	86.3	123.7	54.6
T3-9	93.4	140.5	114.7
T3-10	82.3	97.6	73.2
T4-1	104.6	111.3	106.7
T4-2	91.0	118.5	79.3
T4-3	124.7	126.1	102.6
T4-4	108.9	109.8	102.3
T4-5	124.4	68.5	24.2
T4-6	99.4	53.1	38.7
T4-7	104.9	160.9	141.5
T4-8	118.9	103.2	81.5
T4-9		LVDT reading corrupt	
T4-10	103.8	126.2	81.1
T5-1	142.8	93.1	121.6
T5-2	139.0	89.1	94.1
T5-3	144.6	68.4	73.6
T5-4	142.6	78.3	59.5
T5-5	145.6	196.1	129.5
T5-6	144.8	145.6	97.5
T5-7	141.8	120.0	102.4
T5-8	159.2	212.8	155.7
T5-9	158.8	101.9	83.7
T5-10	153.4	386.3	215.4

Table A.6 Cylinder compression test data of concrete of TCC beams

Test		Dimensions (mm)		Weight (g)		Load	Compressive strength
		Diameter	Height	After 24 hrs	At testing time	kN	(MPa)
Group 1, 7 days	A	100.1	202.0	3792.0	3860.0	188.0	23.9
	B	100.2	202.0	3778.0	3837.0	187.5	23.8
	C	100.3	202.0	3796.0	3854.0	184.5	23.4
Group 2, 28 days	A	100.5	200.0	3762.0	3808.0	316.5	39.9
	B	100.2	201.0	3774.0	3821.0	299.5	38.0
	C	99.9	199.0	3720.0	3763.0	319.0	40.7
Group 3, 56 days	A	100.0	201.0	3769.0	3824.0	347.5	44.3
	B	100.2	201.0	3780.0	3839.0	339.0	43.0
	C	100.1	200.0	3768.0	3812.0	359.5	45.7
Group 4, 91 days	A	100.1	201.0	3782.0	3832.0	387.5	49.3
	B	99.8	201.0	3720.0	3783.0	387.0	49.5
	C	101.5	203.0	3968.0	4027.0	422.5	52.2

Table A.7 Summary of natural frequencies and damping ratios of TCC beams

Beam	Natural frequencies (Hz)			Damping ratios (%)		
	Mode 1	Mode 2	Mode 3	Mode 1	Mode 2	Mode 3
Beam-1	9.00	31.61	57.93	0.90	0.39	1.73
	8.97	31.70	57.86	1.01	0.49	1.55
	9.03	31.57	57.86	1.10	0.55	1.61
Mean	9.00	31.63	57.88	1.00	0.48	1.63
CoV (%)	0.27	0.17	0.06	8.15	13.85	4.59
Beam-2	8.95	30.39	52.82	0.99	0.85	2.33
	8.91	30.05	52.76	0.99	0.77	2.52
	8.93	30.25	53.12	1.04	0.73	2.26
Mean	8.93	30.23	52.90	1.01	0.78	2.37
CoV (%)	0.18	0.46	0.30	2.34	6.37	4.63
Beam-3	10.06	27.77	52.40	1.90	3.55	3.41
	10.10	28.17	52.91	1.85	3.35	2.95
	10.08	28.11	52.79	1.82	3.05	3.13
Mean	10.08	28.02	52.70	1.86	3.32	3.16
CoV (%)	0.16	0.63	0.41	1.78	6.20	5.98
Beam-4	9.77	29.65	52.51	1.00	2.05	1.93
	9.76	29.69	52.13	1.00	2.25	2.20
	9.76	29.78	52.39	0.91	2.02	1.73
Mean	9.76	29.71	52.34	0.97	2.11	1.95
CoV (%)	0.05	0.18	0.30	4.37	4.85	9.86

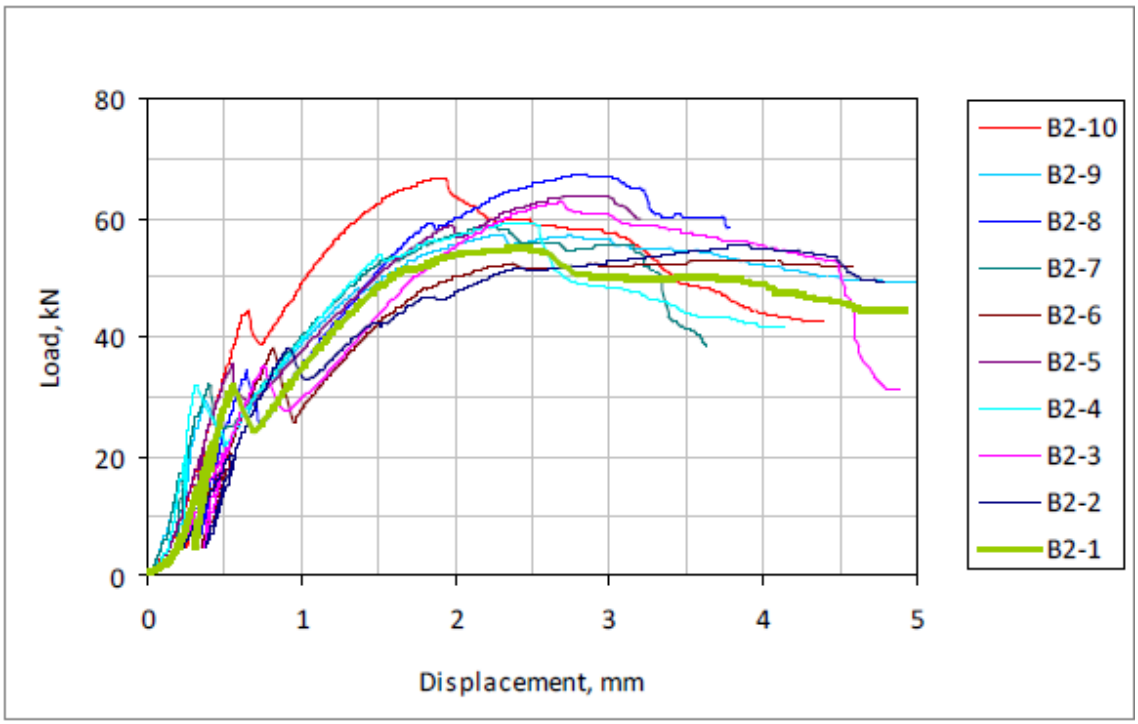

Figure A.1 Load-slip behaviour of bird-mouth notched B2 series specimens.

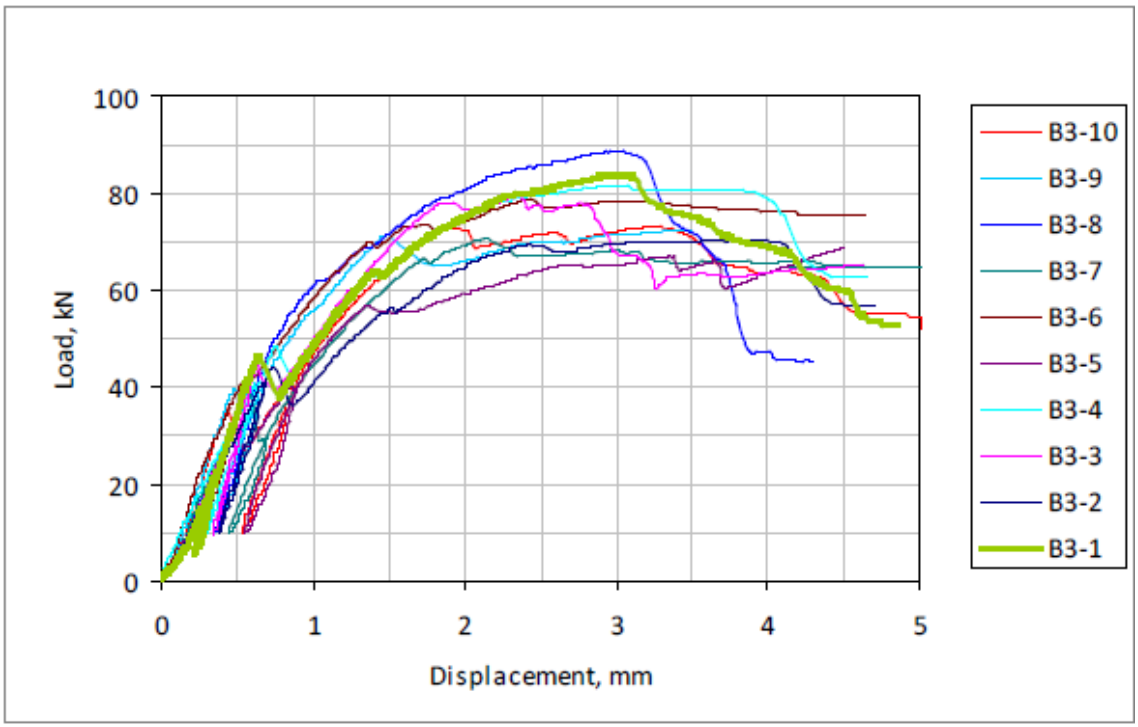

Figure A.2 Load-slip behaviour of bird-mouth notched B3 series specimens.

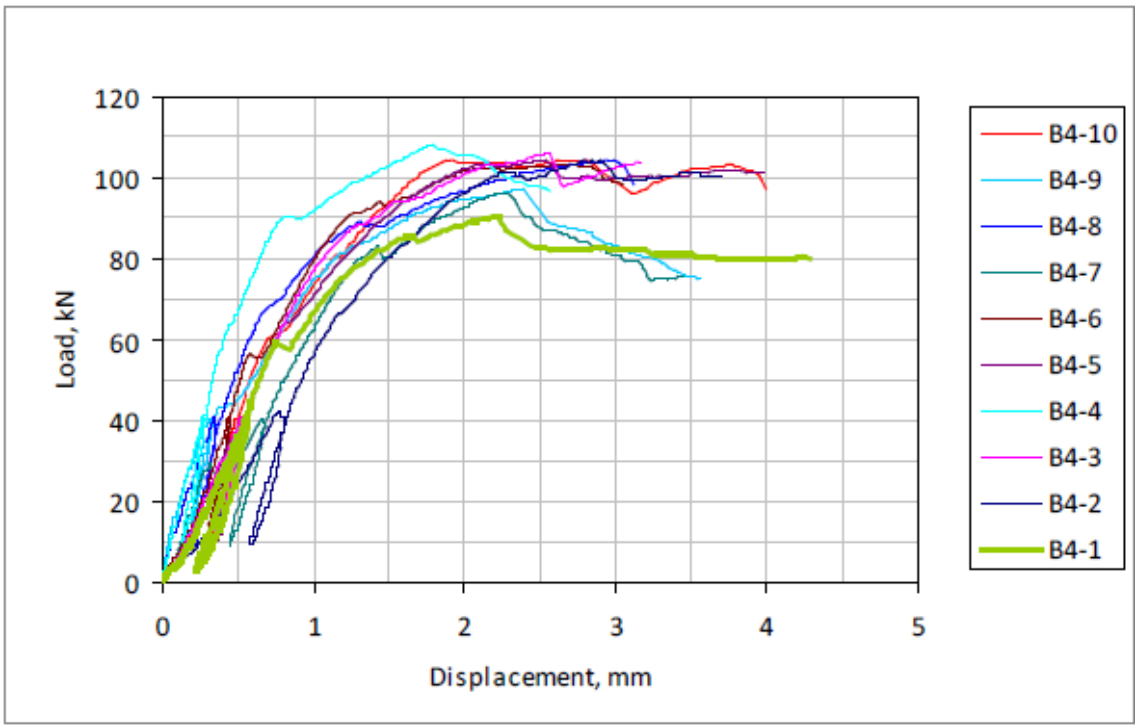

Figure A.3 Load-slip behaviour of bird-mouth notched B4 series specimens.

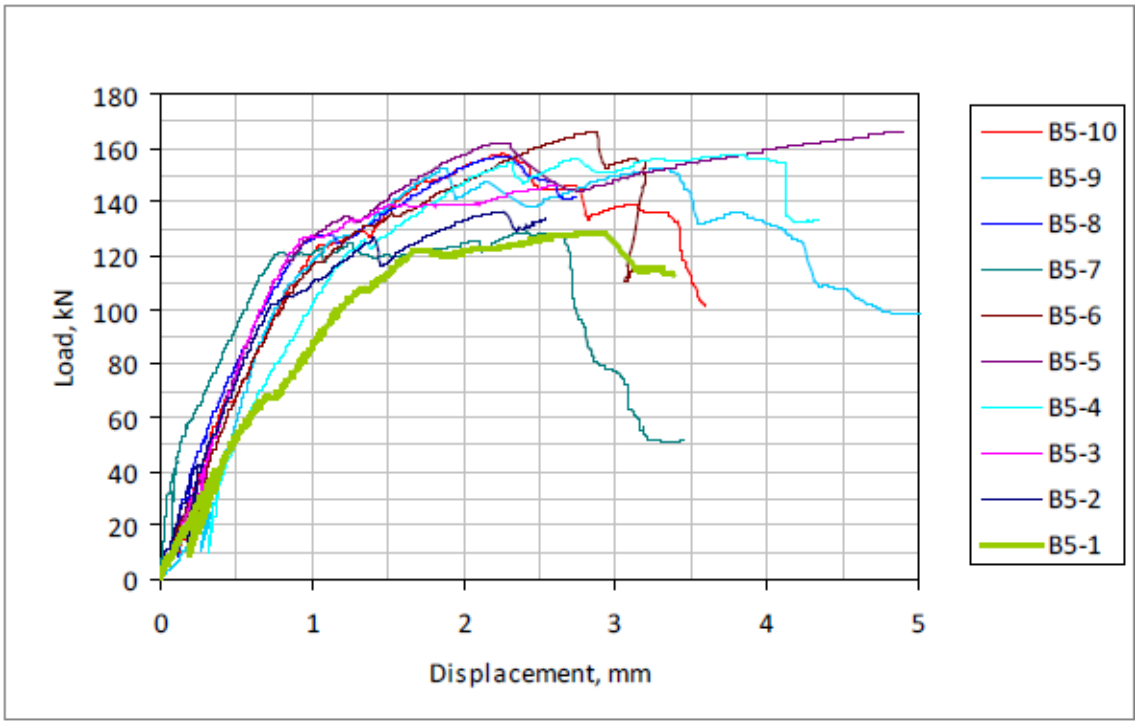

Figure A.4 Load-slip behaviour of bird-mouth notched B5 series specimens.

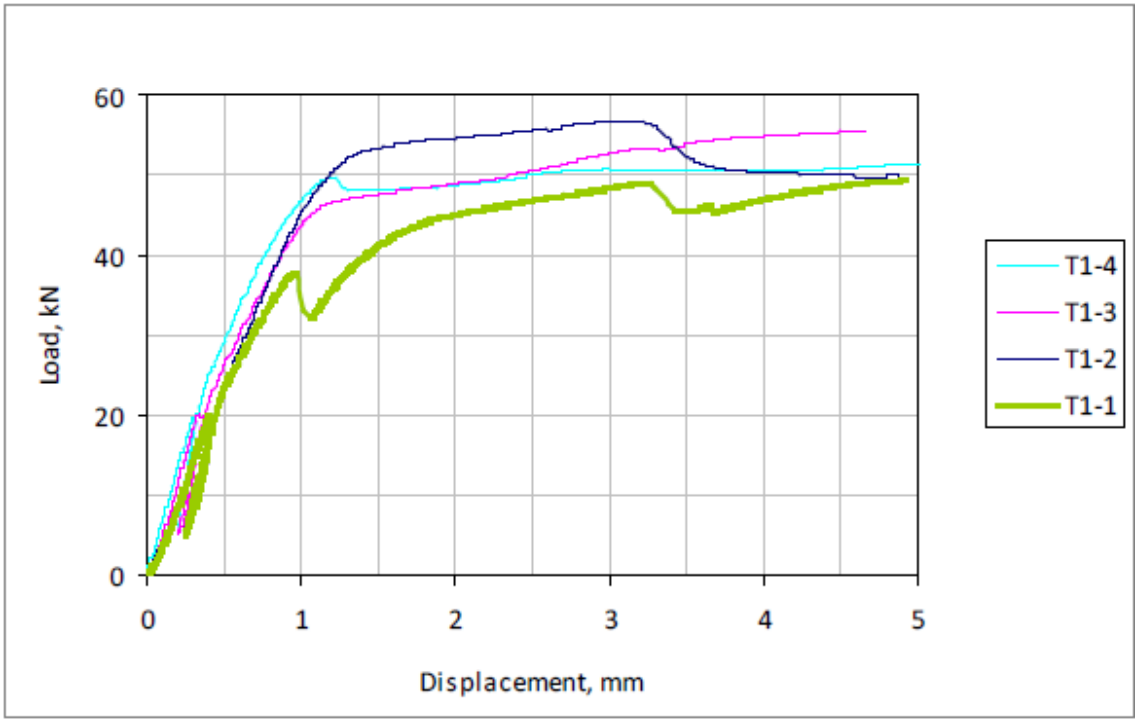

Figure A.5 Load-slip behaviour of trapezoidal notched T1 series specimens.

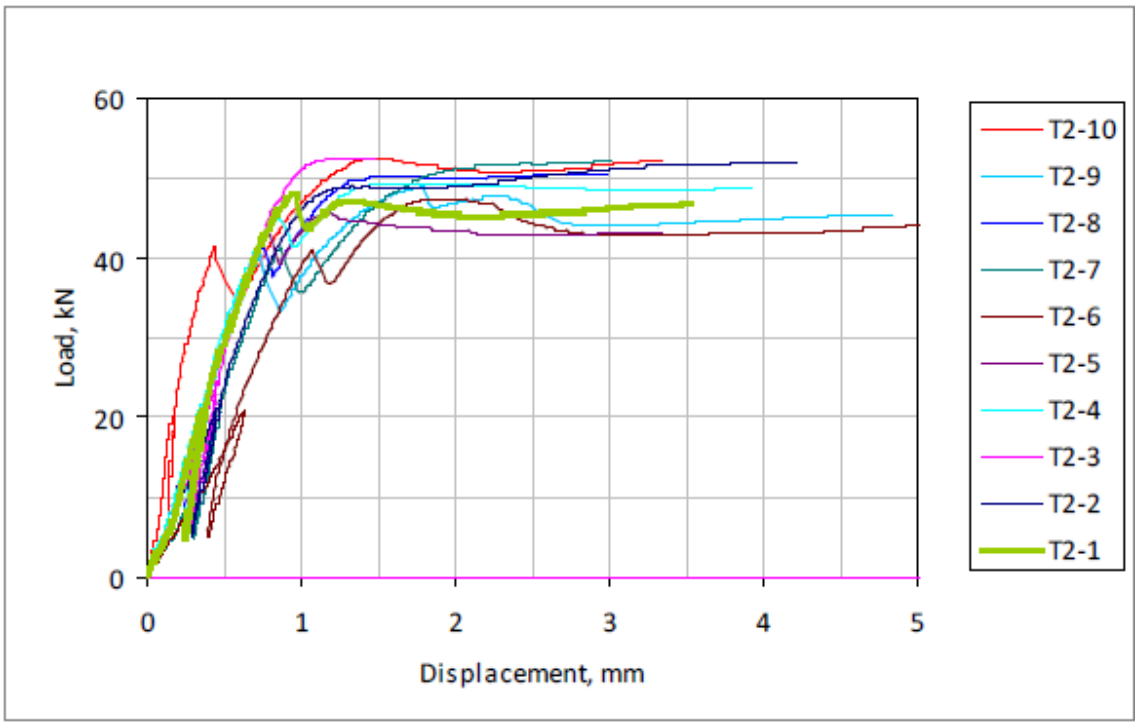

Figure A.6 Load-slip behaviour of trapezoidal notched T2 series specimens.

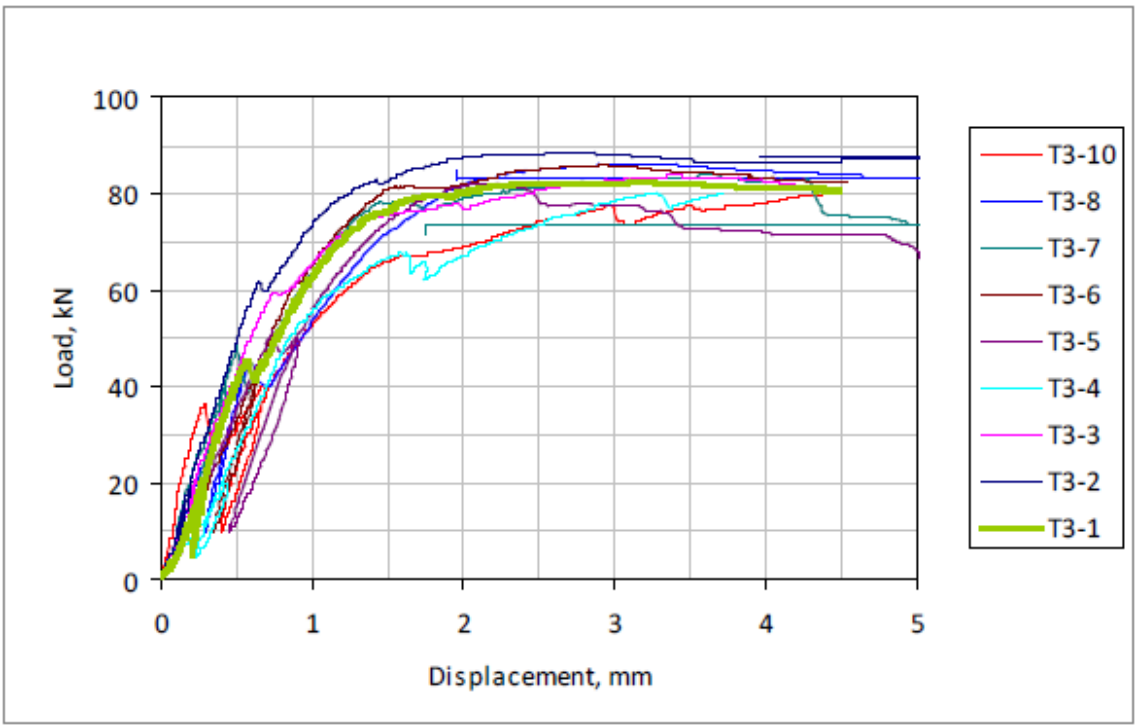

Figure A.7 Load-slip behaviour of trapezoidal notched T3 series specimens.

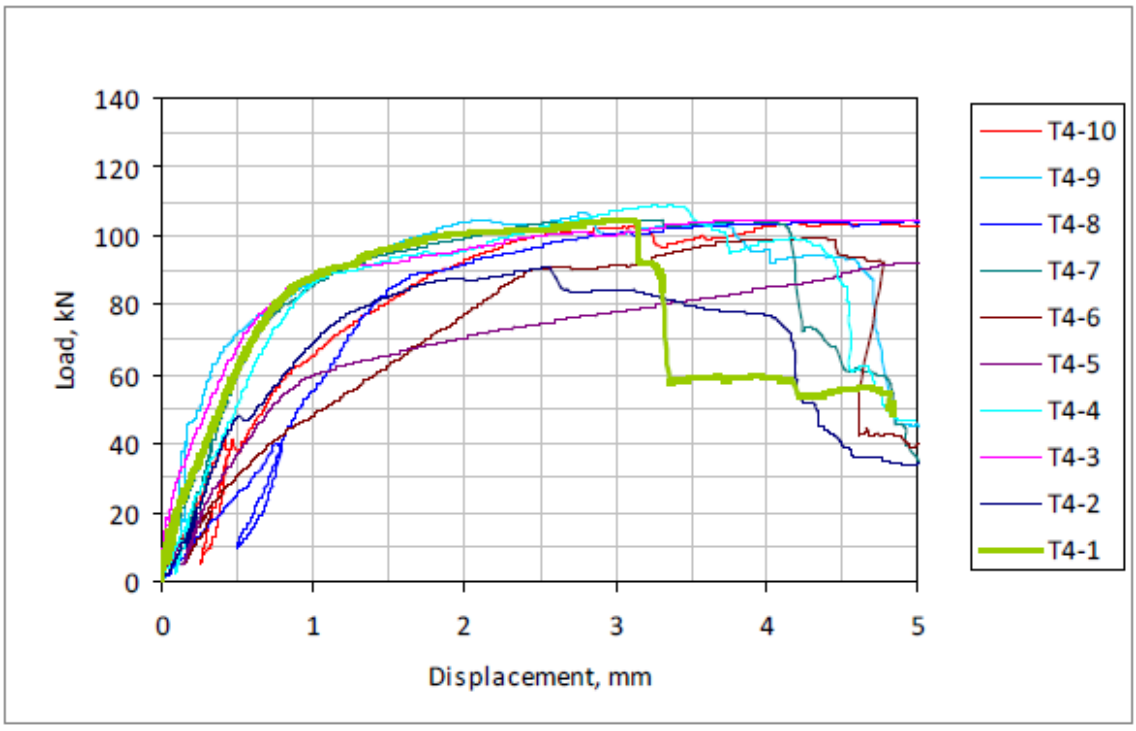

Figure A.8 Load-slip behaviour of trapezoidal notched T4 series specimens.

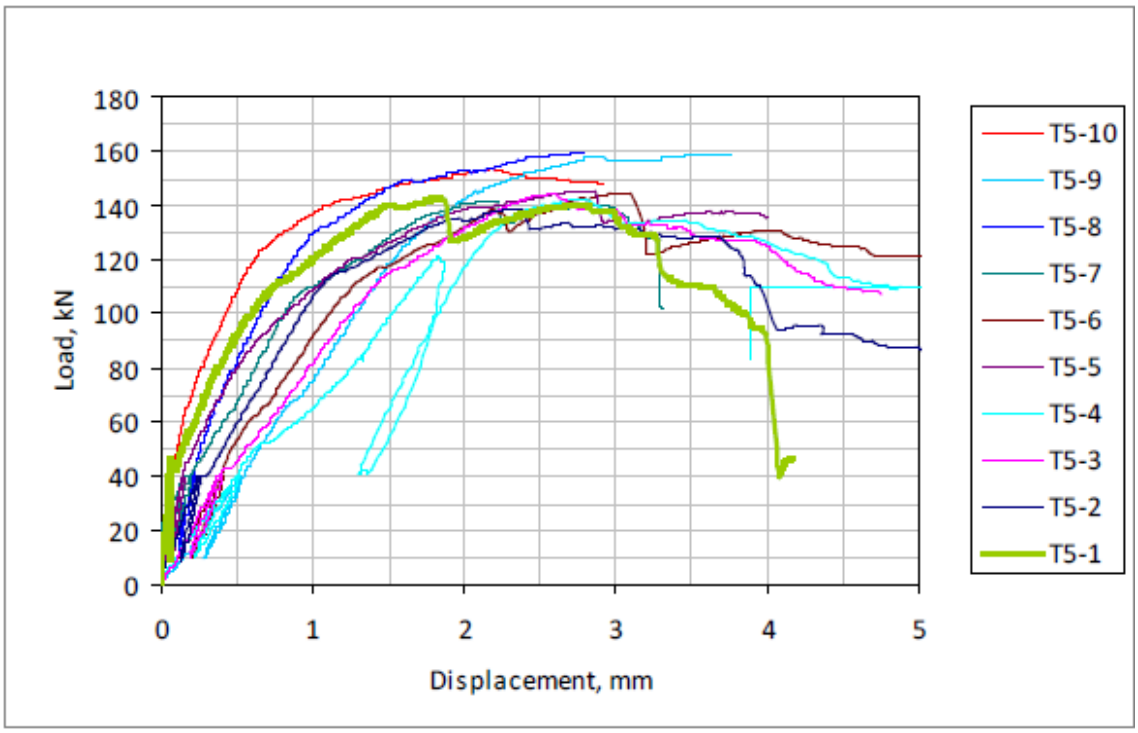

Figure A.9 Load-slip behaviour of trapezoidal notched T5 series specimens.

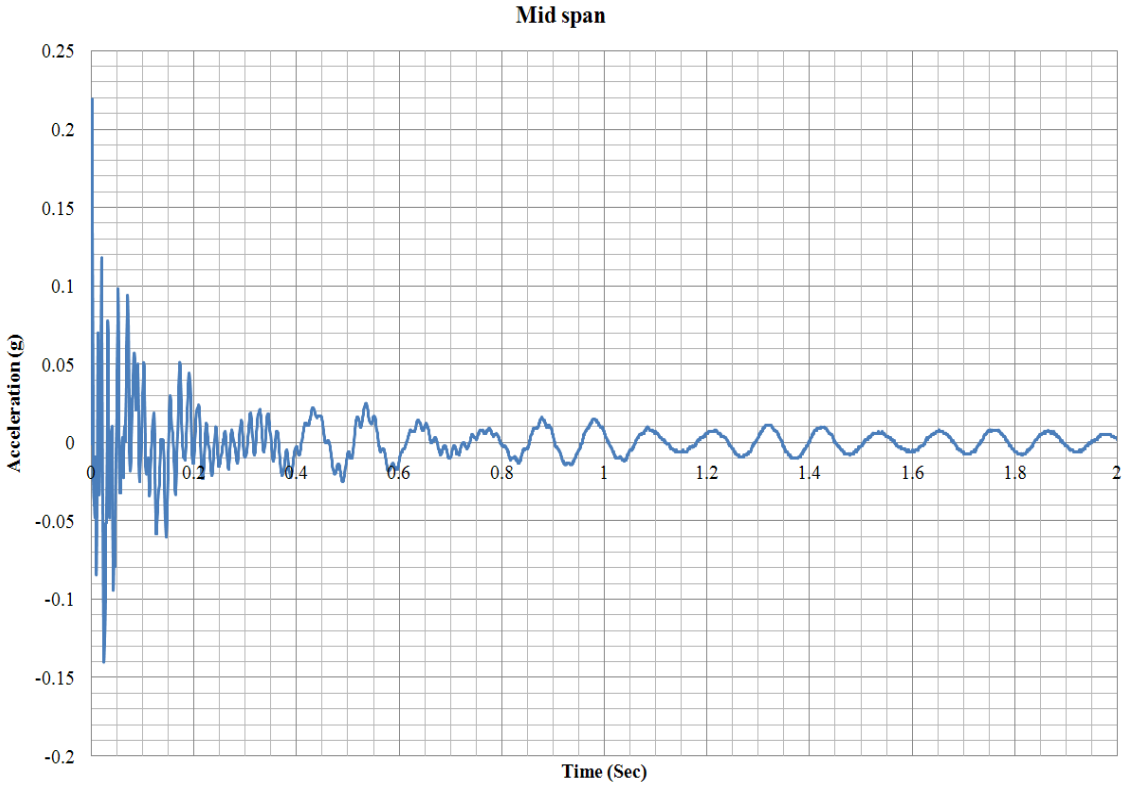

Notes:

a. *This result is a sample of one of the data sets for excitation at mid span.*
b. *This graph presents response of TCC Beam-1 for 2 seconds out of 20 seconds experimental record.*
c. *Response of other TCC beams was also similar to this result.*

Figure A.10 Response of TCC Beam-1 measured at mid span of the beam using accelerometer along centre line of concrete topping in time domain.

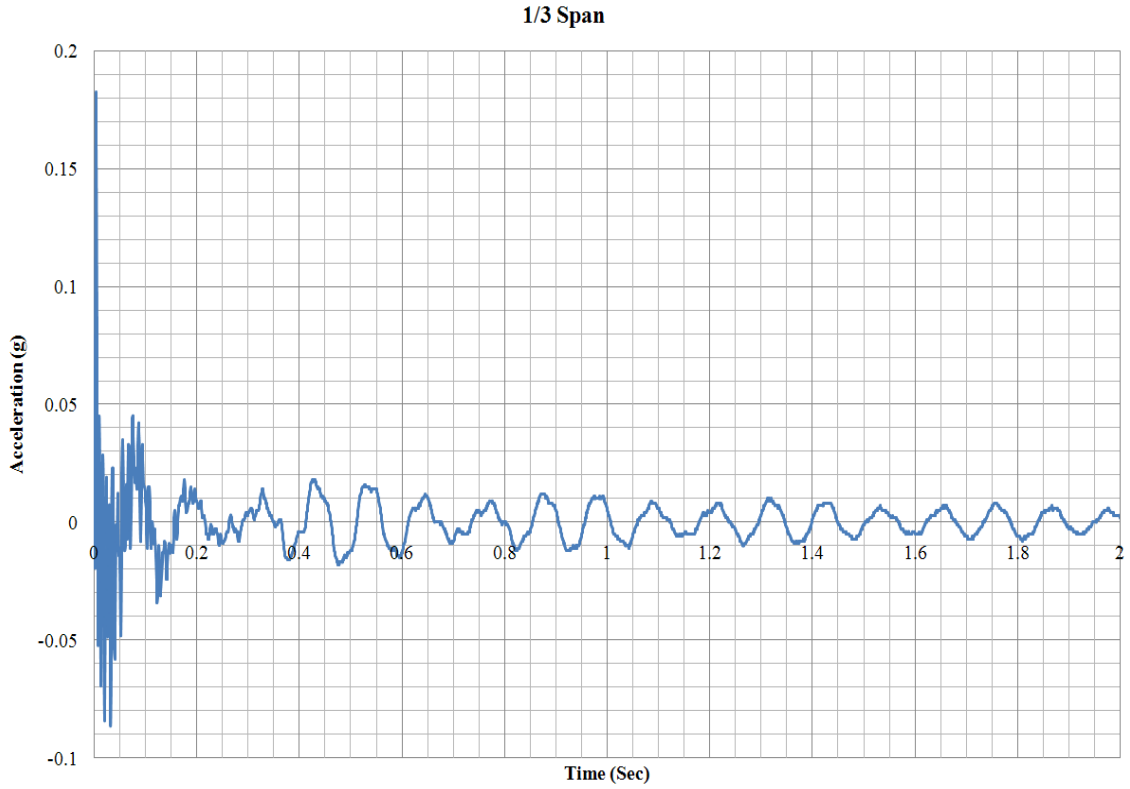

Notes:

a. This result is a sample of one of the data sets for excitation at mid span.

b. This graph presents response of TCC Beam-1 for 2 seconds out of 20 seconds experimental record.

c. Response of other TCC beams was also similar to this result.

Figure A.11 Response of TCC Beam-1 measured at 1/3rd span of the beam using accelerometer along centre line of concrete topping in time domain.

Appendix B (Chapter 4)

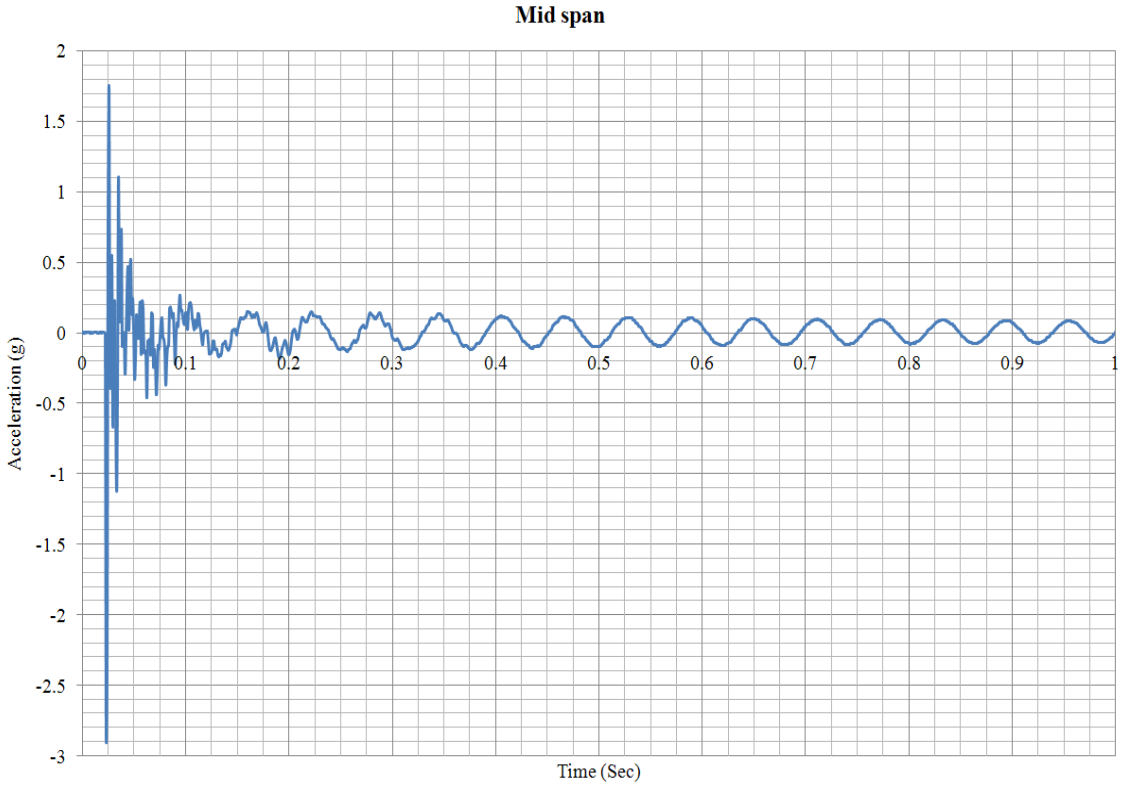

Notes:

a. *This result is a sample of one of the data sets for excitation at mid span.*
b. *This graph presents response of timber beam, L6-01, for 1 second out of 30 seconds experimental record.*
c. *Response of other timber beams with 6 and 8 m spans was also similar to this result.*

Figure B.1 Response of timber beam, L6-01, measured at mid span of the beam using accelerometer along centre line of top flange in time domain.

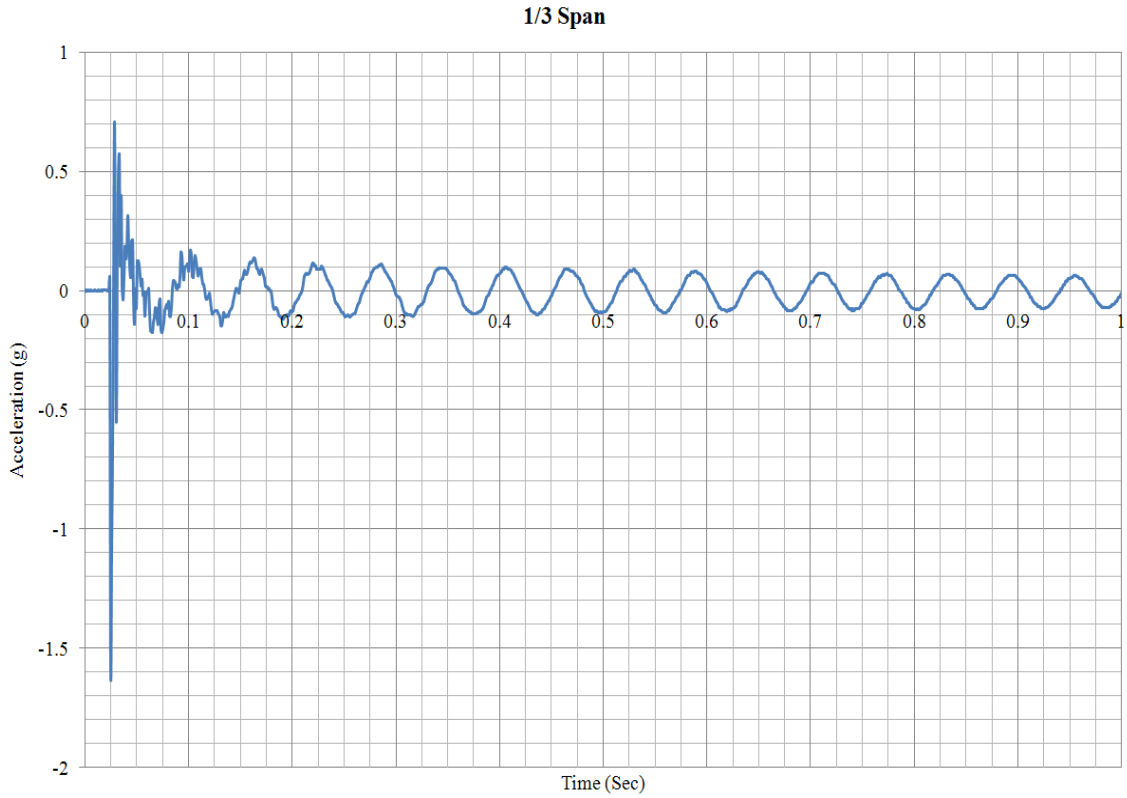

Notes:

a. This result is a sample of one of the data sets for excitation at mid span.

b. This graph presents response of timber beam, L6-01, for 1 second out of 30 seconds experimental record.

c. Response of other timber beams with 6 and 8 m spans was also similar to this result.

Figure B.2 Response of timber beam, L6-01, measured at 1/3rd span of the beam using accelerometer along centre line of top flange in time domain.

Appendix C (Chapter 6)

Table C.1 Natural frequencies of an experimental timber beam

Data set	No. of screws	Flexural natural frequencies, Hz				
		f_1	f_2	f_3	f_4	f_5
1	3	19.5	57.8	118.1	155.2	214.8
2		18.9	57.6	118.0	157.4	213.6
3		19.3	57.4	118.2	159.7	212.8
4		19.5	58.0	118.9	155.2	212.5
5		19.3	57.6	118.7	157.0	213.1
Mean		19.3	57.7	118.4	156.9	213.4
CoV		1.3	0.4	0.3	1.2	0.4
1	5	22.3	78.0	133.7	212.2	285.1
2		22.0	78.1	135.7	210.1	270.7
3		22.1	75.0	131.1	206.1	269.3
4		22.0	77.6	135.6	202.6	260.9
5		22.1	74.6	128.8	207.1	259.7
Mean		22.1	76.7	133.0	207.6	269.1
CoV		0.5	2.2	2.3	1.8	3.8
1	9	23.0	79.7	139.4	221.9	320.9
2		22.8	80.1	140.0	220.0	317.5
3		23.1	80.4	136.9	222.0	324.0
4		22.9	80.8	139.4	221.5	313.1
5		23.3	81.3	139.3	225.2	317.8
Mean		23.0	80.4	139.0	222.1	318.7
CoV		0.8	0.8	0.9	0.9	1.3
1	17	23.8	83.6	154.7	241.8	336.3
2		23.7	83.8	158.5	240.4	339.5
3		23.8	85.2	154.3	239.9	326.2
4		23.7	83.3	154.0	242.4	337.2
5		23.7	83.8	153.1	237.1	341.1
Mean		23.8	83.9	154.9	240.3	336.0
CoV		0.2	0.9	1.3	0.9	1.7
1	33	24.1	85.8	162.3	256.6	341.4
2		24.1	86.0	163.0	258.2	356.4
3		24.1	86.0	161.9	255.5	365.4
4		24.0	85.7	160.7	256.7	347.8
5		24.1	85.7	159.0	254.3	341.8
Mean		24.1	85.8	161.4	256.3	350.6
CoV		0.2	0.2	1.0	0.6	2.9

Table C.2 Corresponding damping ratios, ξ (%) of an experimental timber beam

Data set	No. of screws	ξ_1	ξ_2	ξ_3	ξ_4	ξ_5
		2.04	1.77	1.18	1.45	0.95
2		2.14	1.83	1.40	3.92	1.11
3	3	2.17	2.03	1.60	1.63	1.11
4		2.15	1.96	1.40	1.13	0.79
5		1.83	1.74	1.16	2.17	1.06
Mean		2.07	1.87	1.35	2.06	1.00
CoV		6.83	6.68	13.50	53.69	13.58
1		2.56	0.80	2.00	3.19	0.10
2		2.26	1.41	0.96	2.68	0.24
3	5	2.57	1.47	1.80	2.18	2.39
4		2.79	1.21	3.77	2.36	2.90
5		1.94	0.68	3.61	3.49	3.72
Mean		2.42	1.11	2.43	2.78	3.00
CoV		13.60	32.07	50.15	19.85	22.34
1		2.78	3.69	4.60	1.99	0.54
2		2.76	4.35	4.89	2.66	0.52
3	9	2.82	2.81	3.65	3.72	0.39
4		2.54	3.10	3.42	2.60	0.30
5		1.97	2.39	3.40	4.34	0.16
Mean		2.57	3.27	3.99	3.06	0.38
CoV		13.78	23.49	17.58	30.94	41.41
1		1.86	2.40	2.92	1.69	0.57
2		1.88	2.07	1.07	3.09	0.09
3	17	1.86	0.98	2.15	2.85	0.07
4		1.86	2.18	2.27	2.43	0.05
5		1.83	2.27	2.13	3.03	1.02
Mean		1.86	1.98	2.11	2.62	0.80
CoV		0.96	28.89	31.51	22.13	40.02
1		1.70	1.87	0.95	1.11	0.01
2		1.38	1.77	2.20	1.17	0.03
3	33	1.47	1.67	1.60	1.11	0.01
4		1.68	1.63	2.08	1.15	0.02
5		1.55	1.70	1.16	1.63	0.01
Mean		1.56	1.73	1.60	1.23	0.02
CoV		8.77	5.47	34.37	18.06	55.90

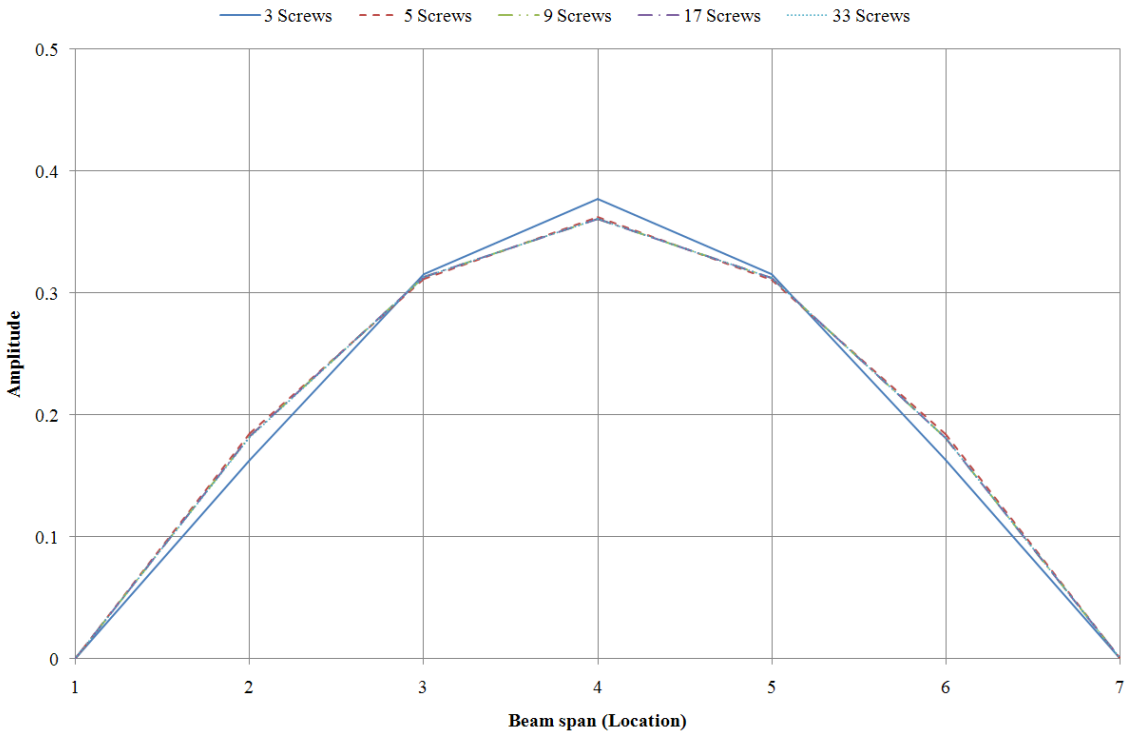

(a) Mode 1

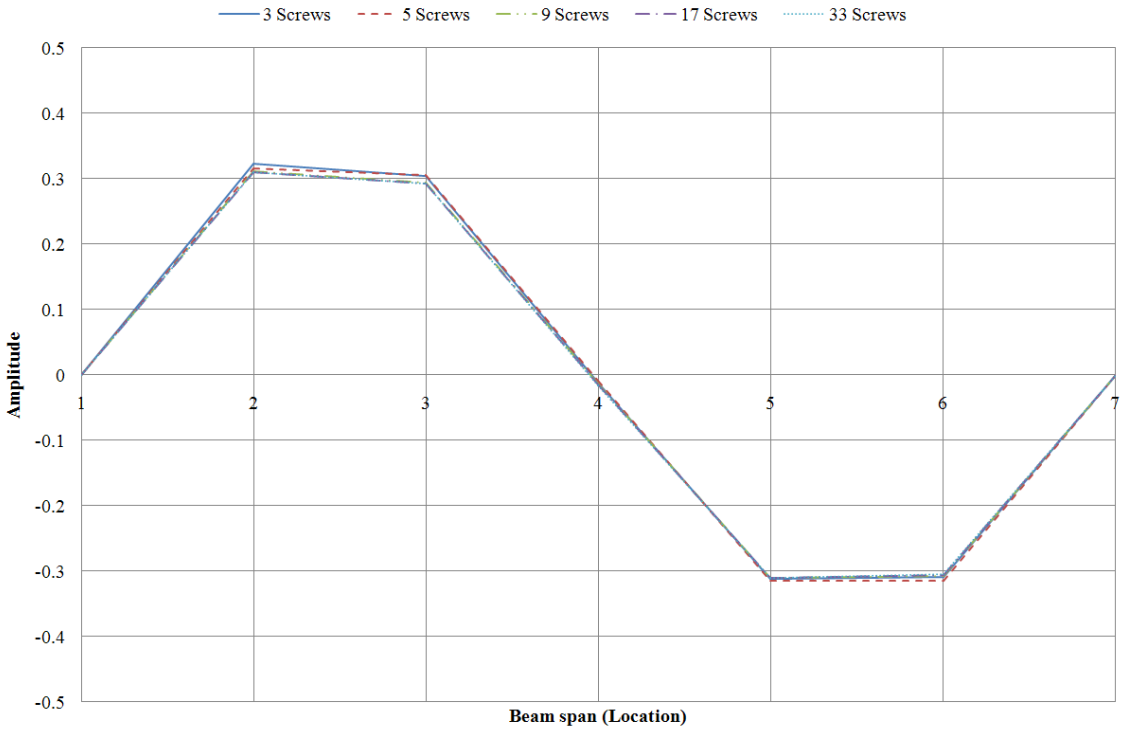

(b) Mode 2

Figure C.1 First two flexural mode shapes of timber composite beam from FE models with different number of screw connections.

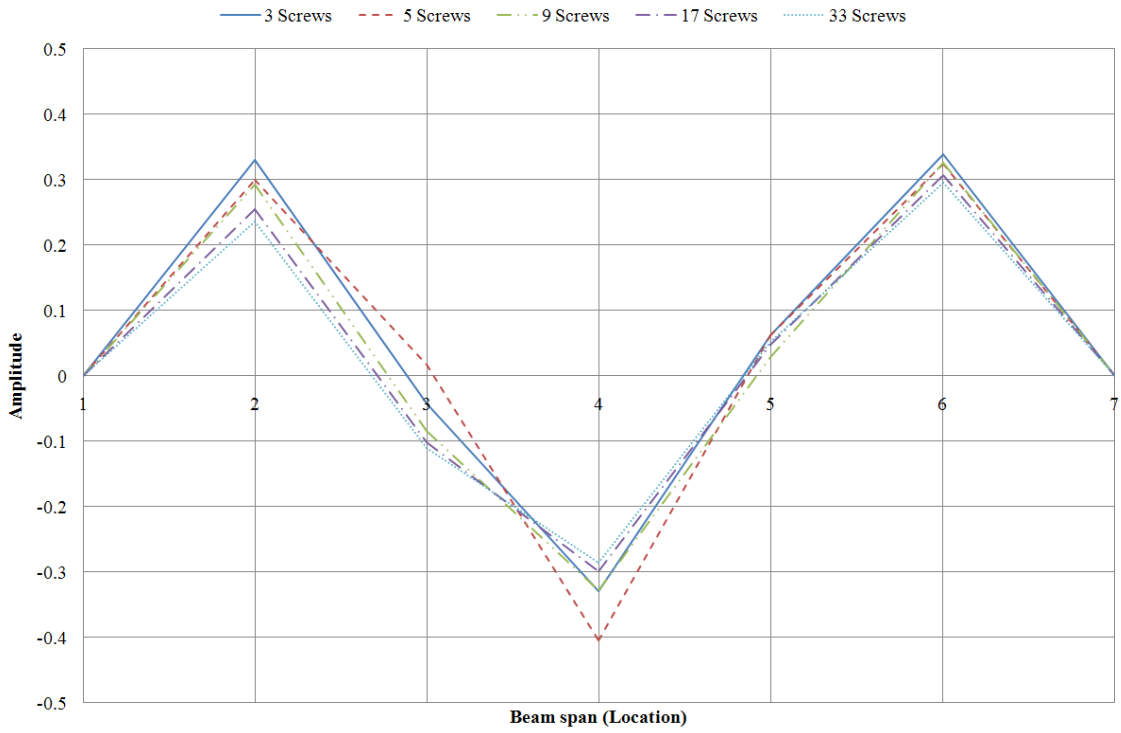

(a) Mode 3

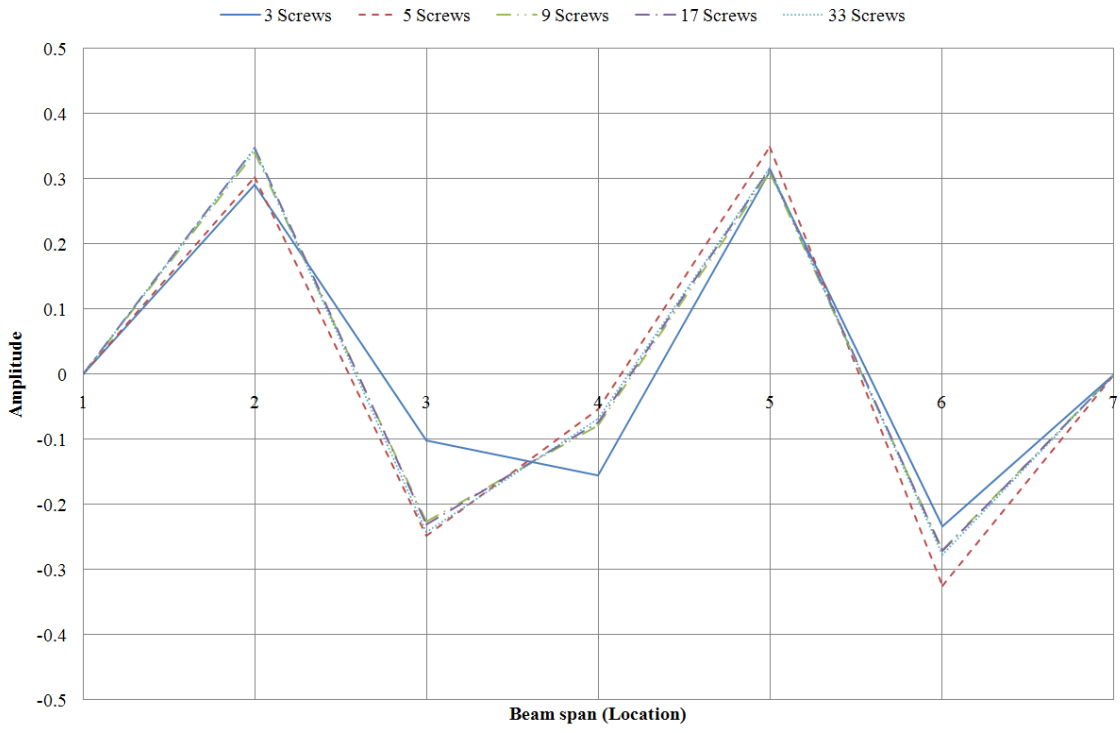

(b) Mode 4

Figure C.2 Third and fourth flexural mode shapes of timber composite beam from FE models with different number of screw connections.

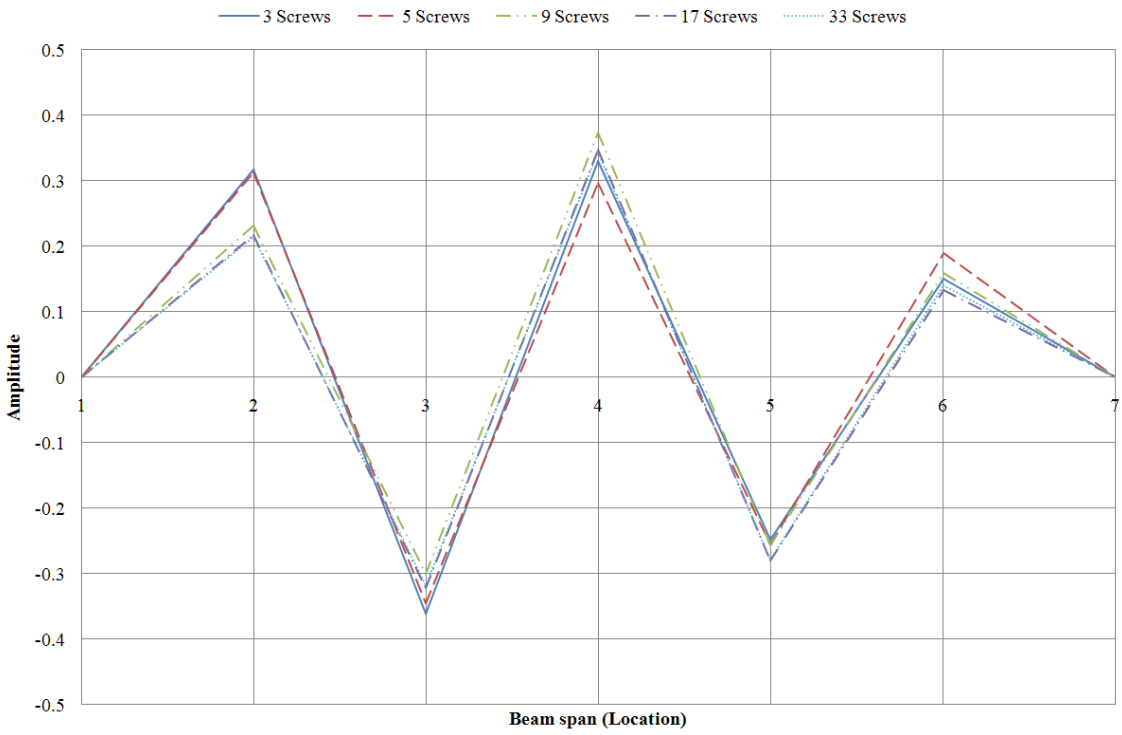

Figure C.3 Fifth flexural mode shape of timber composite beam from FE models with different number of screw connections.

	7 data points	31 data points
Mode 1	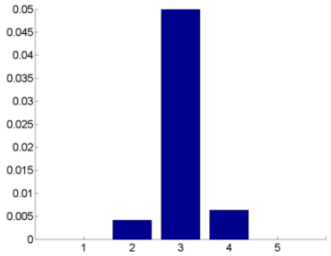	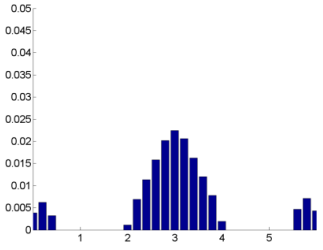
Mode 2	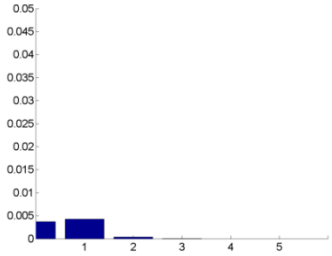	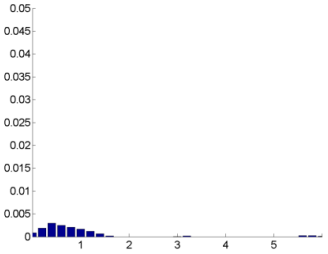
Mode 3	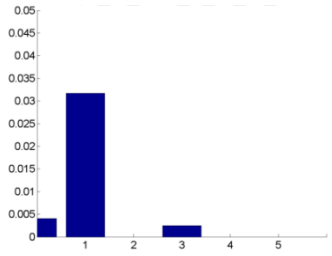	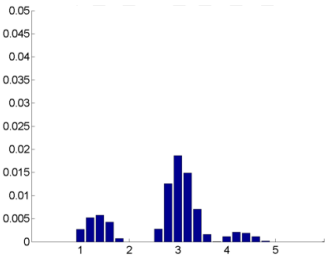
Mode 4	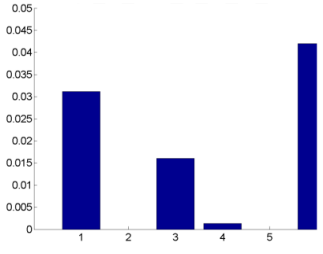	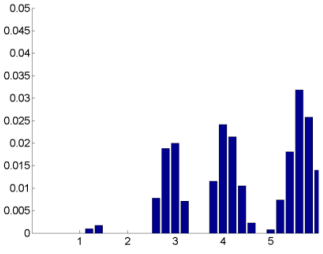
Mode 5	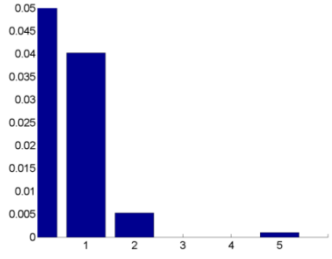	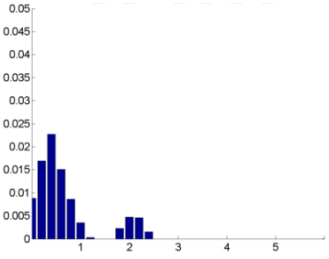

Figure C.4 α values for '3' screws of numerical timber composite beam models derived from 7-point mode shape vectors (7P) and reconstructed 31-point mode shape vectors (31P).

	7 data points	31 data points
Mode 1	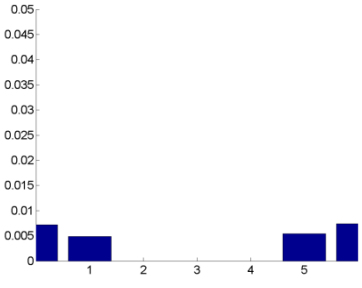	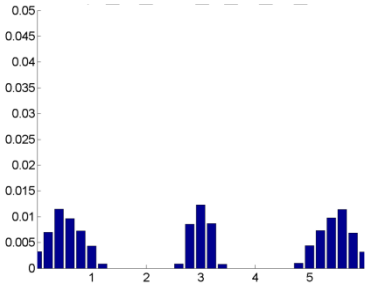
Mode 2	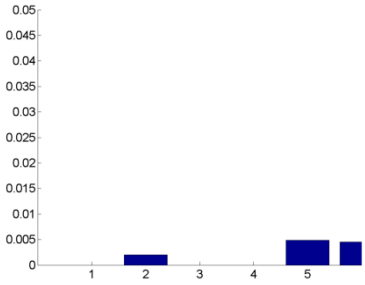	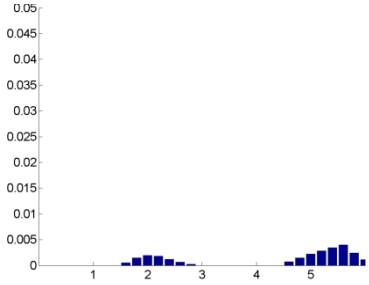
Mode 3	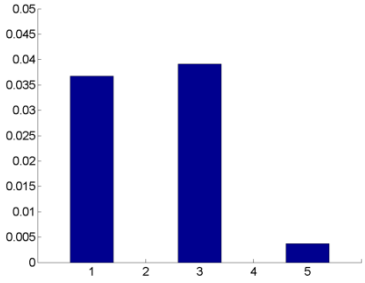	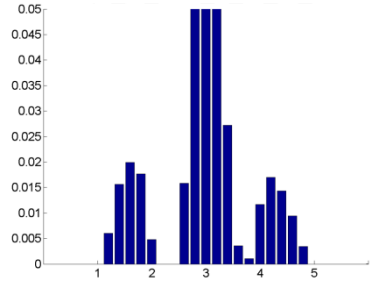
Mode 4	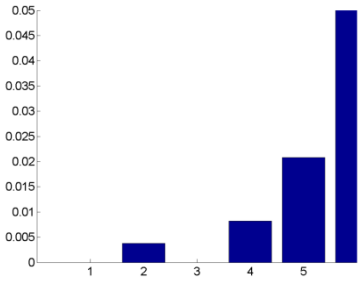	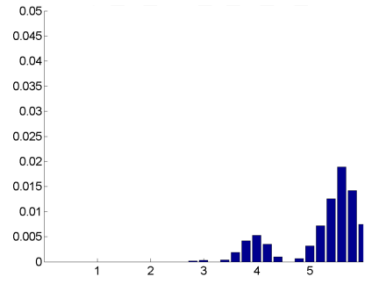
Mode 5	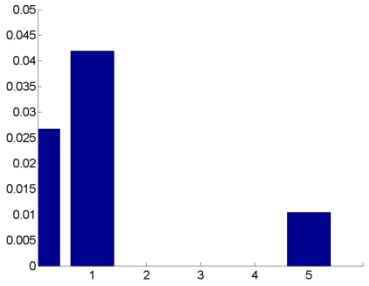	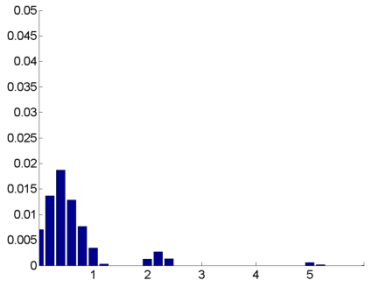

Figure C.5 α values for '5' screws of numerical timber composite beam models derived from 7-point mode shape vectors (7P) and reconstructed 31-point mode shape vectors (31P).

	7 data points	31 data points
Mode 1	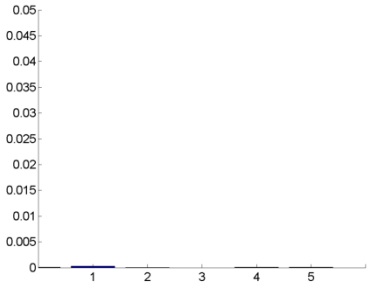	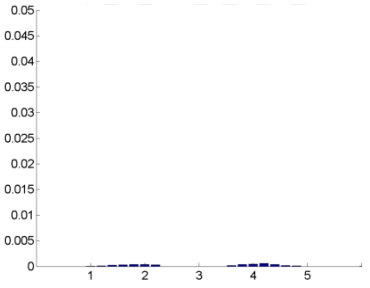
Mode 2	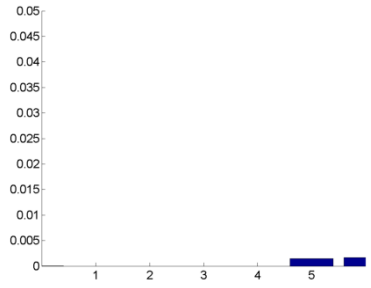	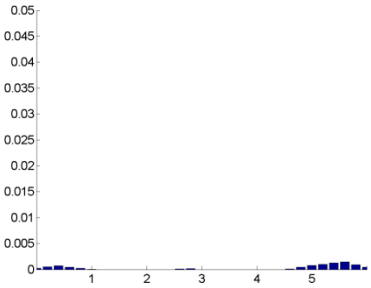
Mode 3	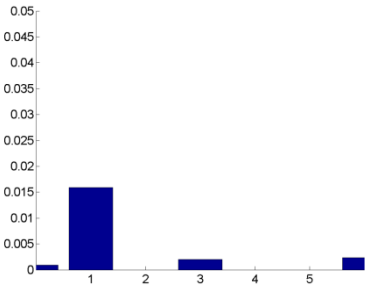	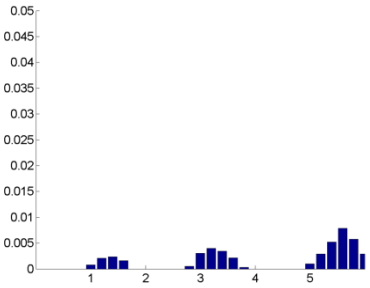
Mode 4	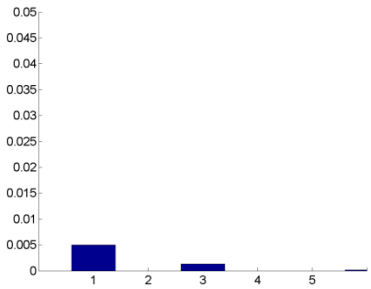	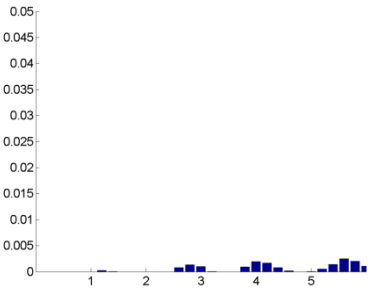
Mode 5	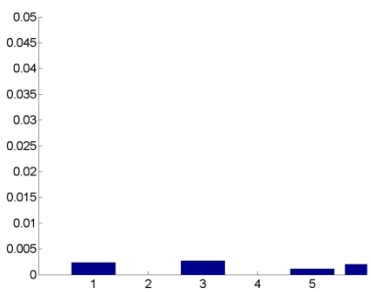	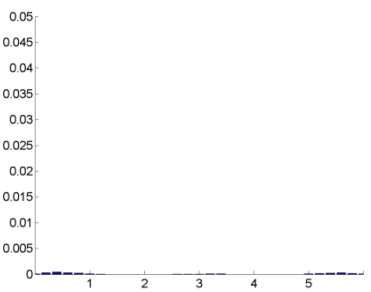

Figure C.6 α values for '9' screws of numerical timber composite beam models derived from 7-point mode shape vectors (7P) and reconstructed 31-point mode shape vectors (31P).

	7 data points	31 data points
Mode 1	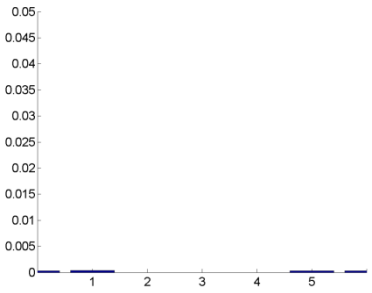	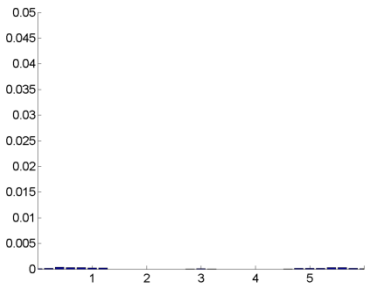
Mode 2	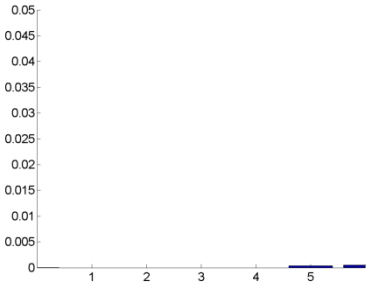	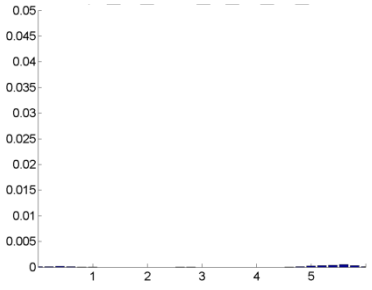
Mode 3	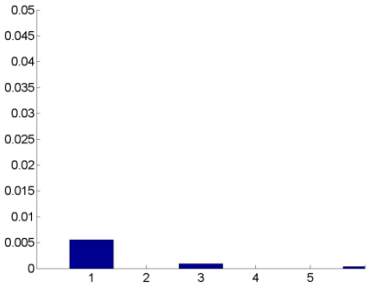	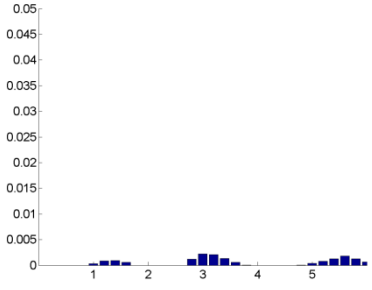
Mode 4	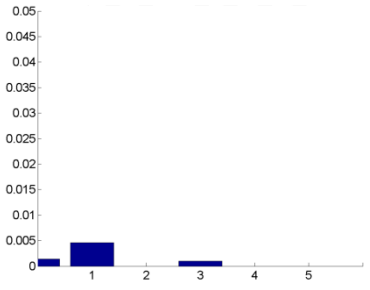	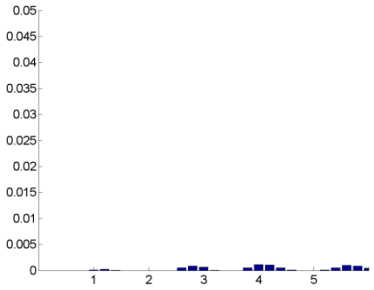
Mode 5	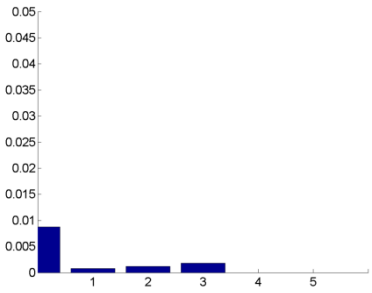	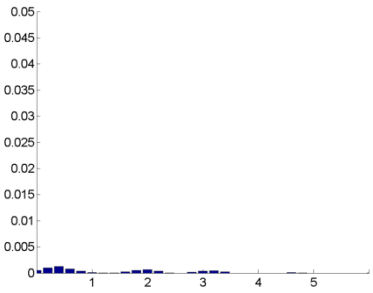

Figure C.7 α values for '17' screws of numerical timber composite beam models derived from 7-point mode shape vectors (7P) and reconstructed 31-point mode shape vectors (31P).

	7 data points	31 data points
Mode 1	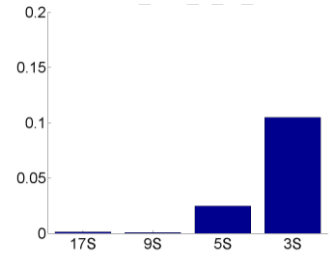	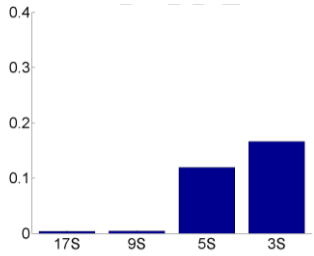
Mode 2	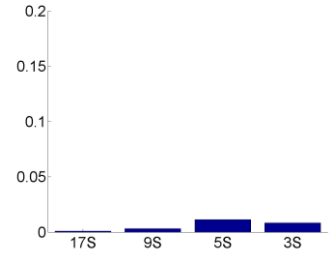	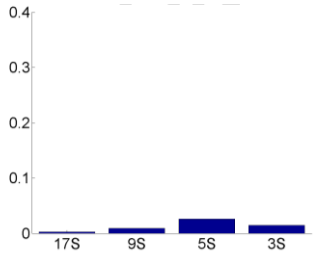
Mode 3	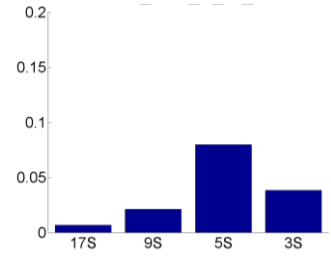	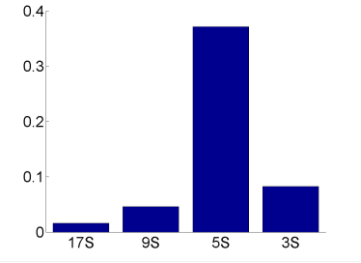
Mode 4	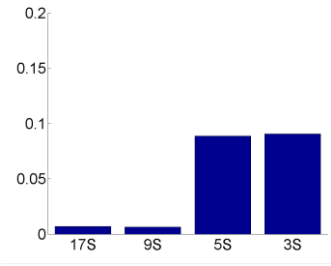	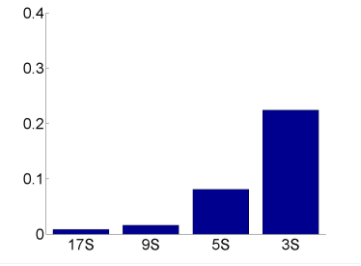
Mode 5	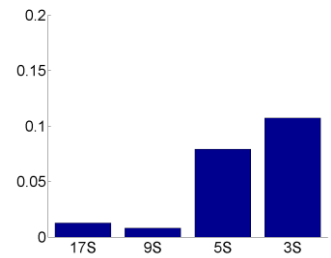	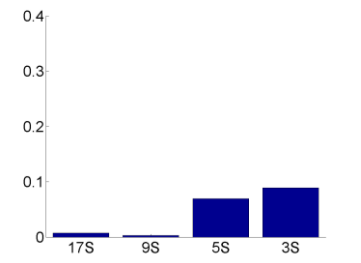

Figure C.8 $LCAI_1$ values for first five flexural modes (for '3', '5', '9' and '17' number of screws) of numerical timber composite beam models derived from 7-point mode shape vectors (7P) and reconstructed 31-point mode shape vectors (31P).

	7 data points	31 data points
Mode 1	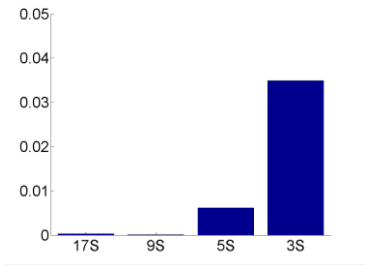	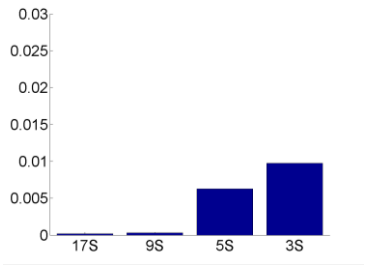
Mode 2	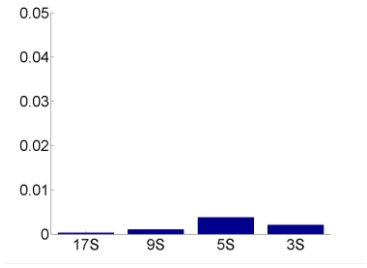	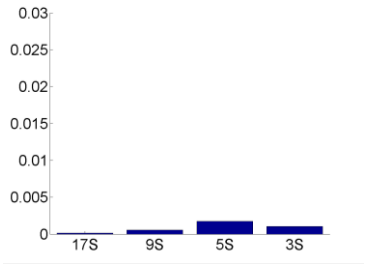
Mode 3	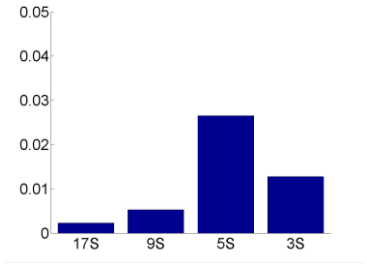	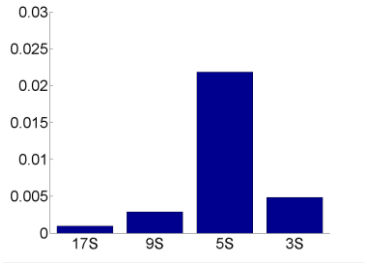
Mode 4	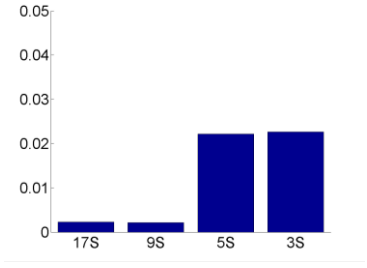	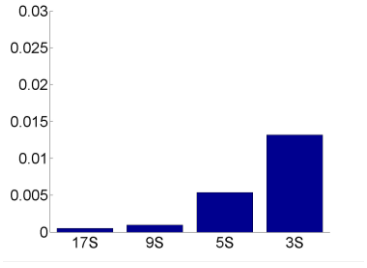
Mode 5	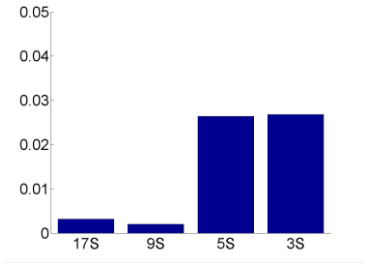	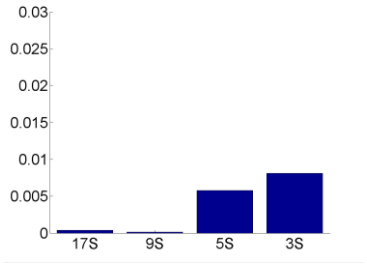

Figure C.9 $LCAI_2$ values for first five flexural modes (for '3', '5', '9' and '17' number of screws) of numerical timber composite beam models derived from 7-point mode shape vectors (7P) and reconstructed 31-point mode shape vectors (31P).

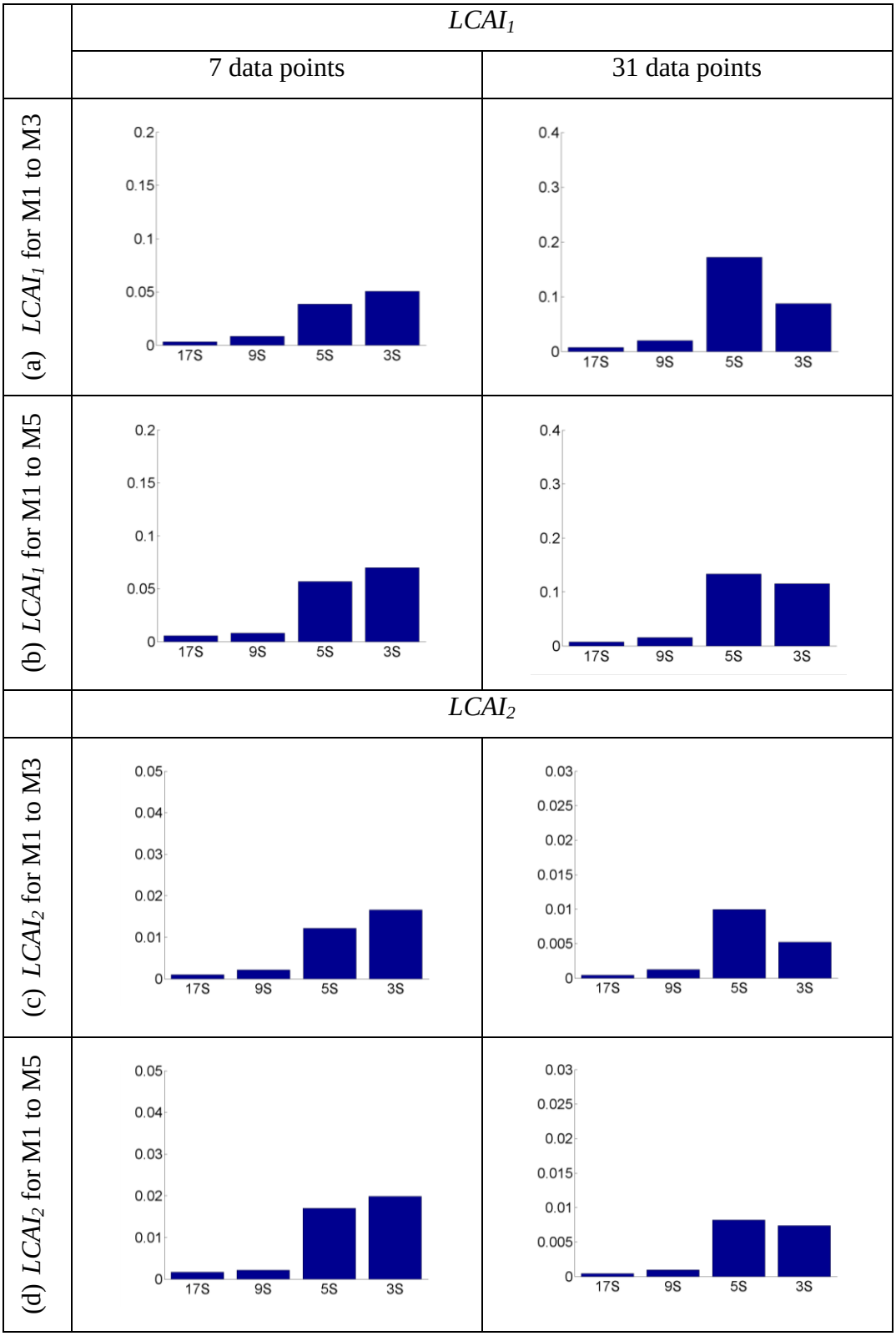

Figure C.10 $LCAI_1$ and $LCAI_2$ values for flexural modes (a) and (c) 1 to 3, (b) and (d) 1 to 5 (for '3', '5', '9' and '17' number of screws) of numerical timber composite beam models derived from 7-point mode shape vectors (7P) and reconstructed 31-point mode shape vectors (31P).

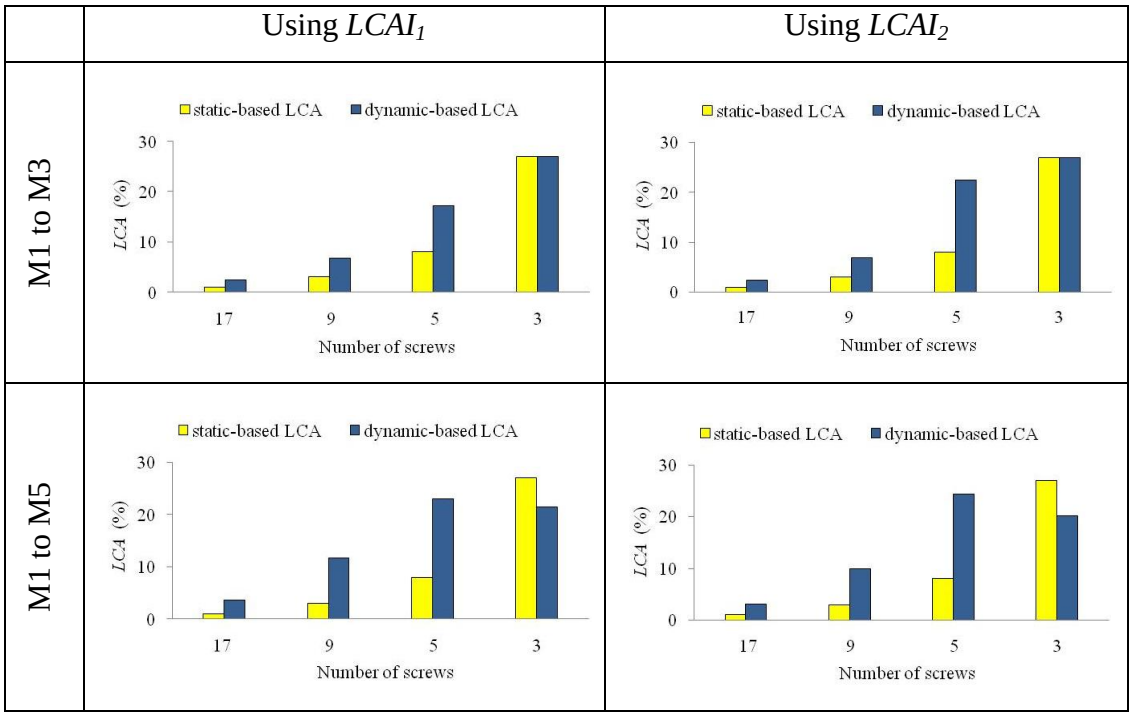

Figure C.11 Loss of composite action of a timber beam for 'case 3' derived from FE models.

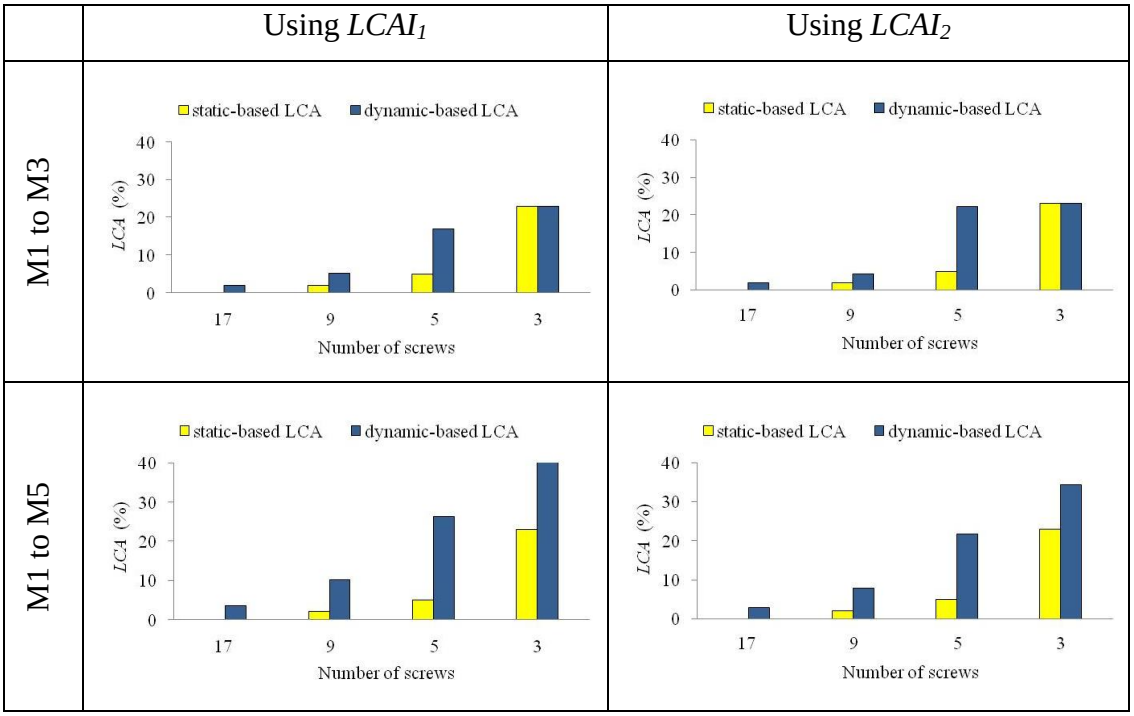

Figure C.12 Loss of composite action of a timber beam for 'case 4' derived from FE models.

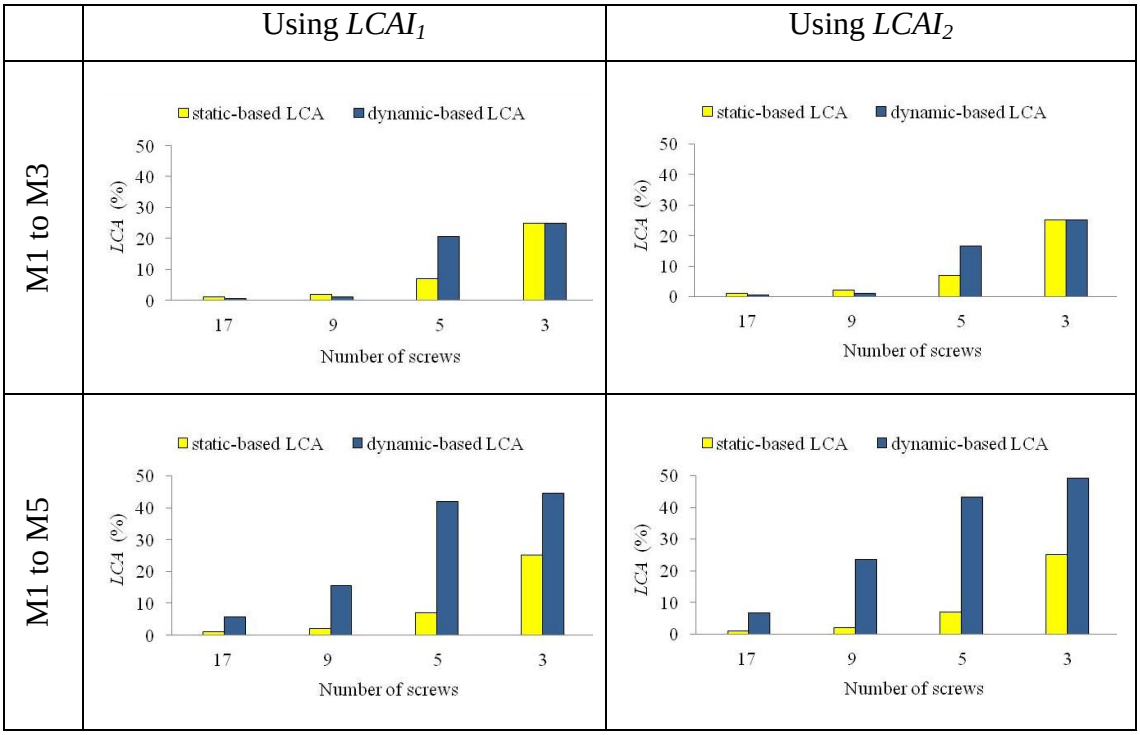

Figure C.13 Loss of composite action of a timber beam for 'case 5' derived from FE models.

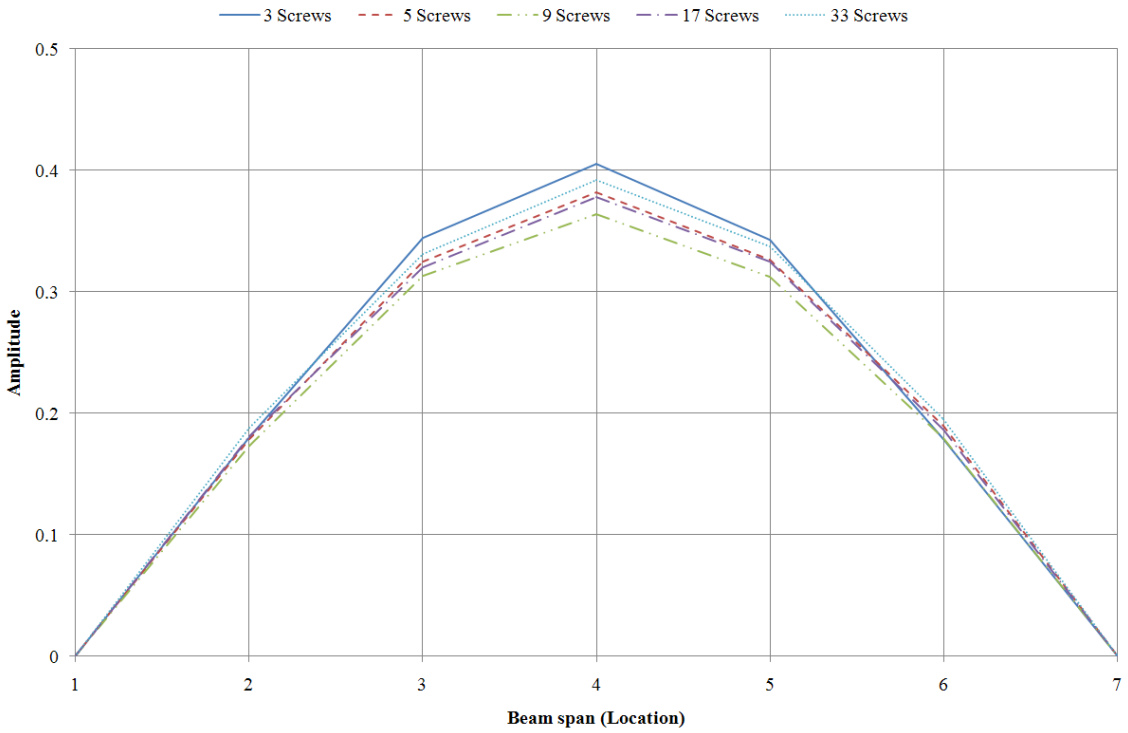

Figure C.14 First flexural mode shape of the experimental timber composite beam with different number of screws.

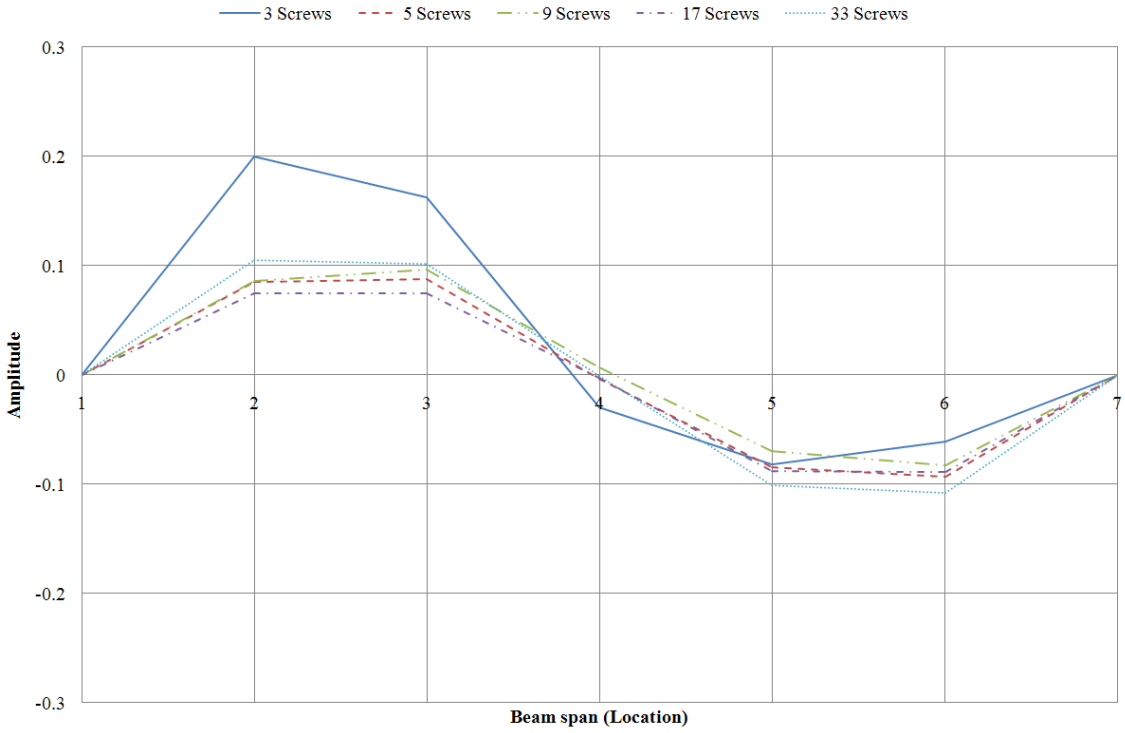

(a) Mode 2

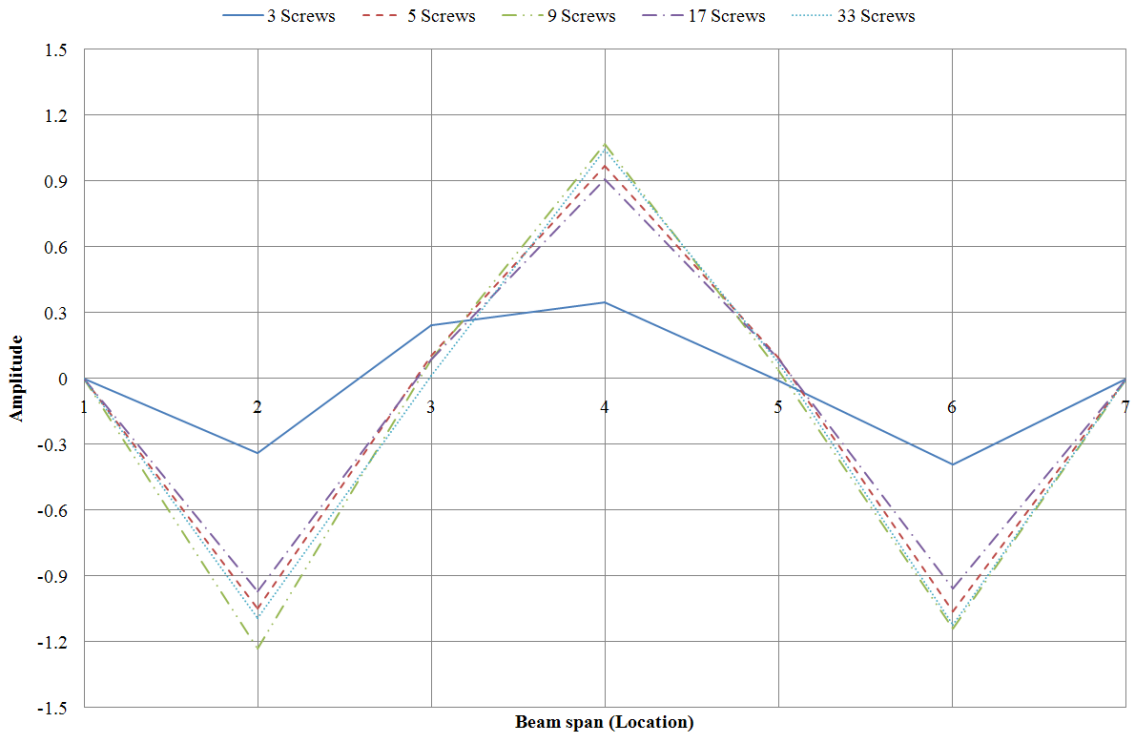

(b) Mode 3

Figure C.15 Second and third flexural mode shapes of the experimental timber composite beam with different number of screws.

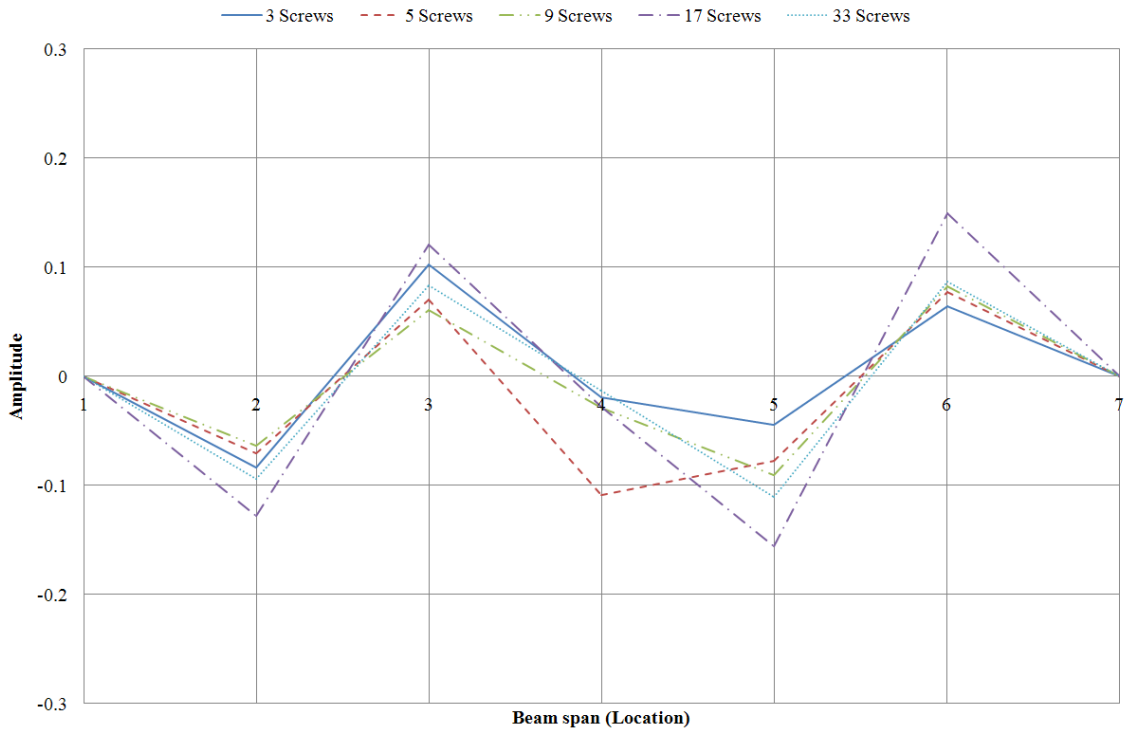

(a) Mode 4

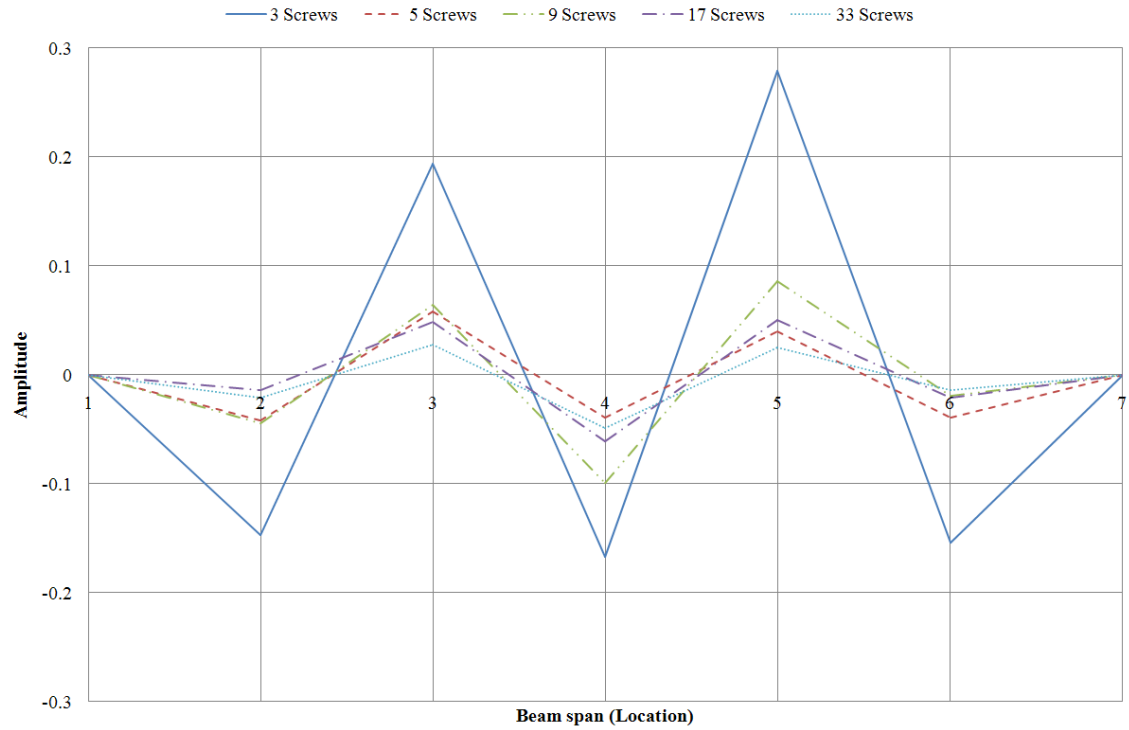

(b) Mode 5

Figure C.16 Fourth and fifth flexural mode shapes of the experimental timber composite beam with different number of screws.